

Discovery of Inhibitors of Bacterial Histidine Kinases

Nadya Velikova

Thesis committee

Promotor

Prof. dr. Jerry M. Wells
Professor of Host-Microbe Interactomics
Wageningen University

Co-promotor

Dr. Alberto Marina
Director of the Department of Genomics and Proteomics
Institute of Biomedicine of Valencia (IBV)
Spanish National Research Council (CSIC), Valencia, Spain

Other members

Dr. Maria Teresa Pellicer, Ferrer, Barcelona, Spain
Dr. Bruno Gonzales Zorn, Computense University of Madrid, Madrid, Spain
Prof. dr. Pedro Alzari, Institute Pasteur, Paris, France
Prof. dr. ir. Geert Wiegertjes, Wageningen University

This research was conducted under the auspices of the Graduate School of
Wageningen Institute of Animal Sciences (WIAS)

Discovery of Inhibitors of Bacterial Histidine Kinases

Nadya Velikova

Thesis

submitted in fulfillment of the requirements for the degree of doctor
at Wageningen University
by the authority of the Rector Magnificus
Prof. dr. M.J. Kropff,
in the presence of the
Thesis Committee appointed by the Academic Board
to be defended in public
on Friday 7 November 2014
at 11 a.m. in the Aula.

2014

Nadya Velikova

Discovery of Inhibitors of Bacterial Histidine Kinases , 219 pages.

Thesis, Wageningen University, Wageningen, NL (2014)

With references, with summaries in English and Dutch

ISBN: 978-94-6257-111-2

*To my family and
all the wholeheartedly devoted teachers*

**На моето семейство и
на всички всеотдайни учители**

2014

TABLE OF CONTENTS

Chapter 1	General Introduction	9
Chapter 2	Discovery of bacterial histidine kinase inhibitors with antibacterial activity against clinical isolates of MRSA and <i>Staphylococcus epidermidis</i>	31
Chapter 3	Histidine-kinase inhibitors with broad-spectrum antibacterial effect identified by fragment-based screens	67
Chapter 4	Broadening the antibacterial spectrum of histidine kinase autophosphorylation inhibitors via the use of ϵ -poly-L-lysine capped mesoporous silica-based nanoparticles	91
Chapter 5	Computer-aided approaches in hit optimisation	123
Chapter 6	Preliminary biochemical studies on the interaction of LactoferricinB-derived peptides with two-component systems	141
Chapter 7	Expression, purification, (co-)crystallization and preliminary X-ray diffraction analysis of Two-component Systems and Two-component System-inhibitor co-crystals	157
Chapter 8	WalK, the Path towards New Antibacterials with Low Potential for Resistance Development	173
Chapter 9	General Discussion	183
Summary		201
Samenvatting		205
Acknowledgements		209
Personalia		215
Curriculum Vitae		
List of Publications		

2014

CHAPTER 1

GENERAL INTRODUCTION

Nadya Velikova

2014

THE GROWING PROBLEM OF BACTERIAL RESISTANCE TO ANTIBIOTICS

Bacterial multi-drug resistance (MDR) is defined as acquisition of non-susceptibility to at least one agent in three categories of antibacterials by pathogenic bacteria¹. MDR is a growing problem worldwide². The World Health Organisation (WHO) has identified antibacterial resistance and the antibiotics crisis as “bigger than AIDS” The so-called “ESKAPE” pathogens (*Enterococcus faecium*, *Staphylococcus aureus*, *Klebsiella pneumonia*, *Acinetobacter baumannii*, *Pseudomonas aeruginosa*, *Enterobacter spp.*) are the main cause of hospital infections and are resistant to virtually all the currently marketed antibiotics^{3, 4}. Infections due to resistant bacteria have 1.3 – 2 fold higher associated healthcare costs than susceptible bacteria due to increased mortality, morbidity and treatment costs⁵. The aging population and growing number of immunocompromised patients due to HIV, cancer therapy or transplantation are making the need for novel antibacterials even more acute.

CLASSICAL AND POST-GENOMIC ANTIBACTERIAL DRUG DISCOVERY

All currently used antibiotic classes have been discovered by screening natural products from various sources or synthetic compounds for antibacterial activities against a spectrum of different bacteria^{6, 2, 7}. Over the past decade the large number of available sequenced genomes from multiple strains of pathogenic bacterial stimulated a change in the screening approaches for antibacterials⁸. Rather than screening for whole-cell antibacterial activity, efforts shifted to screening for inhibitors of rationally preselected targets, otherwise known as target-based drug discovery⁶.

CLASSICAL PHENOTYPIC SCREENING

Phenotypic screening for inhibition of bacterial growth with libraries of chemical compounds, including natural products from soil or marine ecosystems, fungi or plants, and bacterial secondary metabolites, has to date been the most successful way of discovering novel antibacterials⁹. Typically, inhibition of bacterial growth in the pre-clinical screening stage is followed up by isolation and purification of the active compound and evaluation of its toxicity. Promising hits are then optimized by synthesizing a series of similar compounds to investigate their structure-activity relationship and identify a lead compound. Ultimately, the mode of action of the lead and its antibacterial spectrum are determined. Nearly all antibacterials on the market are based on antibiotics produced by *Streptomyces* and their chemically modified derivatives^{10, 11}. However, since the 1950s the number of novel classes of antibiotics discovered by phenotypic screenings has dwindled and novel strategies have been investigated to overcome the raising problem of bacterial multi-drug resistance and the lack of novel antibacterials¹².

TARGET-BASED ANTIBACTERIALS DRUG DISCOVERY

In the genomic era, more potential antibacterial targets were identified and rational target-based antibacterial drug design gained popularity as an approach¹³. This approach is based on the assumption that some targets, proteins or whole biological pathways, are essential or conditionally essential for bacterial survival. Therefore, blocking them will lead to bacterial death¹⁴. In target-based drug discovery, selected targets are purified and used in *in vitro* screenings of compound libraries for inhibitors of the target activity. Typically, screenings are performed in a high-throughput manner (i.e. high-throughput screening, HTS) and libraries of hundreds of thousands of compounds are screened.

Recent advances in computational biology and chemistry made it become possible to screen compound libraries for putative target ligands *in silico* commonly referred to as virtual screening^{15, 16, 17}. This reduced the number of hits that have to be evaluated *in vitro* for the desired biochemical activity. Target-based screening *in silico* (or structure-based virtual screening) utilizes a three-dimensional structure of the target protein obtained experimentally by X-ray crystallography or NMR or a homology model based on the structure of homologous proteins. Then, large virtual libraries of chemical compounds are screened *in silico* to identify ligands predicted to bind to the target site on the protein. The most promising hits with biochemical activity against the target are optimized by iterative rounds of structure-based drug design^{18, 19}.

Another approach combining the principles behind high-throughput *in vitro* screening and structure-based drug design is fragment-based drug discovery (FBDD). In FBDD a library of few thousands fragment-like compounds^{20, 21, 22} is screened for ligands of a selected drug target *in vitro*. Ideally, hits are confirmed by elucidating the target-fragment structure by X-ray crystallography or NMR. The obtained structural information is used to guide structure-based design of more complex inhibitors with enhanced selectivity and potency by chemically linking fragment hits binding to different regions of the target site.

TWO-COMPONENT SYSTEMS AS ANTIBACTERIAL DRUG TARGETS

Signaling by two-component systems (TCS) is one of the promising antibacterial targets to be proposed since the genomics revolution (Figure 1)^{23, 24, 25}.

TCS are the primary regulators used by bacteria to respond and adapt to a large variety of environmental and intracellular signals²⁶. Prototypical TCS consist of two proteins, a sensor histidine kinase (HK) and an effector response regulator (RR) (Figure 1, 2, and 3).

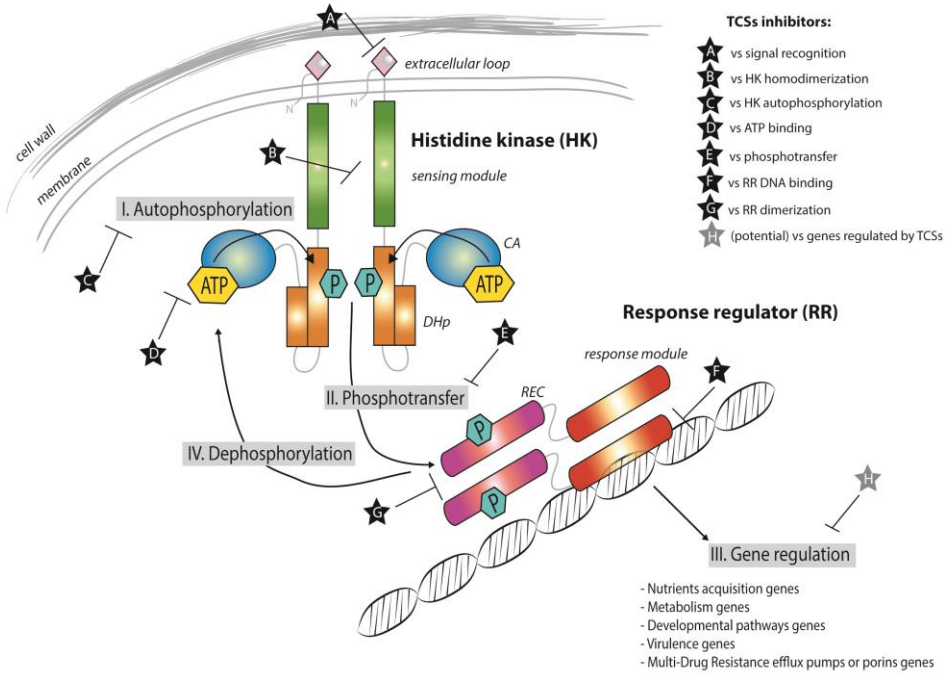


Figure 1. Two-component systems signalling and inhibition. A prototypical two-component system (TCSs) consists of a membrane-bound histidine kinase (HK) and a cognate response regulator (RR). HKs sense environmental stimuli via an extracellular sensor domain (pink) and this triggers HK autophosphorylation at conserved His residues in the dimerization and phosphotransfer (DHp) domain (orange). ATP accommodated in the ATP-binding and catalytic (CA) domain (blue) serves as a phosphodonor. Phosphoryl group is transferred from the bound ATP in the CA domain to the His residue of the DHp domain (autophosphorylation) and then from the DHp domain to Asp residue of the RR (phosphotransfer). RR phosphorylation induces changes of the expression of target genes. RR phosphorylation levels are regulated via dephosphorylation mediated by the phosphatase RR intrinsic or HK-induced phosphatase activity or by ancillary proteins. TCS inhibition can be targeted at different steps of the TCS signalling (indicated A to G) and the most promising and exploited so far is autophosphorylation inhibition.

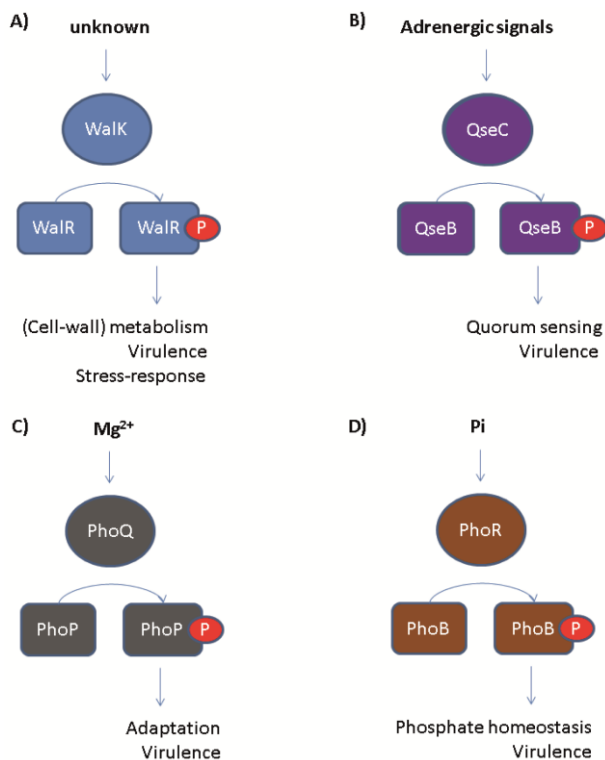


Figure 2. Promising TCS antibacterial drug targets A) WalK is highly conserved among Gram-positive bacteria, conditionally essential for bacterial growth and involved in the regulation of variety of processes including virulence³². B) QseCB is present in a number of Gram-negative bacteria and is involved in the response to host-adrenergic signals and AI-2 mediated quorum sensing. QseC inhibitors were shown to inhibit virulence of susceptible Gram-negatives *in vitro* and *in vivo*³³. C) PhoPQ is involved in response to changes in Mg²⁺ levels and in the regulation of virulence. PhoPQ inhibitors with antibacterial and antivirulence effect have been discovered following structure-based screenings for PhoQ or PhoP inhibitors^{44, 51}. D) PhoRB is involved in responses to inorganic

phosphate and is implicated to the regulation of virulence and pathogenesis of Gram-negative bacteria^{76, 86}.

The sensor HK is membrane-bound and signal recognition alters the phosphorylation state of a cognate response regulator (RR). HK sensing of specific signals occurs via a variable domain, which is commonly exposed to the extracellular milieu, whereas the remaining protein domains are generally conserved, cytoplasmic and required for signal transduction. RRs are usually transcription factors of which the DNA-binding capacity and consequently, gene transcription is determined by their phosphorylation state. TCS may directly or indirectly control numerous genes, including those involved in the regulation of metabolism, cell physiology, virulence and resistance to antibiotics or antimicrobial peptides^{27, 28, 29, 30}. TCS represent an attractive target for novel antibacterial agents as they are pervasive in microorganisms but absent in mammals. Furthermore, some TCS are essential or conditionally essential for viability in several important bacterial pathogens^{27, 31, 32}. Many TCS play

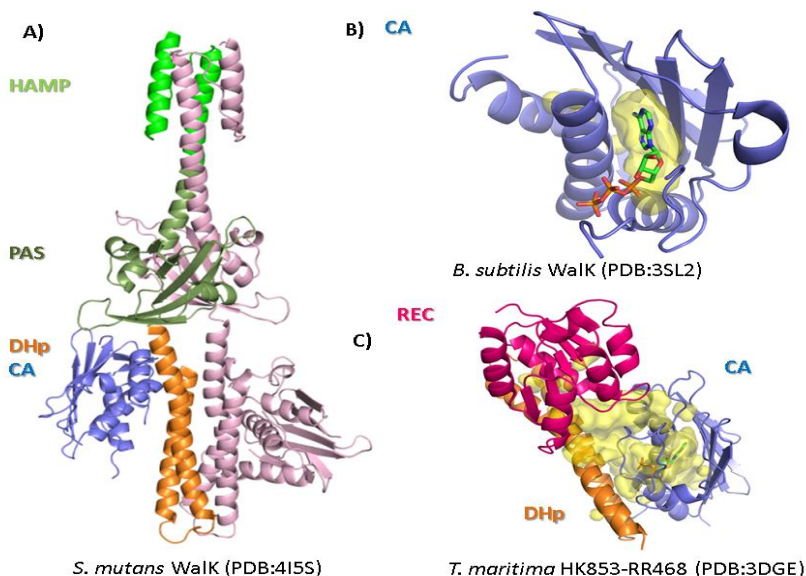


Figure 3. Structural information on TCS has facilitated the discovery of TCS inhibitors using structure-based discovery and rational structure-based design. A) Structure of *S. mutans* Walk (PDB:4I5S). *S. mutans* Walk is a long-rod dimer anchoring a HAMP signal-transducer domain (light green) and a PAS sensor domain (dark green) directly connected to the catalytic DHp (orange) and CA (blue) domains. High-resolution structures of full-length HKs will shed light on how the different domains interact with each other and how this can be used for inhibitor design B) Structure of the CA domain of *B. subtilis* Walk (PDB:3SL2). CA is the most exploited domain in structure-based TCS inhibitors discovery so far because of its well defined and generally conserved ATP-binding site (shown as yellow surface) C) Structure of the *T. maritima* HK853-RR468 (PDB:3DGE) reveals the interaction between the catalytic DHp (orange) and CA (blue) domains of the HK with the response receiver (REC) domain of the cognate RR (magenta). TCS catalytic domains, especially the CA domain, are highly conserved and suitable for the development of broad-spectrum inhibitors. Narrow -spectrum inhibitors can be designed/ discovered by targeting the interaction of a HK and its cognate RR. For this high-resolution structures of TCS complexes are needed Putative ligand binding sites were calculated with PyMol and are shown as yellow surface (detection radius and detection cut-off is 5 solvent radii). Ligands are shown as sticks.

role in bacterial adaption to environmental stresses and the regulation of virulence factor production. Thus drugs inhibiting TCS function are expected to attenuate pathogen virulence and/ or compromise pathogen growth under a range of physiological stresses^{23, 33, 34}. Moreover, HKs and RRs possess a high degree of homology in their active sites, suggesting that it might be possible to identify inhibitors targeting multiple TCS^{35, 36}. Developing resistance to a drug with multiple targets is expected to be slower than to a drug with a single target¹⁹.

TWO-COMPONENT SYSTEM SIGNALLING

Upon sensing of a ligand or physiological stimulus TCS signal transduction is initiated by autophosphorylation of a conserved histidine (His) residue in the dimerization and phosphotransfer (DHp) domain³⁷. Autophosphorylation involves the helical DHp domain hosting the conserved His and the C-terminal catalytic and ATP-binding (CA) domain that binds ATP and phosphorylates the His (Figure 1 and 3). The phosphoryl group from the phosphorylated His in the DHp domain is then transferred to an exposed Asp that belongs to the response receiver (REC) domain of the cognate RR. Phosphotransfer, i.e. phosphorylation of the RR, triggers changes in the conformation of the RR, modulating the affinity of the effector domain for its targets, typically DNA binding motifs in specific gene promoters^{38, 26}. In some cases the RR lacks the effector domain and the REC domain takes over the effector role. The phosphorylation levels of the RR are tightly regulated by the phosphatase activity of the HK; the RR itself or a partner protein^{26, 39, 40, 41}. The DHp, CA, and REC domains are always present in all TCS and relatively well conserved in amino-acid sequence (Figure 4), compared to the sensor domains of HKs (the periplasmic domain, HAMP, PAS and GAF domains) or the effector domains of RRs. The presence or absence and the variability of the sensor and effector domains is determined by the wide range of specific signals or targets to be recognized by the different TCS^{38, 26}. Therefore, inhibitors of the catalytic activity of the highly conserved DHp, CA and REC domain are expected to possess broad-spectrum antibacterial activity.

DISCOVERY OF TWO-COMPONENT SYSTEM INHIBITORS

There are several publications describing the discovery of TCS inhibitors which have been reviewed elsewhere^{34, 36, 42} and some aspects are discussed in more detail in the following sections. The target TCS include among others, *S. pneumoniae* and *S. epidermidis* WalKR^{43, 43}, *E. coli* QseCB⁴³, *S. flexnerii* and *S. enterica* PhoQP^{44, 45, 45}. The identified TCS inhibitors were from libraries of natural products⁴⁶, small molecules³⁴ and antibacterial peptides⁴⁷ (Figure 5). Different approaches have been employed to discover TCS inhibitors, including high-throughput target-based screening^{48, 33, 49} and virtual structure-based screening^{43, 50, 51, 44, 35}.

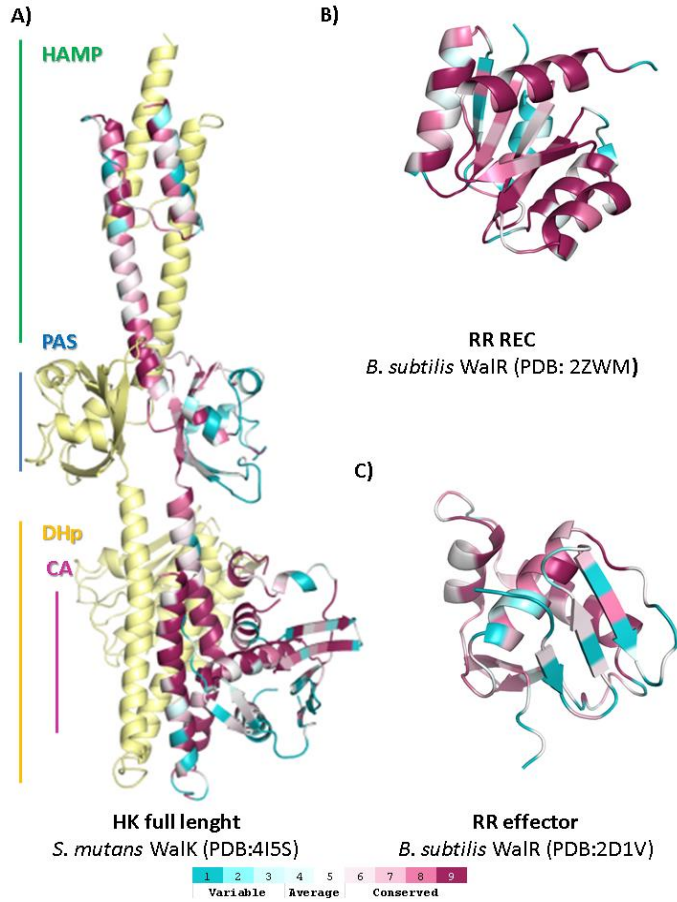


Figure 4. Conservation of the different domains of TCS A) *S. mutans* WalK (PDB:4I5S) the catalytic domains (DHp and CA) are relatively more conserved than the sensor domains (HAMP and PAS). Furthermore DHp and CA domains are always present in all HK, whereas the sensor domains vary. B) REC domain of *B. subtilis* WalR is relatively more conserved than C) the DNA-binding effector domain of *B. subtilis* WalR. The variability of the HK sensor domains and the RR effector domains are determined by the variety of input signals and adaptation responses TCS are involved in. Targeting the relatively more conserved DHp, CA and REC domain might facilitate the development of broad-spectrum antibacterials with low potential of resistance development.

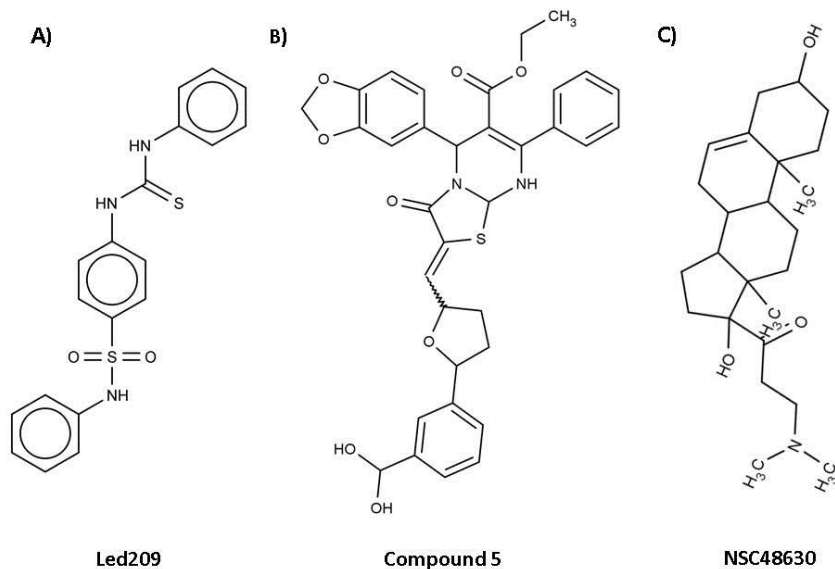


Figure 4 Published two-component systems inhibitors can be used as starting point for the design of more potent inhibitors following structure-based drug design approaches A) Led209 inhibits the binding of adrenergic signals to the periplasmic domain of *E. coli* QseC, preventing its autophosphorylation and consequently inhibiting QseC-mediated activation of virulence gene expression ³³. B) Compound 5 was identified in a structure-based screening for ligands of the CA domain of *S. epidermidis* WalK ⁴³. Compound 5 inhibited *S. epidermidis* WalK autophosphorylation with $IC_{50} = 14 \mu\text{M}$ and showed antibacterial effect against Gram-positive bacteria with minimal inhibitory concentrations (MICs) in the range of 2 – 6 μM . C) NSC48630 inhibited the formation of *S. enterica* PhoP-DNA complex with $IC_{50} = 3.6 \mu\text{M}$. NSC4836 was identified as putative PhoP ligand in a structure-based screening for ligands of the activated response regulator PhoP (PDB: 2PL1) ⁵¹. Compound 5 and NSC48630 and other TCS inhibitors identified by structure-based virtual screenings indicate the potential of structure-based approaches to discover promising TCS inhibitors with antibacterial and therapeutic effect ^{43, 50, 44, 51, 35}.

PROMISING TWO-COMPONENT SYSTEM TARGETS

WalKR

WalKR (aka YycF/G, MicA/B, VicK/R) is highly conserved and has been identified in the genomes of the major group of Gram-positive bacteria with a low genomic GC-content (Figure 2A)^{52, 53, 54, 55, 32, 30}. This includes pathogenic species belonging to the genus *Staphylococcus*, *Streptococcus*, *Enterococcus*, *Clostridium*, and *Listeria*. In the important pathogens *S. aureus*, *S. pneumoniae*, and *Enterococcus faecalis* WalKR has been shown to be essential for viability in rich laboratory growth medium^{52, 30, 56}. WalKR regulates genes responsible for cell wall metabolism and cell wall homeostasis^{55, 57, 53} but the specific genes and pathways regulated by WalKR may differ from species to species. Additionally, *walKR* regulates genes involved in metabolism, stress response, virulence, host-microbe interactions, transport and regulatory pathways depending on the species^{27, 58}.

Of all the TCS WalKR is considered one of the most attractive targets for antibacterial drugs due to its essentiality, links to virulence and antibiotic resistance. Imidazole and zerumbone derivatives were the first inhibitors of WalK to be identified^{59, 46}. Following this pioneering discovery, Utsumi's group developed biochemical and genetic high-throughput screening methods to search for WalK and WalR inhibitors. This led to the discovery of WalK inhibitors such as aranorosinol, walkmycin B, waldiomycin, signermycin B and the WalR inhibitors, walrycin A and B^{48, 49}. Later, some of these inhibitors were not proven to be selective to WalKR and other mechanisms such as membrane damage and adverse effects on macromolecules biosynthesis most likely account for the observed antibacterial effects.

Elucidation of the structure of HK catalytic domains opened up the possibility for structure-based virtual screening (SBVS) for WalK inhibitors^{60, 61, 43, 43}. The catalytic ATP-binding domain (CA domain) appeared to be the most promising target for this approach as this domain contains a well-defined and partially conserved pocket where ATP is accommodated (Figure 3B). Before the elucidation of WalK structure (PDB: 3SL2 and PDB:4I5S), homology models of the CA domains of *S. pneumoniae* and *S. epidermidis* WalK based on the three-dimensional structures of *Thermotoga maritima* HK853 (PDB: 2C2A) and *E. coli* EnvZ (PDB: 1BXD) HKs were used for SBVS of drug-lead compound libraries. These screenings yielded WalK autophosphorylation inhibitors belonging to different classes of chemical structures, such as imidazole analogues and derivatives of furan, thiophene, thiazolidinone, benzamide and pyrimidinone (Figure 4). The SBVS hits inhibited the growth of *S. pneumoniae* and *S. epidermidis* and showed bactericidal effects towards both planktonic and biofilm cells^{62, 63}. Furthermore, some of these inhibitors decreased the mortality of mice infected with *S. pneumoniae* in an *in vivo* sepsis model, demonstrating that SBVS is a valuable tool for the identification of WalK inhibitors with therapeutic effect⁴³. Nevertheless,

the design of potent ATP-competitive inhibitors specific for WalK is challenging, even more so when structural homology models are used instead of experimental (e.g. X-ray) data. This issue is crucial when attempting to generate a WalK inhibitor with higher specificity and affinity in the hit-to-lead optimization phase. Although the overall fold of the CA domain as well as the catalytic residues is generally conserved, there are large variations in size and sequence in the ATP-lid, a HK distinctive flexible loop that covers the ATP-binding pocket and is crucially involved in ATP binding and in HK catalytic reactions^{26, 64, 65}. The recently published WalK structures of the entire intracellular portion from *Streptococcus mutans* (PDB: 4I5S) (Figure 3A) and the CA domain from *Bacillus subtilis* (PDB: 3SL2, Figure 3B) might provide the key to design of improved WalK inhibitors^{66, 67}. These structures have not only revealed specific characteristics of the WalK CA domain but also insights into the molecular mechanism of WalK autokinase activation and clues how it can be effectively inhibited by exploring HK domains for structure-based drug design²⁵.

QseCB

Targeting microbial virulence without inhibiting growth has been proposed as promising strategy in antibacterial drug discovery as it was proposed that antivirulence drugs present less selective pressure for resistance development^{33, 24, 51}. QseCB is a TCS involved in recognizing the host-derived adrenergic signals and the bacterial aromatic signal autoinducer-3 AI-3 (epinephrine, norepinephrine) to trigger expression of virulence genes (Figure 2B)⁶⁸. Homologues of QseC are present in at least 25 important human and plant pathogens, therefore, a QseC inhibitor is expected to be a promising drug for antivirulence therapy against a wide range of pathogenic bacteria³³.

Adrenergic signals, as well as, AI-3 are recognized by QseC periplasmic domain⁶⁸. Drugs targeting QseC periplasmic domain have an advantage compared to drugs with intracellular targets of Gram-negative bacteria as they only need to pass the outer membrane to reach the target.

High-throughput screening to search for a compound that inhibits the activation of QseC by AI-3 has been reported³³. LED209 (Figure 4) was identified as inhibitor of the binding of the signaling molecules to QseC from different Gram-negative pathogenic bacteria. LED209 inhibited QseC autophosphorylation, bacterial pathogenicity *in vitro* and *in vivo*, but did not inhibit cell growth. The discovery of LED209 demonstrates that targeting microbial virulence without inhibiting growth is a promising strategy to identify antibacterials with therapeutic effect³³.

PhoPQ

The PhoQ/PhoP two-component regulatory system is a major regulator of virulence in the enteric pathogen *Salmonella enterica* serovar Typhimurium^{69,70} and is present in a range of Gram-negative bacteria. It also controls the adaptation to low Mg^{2+} environments by governing the expression and/or activity of Mg^{2+} transporters and of enzymes modifying the Mg^{2+} -binding sites on the bacterial cell surface (Figure 2C). The RR PhoP modifies expression of about 3% of the *Salmonella* genes in response to the periplasmic Mg^{2+} concentration detected by the HK PhoQ⁷¹. Genes that are directly controlled by PhoP often differ in their promoter structures, resulting in distinct expression levels and kinetics in response to the low Mg^{2+} inducing signal. PhoP regulates a large number of genes indirectly via other transcription factors and TCS that form a panoply of regulatory networks. These regulatory networks include transcriptional cascades, feed-forward loops and the use of connector proteins to modify the activity of RRs⁷². These networks confer distinct expression properties that may be important contributors to the lifestyle of *Salmonella*.

The structure of the catalytic domain of PhoQ has been well studied⁷³. PhoQ has also been co-crystallized with the inhibitor radicicol⁴⁵. The available structural information has been exploited in structure-based screening for PhoQ inhibitors that attenuate the virulence of *S. flexneri* *in vitro* and *in vivo*⁴⁴. PhoP inhibitors have also been discovered via structure-based screenings and shown to inhibit PhoP-DNA complex formation (Figure 4)⁵¹. Taken together these findings highlight good potential to develop novel antibacterials against PhoPQ using structure-based screening and design.

PhoRB

PhoRB is a two-component system sensing the extracellular concentration of phosphate (Figure 2D)⁷⁴. It consists of the HK PhoR and its cognate RR PhoB. PhoRB responds to phosphate limitation, when the extracellular concentration of phosphate falls below 4 μ M. In phosphate-limiting conditions, PhoR phosphorylates PhoB, which then binds to specific DNA sequences, known as Pho boxes. PhoB binding either induces or represses the genes belonging to the Pho (phosphate) regulon, which includes genes involved in acquisition and metabolism of different phosphates.

The Pho regulon in *E. coli* K12 comprises of 31 genes, and it is not only involved in phosphate homeostasis, but it is also related to bacterial virulence as the induction of Pho regulon results in attenuated pathogenesis^{75,76}. Examples of virulence attributes altered by induction of the Pho regulon are a significant reduction in the amount of capsular antigen at the cell surface, resistance to the bactericidal effect of serum, to cationic antimicrobial peptides, and to acid and oxidative stress, as well as the production of type 1 fimbriae^{75,76}. Therefore, PhoRB presents a promising target for antibacterials that inhibit bacterial virulence.

ANTIMICROBIAL PEPTIDES INHIBITING TCS SIGNALING

Antimicrobial peptides (AMPs) have been proposed as promising strategy to address the growing problem of MDR^{77, 78}. Eukaryotic cationic AMPs are produced at sites of infection or inflammation in many different organisms^{79, 80}. Typically they are peptides of 12 to 45 amino acids with a net positive charge and a high proportion of hydrophobic amino acids⁸¹. Bovine lactoferricin (LfcinB; Figure 6) is a typical cationic antibacterial peptide generated by proteolytic cleavage of lactoferrin that has a broad-spectrum antibacterial activity^{82, 83, 84, 82}.

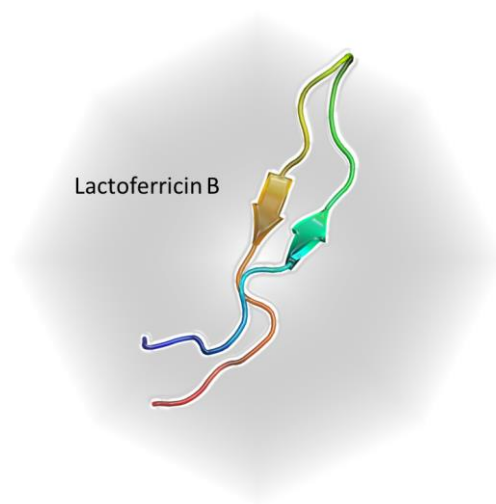


Figure 5. LactoferricinB is an antimicrobial peptide identified as a TCS inhibitor. LactoferricinB was shown to inhibit the phosphorylation activity of *E. coli* BasR-BasS and the ability of CreC to recognize CreB⁴⁷.

It has been shown that LfcinB derived peptides (LfcinB₁₇₋₄₁, LfcinB₁₇₋₃₁ and D-LfcinB₁₇₋₃₁) enter the cytoplasm of *E. coli* and *S. aureus*⁸⁵. In a recent study aimed at elucidation of the intracellular targets of LfcinB, the TCS BasSR and CreCB were among the 16 proteins shown to specifically interact with LfcinB⁴⁷. This discovery suggested that LfcinB-derived peptides were a promising starting point for the development of AMP-based TCS inhibitors.

THESIS OUTLINE AND AIMS

The main aims of the current thesis were:

1. To discover hits that can be further developed to broad-spectrum TCS inhibitors following a multidisciplinary approach.
2. To provide structural-knowledge on TCS inhibition to facilitate the optimization of the identified TCS inhibitors using structure-based drug design.
3. To evaluate the identified hits for their biochemical, antibacterial and cytotoxic effects *in vitro*
4. To explore ways to improve hit compound permeability of the Gram-negative bacteria outer membrane using nanoparticles and AMPs

In **Chapter 2**, we describe the discovery of histidine kinase (HK) autophosphorylation inhibitors targeted at the ATP-binding and catalytic (CA) domain of multiple HKs using combined structure-based and ligand-based virtual screening approaches.

In **Chapter 3**, we describe the application of fragment-based screenings by differential scanning fluorimetry and ligand-based similarity searches to discover fragment-like HK autophosphorylation inhibitors targeted at the CA domain of multiple HKs.

Due to the weak or absent antibacterial effect of identified HK inhibitors (Chapter 2 and 3) against Gram-negative bacteria, nanoparticles were investigated as potential drug delivery vehicles. Silica-based mesoporous nanoparticles capped with ϵ -poly-L-lysine were loaded with HK autophosphorylation inhibitors and their antibacterial effect, cytotoxicity and immunotoxicity were studied and described in **Chapter 4**.

In **Chapter 5** we used computer-aided approaches in an attempt to discover improved HK inhibitors.

As lactoferricinB-derived peptides seemed to present a promising starting point for the development of antimicrobial-peptides-based TCS inhibitors, in **Chapter 6** we investigated the possibility to use *T. maritima* HK853-RR468 and *E. coli* PhoRB for structural studies of TCS inhibition by LactoferricinB – derived peptides.

In **Chapter 7** the (co-)crystallization and preliminary X-ray diffraction analysis of the *T. maritima* CheA-inhibitors co-crystals and CopM periplasmic domain are described.

In **Chapter 8** the potential of targeting WalK for developing antibacterial drugs with low potential of resistance development is discussed in the light of current literature and results.

Chapter 9 is a concluding discussion on the results described in the thesis and their implications for antibacterial drug discovery and development.

REFERENCES

1. Magiorakos, A., Multidrug-resistant, extensively drug-resistant and pandrug-resistant bacteria: an international expert proposal for interim standard definitions for acquired resistance. *Clin Microbiol Infect* 2012, 18, 268-281.
2. Bassetti, M.; Merelli, M.; Temperoni, C.; Astilean, A., New antibiotics for bad bugs: where are we? *Annals of clinical microbiology and antimicrobials* 2013, 12, 22.
3. Boucher, H. W., Bad Bugs, No Drugs: No ESCAPE! An Update from the Infectious Diseases Society of America. *Clin Infect Dis* 2009, 48, 1-12.
4. Peterson, L. R., Bad bugs, no drugs: no ESCAPE revisited. *Clinical infectious diseases : an official publication of the Infectious Diseases Society of America* 2009, 49 (6), 992-3.
5. Cosgrove, S. E.; Carmeli, Y., The impact of antimicrobial resistance on health and economic outcomes. *Clinical infectious diseases : an official publication of the Infectious Diseases Society of America* 2003, 36 (11), 1433-7.
6. Brotz-Oesterhelt, H.; Sass, P., Postgenomic strategies in antibacterial drug discovery. *Future microbiology* 2010, 5 (10), 1553-79.
7. Butler, M. S.; Blaskovich, M. A.; Cooper, M. A., Antibiotics in the clinical pipeline in 2013. *The Journal of antibiotics* 2013, 66 (10), 571-91.
8. Dougherty, T. J.; Miller, P. F., Microbial genomics and drug discovery: exploring innovative routes of drug discovery in the postgenomic era. *IDrugs : the investigational drugs journal* 2006, 9 (6), 420-2.
9. Aminov, R. I., A brief history of the antibiotic era: lessons learned and challenges for the future. *Frontiers in microbiology* 2010, 1, 134.
10. Fernandes, P., Antibacterial discovery and development--the failure of success? *Nature biotechnology* 2006, 24 (12), 1497-503.
11. Singh, S. B.; Barrett, J. F., Empirical antibacterial drug discovery--foundation in natural products. *Biochemical pharmacology* 2006, 71 (7), 1006-15.
12. Talbot, G. H.; Bradley, J.; Edwards, J. E., Jr.; Gilbert, D.; Scheld, M.; Bartlett, J. G.; Antimicrobial Availability Task Force of the Infectious Diseases Society of A., Bad bugs need drugs: an update on the development pipeline from the Antimicrobial Availability Task Force of the Infectious Diseases Society of America. *Clinical infectious diseases : an official publication of the Infectious Diseases Society of America* 2006, 42 (5), 657-68.
13. Alksne, L. E.; Dunman, P. M., Target-based antimicrobial drug discovery. *Methods in molecular biology* 2008, 431, 271-83.
14. Pucci, M. J., Overview of antibacterial target selection. *Current protocols in pharmacology / editorial board, S.J. Enna* 2006, Chapter 13, Unit13A 2.
15. Waszkowycz, B., Structure-based approaches to drug design and virtual screening. *Current opinion in drug discovery & development* 2002, 5 (3), 407-13.
16. Muegge, I., Synergies of virtual screening approaches. *Mini reviews in medicinal chemistry* 2008, 8 (9), 927-33.
17. Wildman, S. A., Approaches to virtual screening and screening library selection. *Current pharmaceutical design* 2013, 19 (26), 4787-96.
18. Simmons, K. J.; Chopra, I.; Fishwick, C. W., Structure-based discovery of antibacterial drugs. *Nature reviews. Microbiology* 2010, 8 (7), 501-10.
19. Ferreira, R. S.; Andricopulo, A. D., Structure-based drug design to overcome drug resistance: Challenges and opportunities. *Current pharmaceutical design* 2014, 20 (5), 687-693.
20. Rule of three. *Nature biotechnology* 2000, 18 (10), 1025.

21. Jhoti, H.; Williams, G.; Rees, D. C.; Murray, C. W., The 'rule of three' for fragment-based drug discovery: where are we now? *Nature reviews. Drug discovery* 2013, 12 (8), 644-5.
22. Baker, M., Fragment-based lead discovery grows up. *Nature reviews. Drug discovery* 2013, 12 (1), 5-7.
23. Froscio, M.; Barrett, J. F., Bacterial two-component systems as antimicrobial drug discovery targets. *Drug News and Perspectives* 1999, 12 (5), 293-299.
24. Gotoh, Y.; Eguchi, Y.; Watanabe, T.; Okamoto, S.; Doi, A.; Utsumi, R., Two-component signal transduction as potential drug targets in pathogenic bacteria. *Current opinion in microbiology* 2010, 13 (2), 232-9.
25. Velikova, N.; Bem, A. E.; van Baarlen, P.; Wells, J. M.; Marina, A., Walk, the Path towards New Antibacterials with Low Potential for Resistance Development. *ACS Medicinal Chemistry Letters* 2013, 4 (10), 891-894.
26. Casino, P.; Rubio, V.; Marina, A., The mechanism of signal transduction by two-component systems. *Current opinion in structural biology* 2010, 20 (6), 763-71.
27. Dubrac, S.; Msadek, T., Identification of Genes Controlled by the Essential YycG/YycF Two-Component System of *Staphylococcus aureus*. *Journal of bacteriology* 2004, 186 (4), 1175-1181.
28. Dubrac, S.; Msadek, T., Tearing down the wall: peptidoglycan metabolism and the Walk/WalR (YycG/YycF) essential two-component system. *Advances in experimental medicine and biology* 2008, 631, 214-28.
29. Paterson, G. K.; Blue, C. E.; Mitchell, T. J., Role of two-component systems in the virulence of *Streptococcus pneumoniae*. *Journal of medical microbiology* 2006, 55 (Pt 4), 355-63.
30. Mohedano, M. L.; Overweg, K.; de la Fuente, A.; Reuter, M.; Altabe, S.; Mulholland, F.; de Mendoza, D.; Lopez, P.; Wells, J. M., Evidence that the essential response regulator YycF in *Streptococcus pneumoniae* modulates expression of fatty acid biosynthesis genes and alters membrane composition. *Journal of bacteriology* 2005, 187 (7), 2357-67.
31. Fukuchi, K.; Kasahara, Y.; Asai, K.; Kobayashi, K.; Moriya, S.; Ogasawara, N., The essential two-component regulatory system encoded by *yycF* and *yycG* modulates expression of the *ftsAZ* operon in *Bacillus subtilis*. *Microbiology* 2000, 146 (Pt 7), 1573-83.
32. Winkler, M. E.; Hoch, J. A., Essentiality, bypass, and targeting of the YycFG (VicRK) two-component regulatory system in gram-positive bacteria. *Journal of bacteriology* 2008, 190 (8), 2645-8.
33. Rasko, D. A.; Moreira, C. G.; Li de, R.; Reading, N. C.; Ritchie, J. M.; Waldor, M. K.; Williams, N.; Taussig, R.; Wei, S.; Roth, M.; Hughes, D. T.; Huntley, J. F.; Fina, M. W.; Falck, J. R.; Sperandio, V., Targeting QseC signaling and virulence for antibiotic development. *Science* 2008, 321 (5892), 1078-80.
34. Worthington, R. J.; Blackledge, M. S.; Melander, C., Small-molecule inhibition of bacterial two-component systems to combat antibiotic resistance and virulence. *Future medicinal chemistry* 2013, 5 (11), 1265-84.
35. Francis, S.; Wilke, K. E.; Brown, D. E.; Carlson, E. E., Mechanistic insight into inhibition of two-component system signaling. *MedChemComm* 2013, 4 (1), 269-277.
36. Hilliard, J. J.; Goldschmidt, R. M.; Licata, L.; Baum, E. Z.; Bush, K., Multiple mechanisms of action for inhibitors of histidine protein kinases from bacterial two-component systems. *Antimicrobial agents and chemotherapy* 1999, 43 (7), 1693-9.
37. Mascher, T.; Helmann, J. D.; Unden, G., Stimulus perception in bacterial signal-transducing histidine kinases. *Microbiology and molecular biology reviews : MMBR* 2006, 70 (4), 910-38.

38. Gao, R.; Stock, A. M., Biological insights from structures of two-component proteins. *Annual review of microbiology* 2009, 63, 133-54.
39. Kenney, L. J., How important is the phosphatase activity of sensor kinases? *Current opinion in microbiology* 2010, 13 (2), 168-76.
40. Zhu, Y.; Qin, L.; Yoshida, T.; Inouye, M., Phosphatase activity of histidine kinase EnvZ without kinase catalytic domain. *Proceedings of the National Academy of Sciences of the United States of America* 2000, 97 (14), 7808-13.
41. Gutu, A. D.; Wayne, K. J.; Sham, L. T.; Winkler, M. E., Kinetic characterization of the WalRKSpn (VicRK) two-component system of *Streptococcus pneumoniae*: dependence of WalkSpn (VicK) phosphatase activity on its PAS domain. *Journal of bacteriology* 2010, 192 (9), 2346-58.
42. Kurosu, M.; Begari, E., Bacterial protein kinase inhibitors. *Drug Development Research* 2010, 71 (3), 168-187.
43. Qin, Z.; Zhang, J.; Xu, B.; Chen, L.; Wu, Y.; Yang, X.; Shen, X.; Molin, S.; Danchin, A.; Jiang, H.; Qu, D., Structure-based discovery of inhibitors of the YycG histidine kinase: new chemical leads to combat *Staphylococcus epidermidis* infections. *BMC microbiology* 2006, 6, 96.
44. Cai, X.; Zhang, J.; Chen, M.; Wu, Y.; Wang, X.; Chen, J.; Zhang, J.; Shen, X.; Qu, D.; Jiang, H., The effect of the potential PhoQ histidine kinase inhibitors on *Shigella flexneri* virulence. *PloS one* 2011, 6 (8), e23100.
45. Guarnieri, M. T.; Zhang, L.; Shen, J.; Zhao, R., The Hsp90 inhibitor radicicol interacts with the ATP-binding pocket of bacterial sensor kinase PhoQ. *Journal of molecular biology* 2008, 379 (1), 82-93.
46. Watanabe, T.; Okada, A.; Gotoh, Y.; Utsumi, R., Inhibitors targeting two-component signal transduction. *Advances in experimental medicine and biology* 2008, 631, 229-36.
47. Ho, Y. H.; Sung, T. C.; Chen, C. S., Lactoferricin B inhibits the phosphorylation of the two-component system response regulators BasR and CreB. *Molecular & cellular proteomics : MCP* 2012, 11 (4), M111 014720.
48. Okada, A.; Igarashi, M.; Okajima, T.; Kinoshita, N.; Umekita, M.; Sawa, R.; Inoue, K.; Watanabe, T.; Doi, A.; Martin, A.; Quinn, J.; Nishimura, Y.; Utsumi, R., Walkmycin B targets Walk (YycG), a histidine kinase essential for bacterial cell growth. *The Journal of antibiotics* 2010, 63 (2), 89-94.
49. Gotoh, Y.; Doi, A.; Furuta, E.; Dubrac, S.; Ishizaki, Y.; Okada, M.; Igarashi, M.; Misawa, N.; Yoshikawa, H.; Okajima, T.; Msadek, T.; Utsumi, R., Novel antibacterial compounds specifically targeting the essential WalR response regulator. *The Journal of antibiotics* 2010, 63 (3), 127-34.
50. Li, N.; Wang, F.; Niu, S.; Cao, J.; Wu, K.; Li, Y.; Yin, N.; Zhang, X.; Zhu, W.; Yin, Y., Discovery of novel inhibitors of *Streptococcus pneumoniae* based on the virtual screening with the homology-modeled structure of histidine kinase (VicK). *BMC microbiology* 2009, 9, 129.
51. Tang, Y. T.; Gao, R.; Havranek, J. J.; Groisman, E. A.; Stock, A. M.; Marshall, G. R., Inhibition of bacterial virulence: drug-like molecules targeting the *Salmonella enterica* PhoP response regulator. *Chemical biology & drug design* 2012, 79 (6), 1007-17.
52. Dubrac, S.; Boneca, I. G.; Poupel, O.; Msadek, T., New insights into the Walk/WalR (YycG/YycF) essential signal transduction pathway reveal a major role in controlling cell wall metabolism and biofilm formation in *Staphylococcus aureus*. *Journal of bacteriology* 2007, 189 (22), 8257-69.
53. Delaune, A.; Dubrac, S.; Blanchet, C.; Poupel, O.; Mader, U.; Hiron, A.; Leduc, A.; Fitting, C.; Nicolas, P.; Cavillon, J. M.; Adib-Conquy, M.; Msadek, T., The WalkR system

controls major staphylococcal virulence genes and is involved in triggering the host inflammatory response. *Infection and immunity* 2012, 80 (10), 3438-53.

54. Delaune, A., Poupel O., Mallet A., Coic YM., Msadek T., Dubrac S., Peptidoglycan Crosslinking Relaxation Plays an Important Role in Staphylococcus aureus WalkR Dependent Cell Viability. *PloS one* 2010, 6 (2).

55. Howell, A.; Dubrac, S.; Andersen, K. K.; Noone, D.; Fert, J.; Msadek, T.; Devine, K., Genes controlled by the essential YycG/YycF two-component system of *Bacillus subtilis* revealed through a novel hybrid regulator approach. *Molecular microbiology* 2003, 49 (6), 1639-1655.

56. JA, F. C. a. H., Two-Component Signal Transduction System Essential for Growth of *Bacillus subtilis*: Implications for Anti-Infective Therapy. *Journal of bacteriology* 1998, 180 (23), 6375-6383.

57. Howden, B. P.; McEvoy, C. R.; Allen, D. L.; Chua, K.; Gao, W.; Harrison, P. F.; Bell, J.; Coombs, G.; Bennett-Wood, V.; Porter, J. L.; Robins-Browne, R.; Davies, J. K.; Seemann, T.; Stinear, T. P., Evolution of multidrug resistance during *Staphylococcus aureus* infection involves mutation of the essential two component regulator WalkR. *PLoS pathogens* 2011, 7 (11), e1002359.

58. Luz Mohedano, M., Evidence that the Essential Response Regulator YycF in *Streptococcus pneumoniae* Modulates Expression of Fatty Acid Biosynthesis Genes and Alters Membrane Composition. *Journal of Bacteriology* 2005, 187 (7), 2357-2367.

59. Okada, A.; Gotoh, Y.; Watanabe, T.; Furuta, E.; Yamamoto, K.; Utsumi, R., Targeting two-component signal transduction: a novel drug discovery system. *Methods in enzymology* 2007, 422, 386-95.

60. Marina, A.; Waldburger, C. D.; Hendrickson, W. A., Structure of the entire cytoplasmic portion of a sensor histidine-kinase protein. *The EMBO journal* 2005, 24 (24), 4247-59.

61. Tanaka, T.; Saha, S. K.; Tomomori, C.; Ishima, R.; Liu, D.; Tong, K. I.; Park, H.; Dutta, R.; Qin, L.; Swindells, M. B.; Yamazaki, T.; Ono, A. M.; Kainosho, M.; Inouye, M.; Ikura, M., NMR structure of the histidine kinase domain of the *E. coli* osmosensor EnvZ. *Nature* 1998, 396 (6706), 88-92.

62. Huang, R. Z.; Zheng, L. K.; Liu, H. Y.; Pan, B.; Hu, J.; Zhu, T.; Wang, W.; Jiang, D. B.; Wu, Y.; Wu, Y. C.; Han, S. Q.; Qu, D., Thiazolidione derivatives targeting the histidine kinase YycG are effective against both planktonic and biofilm-associated *Staphylococcus epidermidis*. *Acta pharmacologica Sinica* 2012, 33 (3), 418-25.

63. Liu, H.; Zhao, D.; Chang, J.; Yan, L.; Zhao, F.; Wu, Y.; Xu, T.; Gong, T.; Chen, L.; He, N.; Wu, Y.; Han, S.; Qu, D., Efficacy of novel antibacterial compounds targeting histidine kinase YycG protein. *Applied microbiology and biotechnology* 2014, 98 (13), 6003-13.

64. Podgornaia, A. I.; Casino, P.; Marina, A.; Laub, M. T., Structural basis of a rationally rewired protein-protein interface critical to bacterial signaling. *Structure* 2013, 21 (9), 1636-47.

65. Casino, P., Miquel-Romero, L., Marina, A., Visualizing autophosphorylation in histidine kinases. *Nat Commun* 2014.

66. Wang, C.; Sang, J.; Wang, J.; Su, M.; Downey, J. S.; Wu, Q.; Wang, S.; Cai, Y.; Xu, X.; Wu, J.; Senadheera, D. B.; Cvitkovitch, D. G.; Chen, L.; Goodman, S. D.; Han, A., Mechanistic insights revealed by the crystal structure of a histidine kinase with signal transducer and sensor domains. *PLoS biology* 2013, 11 (2), e1001493.

67. Celikel, R.; Veldore, V. H.; Mathews, I.; Devine, K. M.; Varughese, K. I., ATP forms a stable complex with the essential histidine kinase Walk (YycG) domain. *Acta crystallographica. Section D, Biological crystallography* 2012, 68 (Pt 7), 839-45.

68. Clarke, M. B.; Hughes, D. T.; Zhu, C.; Boedeker, E. C.; Sperandio, V., The QseC sensor kinase: a bacterial adrenergic receptor. *Proceedings of the National Academy of Sciences of the United States of America* 2006, 103 (27), 10420-5.
69. Groisman, E. A., The pleiotropic two-component regulatory system PhoP-PhoQ. *Journal of bacteriology* 2001, 183 (6), 1835-42.
70. Miller, S. I.; Kukral, A. M.; Mekalanos, J. J., A two-component regulatory system (phoP phoQ) controls *Salmonella typhimurium* virulence. *Proceedings of the National Academy of Sciences of the United States of America* 1989, 86 (13), 5054-8.
71. Lejona, S.; Aguirre, A.; Cabeza, M. L.; Garcia Vescovi, E.; Soncini, F. C., Molecular characterization of the Mg²⁺-responsive PhoP-PhoQ regulon in *Salmonella enterica*. *Journal of bacteriology* 2003, 185 (21), 6287-94.
72. Park, S. Y.; Groisman, E. A., Signal-specific temporal response by the *Salmonella* PhoP/PhoQ regulatory system. *Molecular microbiology* 2014, 91 (1), 135-44.
73. Marina, A.; Mott, C.; Auyzenberg, A.; Hendrickson, W. A.; Waldburger, C. D., Structural and mutational analysis of the PhoQ histidine kinase catalytic domain. Insight into the reaction mechanism. *The Journal of biological chemistry* 2001, 276 (44), 41182-90.
74. Yamada, M.; Makino, K.; Amemura, M.; Shinagawa, H.; Nakata, A., Regulation of the phosphate regulon of *Escherichia coli*: analysis of mutant phoB and phoR genes causing different phenotypes. *Journal of bacteriology* 1989, 171 (10), 5601-6.
75. Chekabab, S. M.; Jubelin, G.; Dozois, C. M.; Harel, J., PhoB activates *Escherichia coli* O157:H7 virulence factors in response to inorganic phosphate limitation. *PLoS one* 2014, 9 (4), e94285.
76. Crepin, S.; Chekabab, S. M.; Le Bihan, G.; Bertrand, N.; Dozois, C. M.; Harel, J., The Pho regulon and the pathogenesis of *Escherichia coli*. *Veterinary microbiology* 2011, 153 (1-2), 82-8.
77. Steckbeck, J. D.; Deslouches, B.; Montelaro, R. C., Antimicrobial peptides: new drugs for bad bugs? *Expert opinion on biological therapy* 2014, 14 (1), 11-4.
78. Hassan, M.; Kjos, M.; Nes, I. F.; Diep, D. B.; Lotfipour, F., Natural antimicrobial peptides from bacteria: characteristics and potential applications to fight against antibiotic resistance. *Journal of applied microbiology* 2012, 113 (4), 723-36.
79. Palffy, R.; Gardlik, R.; Behuliak, M.; Kadasi, L.; Turna, J.; Celec, P., On the physiology and pathophysiology of antimicrobial peptides. *Molecular medicine* 2009, 15 (1-2), 51-9.
80. Pasupuleti, M.; Schmidtchen, A.; Malmsten, M., Antimicrobial peptides: key components of the innate immune system. *Critical Reviews in Biotechnology* 2012, 32 (2), 143-171.
81. Hancock, R. E. W., Peptide antibiotics. *Lancet* 1997, 349 (9049), 418-422.
82. Bellamy, W.; Takase, M.; Wakabayashi, H.; Kawase, K.; Tomita, M., Antibacterial spectrum of lactoferricin B, a potent bactericidal peptide derived from the N-terminal region of bovine lactoferrin. *The Journal of applied bacteriology* 1992, 73 (6), 472-9.
83. Strom, M. B.; Haug, B. E.; Rekdal, O.; Skar, M. L.; Stensen, W.; Svendsen, J. S., Important structural features of 15-residue lactoferricin derivatives and methods for improvement of antimicrobial activity. *Biochemistry and cell biology = Biochimie et biologie cellulaire* 2002, 80 (1), 65-74.
84. (a) Del Olmo, A.; Morales, P.; Nuñez, M., Bactericidal effect of lactoferrin and its amidated and pepsin-digested derivatives on *Pseudomonas fluorescens*: Influence of environmental and physiological factors. *Journal of food protection* 2008, 71 (12), 2468-2474; (b) Roseanu, A.; Florian, P.; Condei, M.; Cristea, D.; Damian, M., Antibacterial activity of lactoferrin and lactoferricin against oral streptococci. *Romanian Biotechnological Letters* 2010, 15 (6), 5788-5792.

85. Haukland, H. H.; Ulvatne, H.; Sandvik, K.; Vorland, L. H., The antimicrobial peptides lactoferricin B and magainin 2 cross over the bacterial cytoplasmic membrane and reside in the cytoplasm. *FEBS letters* 2001, 508 (3), 389-93.
86. Scholten, M.; Janssen, R.; Bogaarts, C.; van Strien, J.; Tommassen, J., The *pho* regulon of *Shigella flexneri*. *Molecular microbiology* 1995, 15 (2), 247-54.

2014

CHAPTER 2

DISCOVERY OF BACTERIAL HISTIDINE KINASE INHIBITORS WITH ANTIBACTERIAL ACTIVITY AGAINST CLINICAL ISOLATES OF MRSA AND *STAPHYLOCOCCUS EPIDERMIDIS*

Nadya Velikova¹, Simone Fulle², Ana Sousa Manso^{3, 4}, Nico Taverne⁶, Milena Mechkarska⁵, J. Michael Conlon⁵, Jerry M. Wells⁶, Marco Rinaldo Oggioni^{3, 4}, Paul Finn², Alberto Marina^{1, 7}

¹Instituto de Biomedicina de Valencia, Consejo Superior de Investigaciones Científicas (CSIC), Jaime Roig 11, 46010 Valencia, Spain;

²InhibOx, Oxford, United Kingdom;

³Dipartimento di Biotecnologie Mediche, Università di Siena, 53100 Siena, Italy;

⁴Department of Genetics, University of Leicester, Leicester, Le1 7RH, United Kingdom;

⁵Department of Biochemistry, College of Medicine and Health Science, United Arab Emirates University, P.O. Box 17666 Al Ain, United Arab Emirates;

⁶Host-Microbe Interactomics Chair Group, Animal Sciences, University of Wageningen, P.O. Box 338, 6700 AH Wageningen, The Netherlands;

⁷CIBER de Enfermedades Raras (CIBERER), ISCIII, Valencia, Spain

TO BE SUBMITTED TO ASM ANTIMICROBIAL AGENTS AND CHEMOTHERAPY

2014

ABSTRACT

The emergence of multi-drug resistant bacteria is an overwhelming world-wide public health problem. Two-component systems, consisting of a sensor histidine kinase (HK) and an effector response regulator, are the main signaling devices in bacteria and have been proposed as promising targets for the development of novel broad-spectrum antibacterials. Rational design of competitive inhibitors for the nucleotide-binding site of HKs that inhibit the autophosphorylation activity is considered a promising strategy to generate a novel class of antibacterials. To discover HK inhibitors we employed a virtual screening approach, including structure-based virtual screening (SBVS) and a ligand-based similarity search (LBSS). Two of the hits identified using SBVS inhibited the autophosphorylation activity of multiple HKs *in vitro* and had a weak antibacterial activity against several Gram-positive bacteria species. Using the two hits as query molecules for LBSS, three compounds were identified with greater autophosphorylation inhibitory capacity ($IC_{50} \geq 16 \mu\text{g}/\text{m}$ for the best hit, B13) and stronger antibacterial activity against different Gram-positive laboratory strains and clinical isolates of *Staphylococcus epidermidis* and methicillin-resistant *Staphylococcus aureus* (MRSA). One of these compounds, B14, inhibits the growth of multi-drug resistant clinical isolates of both Gram-positive and Gram-negative bacteria. Analysis of the predicted binding modes of the reported inhibitors suggests different modes of interaction with the ATP-binding site of HKs and thus can be used as a starting point for designing inhibitors with higher affinity and selectivity for HKs.

INTRODUCTION

There is an urgent need to discover new antibacterials to combat the growing problem of antibiotic resistance world-wide^{1,2}. Two-component systems (TCS) have been proposed for almost two decades as promising antibacterial drug-targets^{3,4,5}. TCS are highly pervasive in bacteria and used for signal transduction but are not present in mammals, making them attractive antibacterial drug targets⁶. Moreover, TCS are involved in the regulation of a variety of processes related to bacterial pathogenicity⁷, including virulence⁸, biofilm formation^{9,10}, antibiotic resistance¹¹, and bacterial persistence¹². Some TCS are essential or conditionally essential for bacterial growth¹³. Furthermore, the high degree of conservation among TCS active sites and the existence of multiple TCS in each bacterium suggest that it should be possible to identify an inhibitor of multiple TCS regulatory networks with a broad-spectrum activity. Overall, targeting TCS is expected to effectively incapacitate the ability of bacteria to adapt to environmental and physiological changes.

A prototypical TCS consists of a membrane-bound histidine kinase (HK) and a cognate response regulator (RR) with transcription activity¹⁴. Upon sensing environmental stimuli, the HK is autophosphorylated at conserved histidine residues. Subsequently, the phosphoryl groups attached to His are transferred to conserved aspartic acid residues in the receiver domains (RECs) of the cognate RRs. For some RRs, phosphorylation has been shown to alter affinity of binding to the operator sites and alter gene transcription due to conformational changes and protein dimerization¹⁴. HK autophosphorylation involves two well-conserved domains, a dimerization and histidine phosphotransfer domain (DHP) containing the phospho-accepting His and a C-terminal catalytic ATP-binding (CA) domain that phosphorylates His through ATP hydrolysis. The structure and amino acid sequence of the ATP-binding domain is well conserved so inhibitors targeted at ATP-binding would be expected to inhibit multiple TCS. Here we describe the identification of HK autophosphorylation inhibitors (HKAI) by combined virtual screening approach including structure-based virtual screening (SBVS), followed by ligand-based similarity search (LBSS) for homologues of the initial hits. The compounds were demonstrated to inhibit *Escherichia coli* and *Staphylococcus aureus* PhoR autophosphorylation and are expected to inhibit the autophosphorylation of other HKs. The HKAI were also tested for their antibacterial activity against reference and multi-drug resistant bacterial strains, including MRSA.

MATERIALS AND METHODS

STRUCTURE-BASED VIRTUAL SCREENING

Target preparation

The chosen molecular targets for molecular docking were the CA domains of *Thermotoga maritima* HK853 (PDB: 3DGE)¹⁵, *Geobacillus stearothermophilus* KinB (PDB: 3D36)¹⁶ and *T. maritima* CheA (PDB: I58B)¹⁷. Residues corresponding to the CA domain of each A chain (320-480 for 3DGE, 270-415 for 3D36 and 354-540 for I58B) were selected for each structure and additional atoms corresponding to water molecules, ions or ligands were removed. Hydrogen atoms were added in the absence of the cognate ligand using the GOLD program¹⁸.

Docking parameters

All docking calculations were performed with the GOLD docking software (version 5.2) using ChemPLP as a scoring function¹⁹. Binding sites were defined as being 10 Å around the geometric center of the cognate ligand.

Library

For the initial screening, a diversity set (600 000) of the Scopius – CSpace database (over 6 million commercially available drug-like compounds)^{20, 21} was docked into each of the three HK structures. The search efficiency parameter was set to 30 % and 10 solutions were generated for each compound of which only the highest-scoring poses were saved.

Post-processing of docking results

Compounds with unwanted functional groups (in-house rules used by InhibOx) were removed and the resulting set of compounds was ranked in two lists: i) by the ChemPLP GOLD docking score (ChemPLP) and ii) by a ligand efficiency score (i.e.) which is ChemPLP divided by the number of non-hydrogen atoms in the compound²². The top 3500 compounds in each list were used to extract the top 100 compounds docking to all three HK CA domain structures. This resulted in two final lists of compounds: one with respect to ChemPLP and one with respect to ligand efficiency. The top 100 compounds of each list were finally visually inspected and ten compounds were purchased for experimental testing.

LIGAND-BASED SIMILARITY SEARCH

The database from the Developmental Therapeutics program of the National Cancer Institute and the National Institute of Health (DTP) was searched for analogue structures of the initial hits A5 and A6. The similarity search with A5 or A6 as query molecules was performed using the Morgan fingerprint as implemented in RDKit²³, which is a variation of the “extended connectivity fingerprints” (ECFP)²⁴. The top 100 hits of each similarity search were visually inspected of which in total 25 compounds were ordered and experimentally tested.

BINDING AND INTERACTION MODE PREDICTION

Docking calculations to predict the binding mode of selected inhibitors were performed with the initial hits, A5 and A6, and the LBSS hits showing antibacterial effect, B7, B13 and B14, using the CA domain of *T. maritima* HK853 (PDB: 3DGE, chain A) and GOLD docking software. For each ligand 100 solutions were generated, of which the top 20 were visually inspected.

CHEMICAL REAGENTS

Compounds A1 to A10 from the initial SBVS screening were purchased from Ukrainian Organic Synthesis (Kiev, Ukraine). Compounds B1 to B25 from the ligand-based similarity search (LBSS) were obtained from DTP. Compounds were dissolved in 100% DMSO and stored at 4°C protected from direct light. [γ -³²] ATP was purchased from Perkin Elmer.

CLONING

Streptococcus pneumoniae *walk* encoding the catalytic portion (DHp and CA domain) of Walk (amino acids from 208 to 449) was amplified by PCR from *S. pneumoniae* CDC3059-06 genomic DNA using the following primers: forward 5'-aagttctgttcaggcccgatggagcaggagaaggagaacgc-3' and reverse 5'-atggtctagaagctctagctcttctacttcatccac-3'. The PCR product was purified by PCR product purification kit (Macherey-Nagel) and cloned into a gel-purified pOpinF vector (kindly provided by Nick Berow, IRB, Spain) linearized with KpnI and HindIII (Fischer Scientific). The insert was cloned into the pOpinF vector with In-Fusion HD cloning system (Clontech). Positive clones were confirmed by colony PCR and DNA sequencing.

PROTEIN EXPRESSION AND PURIFICATION

The catalytic portions (DHp and CA domain) of *T. maritima* HK853 (HK853), *E. coli* PhoR (PhoR^E) and *S. aureus* PhoR (PhoR^S) were expressed and purified as previously described^{15, 25}. In brief, the proteins were expressed in *E. coli* RIL and purified by Ni-affinity (PhoR^E and PhoR^S) or anion-exchange (HK853) and size-exclusion chromatography. *S. pneumoniae* Walk (Walk) was expressed in *E. coli* RIL. Luria Broth (LB) media supplemented with 100 µg/ml ampicillin and 33 µg/ml chloramphenicol was inoculated with an overnight pre-culture (1/50 of the culture volume). At exponential phase (OD₆₀₀ 0.2 – 0.4) protein expression was induced by addition of 1 mM IPTG for 3 to 5 h at 37°C. The cells were harvested by centrifugation at 4000 g, 4 ° C for 25 min and the pellets were stored at -80°C until use. The cell pellets were resuspended in lysis buffer (100 mM Tris pH 8.0, 150 mM NaCl, 0.1 mM PMSF) and sonicated at 4°C for 5 min with pulses of 15 sec at intervals

of 1 minute. The cell debris and the supernatant were separated by centrifugation at 11 000 g, 4°C for 60 min. The cell debris were resuspended in equilibration buffer (100 mM Tris pH 8.0, 150 mM NaCl) containing 2M urea and incubated overnight at 4°C with rotation. After centrifugation at 11 000 g, the supernatant was injected into a Ni-affinity chromatography column (GE Healthcare) equilibrated with equilibration buffer, washed with 5 volumes of equilibration buffer and eluted with equilibration buffer containing 0.5 M imidazole. WalK was concentrated with AmiconUltra (Millipore) centrifugal filters, aliquoted and stored at -80°C until use. The yield was \leq 0.5 mg/L culture.

KINASE ASSAY

Kinase assay was performed as previously described²⁶. When comparing the inhibitory capacity of ligands and measuring IC_{50} , the final DMSO concentration in the assay was 10% (v/v). Controls lacking ligands and containing an equal concentration of DMSO were carried out in parallel. Inhibition of HK autophosphorylation was determined by incubating 0.12 mg/ml (\approx 4 μ M HK) and up to 20 mM compound in kinase buffer (50 mM Tris HCl, pH 8.5, 50 mM KCl, 5 mM $MgCl_2$, 0.5 mM EDTA and 0.1 mM DTT). Autophosphorylation reactions were initiated by addition of 0.1 μ Ci/ μ l [γ -³²P] ATP containing from 0.03 to 0.06 μ M ATP (final concentrations). Autophosphorylation was quenched with 2x SDS-PAGE sample buffer supplemented with 50 mM EDTA. Samples were applied without heating to 15% (w/v) Tris-glycine SDS-polyacrylamide gels. After electrophoresis, the bottoms of the gels were removed to lower the background signal from the unincorporated radiolabeled ATP. Gels were dried without staining on a Bio-Rad Gel Air drying system and the phosphorylated protein was quantified by phosphor-imaging using a Fluoro Image Analyzer FLA-5000 (Fujifilm) and evaluated with the MultiGauge software (Fujifilm). IC_{50} is the concentration at which 50% residual enzyme activity was observed compared to the negative control, DMSO. Prism GraphPad v.4 was used for curve fitting and statistical analysis²⁷.

AGGREGATION ANALYSIS BY NATIVE POLYACRYLAMIDE GEL ELECTROPHORESIS

PhoR^E and PhoR^S (0.12 μ g/ml, final concentration) were prepared in kinase buffer. Compounds were added to a final concentration of 5 mM or 2 mM for the initial SBVS or the secondary LBSS hits, respectively. DMSO in the assays was maintained to a final concentration 10% (v/v). After 30 min of incubation at room temperature Native polyacrylamide gel electrophoresis (Native-PAGE) loading buffer was added and samples loaded. Coomassie blue staining was used for protein visualization.

BACTERIAL STRAINS

Bacterial strains used in this study for antibacterial susceptibility testing are listed in Table S3. The strains (Table S3) were propagated using standard microbiological procedures.

Uropathogenic *Escherichia coli* CFT 073, *S. aureus* DSM 20231 and *S. epidermidis* DSM 20044 were obtained from the German Collection of Microorganisms and Cell culture (DSMZ). *S. aureus* ATCC 25293, *S. epidermidis* RP62A and RP62A/1, *E. coli* ATCC 25276, *Klebsiella pneumoniae* ATCC 700603, *Pseudomonas aeruginosa* ATCC 27853, and *S. pneumoniae* ATCC 49619 were obtained from the American Type Culture Collection (ATCC). *Streptococcus suis* 3881/S10 was provided by the Central Veterinary Institute of Wageningen University and Research Centre (CVI, Lelystad, The Netherlands).

Six clinical sporadic isolates of MRSA (127/08, 145/08, 274/08, V4180, S908, and T4/6) were obtained from wounds of patients admitted to Tawam hospital (Al Ain, UAE). Characterization of the MRSA strains by multilocus sequence typing (MLST), staphylococcal cassette chromosome (*SCCmec*) typing, accessory gene regulator (*agr*) typing, *Staphylococcus* protein A (*spa*) typing, and toxin gene carriage has been described previously [36]. The MRSA strains were resistant to all β -lactam antibiotics tested and to a range of non- β -lactam antibiotics²⁸.

Three isolates of *S. epidermidis* (T7/3, T6/19, and T37/8) were obtained from wounds of patients admitted to Tawam hospital (Al Ain, UAE). The biofilm-producing *Staphylococcus epidermidis* RP62A strain produces polysaccharide intercellular adhesin that protects the bacteria against the components of the human innate immune system. Its full genome sequence is in the GenBank: NC002976. *S. epidermidis* RP62A/1 is a stable biofilm non-producer phase variant of RP62A²⁹.

Five independent well-characterized multidrug-resistant *Acinetobacter baumannii* strains (NM8, NM35, NM75, NM109, and NM124) and three *Stenotrophomonas maltophilia* strains (B32/1, B5/5, and B6/2) were included in the study. These strains were isolated at four different hospitals in Abu Dhabi Emirate, UAE and their clonal lineages and antibiotic susceptibilities have been previously described^{30,31}.

ANTIBACTERIAL SUSCEPTIBILITY TESTING

For all microorganisms tested except *S. pneumoniae*, the minimal inhibitory concentrations (MICs) were determined as previously described following a standard double-dilution method^{32,33,34}. MICs were recorded as the lowest concentration of the compound where no visible growth was observed. After plating the dilutions around the MIC, MBC was recorded as the lowest concentration of the compound at which no colonies were formed after 24h of incubation at 37°C. For *S. pneumoniae* MICs were determined by adapting the standard double-dilution method of this microorganism (use of Todd Hewitt Yeast extract (THY) with 200U/mL of catalase and continuous monitoring of growth) to anaerobic conditions³⁴. MBCs for *S. pneumoniae* were determined by inoculation of 10 μ l from each well that did not show visible bacterial growth on THY 0,5% 3% blood agar plates. After 24 h of incubation at 37°C 5% CO₂,

the first dilution yielding three colonies or fewer was scored as the MBC, as described by the CLSI for starting inoculate of 1×10^5 CFU/ml³⁵.

HEMOLYSIS ASSAY

Hemolytic activity against human erythrocytes taken from a healthy donor was measured as previously described³⁶. Erythrocytes were incubated with up to 500 µg/ml compounds and the LC_{50} value was recorded as the mean concentration of compound producing 50% hemolysis in three independent incubations.

CELL LINES AND MEDIUM

Caco-2 BBE cells (CRL 2102) were purchased from the American Type Culture Center (Manassas, VA) and grown in DMEM (Invitrogen, Paisley, UK) containing Glutamax and supplemented with 10% fetal bovine serum (FBS; PAA Laboratories, Colbe, Germany) and 100 U/ml penicillin/100 µg streptomycin (Sigma, St. Louis, MO) in an atmosphere of 5% CO_2 -95% O_2 at 37°C. Cells were trypsinized weekly.

NEUTRAL RED UPTAKE ASSAY OF CELL VIABILITY

Neutral red uptake assay of cell viability with Caco-2 cells was performed as previously described³⁷. Briefly, after overnight incubation (16 to 24 h) with concentration ranges of B7, B13 or B14, 10 µl of neutral red solution (33 µg/ml) was added to the wells. After 3 h of incubation at 37°C the medium was removed and cells were washed rapidly with PBS. Neutral red was extracted from the cells with 150 µl 1% acetic acid-50% ethanol, shaken for 10 min at RT. The neutral red content was measured on a SpectraMax M5 microplate reader (Molecular Devices) at 540 nm. The readings were expressed as neutral-red uptake relative to the neutral-red uptake of the cells exposed to DMSO. IC_{50} is the concentration causing 50% reduction in neutral-red uptake. Prism GraphPad v.4 was used for curve fitting and statistical analysis²⁷.

HUMAN PBMCs ISOLATION AND FLOW CYTOMETRY

This study was approved by Wageningen University Ethical Committee and was performed according to the principles of the Declaration of Helsinki. Buffy coats from healthy blood donors were obtained from the Sanquin Blood bank in Nijmegen (The Netherlands). A written informed consent was obtained from each volunteer before sample collection.

PBMCs were isolated from buffy coats of healthy donors using Ficoll Paque Plus density gradient (GE Healthcare, Diegem Belgium) according to the manufacturer's protocol. After centrifugation, the mononuclear cells were collected, washed in IMDM + glutamax (Invitrogen, Breda, The Netherlands) and resuspended in IMDM + glutamax supplemented with 10% foetal calf serum (FCS), 100 U/ml penicillin and

2014

100 µg/ml streptomycin (Sigma, St. Louis, MO). PBMCs were seeded at 1×10^6 cells/well in 48-well plates and, treated with B7 and B13. After 24 hours, the cells were stained with annexin V and PI (BD Biosciences, Breda, The Netherlands) and analysed on a flow cytometer (FACS Canto II, BD).

RESULTS

VIRTUAL SCREENING STRATEGY FOR POTENTIAL HISTIDINE-KINASE INHIBITORS

The ATP-binding pocket of the CA domains of HKs is considered to be the most promising target for inhibition of TCS HKs and has been used previously in structure-based virtual screenings^{38, 39, 40, 41}. To identify drug-like ligands of the ATP-binding sites of the HK CA domains with putative broad spectrum of inhibition, a diverse set of 600 000 compounds was screened via *in silico* docking calculation using as target receptors the ATP-binding sites of the CA domains of three different HKs: *T. maritima* HK853 (PDB: 3DGE)⁴², *T. maritima* CheA (PDB: 1I58)¹⁷ and *G. stearothermophilus* KinB (PDB: 3D36)¹⁶. These three CA domains were selected because the structures were solved in the presence of a nucleotide and re-docking of the cognate ligand was successful (RMSD 1 Å for 3DGE and 3D36, and 3 Å for 1I58). Virtual screening with the three structures that have some sequence variability at the ATP-binding site was expected to facilitate the identification of broad-spectrum histidine kinase autophosphorylation inhibitors (HKAI). The screened compounds were ranked based on the raw docking score, ChemPLP, as well as ligand efficiency. The top 100 docked compounds in common for the three HKs were ranked on both scoring schemes (i.e. ChemPLP and ligand efficiency) and then visually inspected to select 10 compounds, A1-A10 (Figure 1, Tables 1, S1 and S2), for experimental testing.

INHIBITION OF HK AUTOPHOSPHORYLATION IN VITRO AND ANTIBACTERIAL SUSCEPTIBILITY TESTING REVEALED TWO HIT COMPOUNDS

The inhibitory activity of the 10 selected compounds from the SBVS on HKs autophosphorylation was tested *in vitro* using four different HKs: *T. maritima* HK853 (HK853), as a representative of the structures used in the docking assays, the highly extended HK PhoR from a Gram-negative (*E. coli*; PhoR^E), and Gram-positive (*S. aureus*; PhoR^S) representative and *S. pneumoniae* WalK (WalK) as a representative of the essential WalKR TCS ubiquitous among Gram-positive bacteria⁴³. As a fast way to compare the autophosphorylation inhibitory capacity of the 10 selected compounds the kinase assays were performed at a single and high (5 mM) compound concentration and at one time point (30 sec). Autophosphorylation activity of HK853 was not or weakly (up to 30%) inhibited by the 10 compounds compared to the

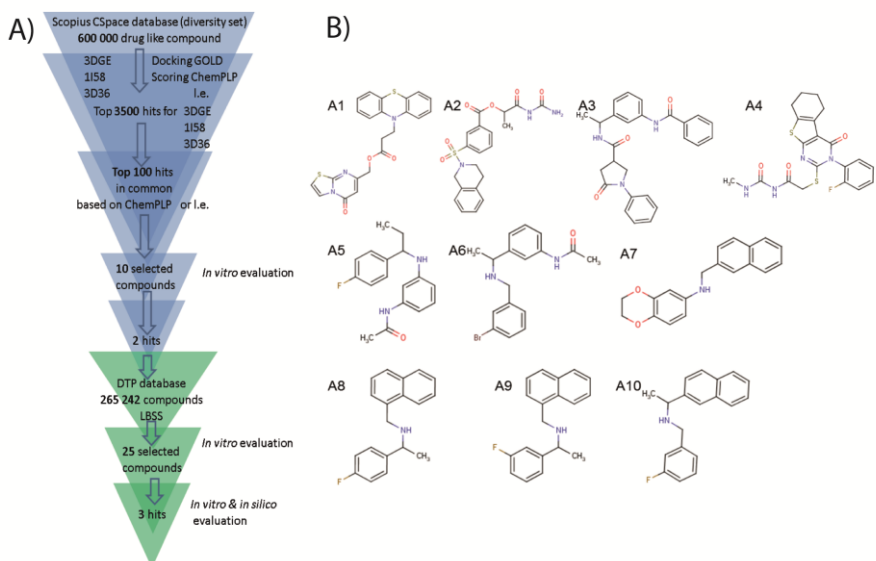


Figure 1. Identification of antibacterial compounds from virtual screening. (A) Schematic representation of the screening workflow including structure-based virtual screening (SBVS; blue) followed by ligand-based similarity search (LBSS; green). In the SBVS a diversity set of the Scopius CSpace database was screened for putative ligands of the ATP-binding site of the CA domain of three HK structures using GOLD. Out of the top 3500 hits for each HK the top 100 in common for the three HKs based on ChemPLP or ligand efficiency were visually inspected and 10 compounds (B) were selected for experimental testing. The results of the *in vitro* evaluation by kinase assay and antibacterial susceptibility testing of these 10 compounds are provided in Table 1.

negative control (Fig S1A) and it was not possible to identify (a) more potent inhibitor(s) based on HK853 autophosphorylation inhibition. The kinase assays with WalK, PhoR^E and PhoR^S revealed that compounds A5 and A6 had a higher autophosphorylation inhibitory activity than the other selected compounds identified by SBVS and were general inhibitors of HK autophosphorylation (Figure 1B, Table 1). A5 and A6 inhibit HK autophosphorylation activity in a dose-dependent manner, with IC₅₀ in the high micromolar / millimolar range (Table 1, Figure S2). A5 inhibits PhoR^E, PhoR^S and WalK with IC₅₀ ≈ 1000 μM and it seems it is not soluble in kinase buffer in the presence of 10% DMSO at concentrations higher than 1.3 mM.

Table 1. Selected compounds from the SBVS and their corresponding IC₅₀ and MICs

Initial hits Name	IC ₅₀ [mM]				MIC µg/ml		
	PhoR ^S	PhoR ^E	HK853	WalK	<i>S. aureus</i> DSM 20231	<i>S. epidermidis</i> DSM 20044	<i>E. coli</i> CFT 073
A1	> 5	> 5	> 5	> 5	>500	>500	>500
A2	> 5	> 5	> 5	> 5	>500	>500	>500
A3	> 5	> 5	> 5	> 5	>500	>500	>500
A4	> 5	> 5	> 5	> 5	>500	>500	>500
A5	≈ 1	≈ 1	> 5	>1	>500	500 [#]	>500
A6	1.14	0.37	> 5	>1	>500	500 [#]	500 [#]
A7	< 5 [*]	> 5	> 5	> 5	>500	>500	>500
A8	< 5 [*]	> 5	> 5	> 5	>500	>500	>500
A9	> 5	> 5	> 5	> 5	>500	>500	>500
A10	> 5	> 5	> 5	> 5	>500	>500	>500

* % Inhibition at 5 mM ≥ 70%, i.e. IC₅₀ < 5 mM

[#]MBC > 500 µg/ml

A6 inhibits PhoR^E, PhoR^S and WalK autophosphorylation with IC₅₀ of 372 µM, 1141 µM and > 1000 µM, respectively (Table 1, Figure S2). The inhibitory activity on HK autophosphorylation was most likely due to inhibition of ATP binding in the CA domain as neither inhibitor caused PhoR^E or PhoR^S protein aggregation when added in high concentrations (Figure S3).

To evaluate the antibacterial effect of the 10 selected compounds from SBVS, their minimal inhibitory concentrations (MICs) and minimal bactericidal concentrations (MBCs) were determined for Gram-positive (*S. aureus* DSM 20231 and *S. epidermidis* DSM 20044) and Gram-negative (*E. coli* UCF 073) bacteria. Only A5 and A6 were able to inhibit bacterial growth at high compound concentrations, which is in agreement with their inhibitory activity on HKs (Table 1). *S. epidermidis* DSM 20044 growth was inhibited by A5 and A6 while *E. coli* UCF 073 growth was only inhibited by A6, in all the cases with a modest MICs of 500 µg/ml that are in line with the low HK affinity suggested by the measured IC₅₀ (Table 1 and Figure S1). Both compounds were bacteriostatic against the three bacterial strains in the tested concentration range (MBC > 500 µg/ml). On the basis of these results, A5 and A6 were used for a ligand-based similarity search (LBSS) in order to identify more potent inhibitors with stronger antibacterial effect.

LIGAND-BASED SIMILARITY SEARCH

It is a well-accepted assumption that similar compounds have similar activity; however, small structural changes in a compound can result in significant difference in potency (so called ‘activity cliffs’) ⁴⁴. The latter is exemplified by A5 and A6 since the two compounds are structurally similar but they show different inhibitory capacity toward the HKs assayed (Figures 1B and S1, Table 1). Thus, to explore the chemical space around the scaffolds represented by the initial hits from the SBVS and to identify more potent HK inhibitors with stronger antibacterial effect, analogue compounds of A5 and A6 in the database from the Developmental Therapeutics Program of the National Cancer Institute and the National Institute of Health (DTP) were identified using LBSS (i.e. by circular topological fingerprints). The top 100 hits for the LBSS with A5 or A6 were visually investigated and 25 representative compounds, B1-B25 (Figure 2 and Table S1), were experimentally evaluated for their HK autophosphorylation inhibitory capacity and antibacterial effect *in vitro*.

LBSS IDENTIFIED MORE POTENT HKs INHIBITORS WITH STRONGER ANTIBACTERIAL ACTIVITY AGAINST GRAM-POSITIVE BACTERIA

To evaluate the 25 selected hits from LBSS, inhibition of autophosphorylation was measured at a single time point (30 sec) using one concentration of each putative inhibitor. PhoR^S and PhoR^E were used as targets as these HKs were more strongly inhibited by A5 and A6 than WalK and HK853. The concentration of putative inhibitors was reduced from 5 mM to 2 mM in order to identify inhibitors with higher potency than A5 and A6. B2, B11, B13 inhibit autophosphorylation activity of both PhoR^S and PhoR^E by more than 75%. B7, B14 and B15 inhibit PhoR^S and PhoR^E autophosphorylation by more than 75% and more than 40 % compared to the negative control, respectively (Figure S2).

The antibacterial effect evaluation of the 25 compounds identified using LBSS showed that B7 was bacteriostatic for *S. aureus* DSM 20231 with a MIC of 250 µg/ml (Table 2). B13 was bactericidal for *S. aureus* DSM 20231 and *S. epidermidis* DSM 20044 with MIC of 8 and 1 µg/ml, respectively, and MBCs of 33 and 8 µg/ml, respectively (Table 2). Additionally, B14 was bactericidal for *S. aureus* DSM 20231 and *S. epidermidis* DSM 20044 at a MIC and MBC of 500 µg/ml (Table 2). The rest of the tested compounds did not inhibit the growth of *S. aureus* DSM 20231 or *S. epidermidis* DSM 20044 at the highest tested concentration of 500 µg/ml (MICs > 500 µg/ml). None of the 25 tested LBSS hits inhibited the growth of *E. coli* CFT 073 at the highest tested concentration of 500 µg/ml (MICs > 500 µg/ml; Table 2). Compounds B7, B13 and B14, which had the highest inhibitory activity in the biochemical assays

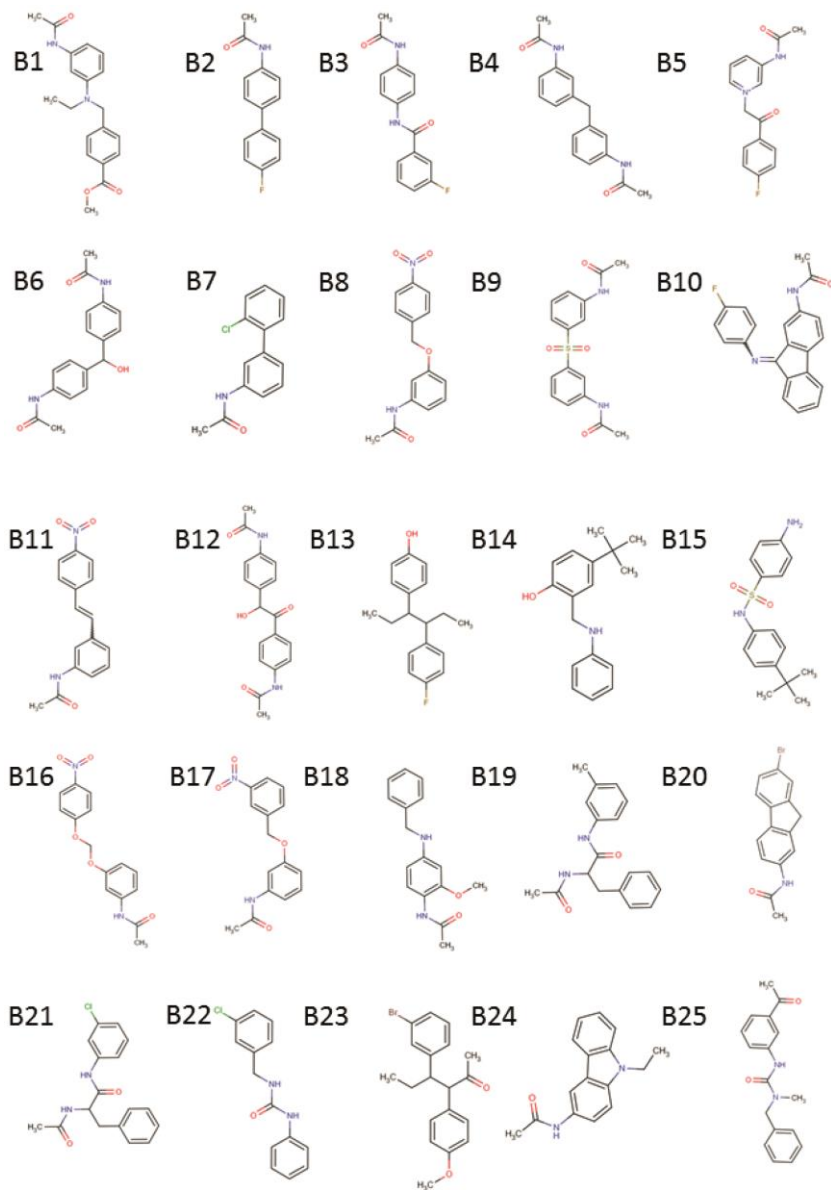


Figure 2. Chemical structures of LBSS selected hits. The results of the *in vitro* evaluation by kinase assay and antibacterial susceptibility testing are presented in Table 2.

Table 2. LBSS hits and their corresponding IC₅₀ and MICs

Secondary hits Name	IC ₅₀ [mM]		MIC [µg/ml]		
	PhoR ^S	PhoR ^E	<i>S. aureus</i> DSM 20231	<i>S. epidermidis</i> DSM 20044	<i>E. coli</i> CFT 073
B1	> 2	> 2	>500	>500	>500
B2	<2	<2	>500	>500	>500
B3	> 2	> 2	>500	>500	>500
B4	> 2	> 2	>500	>500	>500
B5	> 2	> 2	>500	>500	>500
B6	> 2	> 2	>500	>500	>500
B7	≈ 1	≈ 0.1	250 [#]	>500	>500
B8	> 2	> 2	>500	>500	>500
B9	> 2	> 2	>500	>500	>500
B10	> 2	> 2	>500	>500	>500
B11	<2	<2	>500	>500	>500
B12	> 2	> 2	>500	>500	>500
B13	0.212	0.016	8 [¥]	1 [¥]	>500
B14	1.48	> 2	500 [†]	500 [†]	>500
B15	<2	> 2	>500	>500	>500
B16	> 2	> 2	>500	>500	>500
B17	> 2	> 2	>500	>500	>500
B18	> 2	> 2	>500	>500	>500
B19	> 2	> 2	>500	>500	>500
B20	> 2	> 2	>500	>500	>500
B21	> 2	> 2	>500	>500	>500
B22	> 2	> 2	>500	>500	>500
B23	> 2	> 2	>500	>500	>500
B24	> 2	> 2	>500	>500	>500
B25	> 2	> 2	>500	>500	>500

[#] A7 *S. aureus* MBC > 500 µg/ml

[¥] B13 MBC *S. aureus* DSM20231 31 µg/ml; B13 MBC *S. epidermidis* DSM20044 8 µg/ml

[†] B14 MBC *S. aureus* DSM20231 and B14 MBC *S. epidermidis* DSM20044 500 µg/ml

and antibacterial activity were selected for further evaluation *in vitro*. First, their IC₅₀ against PhoR^E and PhoR^S was measured (Figure S2, Table 2). B7 inhibits PhoR^E autophosphorylation with IC₅₀ in the lower micromolar range ($\geq 100 \mu\text{M}$) and PhoR^S in the higher micromolar/ millimolar range (IC₅₀ PhoR^S $\geq 1000 \mu\text{M}$). The IC₅₀ curves indicated that B7 is not soluble in concentrations higher than 1000 μM in kinase buffer in the presence of 10% DMSO. B13 inhibits PhoR^E and PhoR^S with IC₅₀ PhoR^E $< 100 \mu\text{M}$ and IC₅₀ PhoR^S = 212 μM and possess good solubility in kinase buffer in the presence of 10% DMSO. B14 IC₅₀ against PhoR^E and PhoR^S is higher than 2000 μM and higher than 1000 μM , respectively. The possibility of non-specific inhibition by aggregation was ruled out since none of the compounds caused protein aggregation of PhoR^S or PhoR^E at 2 mM in native PAGE (Figure S3). Another reported side effect of previously published TCS inhibitors is membrane damage. To exclude that the antibacterial activity of these compounds could be mediated by this mechanism, the hemolytic activity of B7, B13 and B14 was tested. B7 and B14 did not cause hemolysis at 500 $\mu\text{g/ml}$ (i.e. LC₅₀ $> 500 \mu\text{g/ml}$). Hemolysis was observed with compound B13 at concentrations higher than the observed MICs (LC₅₀ 277 $\mu\text{g/ml}$).

CLINICAL ISOLATES OF MULTIDRUG RESISTANT BACTERIA ARE SUSCEPTIBLE TO SELECTED HKAs *IN VITRO*

The most promising LBSS hits B7, B13 and B14 (Figure 2) were tested for their ability to inhibit the growth of well-characterized methicillin resistant clinical isolates of *S. aureus* (MRSA)²⁸ and clinical isolates of *S. epidermidis*, as well as reference strains of *S. pneumoniae* and *S. suis* and additional reference strains of *S. aureus* and *S. epidermidis*. Since B7, B13 and B14 are expected to inhibit the autophosphorylation of multiple HKs, including HKs from Gram-negative bacteria, their antibacterial effect against multi-drug resistant clinical isolates of the important pathogens *A. baumannii*^{45, 46} and *S. maltophilia*³¹ and against reference strains from *Klebsiella pneumoniae* and *Pseudomonas aeruginosa* were also tested (Table 3, Table S3). B7 inhibited the growth of two of the 6 MRSA strains *in vitro* with MICs $\geq 250 \mu\text{g/ml}$, which was comparable to the MICs for the *S. aureus* reference strains 25293 and DSM 202231. The other four MRSA strains were not susceptible to B7. As expected from the results of the antibacterial susceptibility testing with *S. epidermidis* DSM 20044, compound B7 had no antibacterial effect on the clinical isolates of *S. epidermidis*. B7 inhibits the growth of all tested *S. pneumoniae* strains with MIC of 128 $\mu\text{g/ml}$, which was similar to the MICs for the reference strains of *S. aureus*. B7 did not inhibit the growth of the *S. suis* 3881/ S10 strain in the tested concentration range ($\leq 500 \mu\text{g/ml}$).

B13 inhibited the growth of all tested MRSA stains with MICs between 8 and 16 $\mu\text{g/ml}$, which was comparable to the MICs for the reference strains of *S. aureus*. B13 also inhibited the growth of clinical isolates of *S. epidermidis* with MICs between 8 and 16 $\mu\text{g/ml}$, which is similar to the MICs for, the biofilm forming *S. epidermidis* RP62A and non-biofilm forming *S. epidermidis* RP62A/1. Like B7, B13 inhibited the growth of the *S. pneumoniae* strains with MIC of 16 $\mu\text{g/ml}$.

B14 inhibits growth of MRSA with MICs of 250 $\mu\text{g/ml}$, which was comparable to the MICs for the reference strains of *S. aureus*. B14 inhibited growth of all *S.*

epidermidis strains except *S. epidermidis* strain RP62A, with MICs in the range of 250 to 500 µg/ml. B14 was not active against *S. pneumoniae* strains but inhibited growth of the *S. suis* S10 with MIC of 125 µg/ml.

Even though the three selected HKAI, B7, B13 and B14, inhibit PhoR^E, homologues of which are present in many Gram-negative bacteria, only B14 inhibits the growth of the Gram-negative *A. baumannii* and *S. maltophilia* strains with MICs from 250 µg/ml to 500 µg/ml. None of the 3 selected inhibitors inhibit the growth of *K. pneumoniae* ATCC 700603 and *P. aeruginosa* ATCC 27853 at the highest tested concentration (MIC > 500 µg/ml).

INCREASED ANTIBACTERIAL ACTIVITY IS NOT RELATED TO INCREASED CYTOTOXICITY TO MAMMALIAN CELLS

To check the effect of the most promising inhibitors (B7, B13 and B14) on mammalian cell viability, cytotoxicity was evaluated i) with neutral-red uptake assays with Caco-2 cells (Figure 3) and ii) measurement of dead (propidium iodide positive) and apoptotic (annexin V positive) freshly isolated human peripheral blood mononuclear cells (PBMCs) by flow cytometry (Figure 4). After overnight incubation (16 to 20 h), B7, B13 and B14 inhibited neutral-red uptake with IC₅₀ values of 105, 29 and 3 µg/ml, respectively. B7 and B14 IC₅₀ are lower than the observed MICs. However, B13 IC₅₀ is from 1.8 to 29 times higher than the observed MICs for the panel of Gram-positive strains tested. PBMCs were incubated with 0.2, 1, 3, 13 and 50 µg/ml B7 and B13 for 24 h. There was no significant difference in the number of dead cells in the control (DMSO treated) and B13 treated samples. However, the number of cells binding annexin V, a marker of early apoptosis, was significantly higher in cells incubated with 50 µg/ml of B13 than the control cells (DMSO). This is reflected in a reduction of viable (PI and annexin V negative) cells (Figure 4). Similar results were obtained for compound B7 (Figure 4C) suggesting that a concentration between 13 and 50 µg/ml induces apoptosis in a proportion of the PBMCs after 24 h incubation.

Table 3. Antibacterial effect of selected HK inhibitors against reference strains (marked with *) and (multi-drug resistant) clinical isolates

Strain	MIC ($\mu\text{g/ml}$)		
	B7	B13	B14
<i>Staphylococcus aureus</i>			
DSM 20231*	250	8	500
25293*	125	8	125
274/08	250	16	250
V4180	>500	8	250
T4/6	250	8	250
145/08	>500	8	250
127/08	>500	16	250
S908	>500	16	250
<i>Staphylococcus epidermidis</i>			
DSM 20044*	>500	1	500
RP62A*	>500	8	>500
RP62A/1*	>500	8	500
T7/3	>500	8	250
T37/8	>500	16	500
T6119	>500	8	500
<i>Streptococcus pneumoniae</i>			
DP1004*	128	16	>500
TIGR4*	128	16	>500
ATCC 49619*	128	16	>500
<i>Streptococcus suis</i>			
3881/ S10	> 500	8	125
<i>Acinetobacter baumannii</i>			
NM109	>500	>500	250
NM124	>500	>500	250
NM8	>500	>500	500
NM35	>500	>500	500
NM75	>500	>500	500
<i>Stenotrophomonas maltophilia</i>			
B5/5	>500	>500	500
B6/2	>500	>500	500
B32/1	>500	>500	500

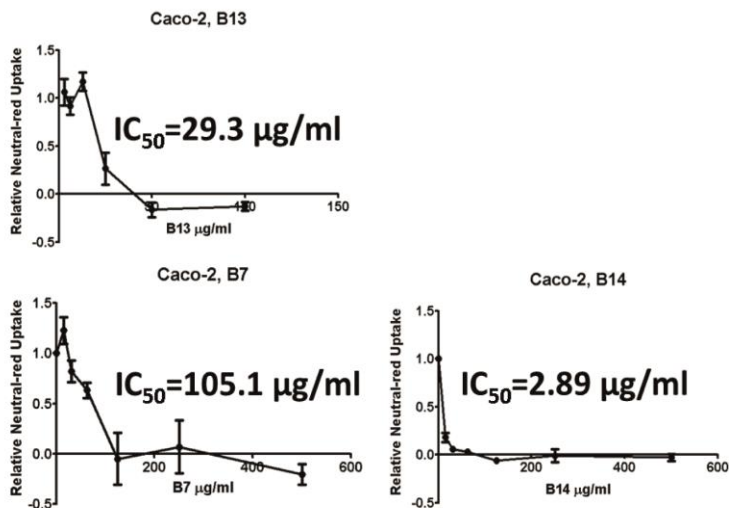


Figure 4. Mammalian cell viability assessed by neutral-red uptake assays with Caco-2 cell line. The error bars represent the SEM of at least two independent experiments in duplicate. IC_{50} is the concentration at which 50% reduction of neutral-red uptake is observed compared to the negative control (DMSO).

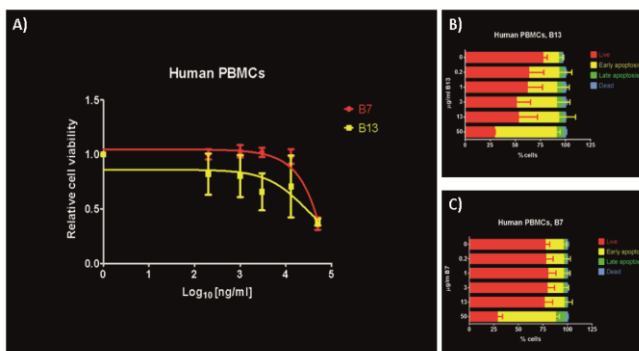


Figure 5. Dose effect of HKAI on PBMCs viability (A) and apoptosis evaluated by propidium iodide and annexin V (AV) staining. The highest tested concentration (50 µg/ml) of both B7 (C) and B13 (B) induces expression of the early apoptotic marker AV which is reflected in reduction of the live cells with more than 50% compared to the control (DMSO-treated PBMCs). The error bars represent the SEM of three independent donors.

THE HK AIs ARE PREDICTED TO INTERACT WITH CONSERVED RESIDUES IN THE ATP-BINDING SITE OF THE HK CA DOMAIN

To gain insights into the mechanism of inhibition at the atomic level, the binding modes of A5, A6, B7, B13 and B14 to *T. maritima* HK853 (PDB: 3DGE) were predicted with GOLD and visually investigated. All selected inhibitors were predicted to occupy the ATP-binding pocket and interact with key residues involved in binding of the natural substrate. A common feature for all the compounds was the presence of an aromatic ring that accommodates into the hydrophobic cavity occupied by the pyrimidine ring of adenine. (Figure 6) The aromatic ring forms $\pi - \pi$ stacking interactions with Y384 on one side and van der Waals contacts with I416 on the other side of the ring. Similar hydrophobic interactions have been observed for the adenine in the structures of *T. maritima* HK853 and other HKs in complex with nucleotides^{26, 42}. Located at the bottom of the hydrophobic pocket is the conserved Asp (D411) in the G1 box that gives specificity for recognition of the N6 amino group in the pyrimidine ring of adenine (Figure 3). For B13, the most potent inhibitor, and B14, the hydroxyl group of the phenolic ring stacked in the adenine pocket is predicted to be hydrogen bonded to the conserved D411 residue (Figure 5). Similar mode of interaction was observed for the binding of the Hsp90 inhibitor radicicol to the ATP-binding domain of the HK PhoQ⁴⁷. In contrast, A5, A6 and B7 are predicted to exploit their common amide moieties to mediate polar interaction on the other part of the active site, which in HK structures with the native ligand is occupied by the nucleotide phosphates and the Mg^{2+} cation (Figure 5). In all the three compounds, A5, A6, and B7, the nitrogen of the amide moiety is predicted to be hydrogen bonded to the conserved N-box Mg^{2+} chelating residue N380 whereas the oxygen is predicted to bind to the main-chain of the G2-Box residues G443, L444 and G445, mimicking in this way the interactions of the ATP γ -phosphate⁴⁸.

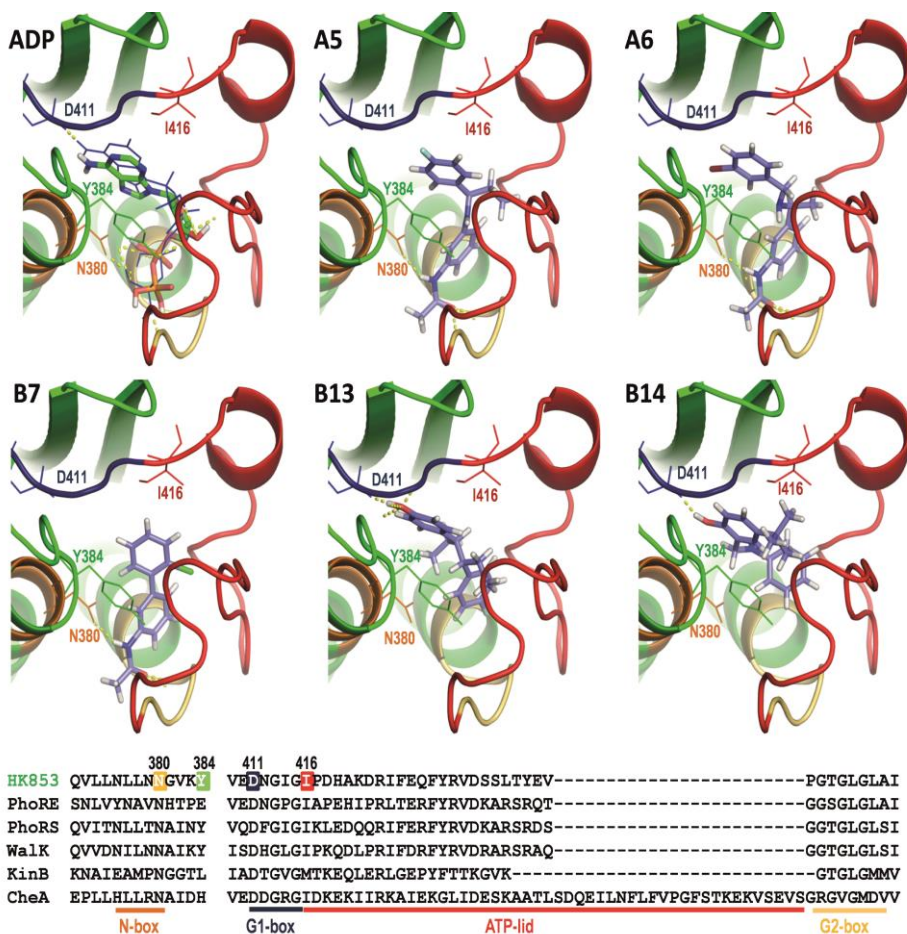


Figure 6. Predicted binding modes of selected HK autophosphorylation inhibitors (HKAI). All HKAI (shown in blue as sticks) dock in the ATP-binding site of HK853 with a predicted binding mode resembling the experimental data (3DGE) for the natural substrate ADP (top left). They interact with key elements involved in ATP-binding and autophosphorylation, i.e the N-, G1-, G2-boxes (shown in orange, blue and yellow, respectively) and the ATP-lid (shown in red).

DISCUSSION

The rapidly growing problem of multi-drug resistant bacteria requires urgent development of a pipeline of new classes of antibiotics. A new class of antibiotics ideally should be broad-spectrum, potent and the initial “hit” scaffold should be amenable to structural changes to allow for optimization of the potency, specificity, efficacy and the ADMET properties⁴⁹. Inhibitors targeting virulence factors including the ability of bacteria to form biofilms^{50, 51} have been proposed as a useful approach. As TCS are involved in the regulation of bacterial pathogenesis, including virulence, and biofilm formation, they are absent in mammals and some TCS are essential or conditionally essential for bacterial growth, TCS in general, and HKs in particular, are recognized as promising antibacterial drug targets⁵¹. The first attempts to discover TCS inhibitors resulted in hydrophobic compounds with non-specific activity, which inhibited HK autophosphorylation by indirect mechanisms such as protein aggregation and showed antibacterial effect due to decreasing membrane integrity^{52, 41, 53}. After the elucidation of HK structures^{54, 26, 42} SBVS for ligands of the CA domain of HK were reported^{38, 39, 40, 41} demonstrating that SBVS is a viable tool for discovery of HKAI with antibacterial, antivirulence and therapeutic effect.

HK CA domains present a characteristic fold with highly conserved residues involved in nucleotide-cation selection and binding⁵⁵. Therefore, autophosphorylation inhibitors discovered using structures of one HK CA are expected to have broad activity against orthologous kinases. However, using one protein structure for SBVS does not take into account the highly flexible and catalytically competent ATP-lid which is variable in length and sequence⁶ or the conformation and target plasticity⁵⁶. To address these and to increase the probability of identifying broad-spectrum HKAI, a SBVS by molecular docking using as receptors the ATP-binding site of three HK CA-domains: *T. maritima* HK853 (PDB: 3DGE), *G. stearothermophilus* KinB (PDB 3D36) and *T. maritima* CheA (PDB: 1I58) was performed. The use of multiple structures in docking experiments increases the chance of finding broad-spectrum ligands because it implicitly considers the receptors plasticity, sequence and conformation variability in the docking approach. This approach mimics an ensemble based docking which has been shown to improve the overall performance of virtual screening experiments⁵⁷. The methodology was validated by “re-docking” experiments where experimental protein-ligand complexes were reproduced with low RMSD values using the computational approach followed in the reported SBVS⁵⁸. This provides some confidence that novel ligands can be found using the same protocol. Encouragingly, two of the selected hits from the SBVS, A5 and A6, inhibited the autophosphorylation of HKs different from the HKs used in the SBVS and showed modest antibacterial effect. It seems that the observed HK autophosphorylation inhibition could be specifically mediated via the binding to the CA domain since A5 and A6 did not cause protein aggregation which is a common non-specific mechanism of action of previously reported HK inhibitors⁴¹. Furthermore, there was a good correlation between the *in vitro* biochemical activity and the antibacterial effects of A5 and A6.

To identify other possible inhibitors with stronger antibacterial effect, A5 and A6 were successfully used as query molecules in a ligand-based similarity search (LBSS). Among the LBSS hits, the most potent inhibitor was B13 (IC_{50} PhoR^E = 16 μ M, IC_{50} PhoR^S = 212 μ M), which inhibited the growth of clinical isolates of MRSA and *S. epidermidis* with MICs \leq 16 μ g/ml. The MICs against multi-drug resistant clinical isolates are comparable with the MICs against reference strains. This suggests that the putative mechanism of action of B13 differs from the known antibiotics and/or the mechanisms of resistance of the tested strains to known antibiotics are not functional against B13. Furthermore, B13 is amenable for chemical modification and further optimization. Encouragingly, the stronger antibacterial effect of B13 was not related to higher cytotoxicity. B13 inhibited neutral-red uptake by Caco-2 cells with IC_{50} of 29 μ g/ml, which is higher than the observed MICs for Gram-positive strains. Furthermore, even 24 h incubation of PBMCs with up to 50 μ g/ml of B13 and B7 did not increase proportion of dead cells. However, the highest B13 concentration tested (50 μ g/ml) increased the proportion cells expressing an early marker of apoptosis. Together these results suggest that B13 is a good lead candidate for the development of antibacterials for Gram-positive bacteria. Even though B13 is the most potent PhoR^E inhibitor among the once here reported it did not inhibit the growth of any of the tested Gram-negative strains at the highest tested concentration (500 μ g/ml). The cell envelope of Gram-negative bacteria is well known to be more effective barrier to penetration of drugs than that of Gram-positive bacteria but ultimately the compound may be modified to promote uptake or penetrate prokaryotic membranes according to experience with other antibacterials entering into Gram-negatives or by applying nanotechnology approaches^{59, 60, 49}.

The predicted binding mode of B14 exploits similar features to B13 as well as polar interaction with the conserved G1-box Asp residue, inhibits Gram-positive (*S. aureus* reference strains and MRSA, *S. epidermidis* strains and *S. suis* 3881/S10) and Gram-negative (*A. baumannii* and *S. maltophilia*) strains with MICs in the range of 125 to 500 μ g/ml. The MICs range is higher than the observed for B13 in close agreement with B14 higher than B13 IC_{50} for PhoR^E and PhoR^S autophosphorylation inhibition. Therefore, B13 and B14 could represent a promising scaffold to re-design new compounds that could be expected to inhibit a broad spectrum of HKs. Furthermore, B14 scaffold seems to possess good safety profile since the screening of B14 with 60-cell lines⁶¹ showed that except for HL-60(TB) and UO-31, the compound was not cytotoxic (cell growth > 90%).

On the other hand, the relatively weaker than B13 HKAI B7 (IC_{50} PhoR^E \approx 100 μ M, IC_{50} PhoR^S \geq 1000 μ M) inhibits the growth of the two reference *S. aureus* strains and 2 of 6 tested MRSA strains. B7 inhibited the growth of *S. pneumoniae* with MICs in the same range as the MICs for the *S. aureus* strains. However, B7 was not active against *S. epidermidis* or any of the Gram-negative bacteria tested. This strain specificity of B7 correlated with the quite different IC_{50} observed for PhoR^E and PhoR^S HKs. A tentative explanation for this fact can arise from the predicted binding mode of B7 that suggests a main interaction mediated by its amide group with the variable part of the ATP-binding site, the ATP lid. All together these indicate that B7 would inhibit autophosphorylation of different HKs with affinity affected by sequence variability. B7 did not cause protein aggregation or hemolysis and seems to possess good toxicity properties as intraperitoneal injection on mice leukemia model L1210⁶²

with up to 400 mg/kg of B7 led to from 93 to 98% survival of the treated animals, showing B7 was nontoxic *in vivo*. All together these data⁶², indicate B7 as a good hit candidate for development of an antibacterial drug. Furthermore, the effect of B7 on PBMCs was similar to that of B13 and B7 (Fig 5). As B7 has been shown to be nontoxic *in vivo* it could be expected that B13 would also be nontoxic *in vivo*.

Except of the number of rotatable bonds, the reported inhibitors B7, B13 and B14 are fragment-like, i.e. they follow the so called "rule of 3" (MW < 300 DA, hydrogen bond donors (HBD) < 3, hydrogen bond acceptors (HBA) < 3). Therefore, they present a promising starting point for the rational re-design of more potent and/ or specific HKAI. The predicted binding modes of these candidates point to different ways of compound binding to the HK active site that could be exploited in the re-design process. In this way, the interaction with the conserved Asp in the G1 box mediated by the phenolic ring predicted for B13, the most potent inhibitor, and B14 could be combined with the amide group of B7 that could interact with the ATP-lid at the other side of the active center. This new generation of structure-based re-designed compounds could increase potency following the features of B13 and/or specificity exploiting the sequence and structural differences between HKs, mainly located at the ATP-lid, to generate general or strain-specific HK inhibitors.

REFERENCES

1. Gootz, T. D., The global problem of antibiotic resistance. *Critical reviews in immunology* 2010, 30 (1), 79-93.
2. Worthington, R. J.; Melander, C., Overcoming resistance to beta-lactam antibiotics. *The Journal of organic chemistry* 2013, 78 (9), 4207-13.
3. Desnottes, J. F., New targets and strategies for the development of antibacterial agents. *Trends in biotechnology* 1996, 14 (4), 134-40.
4. Froscio, M.; Barrett, J. F., Bacterial two-component systems as antimicrobial drug discovery targets. *Drug News and Perspectives* 1999, 12 (5), 293-299.
5. Matsushita, M.; Janda, K. D., Histidine kinases as targets for new antimicrobial agents. *Bioorganic & medicinal chemistry* 2002, 10 (4), 855-67.
6. Casino, P.; Rubio, V.; Marina, A., The mechanism of signal transduction by two-component systems. *Current opinion in structural biology* 2010, 20 (6), 763-71.
7. Crepin, S.; Chekabab, S. M.; Le Bihan, G.; Bertrand, N.; Dozois, C. M.; Harel, J., The Pho regulon and the pathogenesis of *Escherichia coli*. *Veterinary microbiology* 2011, 153 (1-2), 82-8.
8. Delaune, A.; Dubrac, S.; Blanchet, C.; Poupel, O.; Mader, U.; Hiron, A.; Leduc, A.; Fitting, C.; Nicolas, P.; Cavaillon, J. M.; Adib-Conquy, M.; Msadek, T., The WalkR system controls major staphylococcal virulence genes and is involved in triggering the host inflammatory response. *Infection and immunity* 2012, 80 (10), 3438-53.
9. Dubrac, S.; Boneca, I. G.; Poupel, O.; Msadek, T., New insights into the Walk/WalR (YycG/YycF) essential signal transduction pathway reveal a major role in controlling cell wall metabolism and biofilm formation in *Staphylococcus aureus*. *Journal of bacteriology* 2007, 189 (22), 8257-69.
10. Unal, C. M.; Singh, B.; Fleury, C.; Singh, K.; Chavez de Paz, L.; Svensater, G.; Riesbeck, K., QseC controls biofilm formation of non-typeable *Haemophilus influenzae* in addition to an AI-2-dependent mechanism. *International journal of medical microbiology : IJMM* 2012, 302 (6), 261-9.
11. Howden, B. P.; McEvoy, C. R.; Allen, D. L.; Chua, K.; Gao, W.; Harrison, P. F.; Bell, J.; Coombs, G.; Bennett-Wood, V.; Porter, J. L.; Robins-Browne, R.; Davies, J. K.; Seemann, T.; Steiner, T. P., Evolution of multidrug resistance during *Staphylococcus aureus* infection involves mutation of the essential two component regulator WalkR. *PLoS pathogens* 2011, 7 (11), e1002359.
12. Mirabella, A.; Yanez Villanueva, R. M.; Delrue, R. M.; Uzureau, S.; Zygmunt, M. S.; Cloeckart, A.; De Bolle, X.; Letesson, J. J., The two-component system PrlS/PrIR of *Brucella melitensis* is required for persistence in mice and appears to respond to ionic strength. *Microbiology* 2012, 158 (Pt 10), 2642-51.
13. Dubrac, S.; Bisicchia, P.; Devine, K. M.; Msadek, T., A matter of life and death: cell wall homeostasis and the WalkR (YycGF) essential signal transduction pathway. *Molecular microbiology* 2008, 70 (6), 1307-22.
14. Casino, P.; Rubio, V.; Marina, A.
15. Casino, P.; Rubio, V.; Marina, A., Structural insight into partner specificity and phosphoryl transfer in two-component signal transduction. *Cell* 2009, 139 (2), 325-36.
16. Bick, M. J.; Lamour, V.; Rajashankar, K. R.; Gordiyenko, Y.; Robinson, C. V.; Darst, S. A., How to switch off a histidine kinase: crystal structure of *Geobacillus stearothermophilus* KinB with the inhibitor Sda. *Journal of molecular biology* 2009, 386 (1), 163-77.
17. Bilwes, A. M.; Quezada, C. M.; Croal, L. R.; Crane, B. R.; Simon, M. I., Nucleotide binding by the histidine kinase CheA. *Nat Struct Biol* 2001, 8 (4), 353-60.

18. Verdonk, M. L.; Cole, J. C.; Hartshorn, M. J.; Murray, C. W.; Taylor, R. D., Improved protein-ligand docking using GOLD. *Proteins* 2003, 52 (4), 609-23.
19. Korb, O.; Stutzle, T.; Exner, T. E., Empirical scoring functions for advanced protein-ligand docking with PLANTS. *Journal of chemical information and modeling* 2009, 49 (1), 84-96.
20. Ebejer, J. P.; Fulle, S.; Morris, G. M.; Finn, P. W., The emerging role of cloud computing in molecular modelling. *Journal of molecular graphics & modelling* 2013, 44, 177-87.
21. www.inhibox.com.
22. Hopkins, A. L.; Groom, C. R.; Alex, A., Ligand efficiency: a useful metric for lead selection. *Drug discovery today* 2004, 9 (10), 430-1.
23. RDKit: Open-source cheminformatics.
24. Rogers, D.; Hahn, M., Extended-connectivity fingerprints. *Journal of chemical information and modeling* 2010, 50 (5), 742-54.
25. Podgornaia, A. I.; Casino, P.; Marina, A.; Laub, M. T., Structural basis of a rationally rewired protein-protein interface critical to bacterial signaling. *Structure* 2013, 21 (9), 1636-47.
26. Marina, A.; Mott, C.; Auyzenberg, A.; Hendrickson, W. A.; Waldburger, C. D., Structural and mutational analysis of the PhoQ histidine kinase catalytic domain. Insight into the reaction mechanism. *The Journal of biological chemistry* 2001, 276 (44), 41182-90.
27. Christopoulos, H. M. a. A., *Fitting Models to Biological Data using Linear and Nonlinear Regression. A Practical Guide to Curve Fitting*. Oxford University Press: New York, 2004.
28. Sonnevend, A.; Blair, I.; Alkaabi, M.; Jumaa, P.; Al Haj, M.; Ghazawi, A.; Akawi, N.; Jouhar, F. S.; Hamadeh, M. B.; Pal, T., Change in methicillin-resistant *Staphylococcus aureus* clones at a tertiary care hospital in the United Arab Emirates over a 5-year period. *Journal of clinical pathology* 2012, 65 (2), 178-82.
29. Ziebuhr, W.; Krimmer, V.; Rachid, S.; Lossner, I.; Gotz, F.; Hacker, J., A novel mechanism of phase variation of virulence in *Staphylococcus epidermidis*: evidence for control of the polysaccharide intercellular adhesion synthesis by alternating insertion and excision of the insertion sequence element IS256. *Molecular microbiology* 1999, 32 (2), 345-56.
30. Sonnevend, A.; Ghazawi, A.; Al Munthari, N.; Pitout, M.; Hamadeh, M. B.; Hashmey, R.; Giris, S. K.; Sheikh, F. A.; Al Haj, M.; Nagelkerke, N.; Pal, T., Characteristics of epidemic and sporadic strains of *Acinetobacter baumannii* isolated in Abu Dhabi hospitals. *Journal of medical microbiology* 2013, 62 (Pt 4), 582-90.
31. Jumaa, P. A.; Sonnevend, A.; Pal, T.; El Hag, M.; Amith, R.; Trad, O., The molecular epidemiology of *Stenotrophomonas maltophilia* bacteraemia in a tertiary referral hospital in the United Arab Emirates 2000-2004. *Annals of clinical microbiology and antimicrobials* 2006, 5, 32.
32. Conlon, J. M.; Mechkarska, M.; Prajeep, M.; Sonnevend, A.; Coquet, L.; Leprince, J.; Jouenne, T.; Vaudry, H.; King, J. D., Host-defense peptides in skin secretions of the tetraploid frog *Silurana epittropicalis* with potent activity against methicillin-resistant *Staphylococcus aureus* (MRSA). *Peptides* 2012, 37 (1), 113-9.
33. CLSI, *Methods for dilution antimicrobial susceptibility tests for bacteria that grow aerobically*. CLSI: Wayne, PA, 2009; Vol. 8th ed. M7-A8.
34. Clinical Laboratory and Standards Institute *Methods for Antimicrobial Susceptibility Testing of Anaerobic Bacteria; Approved Standard*. M11-A7. 2007; Vol. 7th ed.

35. NCCLS, Methods for determining bactericidal activity of antimicrobial agents. NCCLS: Wayne, PA, 1999; Vol. M26-A.
36. Mechkarska, M.; Ahmed, E.; Coquet, L.; Leprince, J.; Jouenne, T.; Vaudry, H.; King, J. D.; Conlon, J. M., Antimicrobial peptides with therapeutic potential from skin secretions of the Marsabit clawed frog *Xenopus borealis* (Pipidae). *Comparative biochemistry and physiology. Toxicology & pharmacology* : CBP 2010, 152 (4), 467-72.
37. Repetto, G.; del Peso, A.; Zurita, J. L., Neutral red uptake assay for the estimation of cell viability/cytotoxicity. *Nature protocols* 2008, 3 (7), 1125-31.
38. Qin, Z.; Zhang, J.; Xu, B.; Chen, L.; Wu, Y.; Yang, X.; Shen, X.; Molin, S.; Danchin, A.; Jiang, H.; Qu, D., Structure-based discovery of inhibitors of the YycG histidine kinase: new chemical leads to combat *Staphylococcus epidermidis* infections. *BMC microbiology* 2006, 6, 96.
39. Li, N.; Wang, F.; Xu, W.; Wang, H.; Luo, X.; Zhu, W.; Yin, Y.; Zhang, X., [Histidine kinase (YycG) protein of *Streptococcus pneumoniae*: homology modeling and analysis]. *Sheng wu gong cheng xue bao = Chinese journal of biotechnology* 2009, 25 (2), 207-14.
40. Cai, X.; Zhang, J.; Chen, M.; Wu, Y.; Wang, X.; Chen, J.; Zhang, J.; Shen, X.; Qu, D.; Jiang, H., The effect of the potential PhoQ histidine kinase inhibitors on *Shigella flexneri* virulence. *PLoS one* 2011, 6 (8), e23100.
41. Francis, S.; Wilke, K. E.; Brown, D. E.; Carlson, E. E., Mechanistic insight into inhibition of two-component system signaling. *MedChemComm* 2013, 4 (1), 269-277.
42. Marina, A.; Waldburger, C. D.; Hendrickson, W. A., Structure of the entire cytoplasmic portion of a sensor histidine-kinase protein. *The EMBO journal* 2005, 24 (24), 4247-59.
43. Mohedano, M. L.; Overweg, K.; de la Fuente, A.; Reuter, M.; Altabe, S.; Mulholland, F.; de Mendoza, D.; Lopez, P.; Wells, J. M., Evidence that the essential response regulator YycF in *Streptococcus pneumoniae* modulates expression of fatty acid biosynthesis genes and alters membrane composition. *Journal of bacteriology* 2005, 187 (7), 2357-67.
44. Stumpfe, D.; Bajorath, J., Exploring activity cliffs in medicinal chemistry. *Journal of medicinal chemistry* 2012, 55 (7), 2932-42.
45. Turton, J. F.; Woodford, N.; Glover, J.; Yarde, S.; Kaufmann, M. E.; Pitt, T. L., Identification of *Acinetobacter baumannii* by detection of the bla_{OXA-51}-like carbapenemase gene intrinsic to this species. *Journal of clinical microbiology* 2006, 44 (8), 2974-6.
46. Turton, J. F.; Gabriel, S. N.; Valderrey, C.; Kaufmann, M. E.; Pitt, T. L., Use of sequence-based typing and multiplex PCR to identify clonal lineages of outbreak strains of *Acinetobacter baumannii*. *Clinical microbiology and infection : the official publication of the European Society of Clinical Microbiology and Infectious Diseases* 2007, 13 (8), 807-15.
47. Guarnieri, M. T.; Zhang, L.; Shen, J.; Zhao, R., The Hsp90 inhibitor radicicol interacts with the ATP-binding pocket of bacterial sensor kinase PhoQ. *Journal of molecular biology* 2008, 379 (1), 82-93.
48. Casino, P.; Miquel-Romero, L.; Marina, A., Visualizing autophosphorylation in histidine kinases. *Nat Commun* 2014.
49. O'Shea, R.; Moser, H. E., Physicochemical properties of antibacterial compounds: implications for drug discovery. *Journal of medicinal chemistry* 2008, 51 (10), 2871-8.
50. Rasko, D. A.; Moreira, C. G.; Li de, R.; Reading, N. C.; Ritchie, J. M.; Waldor, M. K.; Williams, N.; Taussig, R.; Wei, S.; Roth, M.; Hughes, D. T.; Huntley, J. F.; Fina, M. W.; Falck, J. R.; Sperandio, V., Targeting QseC signaling and virulence for antibiotic development. *Science* 2008, 321 (5892), 1078-80.

51. Gotoh, Y.; Eguchi, Y.; Watanabe, T.; Okamoto, S.; Doi, A.; Utsumi, R., Two-component signal transduction as potential drug targets in pathogenic bacteria. *Current opinion in microbiology* 2010, 13 (2), 232-9.
52. Watanabe, T.; Okada, A.; Gotoh, Y.; Utsumi, R., Inhibitors targeting two-component signal transduction. *Advances in experimental medicine and biology* 2008, 631, 229-36.
53. Gilmour, R.; Foster, J. E.; Sheng, Q.; McClain, J. R.; Riley, A.; Sun, P. M.; Ng, W. L.; Yan, D.; Nicas, T. I.; Henry, K.; Winkler, M. E., New class of competitive inhibitor of bacterial histidine kinases. *Journal of bacteriology* 2005, 187 (23), 8196-200.
54. Tanaka, T.; Saha, S. K.; Tomomori, C.; Ishima, R.; Liu, D.; Tong, K. I.; Park, H.; Dutta, R.; Qin, L.; Swindells, M. B.; Yamazaki, T.; Ono, A. M.; Kainosho, M.; Inouye, M.; Ikura, M., NMR structure of the histidine kinase domain of the E. coli osmosensor EnvZ. *Nature* 1998, 396 (6706), 88-92.
55. Dutta, R.; Qin, L.; Inouye, M., Histidine kinases: diversity of domain organization. *Molecular microbiology* 1999, 34 (4), 633-40.
56. Li, Y.; Kim, D. J.; Ma, W.; Lubet, R. A.; Bode, A. M.; Dong, Z., Discovery of novel checkpoint kinase 1 inhibitors by virtual screening based on multiple crystal structures. *Journal of chemical information and modeling* 2011, 51 (11), 2904-14.
57. Korb, O.; Olsson, T. S.; Bowden, S. J.; Hall, R. J.; Verdonk, M. L.; Liebeschuetz, J. W.; Cole, J. C., Potential and limitations of ensemble docking. *J. Chem. Inf. Model.* 2012, 52 (5), 1262-1274.
58. Hawkins, P. C.; Warren, G. L.; Skillman, A. G.; Nicholls, A., How to do an evaluation: pitfalls and traps. *Journal of computer-aided molecular design* 2008, 22 (3-4), 179-90.
59. Mas, N.; Galiana, I.; Mondragon, L.; Aznar, E.; Climent, E.; Cabedo, N.; Sancenon, F.; Murguia, J. R.; Martinez-Manez, R.; Marcos, M. D.; Amoros, P., Enhanced efficacy and broadening of antibacterial action of drugs via the use of capped mesoporous nanoparticles. *Chemistry* 2013, 19 (34), 11167-71.
60. Bolla, J. M.; Alibert-Franco, S.; Handzlik, J.; Chevalier, J.; Mahamoud, A.; Boyer, G.; Kiec-Kononowicz, K.; Pages, J. M., Strategies for bypassing the membrane barrier in multidrug resistant Gram-negative bacteria. *FEBS letters* 2011, 585 (11), 1682-90.
61. Shoemaker, R. H., The NCI60 human tumour cell line anticancer drug screen. *Nature reviews. Cancer* 2006, 6 (10), 813-23.
62. Boyd, M., The NCI In Vitro Anticancer Drug Discovery Screen. In *Anticancer Drug Development Guide*, Teicher, B., Ed. Humana Press: 1997; pp 23-42.
63. Tettelin, H.; Nelson, K. E.; Paulsen, I. T.; Eisen, J. A.; Read, T. D.; Peterson, S.; Heidelberg, J.; DeBoy, R. T.; Haft, D. H.; Dodson, R. J.; Durkin, A. S.; Gwinn, M.; Kolonay, J. F.; Nelson, W. C.; Peterson, J. D.; Umayam, L. A.; White, O.; Salzberg, S. L.; Lewis, M. R.; Radune, D.; Holtzapple, E.; Khouri, H.; Wolf, A. M.; Utterback, T. R.; Hansen, C. L.; McDonald, L. A.; Feldblyum, T. V.; Angiuoli, S.; Dickinson, T.; Hickey, E. K.; Holt, I. E.; Loftus, B. J.; Yang, F.; Smith, H. O.; Venter, J. C.; Dougherty, B. A.; Morrison, D. A.; Hollingshead, S. K.; Fraser, C. M., Complete genome sequence of a virulent isolate of *Streptococcus pneumoniae*. *Science* 2001, 293 (5529), 498-506.
64. Wang, Y.; Li, D.; Song, L.; Liu, Y.; He, T.; Liu, H.; Wu, C.; Schwarz, S.; Shen, J., First report of the multiresistance gene *cfr* in *Streptococcus suis*. *Antimicrobial agents and chemotherapy* 2013, 57 (8), 4061-3.

SUPPLEMENTARY MATERIAL CHAPTER 2

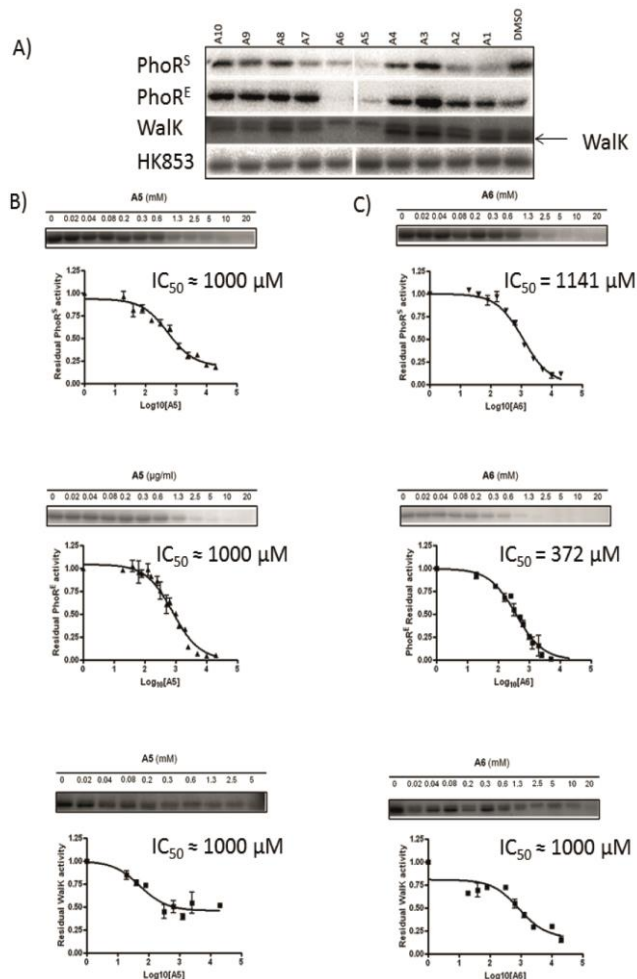


Figure S1. Autophosphorylation inhibitory activity of the initial hits from the SBVS. (A) One-time (30 sec) one-concentration (5 mM) kinase assay with the SBVS hits and PhoS, PhoR^E, WaK and HK853 distinguished A5 and A6 as relatively stronger multiple HKs autophosphorylation inhibitors. The IC₅₀ for PhoS, PhoR^E and WaK in presence of A5 (B) and A6 (C) were calculated from the autophosphorylation reaction assays at different concentrations of compounds. Error bars represent the standard errors of the mean (SEM) of two independent assays with two replicates.

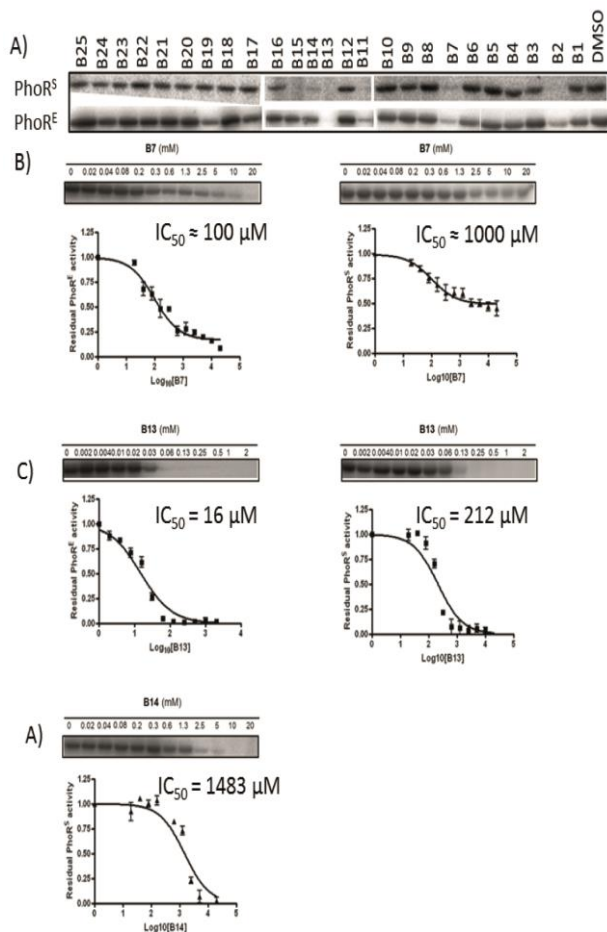


Figure S2 Autophosphorylation inhibitory activity of the LBSS hits. (A) One-time point (30 sec), one-concentration (2 mM) kinase assay with the LBVS hits and PhoR^S and PhoR^E HKs. The IC₅₀ for PhoR^S and PhoR^E in presence of B7 (B), B13 (C) and B14 (D) were calculated from the autophosphorylation reaction assays at different concentrations of compounds. Error bars represent the standard errors of the mean (SEM) of two independent assays with two replicates.

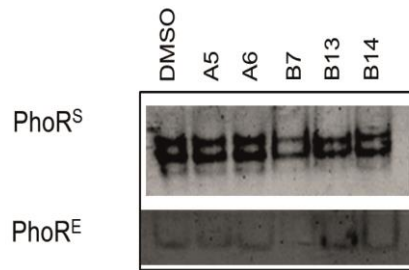


Figure S3. Native PAGE-based aggregation analysis of five inhibitors. A5 and A6 (5 mM), and B7, B13 and B14 (2 mM) do not cause HK aggregation as demonstrated by native-PAGE with PhoR^S and PhoR^E HKs.

Table S1. Selected compounds for experimental testing from SBVS (A1 to A10) and LBSS (B1 to B17)

Name	Provider's Name	Smile
A1	PB-02322356	<chem>O=C(CCN1C2=C(SC3=C1C=CC=C3)C=CC=C2)OCC1=CC(=O)N2C=CSC2=N1</chem>
A2	PB-04723907	<chem>CC(OC(=O)C1=CC(=CC=C1)S(=O)(=O)N1CCC2=C(C1)C=CC=C2)C(=O)NC(N)=O</chem>
A3	PB404910184	<chem>CC(NC(=O)C1CN(C(=O)C1)C1=CC=CC=C1)C1=CC(NC(=O)C2=CC=CC=C2)=CC=C1</chem>
A4	PB-06200251	<chem>CNC(=O)NC(=O)CSC1=NC2=C(C3=C(CCCC3)S2)C(=O)N1C1=C(F)C=CC=C1</chem>
A5	BBV-129624	<chem>CCC(NC1=CC(NC(C)=O)=CC=C1)C1=CC=C(F)C=C1</chem>
A6	BBV-174972	<chem>CC(NCC1=CC(Br)=CC=C1)C1=CC(NC(C)=O)=CC=C1</chem>
A7	BBV-129155	<chem>C(NC1=CC2=C(OCCO2)C=C1)C1=CC2=C(C=CC=C2)C=C1</chem>
A8	BBV-34226801	<chem>CC(NCC1=C2C=CC=CC2=CC=C1)C1=CC=C(F)C=C1</chem>
A9	BBV-34226813	<chem>CC(NCC1=C2C=CC=CC2=CC=C1)C1=CC(F)=CC=C1</chem>
A10	BBV-203039	<chem>CC(NCC1=CC(F)=CC=C1)C1=CC2=C(C=CC=C2)C=C1</chem>
B1	310269	<chem>CCN(CC1=CC=C(C=C1)C(=O)OC)C2=CC(=CC=C2)NC(C)=O</chem>
B2	73090	<chem>CC(=O)NC1=CC=C(C=C1)C2=CC=C(F)C=C2</chem>
B3	214040	<chem>CC(=O)NC1=CC=C(NC(=O)C2=CC(=CC=C2)F)C=C1</chem>
B4	86683	<chem>CC(=O)NC1=CC(=CC=C1)CC2=CC(=CC=C2)NC(C)=O</chem>
B5	400630	<chem>CC(=O)NC1=C[N+](=CC=C1)CC(=O)C2=CC=C(F)C=C2</chem>
B6	4288	<chem>CC(=O)NC1=CC=C(C=C1)C(O)C2=CC=C(NC(C)=O)C=C2</chem>
B7	109741	<chem>CC(=O)NC1=CC(=CC=C1)C2=C(Cl)C=CC=C2</chem>
B8	211557	<chem>CC(=O)NC1=CC(=CC=C1)OCC2=CC=C(C=C2)[N](=O)=O</chem>
B9	85756	<chem>CC(=O)NC1=CC(=CC=C1)[S](=O)(=O)C2=CC(=CC=C2)NC(C)=O</chem>
B10	12323	<chem>CC(=O)NC1=CC2=C(C=C1)C3=CC=CC=C3C2=NC4=CC=C(F)C=C4</chem>
B11	211552	<chem>CC(=O)NC1=CC(=CC=C1)C=CC2=CC=C(C=C2)[N](=O)=O</chem>
B12	106213	<chem>CC(=O)NC1=CC=C(C=C1)C(O)C(=O)C2=CC=C(NC(C)=O)C=C2</chem>
B13	32652	<chem>CCC(C(CC)C1=CC=C(F)C=C1)C2=CC=C(O)C=C2</chem>
B14	48154	<chem>CC(C)(C)C1=CC(=C(O)C=C1)CNC2=CC=CC=C2</chem>
B15	7436	<chem>CC(C)(C)C1=CC=C(N[S](=O)(=O)C2=CC=C(N)C=C2)C=C1</chem>
B16	211556	<chem>CC(=O)NC1=CC(=CC=C1)OCOC2=CC=C(C=C2)[N](=O)=O</chem>
B17	107560	<chem>CC(=O)NC1=CC(=CC=C1)OCC2=CC(=CC=C2)[N](=O)=O</chem>

Table S1 (continued). Selected compounds for experimental testing from LBSS (B18 to B25)

Name	Provider's	
	Name	Smile
B18	118968	<chem>COC1=C(NC(C)=O)C=CC(=C1)NCC2=CC=CC=C2</chem>
B19	408367	<chem>CC(=O)NC(CC1=CC=CC=C1)C(=O)NC2=CC(=CC=C2)C</chem>
B20	68235	<chem>CC(=O)NC1=CC2=C(C=C1)C3=CC=C(Br)C=C3C2</chem>
B21	408365	<chem>CC(=O)NC(CC1=CC=CC=C1)C(=O)NC2=CC(=CC=C2)Cl</chem>
B22	205456	<chem>ClC1=CC=CC(=C1)CNC(=O)NC2=CC=CC=C2</chem>
B23	130858	<chem>CCC(C(C(C)=O)C1=CC=C(OC)C=C1)C2=CC(=CC=C2)Br</chem>
B24	67710	<chem>CC[N]1C2=C(C=CC=C2)C3=C1C=CC(=C3)NC(C)=O</chem>
B25	205718	<chem>CN(CC1=CC=CC=C1)C(=O)NC2=CC=CC(=C2)C(C)=O</chem>

Table S2. Compounds selected from SBVS and their corresponding ChemPLP and ligand efficiency.

Initial hits		Docking score [¥]
Name	ChemPLP	Ligand efficiency
ADP	85.4	3.16
A1	95.12	3.171
A2	96.14	3.214
A3	93.48	2.918
A4	97.21	3.24
A5	82	3.905
A6	80.38	3.828
A7	84.21	3.828
A8	80.11	3.815
A9	81.97	3.903
A10	82.15	3.912

¥ The values for HK853 (PDB: 3DGE, chain A) are presented

Table S3 Bacterial strains

Strain	Source	Resistance
<i>Staphylococcus aureus</i> DSM 20231	DSMZ – German Collection of Microorganisms and Cell culture	Control strain
<i>S. aureus</i> 25293	ATCC	Control strain
<i>S. aureus</i> 274/08 ²⁸	Tawam Hospital, Al Ain, UAE	β-lactams, Ka, Ne, C, E
<i>S. aureus</i> V4180 ²⁸	Tawam Hospital, Al Ain, UAE	β-lactams, A, G, Ka, Ne, S, Sxt, Tet, C, Rif, E, Cl
<i>S. aureus</i> T4/6 ²⁸	Tawam Hospital, Al Ain, UAE	β-lactams, Ka, Ne, C, E, Cl
<i>S. aureus</i> 145/08 ²⁸	Tawam Hospital, Al Ain, UAE	β-lactams, Ka, Ne, S, Tet, Fu
<i>S. aureus</i> 127/08 ²⁸	Tawam Hospital, Al Ain, UAE	β-lactams
<i>S. aureus</i> S908 ²⁸	Tawam Hospital, Al Ain, UAE	β-lactams, C, E, Cl
<i>Staphylococcus epidermidis</i> DSM 20044	DSMZ – German Collection of Microorganisms and Cell culture	Control strain
<i>S. epidermidis</i> RP62A (biofilm producer) ²⁹	ATCC	Control strain
<i>S. epidermidis</i> RP62A/1 (non-biofilm producer) ²⁹	ATCC	Control strain
<i>S. epidermidis</i> T7/3	Tawam Hospital, Al Ain, UAE	
<i>S. epidermidis</i> T37/8	Tawam Hospital, Al Ain, UAE	
<i>S. epidermidis</i> T61/9	Tawam Hospital, Al Ain, UAE	
<i>Streptococcus pneumoniae</i> DP1004		Control strain
<i>S. pneumoniae</i> TIGR4 ⁶³		Control strain
<i>S. pneumoniae</i> ATCC 49619	ATCC	Control strain
<i>Streptococcus suis</i> 3881/ S10 ⁶⁴	CVI, Lelystad	
<i>Acinetobacter baumannii</i> NM109 ³⁰	Hospitals in Abu Dhabi Emirate, UAE	All antibiotics commonly used to treat <i>Acinetobacter</i> infections
<i>A. baumannii</i> NM8 ³⁰	Hospitals in Abu Dhabi Emirate, UAE	All antibiotics commonly used to treat <i>Acinetobacter</i> infections
<i>A. baumannii</i> NM35 ³⁰	Hospitals in Abu Dhabi Emirate, UAE	All antibiotics commonly used to treat <i>Acinetobacter</i> infections
<i>A. baumannii</i> NM75 ³⁰	Hospitals in Abu Dhabi Emirate, UAE	All antibiotics commonly used to treat <i>Acinetobacter</i> infections

Talbe S3 (continued). Bacterial strains

Strain	Source	Resistance
<i>Stenotrophomonas maltophilia</i> B5/5 ³¹	Tawam Hospital, Al Ain, UAE	meropenem
<i>S. maltophilia</i> B6/2 ³¹	Tawam Hospital, Al Ain, UAE	meropenem
<i>S. maltophilia</i> B32/1 ³¹	Tawam Hospital, Al Ain, UAE	meropenem
<i>Escherichia coli</i> CFT 073	ATCC	Control strain
<i>E. coli</i> 25276	ATCC	Control strain
<i>Klebsiella pneumoniae</i> 700603	ATCC	Control strain
<i>Pseudomonas aeruginosa</i> 27853	ATCC	Control strain

*A, amikacin; C, ciprofloxacin; Cl, clindamycin; E, erythromycin; Fu, fusidic acid; G, gentamycin; Ka, kanamycin; Ne, neomycin; Rif, rifampicin; S, streptomycin; Sxt, sulfamethoxazole+trimethoprim; Tet, tetracycline.

Chapter 3

HISTIDINE-KINASE INHIBITORS WITH BROAD-SPECTRUM ANTIBACTERIAL EFFECT IDENTIFIED BY FRAGMENT-BASED SCREENS

Nadya Velikova¹, Simone Fulle², Ana Sousa Manso^{3, 4}, Milena Mechkarska⁵, Nico Taverne⁶, Paul Finn², J. Michael Conlon⁵, Marco Rinaldo Oggioni^{3, 4}, Jerry M. Wells⁶, Alberto Marina^{1, 7}.

¹Instituto de Biomedicina de Valencia, Consejo Superior de Investigaciones Científicas (CSIC), Jaime Roig 11, 46010 Valencia, Spain;

²InhibOx Limited, Oxford, OX1 1BY, United Kingdom;

³Dipartimento di Biotecnologie Mediche, Università di Siena, 53100 Siena, Italy;

⁴Department of Genetics, University of Leicester, Leicester, Le1 7RH, United Kingdom;

⁵Department of Biochemistry, College of Medicine and Health Science, United Arab Emirates University, P.O. Box 17666 Al Ain, United Arab Emirates;

⁶Host-Microbe Interactomics Chair Group, Animal Sciences, University of Wageningen, P.O. Box 338, 6700 AH Wageningen, The Netherlands;

⁷CIBER de Enfermedades Raras (CIBERER), ISCIII, Valencia, Spain

SUBMITTED TO EUROPEAN JOURNAL OF MEDICINAL CHEMISTRY

2014

ABSTRACT

Novel antibacterials are urgently needed to address the growing problem of bacterial resistance to conventional antibiotics. Two-component systems (TCS) have been previously proposed as promising antibacterial targets. TCS are widely used by bacteria to regulate gene expression in response to various environmental stimuli and physiological stress. They consist of a response regulator and a histidine kinase (HK) containing a highly conserved ATP-binding site that could be a good target for broad spectrum antibacterial drugs. Here we describe fragment-based screens using differential scanning fluorimetry and virtual ligand-based similarity searches that yielded HK autophosphorylation inhibitors with antibacterial effect against multi-drug resistant clinical isolates.

Keywords: antibacterials, histidine kinase autophosphorylation inhibitors, fragment-based screening, two-component systems

Abbreviations: TCS – two-component system/s; HK- histidine kinase; RR – response regulator; FBS – fragment-based screening; LBSS – ligand-based similarity search; DSF – differential scanning fluorimetry

INTRODUCTION

Bacterial two-component systems (TCS) are signal transduction systems used by nearly all bacteria. TCS regulate a variety of processes including bacterial growth, cell-wall metabolism, virulence, biofilm formation and resistance to antibiotics¹. A prototypical TCS consist of a membrane bound histidine kinase (HK) and its cognate response regulator (RR)². Upon sensing an environmental stimulus the HK is autophosphorylated on conserved histidine residues in the dimerization and histidine phosphotransfer (DHp) domain. Subsequently, the phosphoryl group from the His is transferred to a conserved aspartic acid residue in the receiver (REC) domain of the RR. The phosphorylated state of the RR affects its binding affinity to a cognate DNA motif and/or other protein partners thereby modulating transcription of target genes². Inhibitors of HK autophosphorylation targeted at the nucleotide binding site of the catalytic and ATP-binding (CA) domains of HKs are expected to simultaneously inhibit multiple TCS due to the conservation between HKs CA domains (Figure S1). Here we describe the step-wise application of fragment-based screenings (FBS) by differential scanning fluorimetry (DSF)³ and ligand-based similarity searches (LBSS)⁴ to identify HKs autophosphorylation inhibitors with antibacterial activity against multi-drug resistant clinical isolates (Figure 1).

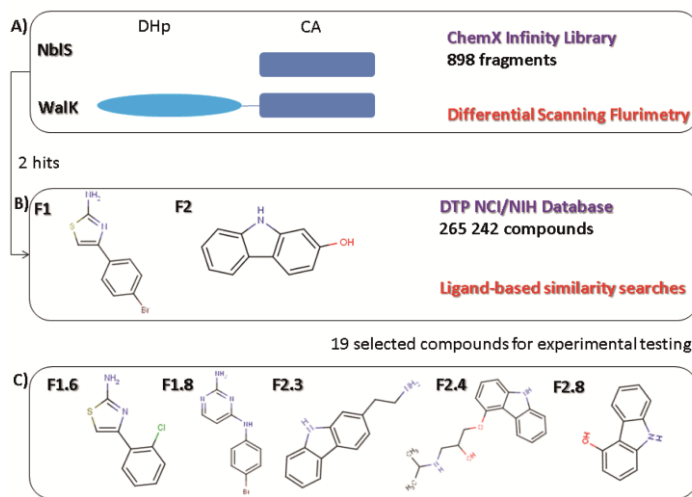


Figure 1. Histidine kinase autophosphorylation inhibitors with antibacterial effect for multi-drug resistant Gram-positive and Gram-negative bacteria were identified by the following workflow (A): First, a fragment library was screened for ligands of both the CA domain

of *Synechococcus sp.* PCC 7942 NbIS and CA and DHp domains of *Streptococcus pneumoniae* Walk. (B) The two hits in common (F1 and F2) were used as query molecules in a ligand-based similarity search of the National Cancer Institute Developmental Therapeutics Programme Database and 19 compounds (Figure S5) were selected for experimental testing. (C) 5 of the 19 tested fragments and F1 inhibited *S. pneumoniae* Walk and *E. coli* PhoR autophosphorylation and showed an antibacterial effect against Gram-positive or both Gram-positive and Gram-negative bacteria (Table 1)

Table 1. Antibacterial activities of selected fragments for a panel of clinical isolates and reference strains.

Strain	MIC ($\mu\text{g/mL}$)					
	F1	F1.6	F1.8	F2.3	F2.4	F2.8
<i>Staphylococcus aureus</i>						
20231	25	125	125	125	250	31
25293	125	250	250	125	125	250
274/08	125	500	250	>500	500	250
V4180	125	>500	250	250	500	250
T4/6	125	250	250	250	>500	250
145/08	125	250	250	250	250	250
127/08	n.d	250	250	250	500	250
S908	n.d	500	250	250	500	n.d.
<i>Staphylococcus epidermidis</i>						
20044	4	500	63	31	500	31
RP62A	>500	>500	500	125	> 500	250
RP62A/1	250	>500	250	125	n. d.	250
T7/3	63	125	31	31	n. d.	63
T37/8	>500	>500	500	125	n. d.	250
T6119	>500	>500	250	125	n. d.	250
<i>Streptococcus suis</i>						
3881/ S10	>500 ^a	>500	250	>500	250	125
<i>Streptococcus pneumoniae</i>						
49619	n. d.	256	128	4	64	n. d.
<i>Acinetobacter baumannii</i>						
NM109	n. d.	n. d.	125	n. d.	500	n. d.
NM124	n. d.	n. d.	125	n. d.	500	n. d.
NM8	>500	>500	125	>500	500	>500
NM35	n. d.	n. d.	125	n. d.	>500	n. d.
NM75	n. d.	n. d.	250	n. d.	>500	n. d.
<i>Stenotrophomonas maltophilia</i>						
B5/5	n. d.	n. d.	n. d.	n. d.	>500	n. d.
B6/2	n. d.	n. d.	n. d.	n. d.	500	n. d.
B32/1	>500	>500	>500	>500	500	>500

Table 1 (continued).

Strain	MIC ($\mu\text{g/mL}$)					
	F1	F1.6	F1.8	F2.3	F2.4	F2.8
<i>Escherichia coli</i>						
CFT 073	>500	>500	250	>500	500	63
ATCC 25276	>500	>500	250	>500	500	500
<i>Klebsiella pneumoniae</i>						
ATCC700603	>500	>500	250	>500	>500	250
<i>Pseudomonas aeruginosa</i>						
ATCC 27853	>500	>500	500	>500	>500	>500

n.d. - not tested

MATERIALS AND METHODS

REAGENTS

A fragment library of 898 compounds (>95% purity) was purchased from Chem-X-Infinity (Romanville, France) and the individual compounds were stored at -80°C at a concentration of 20 mM. For screening purposes cocktails of 10 compounds at final concentrations of 2 mM were prepared in a 96-well-plate. Re-supply of compounds F2 and F2.5 to F2.9 (Table S2) were purchased from Sigma-Aldrich (Spain). Re-supply of F1 was purchased from Apolo Scientific (United Kingdom). Compounds F1.1 to F1.10 and F2.1 to F2.3 (Table S2) were obtained from Developmental Therapeutics program of the National Cancer Institute and the National Institute of Health (DTP NCI/NIH). γ -³²P-ATP was purchased from Perkin Elmer.

CLONING, EXPRESSION AND PURIFICATION

S. pneumoniae *walk* encoding the catalytic portion (DHp and CA domain) of Walk (amino acids from 208 to 449) was amplified by PCR from *S. pneumoniae* CDC3059-06 genomic DNA using the following primers: forward 5'-aagttctgtttcagggcccgatggagcaggagaaggaagaacgc-3' and reverse 5'-atggtctagaagctctagcttctacttcatccac-3'. The PCR product was purified by PCR product purification kit (Macherey-Nagel) and cloned into a gel-purified pOpinF vector (kindly provided by Nick Berow, IRB, Spain) linearized with KpnI and HindIII (Fermentas). The insert was cloned into the pOpinF vector with InFusion HD cloning system (Clontech). Positive clones were confirmed by colony PCR and DNA sequencing.

S. pneumoniae Walk (Walk) was expressed in *E. coli* RIL. Luria Broth (LB) media supplemented with 100 µg/mL ampicillin and 33 µg/mL chloramphenicol was inoculated with an overnight pre-culture (1/50 of the culture volume). At exponential phase (OD₆₀₀ 0.2 – 0.4) protein expression was induced by addition of 1 mM IPTG for 3 to 5 h at 37°C. The cells were harvested by centrifugation at 4000 g, 4°C for 25 min and the pellets were stored at -80°C until use. The cell pellets were resuspended in lysis buffer (100 mM Tris pH 8.0, 150 mM NaCl, 0.1 mM PMSF) and sonicated at 4°C for 5 min at pulses of 15 sec every 1 minute. The cell debris and the supernatant were separated by centrifugation at 11 000 g, 4°C for 60 min. The cell debris were resuspended in equilibration buffer (100 mM Tris pH 8.0, 150 mM NaCl) containing 2M urea and incubated overnight at 4°C with rotation. After centrifugation at 11 000 g, the supernatant was injected into a Ni-affinity chromatography column (GE Healthcare) equilibrated with equilibration buffer, washed with 5 volumes of equilibration buffer and eluted with equilibration buffer containing 0.5 M imidazole. Walk was concentrated with AmiconUltra (Millipore, USA) centrifugal filters, aliquoted and stored at -80°C until use. The yield was ≤ 0.5 mg/L culture.

The catalytic portion (DHp and CA domain) of *E. coli* PhoR (PhoR^E), *E. coli* EnvZ, and *S. aureus* PhoR, and the CA domain of *Synechococcus sp.* PCC 7942 NblS were expressed and purified as previously described^{5, 6, 7, 8}. Shortly, proteins were expressed in *E. coli* RIL and purified by Ni-affinity and size-exclusion chromatography.

Purified proteins were stored in 20 – 50 µl aliquots at -80°C.

DIFFERENTIAL SCANNING FLUORIMETRY

To monitor protein unfolding, the fluorescent dye Sypro orange was used⁹. Differential scanning fluorimetry experiments (DSF) were conducted in the iCycleriQ Real Time Detection System (Bio-Rad, Hercules, CA). Solutions of 20 µl of 0.1 mg/mL protein (final concentration), 200 µM fragment cocktails or individual fragments (final concentration), 10X sypro orange (final concentration) and buffer (100 mM TrisCl pH 8, 150 mM NaCl) were added to the wells of the 96-well iCycler iQ PCR plate. The plate was heated from 20 to 85 or 99 °C at a heating rate of 1 °C/min. The fluorescent intensity was measured with Ex/Em: 490/530 nm. Prism GraphPad was used for curve fitting and statistical analysis¹⁰.

KINASE ASSAY

To evaluate the inhibitory capacity of selected hits from DSF and LBSS *in vitro* autophosphorylation kinase assays with γ -³²P-ATP was performed as previously described¹¹. Ligands were dissolved in 100% DMSO. When comparing the inhibitory capacity of ligands in one concentration-one time point experiments or when measuring IC₅₀ (the concentration at which 50% residual HK autophosphorylation activity is observed), the final DMSO concentration in the assay was 10% (v/v). Controls lacking ligands contained an equal concentration of DMSO. Inhibition of autophosphorylation was determined by incubating 0,12 mg/mL (\approx 4 µM) HK and up to 20 mM fragment in kinase buffer (50 mM Tris HCl, pH 8.5, 50 mM KCl, 5 mM MgCl₂, 0.5 mM EDTA and 0.1 mM DTT). Autophosphorylation reactions were initiated by addition of 0.1 µCi/µl γ -³²P-ATP containing from 0.03 to 0.06 µM ATP (final concentrations). Autophosphorylation was quenched with 2xSDS-PAGE sample buffer supplemented with 50 mM EDTA. Samples were applied without heating to 15% (w/v) Tris-glycine SDS-polyacrylamide gels. After electrophoresis, the bottoms of the gels were removed to lower the background from the unincorporated radiolabeled ATP. Gels were dried without staining on a Bio-Rad Gel Air drying system and the phosphorylated protein was quantified by phosphor-imaging. Prism GraphPad was used for curve fitting and statistical analysis¹⁰.

AGGREGATION ANALYSIS BY NATIVE POLYACRYLAMIDE GEL ELECTROPHORESIS

E. coli PhoR and EnvZ, and *S. aureus* PhoR (0.12 µg/mL, final concentration) were prepared in kinase buffer. F1 and F2 were added to a final concentration of 2 mM. DMSO in the assays was maintained to a final concentration 10% (v/v). After 30 min of incubation at room temperature native polyacrylamide gel electrophoresis (native-PAGE) loading buffer was added and samples loaded. Coomassie blue staining was used for protein visualization.

LIGAND-BASED SIMILARITY SEARCH

The database from the National Cancer Institute (NCI) was searched for analogous structures of the F1 and F2 as query molecules; the similarity search was performed using the Morgan fingerprint as implemented in RDKit¹², which is a variation of the ECFP “extended connectivity fingerprints”^{4, 13}. The top 100 compounds of each similarity search were visually inspected of which in total 14 compounds were selected and experimentally tested.

ANTIBACTERIAL SUSCEPTIBILITY TESTING

Bacterial strains used in this study for antibacterial susceptibility testing (Table S3, Chapter 1) were propagated using standard microbiological procedures. Minimal inhibitory concentrations (MICs) were determined following a standard double-dilution method^{14, 15}. MICs were recorded as the lowest concentration of the compound where no visible growth was observed. After plating the dilutions around the MIC or growing them in fresh MH media, minimal bactericidal concentration (MBC) was recorded as the lowest concentration of the compound at which no colonies were formed or no growth was observed, respectively. For *S. pneumoniae* MICs were determined by adapting the standard double-dilution method to anaerobic conditions and of this microorganism (use of Todd Hewitt Yeast extract with 200U/mL of catalase and continuous monitoring of growth)¹⁵. MBCs for *S. pneumoniae* were determined by inoculation of 10 µl from each well that did not shown visible bacterial growth on THY 0,5% 3% blood agar plates. After 24 h of incubation at 37°C 5% CO₂, the first dilution yielding three colonies or fewer was scored as the MBC, as described by the CLSI for starting inoculate of 1 x 10⁵ CFU/mL¹⁶.

HEMOLYSIS ASSAY

Hemolytic activity against human erythrocytes taken from a healthy donor was measured as previously described¹⁷. Erythrocytes were incubated with (up to) 500 µg/mL compounds and the LC₅₀ value was recorded as the mean concentration of compound producing 50% hemolysis in three independent incubations.

BINDING MODE PREDICTION

Docking calculations to predict the binding modes of the reported fragments were performed using the ATP-binding domain of HK853CD (PDB: 3DGE, chain A, residues from 270 to 415) and the GOLD docking software¹⁸. For each ligand 100 solutions were generated of which the top 20 were visually inspected. In Figure 2 the dominant binding mode within the top 20 solutions is shown for the respective ligand.

RESULTS AND DISCUSSION

To identify fragment-like ligands (MW < 300, ClogP < 3, number of hydrogen bond donors and hydrogen bond acceptors < 3, number of rotatable bonds < 3¹⁹) of the CA domains of HKs we used the Chem-X-Infinity library (Chem-X-Infinity, Romanville, France) comprising 898 fragments and differential scanning fluorimetry (DSF) as screening method³. As targets, we selected the HKs of two essential TCS, WalK-WalR of *Streptococcus pneumoniae* and NblS-RapB of *Synechococcus sp.* PCC 7942. The presence of 4-(4-bromophenyl)-1,3-thiazol-2-amine (F1) and 2-hydroxy-carbazole (F2) increased the temperature at which HK NblS (CA domain) unfolds (Tm) by 2.1 and 2.2 °C, respectively, suggesting that both F1 and F2 are ligands for the CA domain of NblS. Encouragingly, the screening for ligands of HK WalK (DHp and CA domain) showed that F1 and F2 were also among the hits increasing WalK Tm. F1 and F2 increased WalK Tm by 4.5 and 3.9 °C, respectively (Figure S2). Furthermore, *in vitro* kinase assays with γ -³²P-ATP showed that F1 and F2 inhibited the autophosphorylation of the screened catalytic portion of WalK. In addition, these compounds also inhibited the autophosphorylation of PhoR from the Gram-negative *Escherichia coli* (PhoR^E, Figure S3), suggesting a general HK inhibitory activity for F1 and F2.

Compound library screens have previously identified non-drug like inhibitors of HK autophosphorylation with an unspecific mechanism of action due to protein aggregation²⁰. However, even at high concentrations (up to 2 mM) F1 and F2 did not cause protein aggregation of the catalytic portions (DHp and CA domains) of *E. coli* PhoR, *E. coli* EnvZ or *S. aureus* PhoR as determined by native polyacrylamide gel electrophoresis (Figure S4).

In an attempt to identify more potent HK autophosphorylation inhibitors than F1 and F2, LBSS were performed using the Morgan fingerprint as implemented in RDKit^{4,7}, the National Cancer Institute Developmental Therapeutics Programme database (NCI/DTP) and F1 and F2 as query molecules. From the LBSS 14 compounds were selected plus 5 additional substituted carbazoles similar to F2, to a final pool of 19 compounds (Figure S5) that was evaluated for WalK and PhoR^E autophosphorylation inhibitory activity and antibacterial effect *in vitro*.

WalK and PhoR^E kinase assays with γ -³²P-ATP and the 19 compounds at one concentration (2 mM) and one time point (30 sec) showed that the fragments inhibited WalK and PhoR^E autophosphorylation activity compared to the negative control from 11 to 62% and 17 to 80%, respectively (Figure S3A). Only F1.6 inhibited WalK autophosphorylation by more than 50% at a concentration of 2 mM meaning that the remaining 18 of the tested compounds are weak (K_i >> 2 mM) WalK autophosphorylation inhibitors. Inhibition of PhoR^E autophosphorylation was greater than 50% for F1, F1.8, F2, F2.1, F2.2, F2.8 and F2.9 meaning that the remaining 12 of the tested compounds are weak PhoR^E autophosphorylation inhibitors. The IC₅₀ of the active compounds (F2.2. and F2.9 were excluded since they did not show antibacterial effect, see below) were measured in a multiple concentrations one time point (30 sec) PhoR^E kinase assays (Table 1, Figure S3B). F1 and F1.8 inhibited PhoR^E

autophosphorylation with $IC_{50} \approx 2$ mM and ≤ 1 mM, respectively, and the two compounds were not soluble in kinase buffer in the presence of 10% DMSO at concentrations higher than 1 mM (Table 1, Figure S3B). F2 and F2.1 inhibited PhoR^E autophosphorylation with IC_{50} values of 0.3 and 0.24 mM, respectively, and F2.8 inhibited PhoR^E autophosphorylation with an IC_{50} value of 0.72 mM (Table 1, Figure S2B). F2, F2.1 and F2.8 showed good solubility in kinase buffer in the presence of 10% DMSO.

The antibacterial effect of the 19 selected compounds was first studied by determining their minimal inhibitory concentrations (MICs) by standard micro-dilution antibacterial susceptibility testing²¹ for two Gram-positive (*Staphylococcus aureus* DSM 20231 and *Staphylococcus epidermidis* DSM 20044) and one Gram-negative (the uropathogenic *E. coli* CFT 073) strains (Table 1, Table S1, and Table S3, Chapter 1). The highest tested concentration was 500 $\mu\text{g}/\text{mL}$. F1, F1.6, F1.8, F2.3, F2.4 and F2.8 showed moderate antibacterial effects with MICs in the range of 31 to 250 $\mu\text{g}/\text{mL}$ for *S. aureus* DSM 20231 and 4 to 500 $\mu\text{g}/\text{mL}$ for *S. epidermidis* DSM 20044 (Table 1). Only F1.8 and F2.8 had antibacterial action on the Gram-negative *E. coli* CFT 073 with MICs < 250 $\mu\text{g}/\text{mL}$. With the exception of F2.2 and F2.9, those compounds showing HK autophosphorylation inhibitory activity also showed antibacterial activity, suggesting the possibility that the antibacterial activity might be mediated through the inhibition of HK autophosphorylation.

Next, we studied the antibacterial effect of F1, F1.6, F1.8, F2.3, F2.4 and F2.8 on a panel of clinical isolates and reference strains of pathogenic bacteria (Table S3, Chapter 1). The methicillin-resistant *S. aureus* (MRSA) strains are well characterized and are resistant to all β -lactam antibiotics and a range of non- β -lactam antibiotics²². *S. epidermidis* clinical isolates were obtained from wounds of patients admitted to Tawam Hospital (Al Ain, United Arab Emirates). The clinical isolates of the Gram-negative *Acinetobacter baumannii*²³ and *Stenotrophomonas maltophilia*²⁴ are well characterized and show multi-drug resistance. Additional reference strains included the Gram-positive *S. aureus* ATCC 25293, *S. epidermidis* RP62A and RP62A, *S. pneumoniae* 49619 and the emerging zoonotic pathogen *Streptococcus suis* 3881/S10, and the Gram-negative of *E. coli* ATCC 25276, *Klebsiella pneumoniae* ATCC 700603 and *Pseudomonas aeruginosa* ATCC 27853.

F1 and F1.6 (halogen-substituted phenyl-thiazoleamines) showed similar antibacterial activities for the panel of clinical isolates and reference strains. Both F1 and F1.6 showed antibacterial effect for the MRSA strains (with the exception of F1.6 for V4180 MRSA strain; Table 2) and *S. aureus* 25293 with MICs in the range of 125 – 500 $\mu\text{g}/\text{mL}$ (Table 2). The V4180 MRSA strain is resistant to a wider range of antibiotics compared to the other MRSA strains tested (Table S3, Chapter 1) including the small molecule antibiotics chloramphenicol and sulfamethoxazole. Given the broad range of antibiotic resistance of V4180 MRSA it is reasonable to propose that the presence of putative efflux pumps for small molecules could be responsible for the lack of susceptibility to F1.6. F1 and F1.6 showed antibacterial effect on one of the three tested *S. epidermidis* clinical isolates with MICs of 63 and 125 $\mu\text{g}/\text{mL}$, respectively. F1.6 MIC for *S. pneumoniae* 49619 was 256 $\mu\text{g}/\text{mL}$. F1 and F1.6 did not show antibacterial effect on *S. suis* 3881/S10 or on any of the Gram-negative strains tested.

F1.8 (bromophenyl-pyrimidinediamine) showed antibacterial effect on all the Gram-positive strains tested. F1.8 MICs for the *S. aureus* reference strains and the MRSA strains were in the range of 125 to 250 µg/mL. F1.8 MICs for the *S. epidermidis* strains were in the range of 31 to 500 µg/mL. F1.8 MICs for *S. suis* 3881/S10 and *S. pneumoniae* 49610 were 250 µg/mL and 128 µg/mL, respectively. F1.8 showed antibacterial effect for all the Gram-negative strains tested except for the *S. maltophilia* B32/1 strain. F1.8 MICs for *A. baumannii* strains, *E. coli* ATCC 25276 and *K. pneumoniae* ATCC 700603 were in the range of 125 – 250 µg/mL and the MIC for *P. aeruginosa* ATCC 27853 was 500 µg/mL. In a similar way to F1.6 with V4180 MRSA, the lack of susceptibility of *S. maltophilia* B32/1 to F1.8 could be explained by the presence of efflux pumps. *S. maltophilia* B32/1 is also resistant to the small-molecule β-lactam antibiotic, meropenem so that efflux pumps with broad substrate specificity may be involved²⁵.

The MICs of F2.3, F2.4 and F2.8 (substituted carbazoles) for the MRSA strains and *S. aureus* 25293 were in the range of 125 – 500 µg/mL. F2.3 and F2.8 MICs for the *S. epidermidis* strains were in the range of 31 – 250 µg/mL. F2.3 and F2.4 MICs for *S. pneumoniae* 49610 were 4 µg/mL and 64 µg/mL, respectively. F2.4 and F2.8 MICs for *S. suis* 3881/S10 were 125 and 250 µg/mL, respectively. F2.3 and F2.8 did not show antibacterial effect for the *A. baumannii* and *S. maltophilia* strains. F2.4 MICs for 3 of the 5 *A. baumannii* strains and 2 of the 3 *S. maltophilia* strains tested were 500 µg/mL. F2.4 and F2.8 MICs for *E. coli* ATCC 25276 were 500 µg/mL. F2.8 MIC for *K. pneumoniae* ATCC 700603 was 250 µg/mL. None of F2.3, F2.4 and F2.8 showed antibacterial effect for *P. aeruginosa* ATCC 27853.

One of the side effects of previously described TCS inhibitors is membrane damage²⁶. To exclude this mechanism of action we performed hemolysis experiments with erythrocytes from a healthy donor. None of the selected inhibitors (F1, F1.6, F1.8, F2.3, F2.4 and F2.8) caused erythrocyte hemolysis at 500 µg/mL ($LC_{50} > 500$ µg/mL) indicating that the inhibitors do not cause loss of integrity of the erythrocyte plasma membrane.

To evaluate the cytotoxic effect of the selected fragments cell viability assays by neutral-red uptake by Caco-2 cells were performed. F1, F1.6, F1.8, F2.3, F2.4 or F2.8 inhibited neutral-red uptake by Caco-2 cells with IC₅₀ values of 294, 121, 134, 30, 51 and 61 µg/ml, respectively, (Figure S6).

Additionally, cytotoxicity was evaluated by 24 h incubation of 0.2, 1, 3, 13 and 50 µg/ml of F1, F1.8, F2, F2.1, F2.3 and F2.8 with freshly isolated human peripheral blood mononuclear cells (PBMCs) and measurement of dead (propidium iodide (PI) positive) and apoptotic (annexin V (AV) positive) cells by flow cytometry. There was no significant difference in the number of dead cells in the control (DMSO treated) and inhibitors-treated samples. However, the number of cells binding annexin V, a marker of early apoptosis, was significantly higher in cells incubated with 50 µg/ml of F1.8, F2.3, and F2.8 (Figure S5) than the control cells (DMSO-treated). This is reflected in a reduction of viable (PI and annexin V negative) cells (Fig S5A). The results suggest that a concentration between 13 and 50 µg/ml of F1.8, F2.3 and F2.8 induces apoptosis in a proportion of the PBMCs after 24 h incubation.

The IC₅₀ values for neutral-red uptake by Caco-2 were mostly higher than the observed MICs and 24 h incubation with some of the hits (F1.8, F2.3 and F2.8)

induced apoptosis in human PBMCs suggesting off-target effects of the described HK autophosphorylation inhibitors. This requires that the further optimization of the hits should be multidirectional, including improving the affinity and specificity to the target bacterial HKs, enhancing the antibacterial effect and improving the toxicity profile of the hits.

To get insights into the putative interaction mode of the described HK autophosphorylation inhibitors with the CA domains of HKs, molecular docking experiments were performed. F1, F1.6, F1.8, F2.3, F2.4, F2.8 and ADP as an internal control were docked to the CA domain of *T. maritima* HK853 (PDB: 3DGE) using the GOLD docking software¹⁸. The root-mean square deviation (RMSD) between the docked ADP and the cognate ADP structure in the KH853 was 1.0 Å. This corresponds to a successful redocking calculation and, therefore, validates the used docking parameters. Due to low molecular weight of the fragments, it is possible that the fragments possess more than one binding mode. Encouragingly, within the top 20 solutions for each fragment only one or two binding modes were predicted and the predicted binding modes of similar fragments were consistent with each other. This together with the low RMSD for the docked ADP gave us confidence about the predicted binding modes of the studied fragments.

The predicted binding modes of the studied fragments resemble the binding mode of the cognate ligand, ADP (Figure 2), by forming also stabilizing hydrogen bonds with the conserved Asp411 (located at the bottom of the hydrophobic ATP-binding pocket in the so called G1 box) as well as with the ATP-lid (i.e. Ile424, Tyr429 and Arg430): All six fragments form hydrogen bonds with Asp411 either by classical hydrogen bond donor groups such as NH₂ or OH (F1.6, F2.8) or by other polar groups such as Br and CH (F1, F1.8, F2.3, F2.4). The ATP-lid interacts by hydrogen bonds with four of the six compounds (F1, F1.8, F2.3, F2.4). The ATP-lid is a HK distinctive flexible and variable loop that covers the ATP-binding pocket and is crucially involved in nucleotide binding and in autophosphorylation reactions^{6, 27}. Overall, the predicted binding modes indicate that stabilizing interactions are formed by all six fragments with binding sites/residues that are conserved and crucial for autophosphorylation. This supports the *in vitro* results and suggests that the fragments might also inhibit further HKs not tested in this study.

CONCLUSIONS

In conclusion, by combining fragment-screenings by differential scanning fluorimetry and ligand-based similarity searches of a public repository database we identified multiple HK autophosphorylation inhibitors with antibacterial effect against Gram-positive and Gram-negative pathogens including multidrug resistant clinical isolates. The reported inhibitors present a promising starting point for the rational design of more potent HK general or specific inhibitors and the discovery of antibacterials with improved physicochemical and ADMET properties.

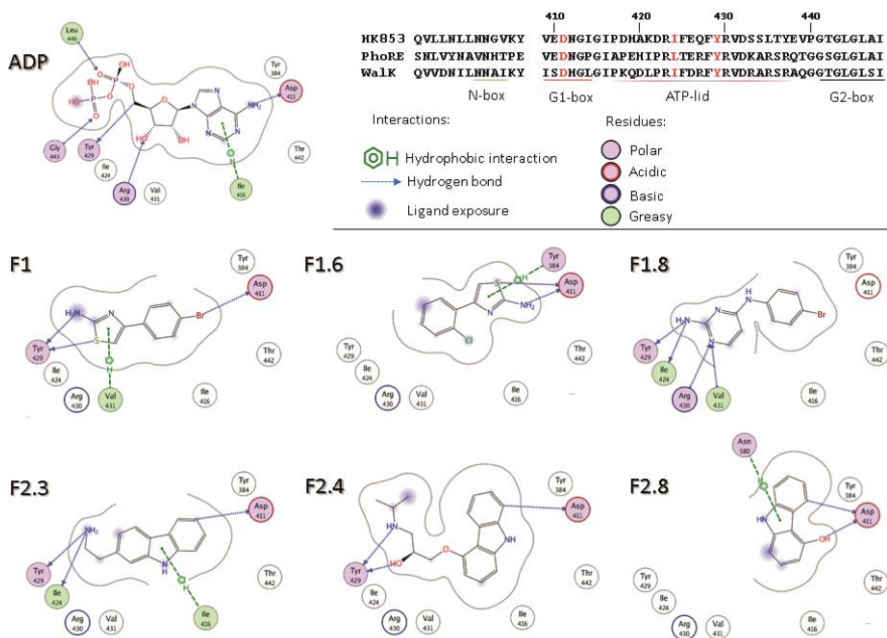


Figure 2. Predicted binding modes of selected fragments to the CA domain of *T. maritima* HK853 (PDB: 3DGE)¹⁵. The predicted binding modes indicate that these fragments form stabilizing hydrogen bonds with conserved elements of the CA domain of HKs represented by *T. maritima* HK853. The formed interactions include the D411 which also forms interactions with the adenine of the natural ligand ADP. Fragments interact as well with residues of the G1 box of the ATP-lid which are crucial for ligand binding and recognition. The binding modes are visualized with MOE²⁸. The sequence alignment in the upper right corner demonstrates that the binding sites residues Ile424, Tyr429, and Asp411, are conserved in HKs suggesting that the compounds might also bind to other HKs not tested in this study.

REFERENCES

1. Stephenson, K.; Hoch, J. A., Virulence- and antibiotic resistance-associated two-component signal transduction systems of Gram-positive pathogenic bacteria as targets for antimicrobial therapy. *Pharmacology & therapeutics* 2002, 93 (2-3), 293-305.
2. Casino, P.; Rubio, V.; Marina, A., The mechanism of signal transduction by two-component systems. *Current opinion in structural biology* 2010, 20 (6), 763-71.
3. Niesen, F. H.; Berglund, H.; Vedadi, M., The use of differential scanning fluorimetry to detect ligand interactions that promote protein stability. *Nature protocols* 2007, 2 (9), 2212-21.
4. Rogers, D.; Hahn, M., Extended-connectivity fingerprints. *Journal of chemical information and modeling* 2010, 50 (5), 742-54.
5. Congreve, M.; Carr, R.; Murray, C.; Jhoti, H., A 'rule of three' for fragment-based lead discovery? *Drug discovery today* 2003, 8 (19), 876-7.
6. Watanabe, T.; Okada, A.; Gotoh, Y.; Utsumi, R., Inhibitors targeting two-component signal transduction. *Advances in experimental medicine and biology* 2008, 631, 229-36.
7. RDKit: Open-source cheminformatics.
8. CLSI, Methods for dilution antimicrobial susceptibility tests for bacteria that grow aerobically. CLSI: Wayne, PA, 2009; Vol. 8th ed. M7-A8.
9. Sonnevend, A.; Blair, I.; Alkaabi, M.; Jumaa, P.; Al Haj, M.; Ghazawi, A.; Akawi, N.; Jouhar, F. S.; Hamadeh, M. B.; Pal, T., Change in methicillin-resistant *Staphylococcus aureus* clones at a tertiary care hospital in the United Arab Emirates over a 5-year period. *Journal of clinical pathology* 2012, 65 (2), 178-82.
10. Sonnevend, A.; Ghazawi, A.; Al Munthari, N.; Pitout, M.; Hamadeh, M. B.; Hashmey, R.; Girgis, S. K.; Sheikh, F. A.; Al Haj, M.; Nagelkerke, N.; Pal, T., Characteristics of epidemic and sporadic strains of *Acinetobacter baumannii* isolated in Abu Dhabi hospitals. *Journal of medical microbiology* 2013, 62 (Pt 4), 582-90.
11. Jumaa, P. A.; Sonnevend, A.; Pal, T.; El Hag, M.; Amith, R.; Trad, O., The molecular epidemiology of *Stenotrophomonas maltophilia* bacteraemia in a tertiary referral hospital in the United Arab Emirates 2000-2004. *Annals of clinical microbiology and antimicrobials* 2006, 5, 32.
12. Pournaras, S.; Maniati, M.; Spanakis, N.; Ikonomidis, A.; Tassios, P. T.; Tsakris, A.; Legakis, N. J.; Maniatis, A. N., Spread of efflux pump-overexpressing, non-metallo-beta-lactamase-producing, meropenem-resistant but ceftazidime-susceptible *Pseudomonas aeruginosa* in a region with blaVIM endemicity. *The Journal of antimicrobial chemotherapy* 2005, 56 (4), 761-4.
13. Hilliard, J. J.; Goldschmidt, R. M.; Licata, L.; Baum, E. Z.; Bush, K., Multiple mechanisms of action for inhibitors of histidine protein kinases from bacterial two-component systems. *Antimicrobial agents and chemotherapy* 1999, 43 (7), 1693-9.
14. Verdonk, M. L.; Cole, J. C.; Hartshorn, M. J.; Murray, C. W.; Taylor, R. D., Improved protein-ligand docking using GOLD. *Proteins* 2003, 52 (4), 609-23.
15. Casino, P.; Rubio, V.; Marina, A., Structural insight into partner specificity and phosphoryl transfer in two-component signal transduction. *Cell* 2009, 139 (2), 325-36.
16. Casino, P.; Miguel-Romero, L.; Marina, A., Visualizing autophosphorylation in histidine kinases. *Nat Commun* 2014, 5, 3258.
17. Molecular Operating Environment (MOE). 2013.
18. Podgornaia, A. I.; Casino, P.; Marina, A.; Laub, M. T., Structural basis of a rationally rewired protein-protein interface critical to bacterial signaling. *Structure* 2013, 21 (9), 1636-47.

19. Casino, P., Miquel-Romero, L., Marina, A., Visualizing autophosphorylation in histidine kinases. *Nat Commun* 2014.
20. Salinas, P.; Ruiz, D.; Cantos, R.; Lopez-Redondo, M. L.; Marina, A.; Contreras, A., The regulatory factor SipA provides a link between NblS and NblR signal transduction pathways in the cyanobacterium *Synechococcus* sp. PCC 7942. *Molecular microbiology* 2007, 66 (6), 1607-19.
21. Uniewicz, K. A.; Ori, A.; Xu, R.; Ahmed, Y.; Wilkinson, M. C.; Fernig, D. G.; Yates, E. A., Differential scanning fluorimetry measurement of protein stability changes upon binding to glycosaminoglycans: a screening test for binding specificity. *Analytical chemistry* 2010, 82 (9), 3796-802.
22. Christopoulos, H. M. a. A., *Fitting Models to Biological Data using Linear and Nonlinear Regression. A Practical Guide to Curve Fitting.* Oxford University Press: New York, 2004.
23. Marina, A.; Mott, C.; Auyzenberg, A.; Hendrickson, W. A.; Waldburger, C. D., Structural and mutational analysis of the PhoQ histidine kinase catalytic domain. Insight into the reaction mechanism. *The Journal of biological chemistry* 2001, 276 (44), 41182-90.
24. Hu, Y.; Lounkine, E.; Bajorath, J., Improving the search performance of extended connectivity fingerprints through activity-oriented feature filtering and application of a bit-density-dependent similarity function. *ChemMedChem* 2009, 4 (4), 540-8.
25. Conlon, J. M.; Mechkarska, M.; Prajeep, M.; Sonnevend, A.; Coquet, L.; Leprince, J.; Jouenne, T.; Vaudry, H.; King, J. D., Host-defense peptides in skin secretions of the tetraploid frog *Silurana epittropicalis* with potent activity against methicillin-resistant *Staphylococcus aureus* (MRSA). *Peptides* 2012, 37 (1), 113-9.
26. Clinical Laboratory and Standards Institute *Methods for Antimicrobial Susceptibility Testing of Anaerobic Bacteria; Approved Standard. M11-A7.* 2007; Vol. 7th ed.
27. NCCLS, *Methods for determining bactericidal activity of antimicrobial agents.* NCCLS: Wayne, PA, 1999; Vol. M26-A.
28. Mechkarska, M.; Ahmed, E.; Coquet, L.; Leprince, J.; Jouenne, T.; Vaudry, H.; King, J. D.; Conlon, J. M., Antimicrobial peptides with therapeutic potential from skin secretions of the Marsabit clawed frog *Xenopus borealis* (Pipidae). *Comparative biochemistry and physiology. Toxicology & pharmacology : CBP* 2010, 152 (4), 467-72.
29. Repetto, G.; del Peso, A.; Zurita, J. L., Neutral red uptake assay for the estimation of cell viability/cytotoxicity. *Nature protocols* 2008, 3 (7), 1125-31.
30. Ashkenazy, H.; Erez, E.; Martz, E.; Pupko, T.; Ben-Tal, N., ConSurf 2010: calculating evolutionary conservation in sequence and structure of proteins and nucleic acids. *Nucleic acids research* 2010, 38 (Web Server issue), W529-33.
31. Seeliger, D.; de Groot, B. L., Ligand docking and binding site analysis with PyMOL and Autodock/Vina. *Journal of computer-aided molecular design* 2010, 24 (5), 417-22.
32. Ziebuhr, W.; Krimmer, V.; Rachid, S.; Lossner, I.; Gotz, F.; Hacker, J., A novel mechanism of phase variation of virulence in *Staphylococcus epidermidis*: evidence for control of the polysaccharide intercellular adhesin synthesis by alternating insertion and excision of the insertion sequence element IS256. *Molecular microbiology* 1999, 32 (2), 345-56.
33. Wang, Y.; Li, D.; Song, L.; Liu, Y.; He, T.; Liu, H.; Wu, C.; Schwarz, S.; Shen, J., First report of the multiresistance gene *cfr* in *Streptococcus suis*. *Antimicrobial agents and chemotherapy* 2013, 57 (8), 4061-3.

SUPPLEMENTARY MATERIAL CHAPTER 3

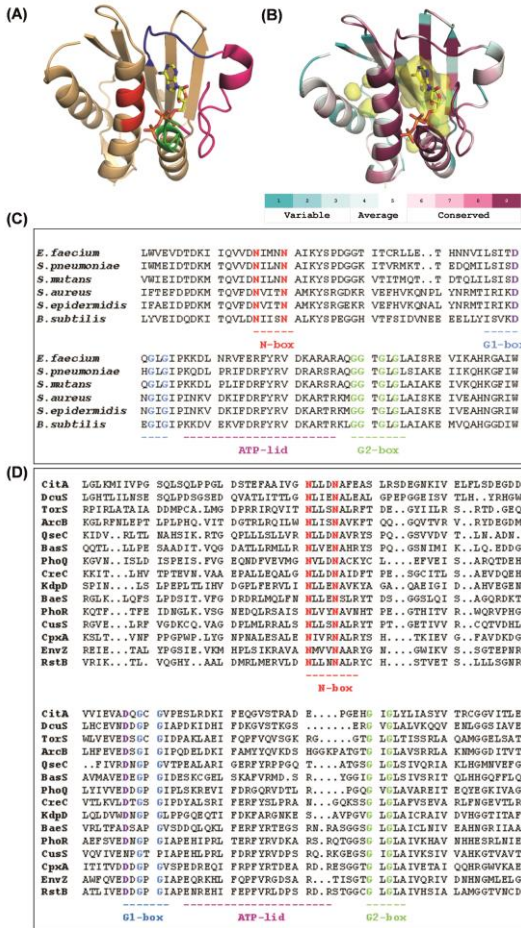


Figure S1. The ATP-binding site of HK CA domain is a well-defined and highly conserved pocket and allows the discovery and design of HK autophosphorylation inhibitors with broad-spectrum antibacterial activity following structure-based approaches A) Structure of *B. subtilis* Walk CA domain (PDB: 3SL2). The conserved N-, G1- and G2-boxes are shown in red, blue and green, respectively. The variable ATP-lid is shown in pink. B) *B. subtilis* Walk CA domain (PDB:3SL2) coloured by conservation. The conservation scores were calculated using ConSurf³⁰. The ATP-binding pocket was calculated using PyMol³¹ and is shown as a semi-transparent yellow surface. ATP is shown in ball-and-stick representation with carbon, nitrogen, oxygen and phosphate atoms in yellow, blue, red and orange, respectively. C) Alignment of Walk CA domains from different organisms D) Alignment of the CA domains of different *E. coli* HKs

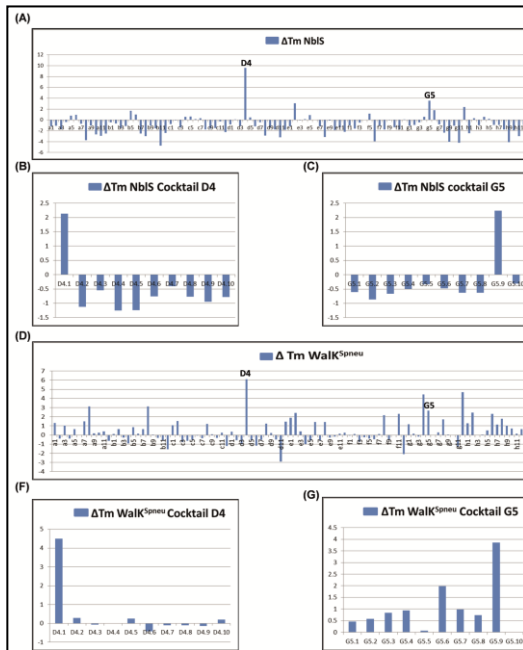


Figure S2. Identification of F1 (D4.1) and F2 (G5.9) as putative CA ligands by DSF. The fragment-library was divided in cocktails of ten fragments, each at a final concentration of 2 mM in a 96-well plates. Each plate included negative controls (DMSO) and positive-control (ADP, ATP, AMP-PNP). A) The individual compounds from the cocktails which increased the T_m of NbIS (A) and the T_m of Walk (D) were tested. F1 (D4.1) and F2 (G5.9) were identified as the compounds present in the D4 and G5 cocktails that most likely caused the observed increase of NbIS and Walk T_m (B, C, E, F).

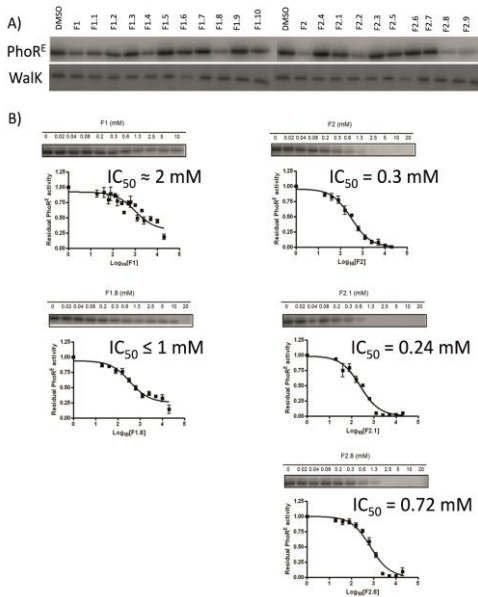


Figure S3. Biochemical evaluation by in vitro kinase assay A) First, the autophosphorylation inhibitory activity was evaluated in a one concentration (2mM) one time-point (30 sec) in vitro kinase assays with Walk and PhoRE. The fragments inhibited Walk and PhoRE autophosphorylation with 10 to 62% and 17 to 80%, respectively. B) IC_{50} of the more potent inhibitors (% inhibition at 2 mM > 50 %) with antibacterial effect were measured in a multiple-concentrations one time-point (30 sec) experiments.

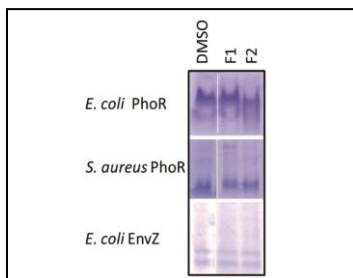


Figure S4. F1 and F2 (2 mM) do not cause HKs aggregation as demonstrated by native-PAGE with *E. coli* PhoR and EnvZ, and *S. aureus* PhoR.

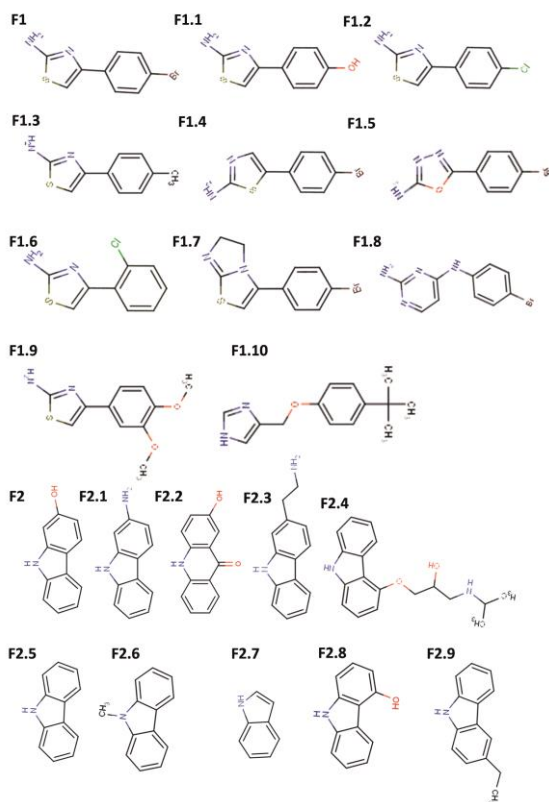


Figure S5. Selected fragments for experimental testing. F1 and F2 were identified as hits in a screening for ligands of both the CA domain of NblS and the CA and DHp domain of WalK. F1.1 to F1.10 and F2.1 to F2.4 were identified by ligand-based similarity searches of the National Cancer Institute Developmental Therapeutics Programme database using F1 and F2 as query molecules.

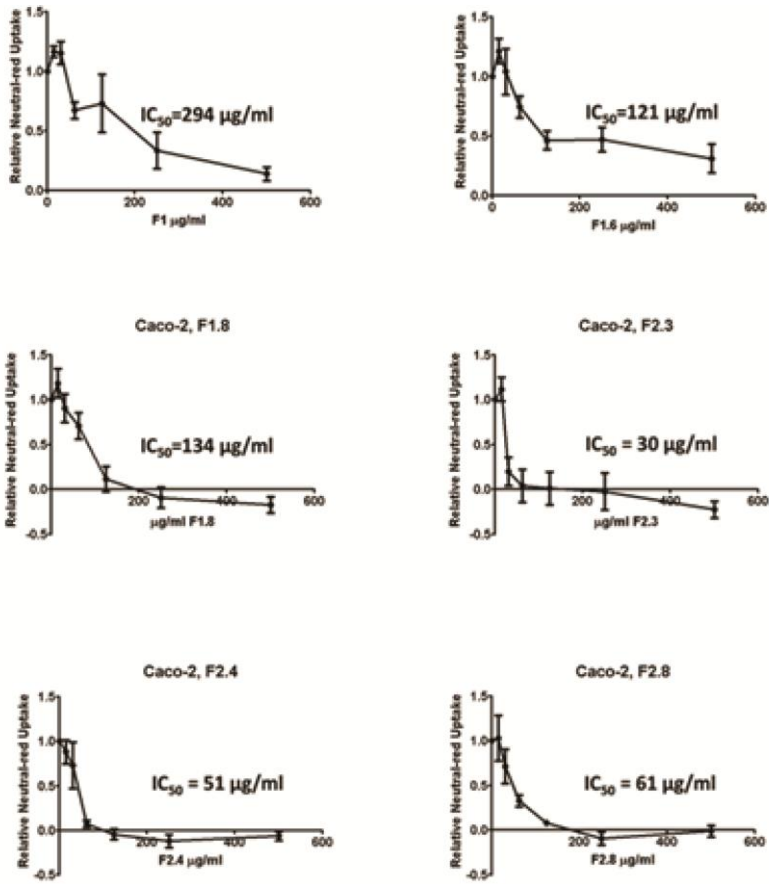


Figure S6. Cell viability assessed by neutral-red uptake assays with Caco-2 cell line. The error bars represent the SEM of at least two independent experiments in duplicate. IC_{50} is the concentration corresponding to 50% reduction of neutral-red uptake by Caco-2 cells.

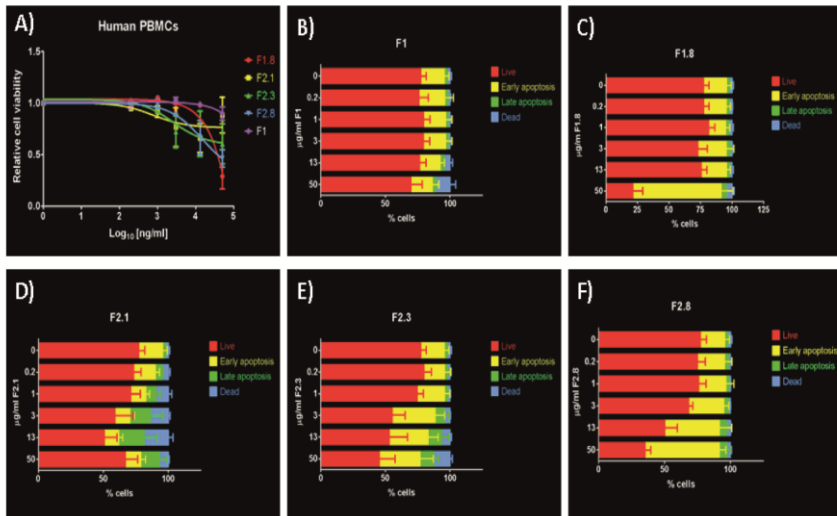


Figure S7. Dose effect of identified inhibitors on PBMCs viability (A) and apoptosis evaluated by propidium iodide and annexin V (AV) staining. 50 $\mu\text{g/ml}$ of F1.8 (C) and F2.3 (E), F2.8 (F) induce stronger expression of the early apoptotic marker AV compared to the control (0 $\mu\text{g/ml}$, DMSO-treated PBMCs) which is reflected in reduction of the live cells (A) with around or more than 50% compared to the control (DMSO-treated PBMCs). Error bars represent SEM for three independent donors.

Table S1. Autophosphorylation inhibitory activities and antibacterial activities of the tested compounds.

name	IC50 [mM]		MIC [μ g/ml]			MBC [μ g/ml]		
	PhoR ^E	WalK	<i>S. aureus</i> DSM 20231	<i>S. epidermidis</i> DSM 20044	<i>E. coli</i> CFT 073	<i>S. aureus</i> DSM 20231	<i>S. epidermidis</i> DSM 20044	<i>E. coli</i> CFT 073
F1	≈ 2	> 2	25	4	>500	>500	250	n.d.
F1.1	> 2	> 2	500	>500	500	>500	n.d.	>500
F1.2	> 2	> 2	>500	>500	>500	n.d.	n.d.	n.d.
F1.3	> 2	> 2	>500	500	>500	n.d.	500	n.d.
F1.4	> 2	> 2	>500	>500	>500	n.d.	n.d.	n.d.
F1.5	> 2	> 2	>500	>500	>500	n.d.	n.d.	n.d.
F1.6	> 2	< 2	125	500	>500	250	500	n.d.
F1.7	> 2	> 2	>500	>500	>500	n.d.	n.d.	n.d.
F1.8	≤ 1	> 2	125	63	250	250	125	500
F1.9	> 2	> 2	>500	>500	>500	n.d.	n.d.	n.d.
F1.10	> 2	> 2	>500	>500	>500	n.d.	n.d.	n.d.
F2	0.3	> 2	31	>500	>500	>500	n.d.	n.d.
F2.4	> 2	> 2	250	500	500	250	500	500
F2.1	0.24	> 2	8	>500	>500	>500	n.d.	n.d.
F2.2	< 2	> 2	>500	>500	>500	n.d.	n.d.	n.d.
F2.3	> 2	> 2	125	31	>500	>500	63	n.d.
F2.5	> 2	> 2	>500	>500	>500	n.d.	n.d.	n.d.
F2.6	> 2	> 2	>500	>500	>500	n.d.	n.d.	500
F2.7	> 2	> 2	500	>500	500	>500	n.d.	n.d.
F2.8	0.72	> 2	31	31	63	63	250	500
F2.9	< 2	> 2	>500	>500	>500	>500	n.d.	n.d.

n.d. – not tested

Table S2. Compounds purchased for experimental testing.

Name	Providers name	Smile
F1 (D4.1)	OR5604	<chem>NC1=NC(=CS1)C2=CC=C(Br)C=C2</chem>
F1.1	NSC 405294	<chem>NC1=NC(=CS1)C2=CC=C(O)C=C2</chem>
F1.2	NSC 372682	<chem>NC1=NC(=CS1)C2=CC=C(Cl)C=C2</chem>
F1.3	NSC 54436	<chem>CC1=CC=C(C=C1)C2=CSC(=N2)N</chem>
F1.4	NSC 176404	<chem>NC1=NC=C(S1)C2=CC=C(Br)C=C2</chem>
F1.5	NSC 614448	<chem>NC1=NN=C(O1)C2=CC=C(Br)C=C2</chem>
F1.6	NSC 13534	<chem>NC1=NC(=CS1)C2=C(Cl)C=CC=C2</chem>
F1.7	NSC 223276	<chem>BrC1=CC=C(C=C1)C2=CSC3=NCCN23</chem>
F1.8	NSC 80819	<chem>NC1=NC(=CC=N1)NC2=CC=C(Br)C=C2</chem>
F1.9	NSC 329206	<chem>COC1=C(OC)C=C(C=C1)C2=CSC(=N2)N</chem>
F1.10	NSC 206952	<chem>CC(C)(C)C1=CC=C(OCC2=C[NH]C=N2)C=C1</chem>
F2 (G5.9)	213497 ALDRICH	<chem>OC1=CC2=C(C=C1)C3=CC=CC=C3[NH]2</chem>
F2.4	NSC 305336	<chem>CC(C)NCC(O)COC1=C2C(=CC=C1)[NH]C3=CC=CC=C23</chem>
F2.1	NSC 171107	<chem>NC1=CC2=C(C=C1)C3=CC=CC=C3[NH]2</chem>
F2.2	NSC 402750	<chem>OC1=CC2=C([NH]C3=C(C=CC=C3)[C]2=O)C=C1</chem>
F2.3	NSC 106510	<chem>NCCC1=CC2=C(C=C1)C3=CC=CC=C3[NH]2</chem>
F2.5	C5132 SIGMA	<chem>[NH]1C2=CC=CC=C2C3=CC=CC=C13</chem>
F2.6	325325 ALDRICH	<chem>C[N]1C2=CC=CC=C2C3=CC=CC=C13</chem>
F2.7	13408 ALDRICH	<chem>[NH]1C=CC2=CC=CC=C12</chem>
F2.8	543896 ALDRICH	<chem>OC1=CC=CC2=C1C3=CC=CC=C3[NH]2</chem>
F2.9	754781 ALDRICH	<chem>CCC1=CC2=C([NH]C3=CC=CC=C23)C=C1</chem>

CHAPTER 4

BROADENING THE ANTIBACTERIAL SPECTRUM OF HISTIDINE KINASE AUTOPHOSPHORYLATION INHIBITORS VIA THE USE OF E-POLY-L-LYSINE CAPPED MESOPOROUS SILICA-BASED NANOPARTICLES

Nadya Velikova^{1,2}, Nuria Mas^{3,4}, Ellen Stolte², Edoardo Zaccaria², Rui Cao², Nico Taverne², José Ramón Murguía^{3,4}, Ramon Martinez-Manez^{3,4}, Alberto Marina^{2,5}, Jerry Wells²

¹ Instituto de Biomedicina de Valencia, Consejo Superior de Investigaciones Científicas (CSIC), Jaime Roig 11, 46010 Valencia, Spain;

² Host-Microbe Interactomics Chair Group, Animal Sciences, University of Wageningen, P.O. Box 338, 6700 AH Wageningen, The Netherlands;

³ Centro de Reconocimiento Molecular y Desarrollo Tecnológico, Departamento de Química, Universidad Politécnica de Valencia, Camino de Vera s/n, 46022 Valencia, Spain;

⁴ CIBER de Bioingeniería, Biomateriales y Nanomedicina, CIBER – BBN;

⁵ CIBER de Enfermedades Raras (CIBERER), ISCIII, Valencia, Spain

TO BE SUBMITTED TO NANOMEDICINE: NANOTECHNOLOGY, BIOLOGY AND
MEDICINE AFTER PUBLISHING OF CHAPTER 2 AND 3

2014

ABBREVIATIONS

Gr- Gram negative

Gr+ Gram positive

TCS Two-component systems

HK Histidine kinase

RR Response regulator

HKAI Histidine-kinase autophosphorylation inhibitor

f n-[(3-trimethoxysilyl)propyl]ethylenediamine triacetic acid trisodium salt

ePLL ε-poly-L-lysine

N.X MCM-41 functionalized with n-[(3-trimethoxysilyl)propyl]ethylenediamine triacetic acid trisodium salt and capped ε-poly-L-lysine (ePLL) cationic polymer and loaded with:

N.Van – vancomycin

N.HKAIs – histidine kinase autophosphorylation inhibitors

N.Rho – rhodamine

F.HKAIs – free histidine kinase autophosphorylation inhibitors

INTRODUCTION

Infections caused by Gram negative (Gr-) multidrug-resistant (MDR) bacteria have become a growing challenge worldwide ¹. The most important resistance problems are encountered in Enterobacteriaceae, *Pseudomonas aeruginosa* and *Acinetobacter spp.* which have developed resistance to last-line antibiotics such as expanded-spectrum cephalosporins and/ or carbapenems ². Urinary tract infections (UTIs) caused by Gr- uropathogenic *Escherichia coli* (UPEC) are among the most common bacterial infections in humans. Recently multi-drug resistant *E. coli* have been reported ^{3, 4, 5}.

Most of the bacterial infections in fish are caused by Gr- bacteria, including *Aeromonas hydrophilia*, *Aeromonas salmonicida*, *Flavobacterium columnare*, *Vibrio*, and *Pseudomonas spp.* ⁶. Currently antimicrobials are routinely used to directly control bacterial infections in pet (ornamental) fish and are added to the water these fish are shipped in to suppress the growth of potential pathogens during transport ⁷. However, this activity has led to high prevalence of multi-drug tolerant or resistant bacteria and associated antimicrobial resistance genes both in ornamental fish and their carriage water ⁷. This might present a potential health risk as studies have suggested that there is bi-directional transfer of resistance genes between aquatic and other Animalia as evidenced by the fact that antimicrobial resistance (AMR) genes of bacteria recovered from the aquatic environment can share very high sequence homology to clinically important AMR genes on plasmids and integrons found in clinical isolates of human pathogens ^{8, 9, 10, 11, 12}. The transmission of zoonotic multidrug resistant Gr- bacteria between food-producing animals and humans and between companion animals and humans has also been reported ^{13, 14, 15}.

Therefore, novel strategies to target infections caused by Gr- bacteria are urgently needed. Two-component systems (TCS) are signal transduction systems found in nearly all bacteria and have been proposed as promising antibacterial drugs targets for both Gram positive (Gr+) and Gr- infections ^{16, 17, 18}. A prototypical TCS consist of membrane bound histidine kinase (HK) and its cognate response regulator (RR) ¹⁹. Upon environmental stimuli the catalytic and ATP-binding (CA) domain of the HK autophosphorylates a conserved histidine found within the dimerization and histidine phosphotransfer (DHp) domain, which subsequently serves as the phosphodonor for a cognate RR ¹⁹. Many HKs are bi-functional and also dephosphorylate their cognate response regulator ^{20, 21}. The changes in the phosphorylation levels of the RR are usually related to changes of the expression of target genes involved in the regulation of variety of processes including growth, virulence, antibacterial resistance and adaptation to environmental changes ^{22, 23, 16}. Following structure-based and fragment-based drug discovery approaches (Chapter 2 and 3), bacterial histidine kinase autophosphorylation inhibitors (HKAI) were identified (Figure 1). The HKAI inhibited the autophosphorylation of HKs from both Gr+ and Gr- bacteria, including *E. coli* PhoR. PhoR belongs to the PhoR-PhoB TCS, which is involved in the regulation of the *pho* regulon. The *pho* regulon is not only a regulatory circuit of phosphate homeostasis but also plays an important adaptive role in stress response and bacterial virulence. ^{24, 25, 26}. Despite the fact that the HKAI inhibited

autophosphorylation of HKs from Gr- bacteria, they showed only moderate to strong antibacterial activity against Gr+ bacteria and not against Gr- bacteria. This was anticipated to be a consequence of the permeability barrier provided by the outer membrane (OM) of Gr- negative bacteria, which are inherently resistant to many hydrophobic antibiotics^{27, 28}. This resistance limits the arsenal of antibiotics that are effective in treating Gr-negative bacterial infections. To overcome this problem several compounds have been used to facilitate permeability of the OM and sensitize Gr- bacteria to hydrophobic antibiotics^{29, 30}. These compounds are typically cationic, amphiphilic molecules that can be prepared from peptides or steroids. Nanotechnology has also been proposed and exploited in addressing the problem related to Gr-membrane permeability³¹.

A nanodevice loaded with vancomycin was shown to possess antibacterial activity against a range of Gr- bacteria including *E. coli* (DH5 α , 100, 405), *Salmonella typhimurium* and *Erwinia carotovora*³². The device consisted of a nanometric mesoporous MCM-41 phase (ca. 100 nm; MCM-41) loaded with vancomycin, functionalized with n-[(3-trimethoxysilyl)propyl]ethylendiamine triacetic acid trisodium salt (*f*) and capped with a cationic polymer of ϵ -poly-L-lysine (ePLL), referred to here as N.Van. Vancomycin is glycopeptide antibiotic that selectively targets Gr+ bacteria³³. Most Gr- bacteria are intrinsically resistant to vancomycin due to its relatively high molecular weight and size and inability to pass through porins in the OM of Gr-.bacteria. Capping the NPs with polycationic ePLL is anticipated to promote ionic bonding with the negatively charged OM and facilitate permeability or antibacterial effects of the inhibitor through its disruptive effects on the bacterial membrane³⁴. Indeed, N.Van broadened the spectrum of vancomycin and enhanced the efficacy of ePLL³².

Here we employed a similar approach to N.Van³² to investigate the potential to deliver novel HKAls to Gr- bacteria. Silica-based nanoparticles were synthesized, loaded with HKAls and capped with ePLL, referred here as N.HKAls. The antibacterial effect of N.HKAls against Gr- bacteria *in vitro* was studied against a range of Gr- bacteria. To facilitate the potential clinical translation of these nanomedicines we tested their potential cytotoxicity using epithelial and immune cells, as well as their possible immunotoxicity to macrophages, which are crucial for immune defence against pathogens. Furthermore, we evaluated the uptake of the nanoparticles in zebrafish models.

MATERIALS AND METHODS

CHEMICALS

The chemicals tetraethylorthosilicate (TEOS) (98 %), *n*-cetyltrimethylammonium bromide (CTAB) (≥ 99 %), sodium hydroxide (≥ 98 %), and rhodamide B were provided by Aldrich. ϵ -poly-L-lysine (ePLL) was purchased from Chengdu Jinkai Biology Engineering Co. Ltd. *N*-[(3-Trimethoxysilyl)propyl]ethylenediamine triacetic acid trisodium salt was purchased from FluoroChem. $\text{Na}_2\text{HPO}_4 \cdot 7\text{H}_2\text{O}$, KH_2PO_4 , NaCl , NH_4Cl , MgSO_4 , glucose and CaCl_2 were purchased from Scharlab (used for the preparation of M9 minimal medium). All reagents were used as received.

Histidine kinase autophosphorylation inhibitors (HKAs; Table S1, Figure 1) were obtained from the National Cancer Institute Developmental Therapeutics Programme (NCI/DTP).

GENERAL TECHNIQUES

Powder XRD, TG analysis, elemental analysis, TEM and N_2 adsorption-desorption techniques were employed to characterize the prepared materials as previously described³². Powder X-ray diffraction measurements were performed on a Philips D8 Advance diffractometer using Cu K radiation. Thermo-gravimetric analysis was carried out on a TGA/SDTA 851e Mettler Toledo balance, using an oxidant atmosphere (air, 80 mL/min) with a heating program consisting on a heating ramp of 10°C per minute from 393 to 1273 K and an isothermal heating step at this temperature for 30 minutes. Elemental analysis was performed in a CE Instrument EA-1110 CHN Elemental Analyzer. TEM images were obtained with a 100 kV Jeol JEM-1010 microscope. N_2 adsorption-desorption isotherms were recorded on a Micromeritics ASAP2010 automated sorption analyser. The samples were degassed at 120°C in vacuum overnight. The specific surface areas were calculated from the adsorption data in the low pressures range using the BET model.

SYNTHESIS OF THE MESOPOROUS SILICA SUPPORT

The starting nanoparticulated MCM-41 mesoporous solid was prepared following well-known procedures using *n*-cetyltrimethylammonium bromide (CTAB) as template and tetraethylorthosilicate (TEOS) as hydrolytic inorganic precursor³². *N*-cetyltrimethylammonium bromide (CTAB, 1.00 g, 2.74 mmol) was first dissolved in 480 mL of deionised water. Then 3.5 mL of NaOH 2.00 M in deionised water were added to the CTAB solution. The solution temperature was adjusted to 80°C . TEOS (5.00 mL, 2.57×10^{-2} mol) was then added dropwise to the surfactant solution. The mixture was stirred for 2 h to give a white precipitate. Finally, the solid product was centrifuged, washed with deionised water and ethanol, and was dried at 60°C (MCM-41 as-synthesised). To prepare the final porous material (MCM-41), the as-synthesised

solid was calcined at 550°C using an oxidant atmosphere for 5 h in order to remove the template phase.

SYNTHESIS OF MESOPOROUS SILICA-BASED NANOPARTICLES LOADED WITH RHODAMINE AND CAPPED WITH ϵ -POLY-L-LYSINE (N.RHO)

The material designed and synthesized in our previous work³², (named in the current paper as N.Rho) was used as control solid in some of the experiments. It consisted on MCM-41 silica nanoparticles loaded with the Rhodamine B dye and externally functionalized with *N*-[(3-Trimethoxysilyl)propyl]ethyldiamine triacetic acid trisodium salt (*f*) and ϵ -poly-L-lysine (ePLL).

SYNTHESIS OF ϵ -POLY-L-LYSINE CAPPED MESOPOROUS NANOPARTICLES LOADED WITH HISTIDINE-KINASE AUTOPHOSPHORYLATION INHIBITORS (N.HKAIS)

ϵ -poly-L-lysine capped mesoporous nanoparticles loaded with histidine-kinase autophosphorylation inhibitors (N.HKAIs; N.B2, N.B11, N.B13, N.B14, N.B15, N.F1.8, N.F2.3) were obtained essentially as previously reported³². The solids N.HKAIs consist of mesoporous nanoparticles loaded with the free HKAI (F.HKAIs; F.B2, F.B11, F.B13, F.B14, F.B15, F.F1.8 and F.F2.3; Table S1), externally functionalized with *N*-[(3-Trimethoxysilyl)propyl]ethyldiamine triacetic acid trisodium salt (*f*) and capped with ϵ -poly-L-lysine (ePLL). In a typical synthesis, 100 mg (except for NB.11 where 30 mg was used) of the template-free MCM-41 was suspended in solution containing the corresponding antibacterial derivative. F.B13, F.B14 and F.F1.8 (corresponding to N.B13, N.B14, N.F1.8 final solids loading) were dissolved in DMSO. The rest of the F.HKAIs (F.B2, F.B7, F.B11, F.B15, F.F2.3) were dissolved in H₂O:2DMSO. After stirring at room temperature for 24 h, an excess (15 mmol/g MCM-41) of *N*-[(3-Trimethoxysilyl)propyl]ethyldiamine triacetic acid trisodium salt (*f*) was added and the mixture stirred for 12 h at room temperature. After that, the solid was centrifuged and washed with 1 mL of water. Then, the solids were dried under vacuum. In a second step, the pre-functionalized solid was suspended in a solution containing ϵ -poly-L-lysine in M9 minimal medium (1.8 mL/100mg of prefunctionalized solid of a 0.033M ϵ -poly-L-lysine solution). This suspension was stirred for 1 h at room temperature. Finally, each solid was filtered and washed once by centrifugation with 1 mL of M9 medium. The final solids were labelled as N.B2, N.B11, N.B13, N.B14, N.B15, N.F1.8 and N.F2.3 and were dried under vacuum for 12 h.

BACTERIAL STRAINS

Escherichia coli CFT 073, *E. coli* DH5 α and *S. marcescens* 21639 were obtained from Leibniz Institute DSMZ – German Collections of Microorganisms and Cell

Cultures (Braunschweig, Germany) and were propagated using standard microbiological procedures.

ANTIMICROBIAL SUSCEPTIBILITY TESTING

Minimal inhibitory concentrations (MICs) of MCM-41, N.Rho, ϵ -poly-L-lysine (ePLL), N.HKAIs (N.B2, N.B7, N.B11, N.B13, N.B14, N.B15, N.F1.8 and N.F2.3), and F.HKAIs (F.B2, F.B7, F.B11, F.B13, F.B14, F.B15, F.F1.8 and F.F2.3) were determined using a standard double dilution method^{35, 36, 37}. Antimicrobial susceptibility testing was performed with inoculum of $1.10^5 - 1.10^6$ CFU/ml. N.HKAIs were suspended in water and Mueller Hinton (MH) broth (1:1) to concentration corresponding to 1.10^5 μ g/ml (N.B2, N.B7, N.B11, N.B13, N.B14, N.B15) or 2.5×10^4 μ g/ml (N.F1.8 and N.F2.3) F.HKAIs and sonicated until obtaining homogenous suspension. The suspensions were serially diluted in MH broth in 96-well plates. The MIC was recorded as the lowest concentration where no visible growth was observed. Minimal bactericidal concentrations (MBCs) were determined by plating 10 μ l of the wells where no growth was observed on MH agar plates and incubating overnight at 37 °C or by inoculating 90 μ l MH broth with 10 μ l of the wells where no growth was observed. MBC was recorded as the lowest concentration where no colonies were formed or no visible growth was observed after overnight incubation at 37°C.

SYNERGY ASSESSMENT

Synergy between ϵ -poly-L-lysine (ePLL) and F.HKAIs (F.B2, F.B7, F.B11, F.B13, F.B14, F.B15, F.F1.8 and F.F2.3) was assessed by the check-board method³⁸ in 96-well-plates. Fractional inhibitory concentrations (FICs) were calculated based on the content in the wells in the growth-no growth area. FIC > 0.5 indicates no synergy³⁸.

CELL LINES AND MEDIUM

Cells were grown in medium supplemented with 10% fetal bovine serum (FBS; PAA Laboratories, Colbe, Germany), 100 U/ml penicillin and 100 μ g/ml streptomycin (Sigma, St. Louis, MO) in an atmosphere of 5% CO₂-95% O₂ at 37°C and were passaged weekly.

Caco-2 BBE cells (CRL 2102), and Raw 264.7 (Mouse leukemic monocyte macrophage cell line) were purchased from the American Type Culture Center (Manassas, VA) and grown in DMEM (Invitrogen, Paisley, UK) containing Glutamax, in RPMI 1640 (Invitrogen, Paisley, UK) supplemented with 2mM Glutamine, in DMEM, respectively.

NEUTRAL RED UPTAKE ASSAY OF CELL VIABILITY

Neutral red uptake assay of cell viability with Caco-2 cells was performed as previously described³⁹. Briefly, after overnight incubation with the NPs (MCM-41, N.Rho and N.HKAIs), the F.HKAIs or ePLL, 10 μ l of neutral red solution (33 μ g/ml) was added to the wells. After 3 h of incubation at 37°C, the medium was removed and cells were washed rapidly with PBS. Neutral red was extracted from the cells with 150 μ l 1% acetic acid-50% ethanol, shaken for 10 min at RT. The neutral red content was measured on a SpectraMax M5 microplate reader (Molecular Devices) at 540 nm. The readings were expressed as neutral-red uptake relative to the uptake of the cells exposed to the negative control (medium or DMSO).

ACTIVATION OF MACROPHAGES AND TREATMENT WITH NPs AND FREE HISTIDINE KINASE AUTOPHOSPHORYLATION INHIBITORS

Raw cells were seeded in 96-well-plates (1.10^5 cells/well) and allowed to attach to the bottom of the wells at 37°C and 5% CO₂ for 1 h. Cells were treated with NPs (MCM-41, N.Rho, N.HKAIs) or F.HKAIs, in the presence or absence of 1 μ g/ml LPS. Controls containing solvent (water or DMSO) were run in parallel. A NO assay and a viability assay (XTT) were run consecutively for every treatment group. The macrophages cultures were incubated at 37°C and 5% CO₂ for 24 h before performing the appropriate assays.

NITRIC OXIDE ASSAY

The NO production of the macrophages was indirectly determined using the Griess reaction, a colorimetric assay to measure the accumulation of the stable end product of NO degradation, nitrite, within the culture supernatant⁴⁰. Briefly, after overnight incubation with NPs or F.HKAIs, plates were centrifuged at 2000 rpm, at RT for 7 min. 75- μ l volumes of the supernatants were transferred to a new 96-well plate. 100 μ l of 1% sulfanilamide (Sigma) in 2.5% phosphoric acid was added to each well. This was followed by addition of 100 μ l of 0.1% N-naphthyl-ethylenediamine (Sigma) in 2.5% phosphoric acid. The plate was gently tapped to mix the contents, incubated at RT for 5 min, and the optical density (OD) at 540 nm with 690 nm as a reference was determined using an automated spectrophotometer SpectraMax M5 microplate reader (Molecular Devices).

CELL RESPIRATION (XTT VIABILITY ASSAY)

Changes in macrophage viability were assessed using the XTT viability assay. This assay measures the respiratory activity of mitochondria by determining the accumulation of a coloured formazan by-product within the supernatants of treated wells⁴¹. Briefly, a 20% volume of 1 mg/ml sodium 3,3'-[1[(phenylamino)carbonyl]-

3,4-tetrazolium]-bis (4-methoxy-6-nitro)benzene sulphonate hydrate (XTT) in 1× RPMI was added to each well of the treatment plate. The plates were gently tapped to mix the contents, incubated for up to 2 h at 37°C and 5% CO₂, and the OD at 450 using 690 nm as a reference was determined using an automated spectrophotometer SpectraMax M5 microplate reader (Molecular Devices).

TUMOR NECROSIS FACTOR ALPHA ELISA

Tumor-necrosis factor alpha (TNF α) protein levels were measured by quantitative enzyme linked immunosorbent assays (ELISA) using the Mouse TNF alpha ELISA Ready-SET-Go!® reagent set (Affymetrix, eBioscience, Netherlands). Briefly, after overnight incubation of Raw cells with NPs or F.HKAIs before or after stimulation with 1 μ g/ml LPS, plates were centrifuged at 2000 rpm, at RT for 7 min. 75- μ l volumes of the supernatants were transferred to a new 96-well plate and ELISA was performed according to the manufactures protocol.

ZEBRAFISH MAINTENANCE

Zebrafish (*Danio rerio*) were bred at the animal facility of Wageningen University and Research Centrum as previously described^{42, 43}. Experiments with zebrafish embryos were conducted in accordance with the guidelines of the Wageningen University Animal Experiments Committee. The breeding tank was cleaned twice a day until hatching by removing debris and unfertilized eggs. Embryos were collected as eggs on different days and maintained in oxygenated water at 28°C. For experiments zebrafish embryos between 1 and 4 days post-hatching were used. After 4 days post-hatching, embryos were killed by incubation on ice for at least 30 minutes.

INCUBATION OF ZEBRAFISH WITH N.RHO

Zebrafish were cultured to 96-well plates (1 embryo/ well) in a total volume of 100 μ l oxygenated water at 28° C. Then 1, 2, 5, 10 μ l of the nanoparticle stock solution (1 mg/ml) were added to the wells. Each treatment group contained 5 embryos 3 days post-hatching and 5 replicates were tested per group. To visualize the NPs two embryos per group were anesthetized using tricaine (MS-222) at standard concentration. Images were taken after 1.5, 6 and 24 hours post incubation using Leica M205 FA Fluorescence Stereo Microscope (Leica Microsystems).

RESULTS AND DISCUSSION

The growing number of reports about the spread of multi-drug resistant (MDR) Gr- pathogens demands urgent development of novel approaches to combat the health risks associated with infections caused by Gr- bacteria¹. Due to low number of new classes of antibacterials entering the market over the past decade and growing incidence of infections due to MDR bacteria, effort is also being directed towards the improving pharmacological properties, potency and delivery of known antibiotics^{30, 44, 32, 45, 31}. Here we describe a new approach using polycationic ϵ -poly-L-lysine capped nanoparticles loaded with bacterial histidine kinase autophosphorylation inhibitors (HKAI) as a mean to enhance permeability of the outer membrane (OM) of Gr-negative bacteria. Newly identified two-component systems (TCSs) inhibitors (Chapter 2 and 3, Figure 1, Table S1) were used to evaluate the nanodelivery approach as they were demonstrated to inhibit HKs from Gr- *in vitro* but lacked antibacterial activity against Gr- bacteria.

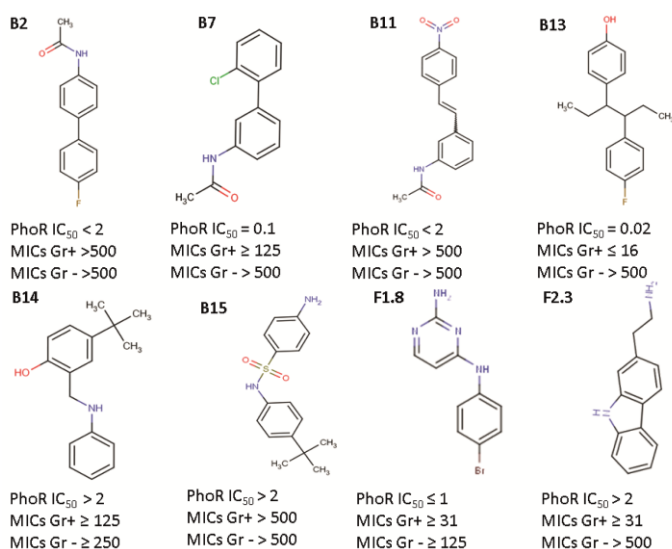


Figure 6. Histidine-kinase autophosphorylation inhibitors (HKAI) Selected HKAI inhibited the autophosphorylation of *E. coli* PhoR with IC₅₀ ranging from 0.2 to > 2 mM. The HKAI showed antibacterial effect for a panel of Gram-positive bacteria (Chapter 2 and 3) with MICs in the range of 8 to > 500 μ g/ml. Only B14

and F1.8 showed antibacterial effect for Gram-negative bacteria with MICs ≥ 250 or ≥ 125, respectively. The IC₅₀ (the concentration causing 50% reduction in autophosphorylation activity; mM) of each HKAI for *E. coli* PhoR (PhoR IC₅₀) is presented together with a consensus MIC (minimal inhibitory concentrations) in antimicrobial susceptibility testing assays with a panel of Gram-positive (Gr+) and Gram-negative (Gr-) bacteria.

SYNTHESIS AND CHARACTERIZATION OF MESOPOROUS SILICA-BASED NANOPARTICLES CAPPED WITH ϵ -POLY-L-LYSINE AND LOADED WITH HK AUTOPHOSPHORYLATION-INHIBITORS

To evaluate the antibacterial effect of the newly identified HKAI to Gr- bacteria, mesoporous silica-based nanoparticles (MCM-41) were loaded with HKAI or rhodamine dye as a control (N.HKAIs or N.Rho) and capped with ϵ -poly-L-lysine (ePLL, Figure 2 and 3) as previously described³². The organic content of N.HKAIs and N.Rho was verified and is shown in Table 1 and details are provided in the Supporting Information. The content of the N.HKAIs was between 5 and 138 mg HKAI/g solid (0.02 to 0.45 mM HKAI/ g solid). The ePLL and silica content for the N.HKAIs or N.Rho was in the same range, between 91 and 220 mg ePLL/ g solid (0.022 – 0.054 mmol ePLL/g solid) and between 51 and 59% silica, respectively.

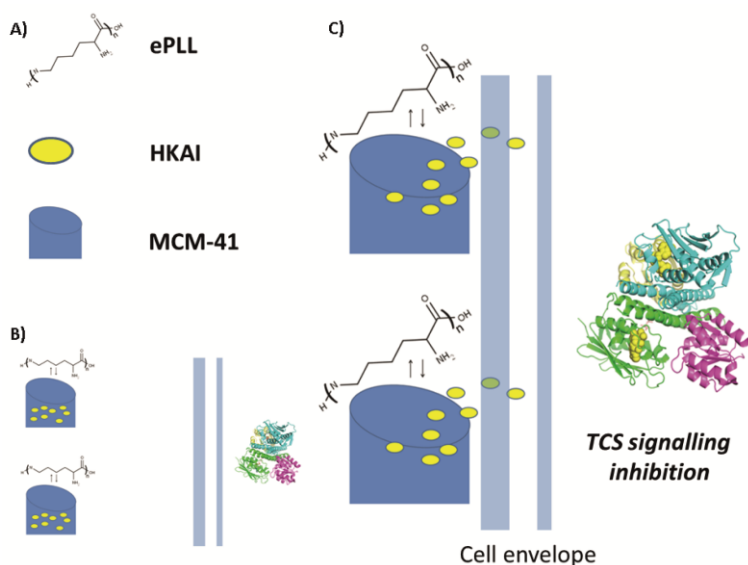


Figure 2.

Schematic representation and putative mechanism of action of the nanoparticles. Nanometric mesoporous MCM-41 phase (ca. 100 nM; MCM-41) functionalized with n-[(3-trimethoxysilyl)propyl]ethylendiamine triacetic acid trisodium salt (blue cylinder) was

capped with ϵ -poly-L-lysine cationic polymer (ePLL) and loaded with histidine kinase autophosphorylation inhibitors (HKAI, yellow balls). Putative mechanism of action of the nanoparticles (NPs) is attributed to interaction of the positively charged capped NPs with the negatively charged Gr- bacterial cell wall (blue lines) and displacement of the capping ePLL which results in release of the loaded HKAI and subsequently to inhibition of two-component systems (TCS) signalling.

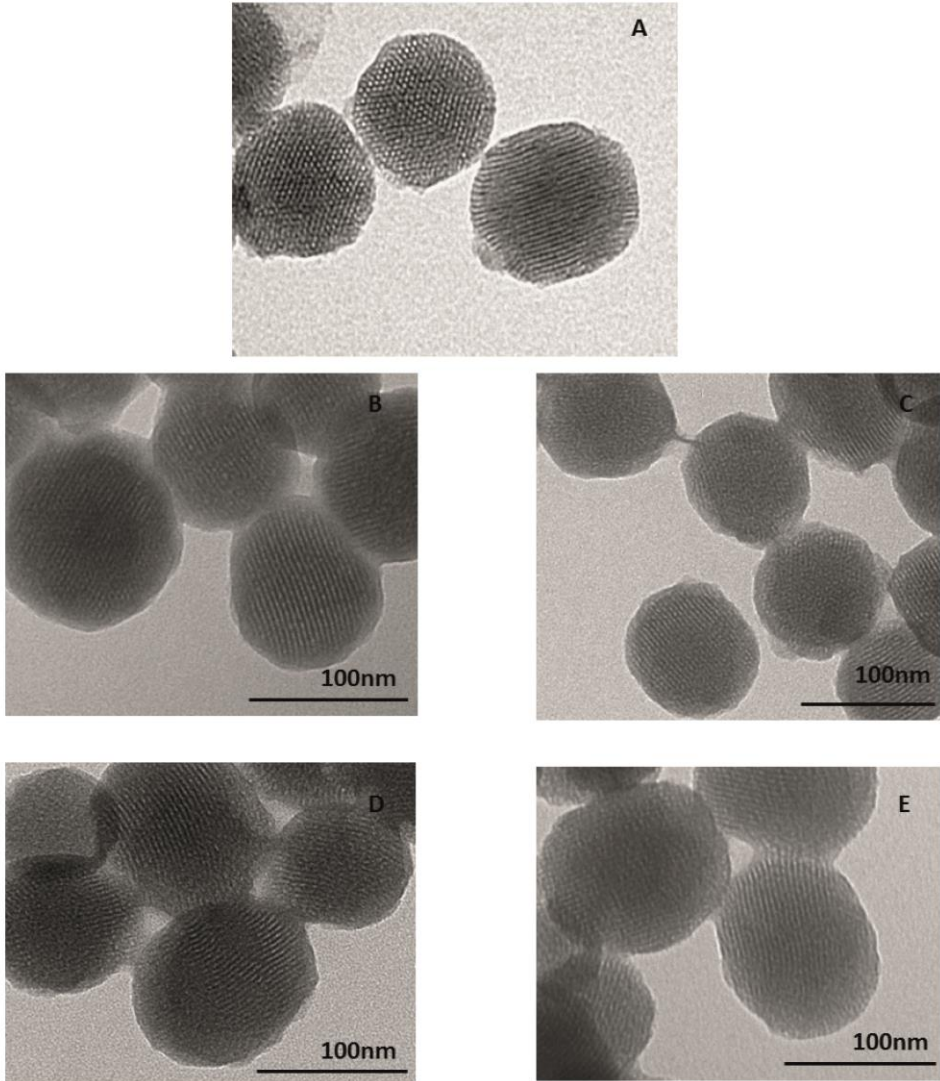


Figure 3. TEM image of the inorganic MCM-41 calcined matrix (A) and some of the final solids (B, C, D and E, correspond to N.Rho, NB.2, NB.14 and NF1.8 final solids, respectively). The images clearly show the mesoporous structure of the matrix which was maintained after capping with ePLL and loading with HKAI.

Table 1. Content (α , mmol/g of solid) of the different HKAls (α_{HKAls}), n-[(3-trimethoxysilyl)propyl]ethylenediamine triacetic acid trisodium salt (f , α_f), ϵ -poly-L-lysine (ePLL, α_{ePLL}) and silica content (silica, %) in the prepared nanoparticles.

	α_{HKAls}	α_f	α_{ePLL}	silica
N.Rho	0.021	0.388	0.025	
NB.2	0.44	0.269	0.036	55
NB.7	0.18	0.325	0.052	55
NB.11	0.05	0.541	0.042	53
NB.13	0.12	0.325	0.054	51
NB.14	0.23	0.465	0.030	54
NB15	0.34	0.034	0.033	57
NF1.8	0.024	0.88	0.022	57
NF2.3	0.026	0.403	0.042	59

MIC $\mu\text{g/ml}$					
<i>E. coli</i> CFT 073 <i>E. coli</i> DH5 α <i>S. marcescens</i>					
	<i>E. coli</i> CFT 073		<i>S. marcescens</i>		
	Nano	Free	Nano	Nano	Free
B2	100	>500	>100	> 100	n.t.
B7	50	>500	50	100	>100
B11	13	>500	>100	100	>500
B13	25	>500	50	100	>500
B14	50	500	>100	>100	500
B15	50	>500	>100	>100	>500
F1.8	6	250	>25	25	250
F2.3	6	>500	>25	25	>500

Table 2. Antibacterial activities of free HK autophosphorylation inhibitors (Free) and HK autophosphorylation inhibitors loaded to silica-based mesoporous nanoparticles capped with ϵ -poly-L-lysine (Nano). HKs inhibitors part of the nanoformulations showed > 10 fold lower MICs for Gram negative strains compared to the free HKs autophosphorylation inhibitors.

	<i>E. coli</i> CFT 073		<i>S. marcescens</i>
	MIC [mg/ml]	MBC [mg/ml]	MIC [mg/ml]
ePLL	0.13	1.6	0.25
N.Rho	> 10	> 10	> 1
ePLL _{nano}	> 1	> 1	> 0.1
MCM-41	> 11	> 11	> 11

Table 3. Antibacterial activity of MCM-41, the control N.Rho and ePLL

ePLL_{nano} ePLL part of the nanoformulation N.Rho

ANTIBACTERIAL ACTIVITIES

The antibacterial activities of N.HKAIs, F.HKAIs, ePLL, MCM-41 and N.Rho were evaluated by determining the optical density at 600 nm (OD_{600}) of bacterial suspensions incubated overnight (16 to 24 h) in 96-well plates. The F.HKAIs did not inhibit bacterial growth at concentrations even as high as 500 $\mu\text{g/ml}$ ($MIC > 500 \mu\text{g/ml}$) except for F.B14 and F.F1.8. F.B14 and F.F1.8 showed antibacterial effect for *E. coli* CFT 073 and *S. marcescens* 21639 with MICs of 500 and 250 $\mu\text{g/ml}$, respectively (Table 2). The N.HKAIs showed antibacterial effect for *E. coli* CFT 073 with MICs corresponding to 3 to 100 $\mu\text{g/ml}$ HK inhibitors (Table 2) which in all cases is more than 10 times lower than the MICs of the F.HKAIs. To exclude the possibility that the observed antibacterial effect is due to the antibacterial action of the MCM-41 or of the ePLL in the nanoformulations, the MICs of MCM-41 and N.Rho were determined. MCM-41 and N.Rho did not inhibit bacterial growth, even at concentrations as high as 11 mg/ml ($MIC > 11 \text{ mg/ml}$) and 10 mg/ml ($MIC > 10 \text{ mg/ml}$), respectively. 10 mg/ml N.Rho corresponds to 1020 $\mu\text{g/ml}$ ePLL ($MIC_{\text{ePLL nanoformulation}} > 1020 \mu\text{g/ml}$, Table 3). The highest tested concentrations of MCM-41 and ePLL as part of N.Rho were higher than the MCM and ePLL content of the highest tested concentrations of the N.HKAIs. To exclude the possibility that the observed antibacterial effect of the N.HKAIs is due to a synergy effect of the HKAIs and ePLL within the nanoformulations, synergy effects against *E. coli* CFT 073 were tested by the checkboard method and no synergy between ePLL and the free HK inhibitors was observed ($FICs > 0.5$). Therefore, the antibacterial effect of the N.HKAIs is solely dependent on the release of the NPs cargo (the HKAIs) and not on the synergistic effect between the HKAIs and ePLL, or due to the presence of MCM-41 and/or ePLL in the nanoformulations.

ADVERSE EFFECTS ON HOST CELLS *IN VITRO*

To be used as effective drugs, antibacterials should not cause adverse effects such as cytotoxicity and immunotoxicity to host cells. Although silica is generally considered to be non-cytotoxic, the formulations of the silica-based NPs described here may affect their biocompatibility because of altered physicochemical properties. Therefore, to assess this we investigated the cytotoxicity and immunotoxicity of the NP formulations described in this chapter with and without incorporation of the HKAI to determine how it affected host toxicity of the HKAI.

Cytotoxicity

Viability of human colon carcinoma cells (Caco-2) incubated with MCM-41, N.Rho, N.HKAIs or F.HKAIs or ePLL was measured using the neutral-red uptake assay³⁹. The N.HKAIs showed lower cytotoxicity compared to the F.HKAIs (Table 4, Figure S3). The IC_{50} (the concentration of test material that causes a 50% decrease in neutral-red uptake, relative to the solvent control) of the N.HKAIs corresponded to $\geq 100 \mu\text{g/ml}$ HKAIs, whereas, the IC_{50} of the F.HKAIs varied between 3 and 134 $\mu\text{g/ml}$. The selectivity index, i.e. mammalian cell cytotoxicity (IC_{50})/antibacterial effect

(MIC), was improved for the N.HKAIs compared to the F.HKAIs. This is an expected result because mesoporous NPs capped with cationic ePLL are designed to interact with the negatively charged OM of Gr- bacteria³². Their proposed mechanism of action is attributed to ionic interaction of the positively charged ePLL capped NPs with the bacterial OM, followed by displacement and binding of ePLL to the Gr- cell membrane, thereby allowing the NKAIs to be released³². Furthermore, MCM-41 and ePLL were not cytotoxic at concentrations as high as 2742 µg/ml and 673 µg/ml, respectively, corresponding to the highest content of MCM-41 and ePLL present in the N.HKAIs. N.Rho was also not cytotoxic at 1000 µg/ml, corresponding to 102 µg/ml ePLL as part of the nanoformulation. This indicates that there is no synergistic effect between MCM-41 and the capping ePLL on cytotoxicity and suggests that ePLL capped mesoporous NPs are safe to be used for antibacterial drug delivery.

	IC ₅₀ [µg/ml] Selectivity index			
	Caco-2		IC ₅₀ /MIC _{E.coli} *	
	Nano	Free	Nano	Free
B2	≥ 100	n.t.	> 1	n.t.
B7	> 100	105	> 2	< 0.21
B11	≥ 100	≥ 500	≥ 7.7	< 1
B13	≥ 100	29	≥ 4	< 0.06
B14	≥ 50	3	≥ 1	0.006
B15	> 100	≈ 500	> 2	< 1
F1.8	> 25	134	> 4.2	0.54
F2.3	> 25	30	> 4.2	< 0.06

**E. coli* CFT 073

Table 4. Effect on cell viability of Caco-2 cells of free HKs autophosphorylation inhibitors (Free) and HKs autophosphorylation inhibitors loaded to silica-based mesoporous nanoparticles capped with ε-poly-L-lysine (Nano) evaluated by neutral-red uptake assay. IC₅₀ is the concentration at which 50% reduction in neutral-red uptake relative to the solvent control is observed. Detailed dose-effect curves are presented in Figure S3

Activation of NO production by macrophages and macrophage viability

The high-output isoform of nitric oxide synthase (NOS2 or iNOS) lies at the interface between the innate and adaptive immune systems⁴⁶. Human NOS2 is most readily observed in monocytes or macrophages from patients with infectious or inflammatory diseases. Sustained production of NO endows macrophages with cytostatic or cytotoxic activity against viruses, bacteria, fungi, protozoa, helminths, and tumor cells. Other macrophage products such as acid, glutathione, cysteine, hydrogen peroxide, or superoxide enhance the antibacterial and cytotoxic actions of NO. To investigate whether the NPs and the HKAI B13 interfered with NO production by immune cells we incubated cultured macrophages with MCM-41, N.Rho, N.B13 and F.B13 with and without LPS (1 μ g/ml) stimulation for 16 to 24 h and then measured NO production (Figure 4 and S4). Simultaneously, the effect of MCM-41, N.Rho, N.B13 and F.B13 on macrophage viability and TNF α protein levels were evaluated using the XTT assay and TNF α ELISA respectively (Figure 5, 6, and S4).

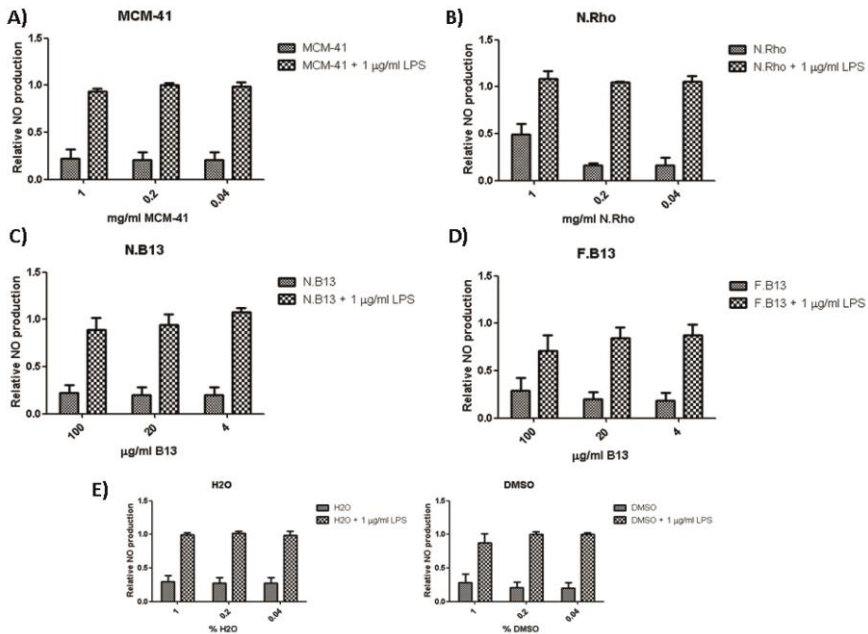


Figure 4. Dose effects of MCM-41 (A), N.Rho (B), N.B13 (C) and F.B13 (D) on NO production by cultured macrophages (Raw cells). NO production is not affected by MCM-41 (A), N.Rho (B), N.B13 (C), F.B13 (D) or the solvents (H2O and DMSO, E) with or without stimulation with 1 μ g/ml LPS. The results are presented relative to the NO production induced by stimulation with 1 μ g/ml LPS. The error bars present the SEM of at least three independent experiments in duplicate.

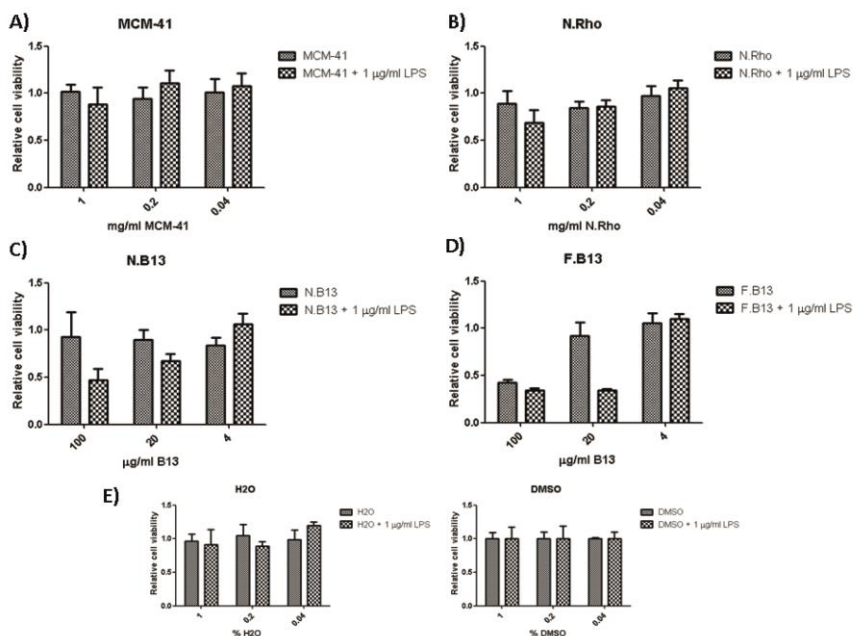


Figure 5. Dose effects of MCM-41 (A), N.Rho (B), N.B13 (C) and F.B13 (D) on cell viability of cultured macrophages (Raw cells). Cell viability is not affected by MCM-41 (A), N.Rho (B) or the solvents (H2O and DMSO, E) with or without stimulation with 1 µg/ml LPS. Reduction in cell viability by N.B13 (C) is observed only at the highest tested concentration (100 µg/ml B13) with stimulation with 1 µg/ml LPS. Reduction of cell viability by F.B13 (D) is observed at the highest tested concentration (100 µg/ml B13) with or without stimulation with 1 µg/ml LPS and at 20 µg/ml B13 with stimulation with 1 µg/ml LPS. The results are presented relative to the viability of the solvent controls (H2O or DMSO). The error bars present the SEM of at least two independent experiments in duplicate.

1 mg/ml MCM-41 or N.Rho did not cause significant changes in NO production by macrophages or in macrophage viability compared to the solvent control before or after stimulation with 1 µg/ml LPS. These results indicate that MCM-41 and N.Rho do not stimulate NO production by themselves and do not inhibit NO production induced by LPS. The production of NO before and after stimulation with 1 µg/ml LPS after incubation with N.B13 and F.B13 at concentrations corresponding to 100 µg/ml B13 was comparable to the solvent control. However, free HKAI F.B13 reduced viability of macrophages stimulated with LPS by more than 50% at a concentration of 100 µg/ml and LPS stimulated macrophage viability by more than 50% at a concentration of 20 µg/ml F.B13. This finding suggests that F.B13 might induce an increase in NO production by macrophages which is masked by its cytotoxic effect. The macrophage viability was decreased by N.B13 at concentrations corresponding to 100 µg/ml B13, implying that N.B13 also stimulates some NO production by macrophages. Nevertheless, these effects are observed at concentrations higher than the MIC of F.B13 for Gr+ bacteria and of N.B13 for Gr- bacteria (Chapter 2 and Table 2,

respectively). As the nanomaterials, MCM-41 and the control N.Rho did not cause significant changes in NO production or in macrophages viability, the N.B13 effect on NO production and macrophage viability can be attributed to release of the cargo, i.e. HKAI B13. This is in agreement with the cell viability study of free HKAI B13 and Caco-2 cells (Table 4 and Figure S3).

Production of tumor necrosis factor alpha by macrophages activated with NPs and F.HKAIs

Tumor-necrosis factor alpha (TNF α) is involved in the process of inflammation and in cellular processes mediating protection to bacterial infections⁴⁷. Antibacterials ideally should not alter the level of TNF α production by activated and resting macrophages. Indeed, neither the NPs (MCM-41, N.Rho or N.B13) nor the HKAI F.B13 caused changes in TNF α secretion by Raw cells before or after stimulation with 1 μ g/ml LPS (Figure 6).

ZEBRAFISH EMBRYOS CAN BE USED IN INFECTION STUDIES WITH MESOPOROUS SILICA-BASED NPS CAPPED WITH EPLL

To evaluate the toxicity of the NPs capped with ePLL and the suitability of zebrafish embryos for future infection studies, the toxicity of N.Rho to zebrafish embryos was evaluated. Given the low toxicity of the HKAI loaded NPs (N.HKAIs) and their antibacterial activity we evaluated the potential to deliver antibacterials via nanoparticles to zebrafish embryos via dispersion in the water.

Zebrafish infection models are becoming a valuable tool in pre-clinical antibacterial drug discovery^{48, 49, 50}. Experimental candidate drugs can be injected via the yolk sack or the blood vessels using a microinjection device. However, microinjection is time-consuming, laborious and not always accurate. Ideally, antibacterials delivered via nanoparticles are dispersed in the water to test their uptake, distribution and adverse effects.

N.Rho was dispersed in the water where the zebrafish embryos were incubated. The dispersion of the N.Rho in the water did not result in signs of toxicity and lethality of the zebrafish embryos for up to 24h hours post incubation (Figure 7) at concentrations of 10, 20 and 50 μ g/ml. Incubation with N.Rho led to concentration dependent increase of rhodamine fluorescence and increased over time in the intestine and in the yolk sac (Figure 7). These can be attributed to uptake of N.Rho via the gills or the skin⁵¹, distribution in the blood and accumulation in the yolk sac and intestine. The gills have been suggested as the main site for antigen uptake in fish, however, the skin was shown to play a significant role in the uptake of antigens as well⁵¹. If N.Rho is taken up via the gills, N.Rho might circulate through the vasculature to the yolk sac and the intestine. A similar distribution in the body was observed with liposomes delivered by immersion⁵². Possible release of the rhodamine cargo due the encounter of the N.Rho with the yolk content or with Gr- negative bacteria normally present in the intestine may also be a factor influencing the results.

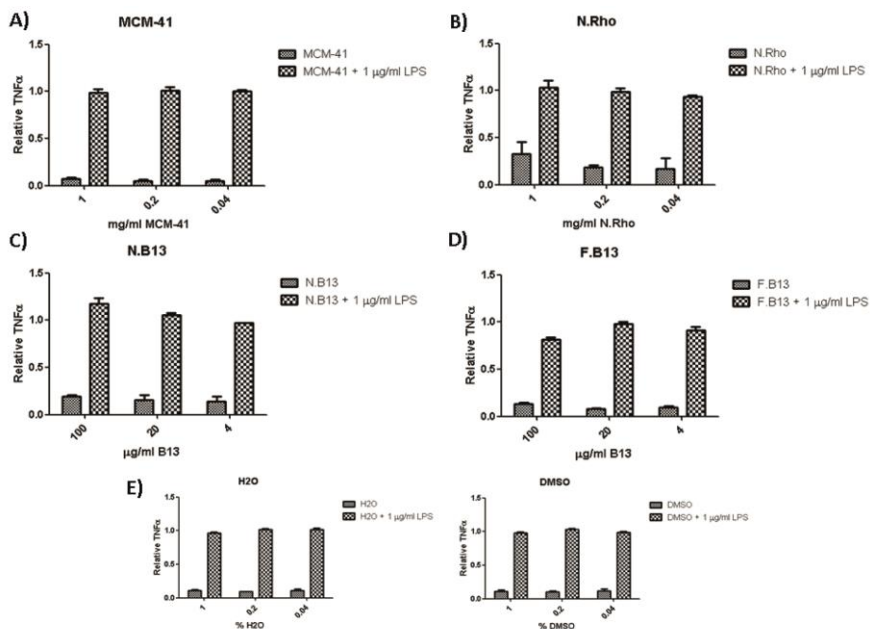


Figure 6. Dose effects of MCM-41 (A), N.Rho (B), N.B13 (C) and F.B13 (D) on TNF α levels of cultured macrophages (Raw cells). TNF α levels in Raw cells are not after incubation with MCM-41 (A), N.Rho (B), N.B13 (C), F.B13 (D) or by the solvents (H₂O and DMSO, E) with or without stimulation with 1 μ g/ml LPS. The results are presented relative to the TNF α levels after stimulation with 1 μ g/ml LPS. The error bars present the SEM of at two independent experiments in duplicate.

The observations made after incubation of N.Rho with zebrafish embryos open up new targeted strategies for treating bacterial infections in aquaculture industry using mesoporous silica-based NPs capped with ePLL thanks to the simplicity, absence of toxicity and accuracy of the cargo delivery.

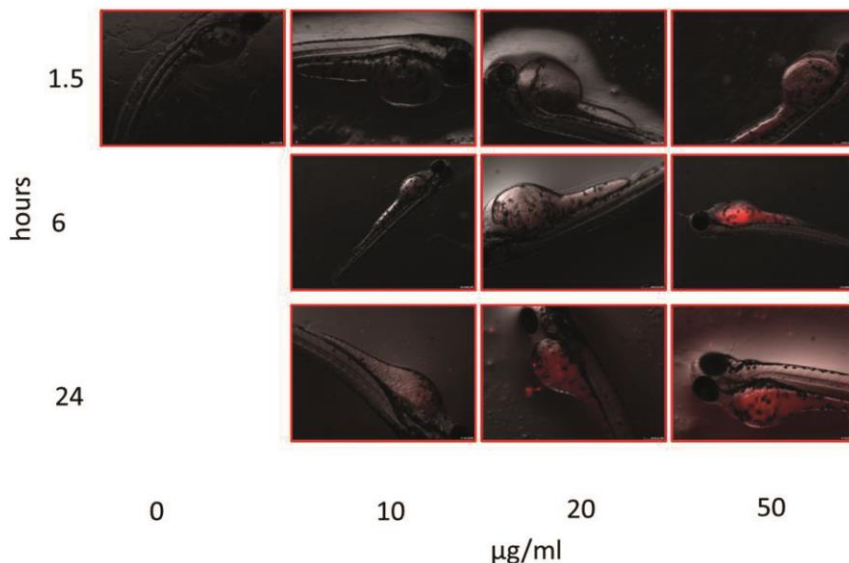


Figure 7. Incubation of zebrafish embryos with N.Rho. Rhodamine fluorescence in the yolk sack and the intestine is increased in concentration-dependent and time-dependent manner.

SUMMARY

By combining two novel strategies, loading of nanoparticles with antibacterials on the one hand, and targeting TCS signalling on the other hand, it was possible to achieve antibacterial effect against Gr- bacteria *in vitro*. The antibacterials-loaded NPs did not show adverse effects to mammalian cell viability, or immunotoxicity *in vitro*. The NPs did not cause adverse effects on zebrafish embryos. All together, these open promising possibilities for the treatment of Gr- infections and development of novel antibacterials and/ or delivery of antibacterials using nanoparticles.

REFERENCES

1. Curcio, D., Multidrug-Resistant Gram-Negative Bacterial Infections: Are you Ready for the Challenge? *Current clinical pharmacology* 2014, 9 (1), 27-38.
2. Dancer, S. J., The problem with cephalosporins. *The Journal of antimicrobial chemotherapy* 2001, 48 (4), 463-78.
3. Ibrahim, M. E.; Bilal, N. E.; Hamid, M. E., Increased multi-drug resistant *Escherichia coli* from hospitals in Khartoum state, Sudan. *African health sciences* 2012, 12 (3), 368-75.
4. Alhashash, F.; Weston, V.; Diggle, M.; McNally, A., Multidrug-resistant *Escherichia coli* bacteremia. *Emerging infectious diseases* 2013, 19 (10), 1699-701.
5. Vigil, K. J.; Adachi, J. A.; Aboufaycal, H.; Hachem, R. Y.; Reitzel, R. A.; Jiang, Y.; Tarrand, J. J.; Chemaly, R. F.; Bodey, G. P.; Rolston, K. V.; Raad, I., Multidrug-resistant *Escherichia coli* bacteremia in cancer patients. *American journal of infection control* 2009, 37 (9), 741-5.
6. UF/IFAS Fact Sheets FA-14 *Aeromonas* Infections, FA-31 *Vibrio* Infections of Fish and FA-11 Columnaris disease.
7. Verner-Jeffreys, D. W.; Welch, T. J.; Schwarz, T.; Pond, M. J.; Woodward, M. J.; Haig, S. J.; Rimmer, G. S.; Roberts, E.; Morrison, V.; Baker-Austin, C., High prevalence of multidrug-tolerant bacteria and associated antimicrobial resistance genes isolated from ornamental fish and their carriage water. *PLoS one* 2009, 4 (12), e8388.
8. Hall, R. M.; Collis, C. M.; Kim, M. J.; Partridge, S. R.; Recchia, G. D.; Stokes, H. W., Mobile gene cassettes and integrons in evolution. *Annals of the New York Academy of Sciences* 1999, 870, 68-80.
9. Schmidt, A. S.; Bruun, M. S.; Dalsgaard, I.; Larsen, J. L., Incidence, distribution, and spread of tetracycline resistance determinants and integron-associated antibiotic resistance genes among motile aeromonads from a fish farming environment. *Applied and environmental microbiology* 2001, 67 (12), 5675-82.
10. Rhodes, G.; Huys, G.; Swings, J.; McGann, P.; Hiney, M.; Smith, P.; Pickup, R. W., Distribution of oxytetracycline resistance plasmids between aeromonads in hospital and aquaculture environments: implication of Tn1721 in dissemination of the tetracycline resistance determinant tet A. *Applied and environmental microbiology* 2000, 66 (9), 3883-90.
11. Furushita, M.; Shiba, T.; Maeda, T.; Yahata, M.; Kaneoka, A.; Takahashi, Y.; Torii, K.; Hasegawa, T.; Ohta, M., Similarity of tetracycline resistance genes isolated from fish farm bacteria to those from clinical isolates. *Applied and environmental microbiology* 2003, 69 (9), 5336-42.
12. Welch, T. J.; Fricke, W. F.; McDermott, P. F.; White, D. G.; Rosso, M. L.; Rasko, D. A.; Mammel, M. K.; Eppinger, M.; Rosovitz, M. J.; Wagner, D.; Rahalison, L.; Leclerc, J. E.; Hinshaw, J. M.; Lindler, L. E.; Cebula, T. A.; Carniel, E.; Ravel, J., Multiple antimicrobial resistance in plague: an emerging public health risk. *PLoS one* 2007, 2 (3), e309.
13. Da Costa, P. M.; Loureiro, L.; Matos, A. J. F., Transfer of multidrug-resistant bacteria between intermingled ecological niches: The interface between humans, animals and the environment. *International journal of environmental research and public health* 2013, 10 (1), 278-294.
14. Ewers, C.; Grobbel, M.; Bethe, A.; Wieler, L. H.; Guenther, S., Extended-spectrum beta-lactamases-producing gram-negative bacteria in companion animals: action is clearly warranted! *Berliner und Munchener tierarztliche Wochenschrift* 2011, 124 (3-4), 94-101.
15. Ahmed, A. M.; Motoi, Y.; Sato, M.; Maruyama, A.; Watanabe, H.; Fukumoto, Y.; Shimamoto, T., Zoo animals as reservoirs of gram-negative bacteria harboring integrons

- and antimicrobial resistance genes. *Applied and environmental microbiology* 2007, 73 (20), 6686-6690.
16. Velikova, N.; Bem, A. E.; van Baarlen, P.; Wells, J. M.; Marina, A., *WalK, the Path towards New Antibacterials with Low Potential for Resistance Development*. *ACS Medicinal Chemistry Letters* 2013, 4 (10), 891-894.
 17. Rutherford, S. T.; Bassler, B. L., *Bacterial quorum sensing: its role in virulence and possibilities for its control*. *Cold Spring Harbor perspectives in medicine* 2012, 2 (11).
 18. Rasko, D. A.; Moreira, C. G.; Li de, R.; Reading, N. C.; Ritchie, J. M.; Waldor, M. K.; Williams, N.; Taussig, R.; Wei, S.; Roth, M.; Hughes, D. T.; Huntley, J. F.; Fina, M. W.; Falck, J. R.; Sperandio, V., *Targeting QseC signaling and virulence for antibiotic development*. *Science* 2008, 321 (5892), 1078-80.
 19. Casino, P.; Rubio, V.; Marina, A., *The mechanism of signal transduction by two-component systems*. *Current opinion in structural biology* 2010, 20 (6), 763-71.
 20. Kenney, L. J., *How important is the phosphatase activity of sensor kinases?* *Current opinion in microbiology* 2010, 13 (2), 168-76.
 21. Zhu, Y.; Qin, L.; Yoshida, T.; Inouye, M., *Phosphatase activity of histidine kinase EnvZ without kinase catalytic domain*. *Proceedings of the National Academy of Sciences of the United States of America* 2000, 97 (14), 7808-13.
 22. Skerker, J. M.; Prasol, M. S.; Perchuk, B. S.; Biondi, E. G.; Laub, M. T., *Two-component signal transduction pathways regulating growth and cell cycle progression in a bacterium: a system-level analysis*. *PLoS biology* 2005, 3 (10), e334.
 23. Wick, L. M.; Gli, T., *Molecular components of physiological stress responses in Escherichia coli*. *Advances in biochemical engineering/biotechnology* 2004, 89, 1-45.
 24. Crepin, S.; Chekabab, S. M.; Le Bihan, G.; Bertrand, N.; Dozois, C. M.; Harel, J., *The Pho regulon and the pathogenesis of Escherichia coli*. *Veterinary microbiology* 2011, 153 (1-2), 82-8.
 25. Chekabab, S. M.; Harel, J.; Dozois, C. M., *Interplay between genetic regulation of phosphate homeostasis and bacterial virulence*. *Virulence* 2014, 5 (5).
 26. Chekabab, S. M.; Jubelin, G.; Dozois, C. M.; Harel, J., *PhoB activates Escherichia coli O157:H7 virulence factors in response to inorganic phosphate limitation*. *PloS one* 2014, 9 (4), e94285.
 27. Nikaido, H., *Molecular basis of bacterial outer membrane permeability revisited*. *Microbiology and molecular biology reviews : MMBR* 2003, 67 (4), 593-656.
 28. Page, M. G., *The role of the outer membrane of Gram-negative bacteria in antibiotic resistance: Ajax' shield or Achilles' heel?* *Handbook of experimental pharmacology* 2012, (211), 67-86.
 29. Brehm-Stecher, B. F.; Johnson, E. A., *Sensitization of Staphylococcus aureus and Escherichia coli to antibiotics by the sesquiterpenoids nerolidol, farnesol, bisabolol, and apritone*. *Antimicrobial agents and chemotherapy* 2003, 47 (10), 3357-60.
 30. Bolla, J. M.; Alibert-Franco, S.; Handzlik, J.; Chevalier, J.; Mahamoud, A.; Boyer, G.; Kiec-Kononowicz, K.; Pages, J. M., *Strategies for bypassing the membrane barrier in multidrug resistant Gram-negative bacteria*. *FEBS letters* 2011, 585 (11), 1682-90.
 31. Huh, A. J.; Kwon, Y. J., *"Nanoantibiotics": a new paradigm for treating infectious diseases using nanomaterials in the antibiotics resistant era*. *Journal of controlled release : official journal of the Controlled Release Society* 2011, 156 (2), 128-45.
 32. Mas, N.; Galiana, I.; Mondragon, L.; Aznar, E.; Climent, E.; Cabedo, N.; Sancenon, F.; Murguia, J. R.; Martinez-Manez, R.; Marcos, M. D.; Amoros, P., *Enhanced efficacy and broadening of antibacterial action of drugs via the use of capped mesoporous nanoparticles*. *Chemistry* 2013, 19 (34), 11167-71.

33. Waltho, J. P.; Williams, D. H., The natural design of vancomycin family antibiotics to bind their target peptides. Ciba Foundation symposium 1991, 158, 73-86; discussion 87-91, 92-7.
34. Ye, R.; Xu, H.; Wan, C.; Peng, S.; Wang, L.; Xu, H.; Aguilar, Z. P.; Xiong, Y.; Zeng, Z.; Wei, H., Antibacterial activity and mechanism of action of epsilon-poly-L-lysine. Biochemical and biophysical research communications 2013, 439 (1), 148-53.
35. Conlon, J. M.; Mechkarska, M.; Prajeep, M.; Sonnevend, A.; Coquet, L.; Leprince, J.; Jouenne, T.; Vaudry, H.; King, J. D., Host-defense peptides in skin secretions of the tetraploid frog *Silurana epittropicalis* with potent activity against methicillin-resistant *Staphylococcus aureus* (MRSA). Peptides 2012, 37 (1), 113-9.
36. Clinical Laboratory and Standards Institute Methods for Antimicrobial Susceptibility Testing of Anaerobic Bacteria; Approved Standard. M11-A7. 2007; Vol. 7th ed.
37. CLSI, Methods for dilution antimicrobial susceptibility tests for bacteria that grow aerobically. CLSI: Wayne, PA, 2009; Vol. 8th ed. M7-A8.
38. Gialdroni Grassi, G.; Ferrara, A.; Peona, V.; Colombo, M. L., [Evaluation of the bactericidal activity of the combination of fosfomycin with other antibiotics by 2 different methods (checkboard and bactericidal curves)]. Giornale italiano di chemioterapia 1983, 30 (2-3), 77-84.
39. Repetto, G.; del Peso, A.; Zurita, J. L., Neutral red uptake assay for the estimation of cell viability/cytotoxicity. Nature protocols 2008, 3 (7), 1125-31.
40. Green, L. C.; Wagner, D. A.; Glogowski, J.; Skipper, P. L.; Wishnok, J. S.; Tannenbaum, S. R., Analysis of nitrate, nitrite, and [15N]nitrate in biological fluids. Analytical biochemistry 1982, 126 (1), 131-8.
41. Roehm, N. W.; Rodgers, G. H.; Hatfield, S. M.; Glasebrook, A. L., An improved colorimetric assay for cell proliferation and viability utilizing the tetrazolium salt XTT. Journal of immunological methods 1991, 142 (2), 257-65.
42. Kessels, M. Y.; Huitema, L. F.; Boeren, S.; Kranenbarg, S.; Schulte-Merker, S.; van Leeuwen, J. L.; de Vries, S. C., Proteomics analysis of the zebrafish skeletal extracellular matrix. PloS one 2014, 9 (3), e90568.
43. Fiaz, A. W.; Leon-Kloosterziel, K. M.; Gort, G.; Schulte-Merker, S.; van Leeuwen, J. L.; Kranenbarg, S., Swim-training changes the spatio-temporal dynamics of skeletogenesis in zebrafish larvae (*Danio rerio*). PloS one 2012, 7 (4), e34072.
44. O'Shea, R.; Moser, H. E., Physicochemical properties of antibacterial compounds: implications for drug discovery. Journal of medicinal chemistry 2008, 51 (10), 2871-8.
45. Abed, N.; Couvreur, P., Nanocarriers for antibiotics: A promising solution to treat intracellular bacterial infections. International journal of antimicrobial agents 2014, 43 (6), 485-96.
46. MacMicking, J.; Xie, Q. W.; Nathan, C., Nitric oxide and macrophage function. Annual review of immunology 1997, 15, 323-50.
47. Cooper, A. M.; Appelberg, R.; Orme, I. M., Immunopathogenesis of *Mycobacterium avium* infection. Frontiers in bioscience : a journal and virtual library 1998, 3, e141-8.
48. van der Sar, A. M.; Musters, R. J.; van Eeden, F. J.; Appelmelk, B. J.; Vandenbroucke-Grauls, C. M.; Bitter, W., Zebrafish embryos as a model host for the real time analysis of *Salmonella typhimurium* infections. Cellular microbiology 2003, 5 (9), 601-11.
49. Medina, C.; Royo, J. L., Zebrafish as a model organism to study host-pathogen interactions. Methods 2013, 62 (3), 241-5.
50. Meijer, A. H.; Spaink, H. P., Host-pathogen interactions made transparent with the zebrafish model. Current drug targets 2011, 12 (7), 1000-17.
51. Nakanishi, T.; Ototake, M., Antigen uptake and immune responses after immersion vaccination. Developments in biological standardization 1997, 90, 59-68.

52. Ruyra, A.; Cano-Sarabia, M.; Garcia-Valtanen, P.; Yero, D.; Gibert, I.; Mackenzie, S. A.; Estepa, A.; Maspoch, D.; Roher, N., Targeting and stimulation of the zebrafish (*Danio rerio*) innate immune system with LPS/dsRNA-loaded nanoliposomes. *Vaccine* 2014, 32 (31), 3955-62.

SUPPLEMENTARY MATERIAL CHAPTER 4

MATERIALS CHARACTERIZATION

MCM-41 as-synthesized, MCM-41 and the final N.Rho and N.HKAIs (N.B2, N.B7, N.B11, N.B13, N.B14, N.B15, N.F1.8 and N.F2.3) synthesized materials were characterized through standard techniques. Figure S1 shows the X-ray diffraction (XRD) patterns of the nanoparticulated MCM-41 matrix as-synthesised, the MCM-41 calcined and the final N.Rho solid. (The rest of X-ray diffraction patterns of the antibacterial loaded solids are not shown due to the low amount of final solids obtained). The MCM-41 as-synthesised (curve a) displayed the four typical low-angle reflections of a hexagonal-ordered matrix indexed at (100), (110), (200) and (210) Bragg peaks. In curve b (MCM-41 calcined), a significant shift of the (100) peak in the XRD and a broadening of the (100) and (200) peaks are observed. These changes are due to the condensation of silanols in the calcination step, which caused an approximate cell contraction of 4 Å. Finally, curve c shows the N.Rho solid XRD pattern.

For this material, reflections (110) and (200) were mostly lost due to a reduction in contrast related to the functionalisation process and to the filling of mesopores with rhodamine B. Although these reductions, the intensity of the (100) peak in this pattern strongly indicates that the loading process with the dye and the additional functionalisation with *N*-[(3-Trimethoxysilyl)propyl]ethylenediamine triacetic acid trisodium salt and the covering with ϵ -poly-L-lysine did not modify the mesoporous MCM-41 scaffold nature.

Likewise, TEM analysis of the different prepared solids was performed. TEM images showed the typical channels of the MCM-41 scaffolding and can be visualised as alternate black and white stripes in which the typical hexagonal porosity of the MCM-41 calcined material can also be observed (see Figure 2). In the same way, TEM images of some of the final solids loaded with the antibacterial products are also shown in Figure 2. The remaining final solids also showed the same morphology under the TEM analysis. TEM images also show that the materials were obtained as spherical nanoparticles of ca 80 - 100 nm. Then, it can be concluded that the spherical shape and mesoporous nature of the inorganic matrix remains after the loading and functionalization processes.

Figure S2 (curve a) displays the N₂ adsorption-desorption isotherms of the MCM-41 calcined nanoparticles. This curve shows an adsorption step with a P/P_0 value between 0.2 and 0.35, due to a type IV isotherm, which is typical of mesoporous materials. This first step corresponds to nitrogen condensation in the mesopore inlets. With the BJH^[3] model on the adsorption curve of the isotherm, a narrow pore size distribution with an average pore diameter of 2.56 nm (see Figure S2 inlet) and a pore volume of 0.64 cm³g⁻¹ were calculated. The absence of a hysteresis loop in this pressure range and the low BJH pore distribution is due to the cylindrical uniformity of mesopores. The total specific area was 916 m²g⁻¹, calculated with the BET model.^[4] The a_0 cell parameter 42.9 Å (d_{100} = 37.17 Å), the pore diameter (2.56 nm) and the wall

thickness value (17.31 Å) were calculated from the XRD, porosimetry and TEM measurements. Other important feature of the curve is the characteristic H1 hysteresis loop that appears in the isotherm at a high relative pressure ($P/P_0 > 0.8$) which can be closely associated with a wide pore size distribution. This hysteresis loop is due to the filling of the large pores among the nanoparticles ($0.22 \text{ cm}^3 \text{ g}^{-1}$ calculated by the BJH model) because of textural porosity. In relation to the control synthesized N.Rho material, the N_2 adsorption-desorption isotherm of this solid was associated to the typical mesoporous systems with filled mesopores (see Figure S2, curve b). Thus, as it was expected, a lower N_2 adsorbed volume (BJH mesopore volume = $0.15 \text{ cm}^3 \text{ g}^{-1}$) and surface area ($204.9 \text{ m}^2 \text{ g}^{-1}$) were found, compared with the initial MCM-41 material. As it can be observed, this solid presents a curve with no gaps at low relative pressure values if compared to the mother MCM-41 matrix (curve a). Another important feature of N.Rho is that no maximum was found in the pore size distribution curve, which can be associated with the closed pores due to the functionalization process. Table S2 shows a summary of the BET-specific surface values, pore volumes and pore sizes calculated from the N_2 adsorption-desorption isotherms for MCM-41 calcined and N.Rho.

Thermogravimetric studies and elemental analyses of all final prepared solids were carried out, in order to quantify the organic contents of each material. In particular, the amount of the different loading products and functionalization with product *f* and ePLL were calculated. All the results are summarized in Table 1 in the body text.

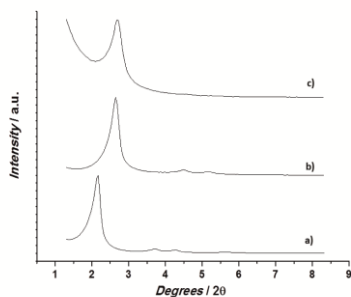


Figure S1. Powder X-Ray diffractograms showing X-Ray patterns of MCM-41 scaffolding as synthesized (a), MCM-41 after the calcination process(b) and the final control solid N.Rho(c).

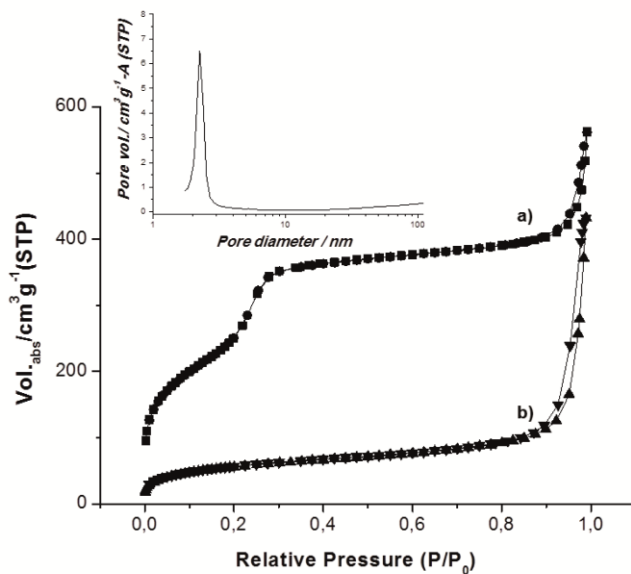


Figure S2. Nitrogen adsorption-desorption isotherms for (a) MCM-41 mesoporous material (b) N.Rho. Inlet:Pore size distributions of the MCM-41 mesoporous material.

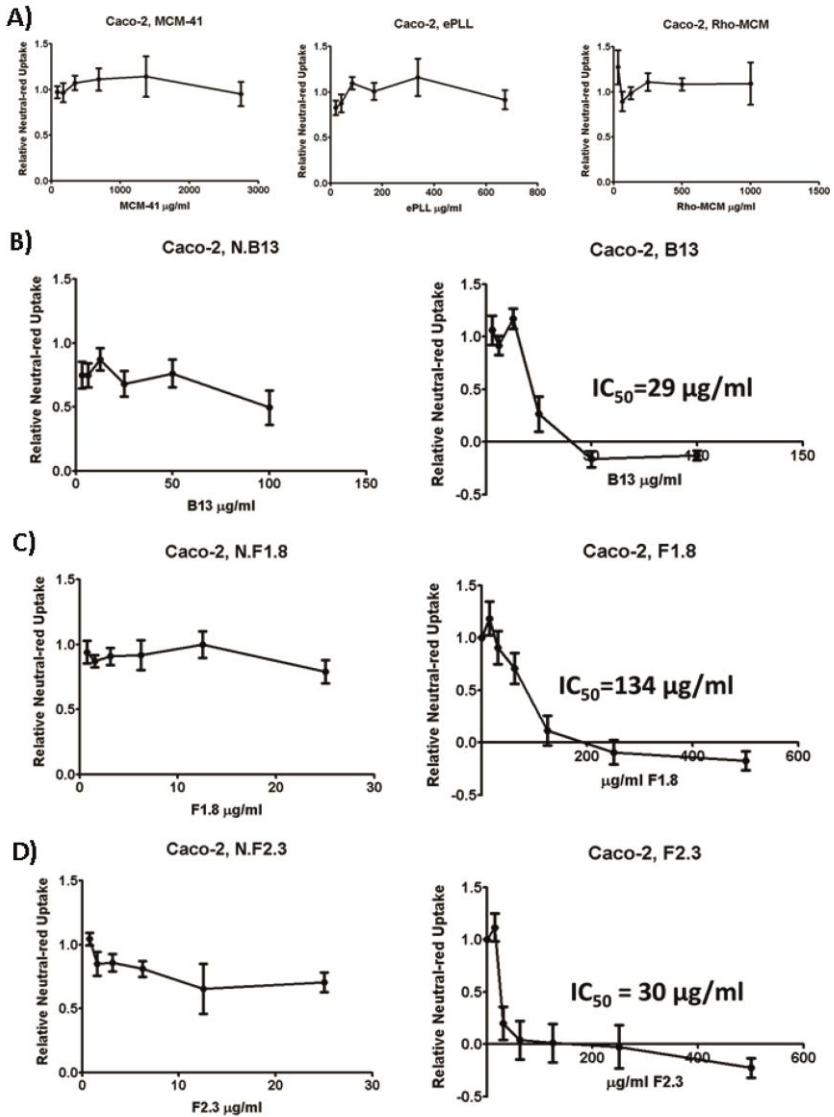


Figure S3. Cell viability of Caco-2 cells assessed by neutral-red uptake after 24 h exposure to NPs or to free HKAls. Error bars represent the SEM of at least two independent experiments in duplicate.

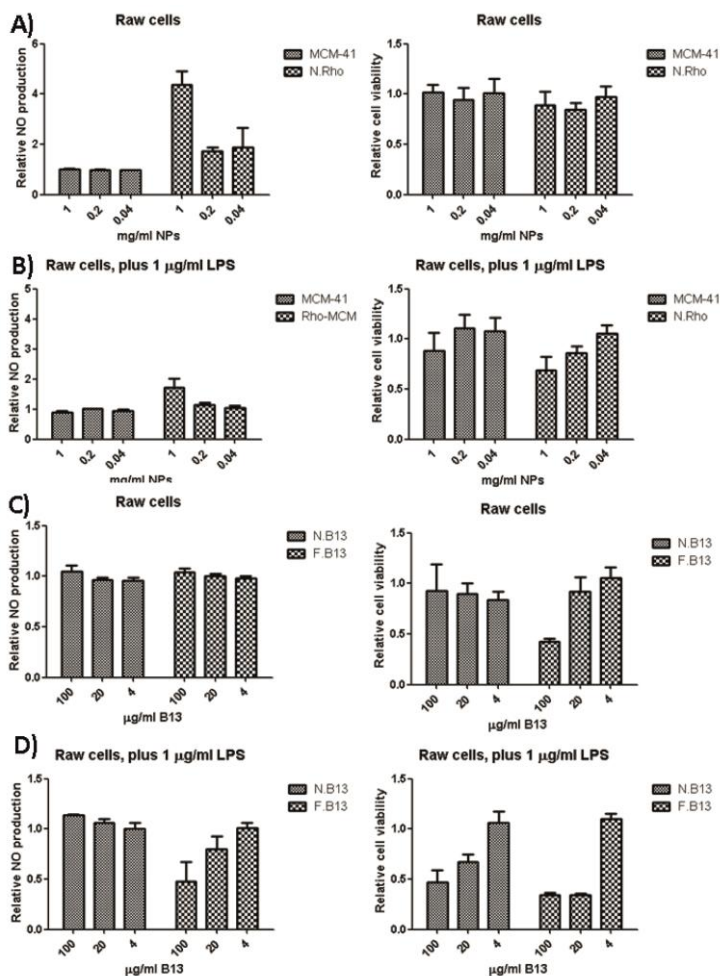


Figure S4. Dose effect of the NPs MCM-41 (A, B), N.Rho (A, B) or N.B13 (C, D) and F.B13 (C, D) on NO production and cell viability of macrophages before (A, C) or after stimulation with 1 µg/ml LPS (B, D). Results are expressed as the effect of the NPs or F.B13 relative to the effect of the solvent controls (water or DMSO, respectively). The error bars represent the SEM of at least two independent experiments in duplicate.

Table S1. Selected histidine kinase autophosphorylation inhibitors (HKAI)s and their physicochemical properties

	NCI number	logS	logP	logD	MW	HBD	HBA	TPSA	Flexibility	RB*
F.B2	73090	2.9	3	3	229	1	2	29.1	0.2	3
F.B7	109741	2.3	3.6	3.6	246	1	2	29.1	0.2	3
F.B11	211552	2.2	3.2	3.2	282	1	5	74.9	0.2	5
F.B13	32652	0.9	5.3	5.3	272	1	1	20.2	0.2	5
F.B14	48154	1.7	4.3	2.3	255	2	2	32.3	0.2	4
F.B15	7436	2.3	3.3	1.7	304	2	4	72.2	0.2	4
F.F1.8	80819	2.4	2.2	1.3	265	2	4	63.8	0.1	2
F.F2.3	106510	3.1	2.5	1.1	210	2	2	41.8	0.1	2

*RB-rotatable bonds

Table S2. BET specific surface values, pore volumes and pore sizes calculated from the N₂ adsorption-desorption isotherms for selected materials.

	S _{BET} (m ² g ⁻¹)	Pore Volume (cm ³ g ⁻¹)	Pore Size (nm)
MCM-41	916	0.64	2.56
N.Rho	204.9	0.15	-

2014

CHAPTER 5

COMPUTER-AIDED APPROACHES IN HIT OPTIMISATION

Nadya Velikova

2014

ABBREVIATIONS

QSAR – quantitative structure-activity relationship

LEI – ligand-efficiency index

SEI – surface-efficiency index

BEI – binding-efficiency index

TCS – two-component systems

HK – histidine kinase

RR – response regulator

INTRODUCTION

Computational chemistry has been applied widely in the pharmaceutical industry for drug discovery, lead optimization, risk assessment, toxicity prediction and regulatory decisions ¹. Over the past four decades, quantitative structure–activity relationship (QSAR) modelling has completely changed the way the interaction of organic compounds with the various forms of life is studied ². It attempts to formulate the relationship between structure and activity as a mathematical model. Therefore, the binding affinity of a new molecule can be predicted using a QSAR model derived from the known inhibitors and their experimental bioassay values ³. Using such an approach, a large library of possible drug candidates can be tested for their predicted selectivity and potency ⁴, saving time and money in drug discovery research. Successful drug discovery requires not only identifying hits with desired biochemical properties (e.g. target affinity) but also hits with optimal physicochemical and ADMET (adsorption, distribution, metabolism, excretion and toxicity) properties ⁵. Once a hit is identified its optimisation should be bidirectional. Ligand-efficiency indices (LEIs) connect the physicochemical properties of hits (e.g. MW and polar surface area [PSA]) with the biological target via the affinity parameter (IC₅₀, enzyme activity or other related measures of affinity) ^{6,7}.

Herein we describe the application of computer-aided drug discovery approaches (including QSAR modelling, ligand-based similarity search and LEIs-based evaluation) for the identification of putative HK autophosphorylation inhibitors with antibacterial activity and low toxicity.

MATERIALS AND METHODS

QSAR PREDICTIVE MODEL BUILDING

The experimental *E. coli* PhoR autophosphorylation inhibition data (% inhibition at 2 mM) of 39 compounds (Chapter 3 and 4) were used as a dataset for building a quantitative structure–activity relationship (QSAR) model for inhibition of *E. coli* PhoR autophosphorylation (Table S1). The percentage inhibition range was from 6 to 85%. Predictive QSAR model was built automatically using the Auto-Modeller module of StarDrop (Optibrium, Cambridge) ⁸.

LIGAND-BASED SIMILARITY SEARCHES

The National Cancer Institute Developmental Therapeutics Programme database (DTP NCI/NIH) was searched for analogue structures of the query molecules B7, B11, B13, B15, F1.8, F2.4, F2 (Figure 1) using the Enhanced NCI database browser v 2.2 ⁹. Molecules with more than 80% similarity to the query molecules (Tanimoto coefficient > 80%) and with predicted drug-like properties were saved for further scoring.

SCORING AND SELECTION OF COMPOUNDS FOR EXPERIMENTAL TESTING

Ligand-based similarity searches (LBSS) hits were evaluated using the StarDrop Oral non central nervous system (CNS) scoring profile (logS>1, importance 90%; positive HIA category, importance 85%; 0<logP<0.35, importance 60%; -0.2<BBB log<1, importance 55%; positive BBB category, importance 55%; P-gp category “no”, importance 50%; hERG IC50≤5, importance 50%; 2C9 pKi≤6, importance 30%; 2D6 affinity category “low to medium”, importance 30%; PPB90 category “low”, importance 20%).

Predicted *E. coli* PhoR autophosphorylation inhibition score was calculated using the QSAR Random Forest Regression model built with StarDrop.

After visual inspection, 18 compounds with oral non-CNS score > 0.4 and predicted *E. coli* PhoR autophosphorylation inhibition higher than 0.45, were purchased for experimental testing.

The predicted *E. coli* PhoR autophosphorylation activity was used as input to calculate binding efficiency indices (nBEIs) and surface efficiency indices (NSEIs) using AtlasCBS ⁶ and the following equations:

$$\text{NSEI} = -\log_{10} \text{pREA} / \text{NPOL}$$
, where pREA stands for predicted residual enzyme activity in one concentration (2 mM) one time-point (30 sec) kinase assay experiments with PhoR^E, and NPOL is number of polar N and O atoms in the compound.

$nBEI = -\log_{10}[\text{pREA}/\text{NHEA}]$, where NHEA is the number of non-hydrogen atoms in the compound.

Out of the 1012 LBSS hits, 36 were purchased for experimental testing following visual inspection.

CHEMICALS

All chemicals (Figure S1 and Table S2) were obtained from DTP NCI/NIH.

ANTIMICROBIAL SUSCEPTIBILITY TESTING

Strains used for antimicrobial susceptibility testing (Table 1) were propagated using standard microbiological procedures and Müller-Hinton (MH) agar or broth. For all microorganisms minimal inhibitory concentrations (MICs) were determined as previously described following a standard double-dilution method^{10, 11}.

PROTEIN EXPRESSION AND PURIFICATION

The catalytic portions (DHp and CA domain) of *E. coli* PhoR (PhoR^E) were expressed and purified as previously described¹². In brief the protein was expressed in *E. coli* RIL and purified by Ni-affinity and size-exclusion chromatography.

KINASE ASSAY

Kinase assay was performed as previously described¹³. When comparing the inhibitory capacity of ligands and measuring IC₅₀, the final DMSO concentration in the assay was 10% (v/v). Controls lacking ligands and containing an equal concentration of DMSO were carried out in parallel. Inhibition of HKs autophosphorylation was determined by incubating 0.12 mg/ml ($\approx 4 \mu\text{M}$ HK) and up to 20 mM of test compound in kinase buffer (50 mM Tris HCl, pH 8.5, 50 mM KCl, 5 mM MgCl₂, 0.5 mM EDTA and 0.1 mM DTT). Autophosphorylation reactions were initiated by addition of 0.1 $\mu\text{Ci}/\mu\text{l}$ [γ -³²P] ATP containing from 0.03 to 0.06 μM ATP (final concentrations). Autophosphorylation was stopped by addition of 2x SDS-PAGE sample buffer supplemented with 50 mM EDTA. Samples were applied without heating to 15% (w/v) Tris-glycine SDS-polyacrylamide gels. After electrophoresis, the bottom part of the gels were removed to lower the background signal from the unincorporated radiolabeled ATP. Gels were dried without staining on a Bio-Rad Gel Air drying system and the phosphorylated protein was quantified by phosphor-imaging using a Fluoro Image Analyzer FLA-5000 (Fujifilm, Japan) and evaluated with the MultiGauge software (Fujifilm, Japan). IC₅₀ is the concentration at which 50% residual enzyme activity was observed compared to the negative control, DMSO. Prism GraphPad v.4 was used for curve fitting and statistical analysis¹⁴.

BINDING MODE PREDICTION

The binding mode of selected ligands to the structure of the CA domain of *B. subtilis* WalK (PDB: 3SL2) was predicted by molecular docking using SwissDock¹⁵. In Figure 2 the lowest energy binding pose is shown.

RESULTS AND DISCUSSION

SELECTION OF COMPOUNDS FOR EXPERIMENTAL TESTING

To facilitate the selection of putative histidine kinase inhibitors for experimental testing in the process of hit-to-lead optimization quantitative structure–activity relationship (QSAR) models were built using a trial version of StarDrop⁸. The best among the generated models was the random forest regression QSAR model however, it was not of high merit with r^2 of 0.71 (Figure 1, Figure S2). In many QSAR studies the criterion r^2 greater than 0.9 is employed to decide whether a model is internally self-consistent. However, r^2 makes no assessment of the intrinsic precision or accuracy of the data itself. Nevertheless, we used this model to predict the *E. coli* PhoR autophosphorylation inhibitory capacity of 1012 hits from ligand-based similarity searches (LBSS) with previously identified histidine kinase autophosphorylation inhibitors as query molecules. The predicted autophosphorylation activities were used to evaluate the physicochemical properties of the selected LBSS hits using AtlasCBS⁶. The hits fell into one of seven groups based on NSEI (surface efficiency index) with the group around B13 showing highest predicted surface efficiency (Figure S3). The following group in terms of NSEI grouped around the F1.8 but with nearly two-fold lower predicted NSEIs. In total 54 compounds were ordered for experimental testing based on the StarDrop and AtlasCBS evaluation and visual inspection of the hits for promising functional groups.

H30 AND H31 SHOW ANTIBACTERIAL EFFECT FOR BOTH GRAM-POSITIVE AND GRAM-NEGATIVE BACTERIA

To evaluate the antibacterial effect of the selected hits, the MICs (minimal inhibitory concentrations) and MBCs (minimal bactericidal concentrations) for *S. aureus* DSM 20231, *S. aureus* CH3657, *S. epidermidis* DSM 20044 and *E. coli* CFT 073 were determined. H30 and H31 showed the strongest antibacterial effect. H30 inhibited *S. aureus* CH3657, *S. epidermidis* DSM 20044 and uropathogenic *E. coli* CFT 073 with MICs of 62.5, 500 $\mu\text{g/ml}$ and 500 $\mu\text{g/ml}$, respectively (Table S4). H31 inhibits *S. aureus* CH3657, *S. epidermidis* DSM 20044 and *E. coli* CFT 073 with MICs of 62.5, 125 and 250 $\mu\text{g/ml}$, respectively. H12 and H27 also showed some antibacterial effect with MICs higher than 250 $\mu\text{g/ml}$. Therefore, only H30 and H31 were tested against a panel of Gram-positive and Gram-negative bacteria and the results are summarized in Table 1. H30 did not show antibacterial effect for any of the additional bacterial strains tested. H31 inhibited the growth of all tested bacterial strains, including the vancomycin resistant *E. faecium* strains with MICs of 125 $\mu\text{g/ml}$

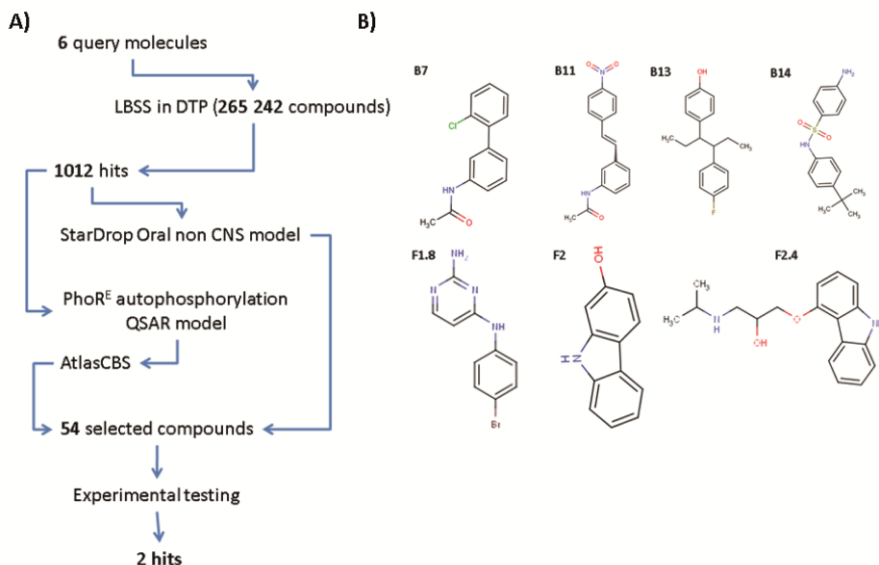


Figure 1. A) Computer-aided drug discovery approach B) Histidine kinase autophosphorylation inhibitors used as query molecules for ligand-based similarity search

H30 INHIBITS *E. COLI* PHOR AUTOPHOSPHORYLATION AND IS PREDICTED TO BIND TO THE ATP-BINDING SITE OF THE CA DOMAIN OF *B. SUBTILIS* WALK

To confirm the autophosphorylation inhibitory capacity of H30 and H31 *in vitro* kinase assay with *E. coli* PhoR was performed. *E. coli* PhoR autophosphorylation activity was inhibited by H30 and H31 in a concentration dependent manner with $IC_{50} \geq 1$ and $IC_{50} > 2$ mM, respectively. Both compounds showed good solubility in kinase buffer. As H30 showed antibacterial effect against *S. aureus* CH3657 and *S. epidermidis* DSM 20044 (Table 1) and not to the other tested Gram-positive strains, we hypothesized that it might interact with WalK. WalK belongs to the WalKR two-component system which is ubiquitous among Gram positive bacteria and in some species it is reported as essential for bacterial growth^{16, 17}.

Table 1. Antibacterial activities of H30 and H31. *E. faecium* Van and VanB strains are vancomycin resistant strains.

Strain	MIC [$\mu\text{g/ml}$]	
	H30	H31
<i>Staphylococcus aureus</i>		
CH3657	63	63
<i>Enterococcus faecalis</i>		
DMS 20478	500	< 4
<i>Streptococcus epidermidis</i>		
DMS 20444	500	125
<i>Enterococcus faecium</i>		
S1	> 500	125
VanA	> 500	125
VanB	>500	125
<i>Escherichia coli</i>		
CFT 073	500	250
<i>Serratia marcescens</i>		
	>500	500

H30 was docked to the structure of the catalytic and ATP-binding domain (CA) of *B. subtilis* WalK (PDB: 3SL2)¹⁸. The predicted binding mode (Figure 2) suggested that H30 interacts with the ATP-binding site of *B. subtilis* WalK and forms contacts with key residues involved in ATP-binding (Figure 2). In the same experimental settings H31 was not docked to *B. subtilis* WalK and this together with the *E. coli* PhoR $\text{IC}_{50} > 2 \text{ mM}$ suggests that the antibacterial effect of H31 against the bacterial strains tested might be mediated via targets different than HKs.

NCI antitumor screen results suggest that H30 scaffold possess good safety profile. 400 mg/kg/injection did not cause death of mice on the toxicity evaluation day. Therefore, H30 might be a good starting point for the development of inhibitors of HK autophosphorylation using a structure-based approach.

100 mg/kg/injection of H31 caused 50% death of mice on the toxicity evaluation day in a NCI antitumor screen. This supports the hypothesis that H31 has (a) target(s) different than HKs.

In summary, we identified H30 as putative HK autophosphorylation inhibitors with weak antibacterial effect using a combined computer-aided drug discovery approach. H30 might serve as a good starting scaffold for the design of more potent HK autophosphorylation inhibitors.

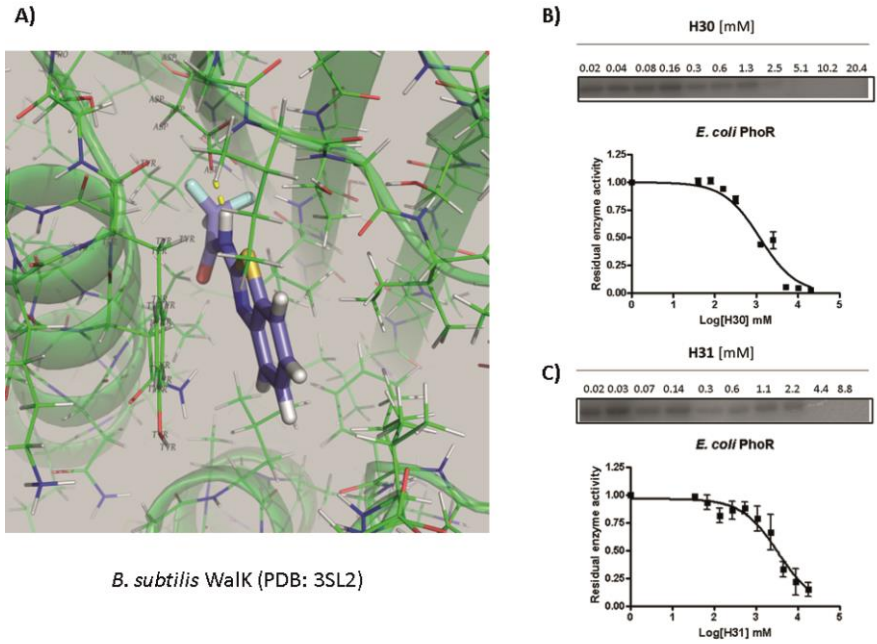


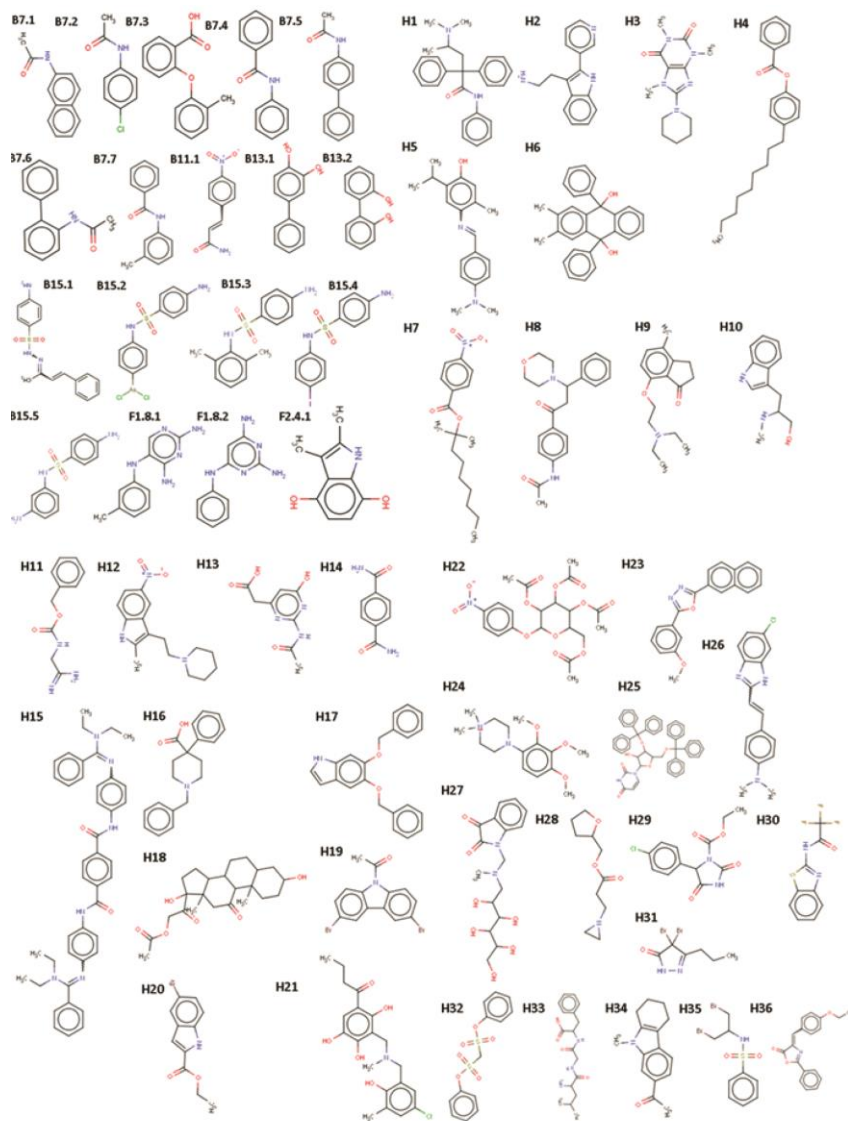
Figure 2. A) predicted binding mode of H30 to the ATP-binding site of *B. subtilis* Walk (PDB:3SL2) B) Concentration-dependent effect of H30 on *E. coli* PhoR autophosphorylation C) Concentration-dependent effect of H31 PhoR autophosphorylation.

REFERENCES

1. Sliwoski, G.; Kothiwale, S.; Meiler, J.; Lowe Jr, E. W., Computational methods in drug discovery. *Pharmacological reviews* 2014, 66 (1), 334-395.
2. Hansch, C.; Hoekman, D.; Leo, A.; Zhang, L.; Li, P., The expanding role of quantitative structure-activity relationships (QSAR) in toxicology. *Toxicology letters* 1995, 79 (1-3), 45-53.
3. Yan, A.; Chong, Y.; Wang, L.; Hu, X.; Wang, K., Prediction of biological activity of Aurora-A kinase inhibitors by multilinear regression analysis and support vector machine. *Bioorganic & medicinal chemistry letters* 2011, 21 (8), 2238-43.
4. Khadikar, P. V.; Sharma, V.; Karmarkar, S.; Supuran, C. T., QSAR studies on benzene sulfonamide carbonic anhydrase inhibitors: need of hydrophobic parameter for topological modeling of binding constants of sulfonamides to human CA-II. *Bioorganic & medicinal chemistry letters* 2005, 15 (4), 923-30.
5. Wang, J., Comprehensive assessment of ADMET risks in drug discovery. *Current pharmaceutical design* 2009, 15 (19), 2195-2219.
6. Abad-Zapatero, C.; Perisic, O.; Wass, J.; Bento, A. P.; Overington, J.; Al-Lazikani, B.; Johnson, M. E., Ligand efficiency indices for an effective mapping of chemico-biological space: the concept of an atlas-like representation. *Drug discovery today* 2010, 15 (19-20), 804-11.
7. Cortes-Cabrera, A.; Morreale, A.; Gago, F.; Abad-Zapatero, C., AtlasCBS: a web server to map and explore chemico-biological space. *Journal of computer-aided molecular design* 2012, 26 (9), 995-1003.
8. Auto-Modeller StarDrop.
9. Enhanced NCI Database Browser 2.2.
10. Conlon, J. M.; Mechkarska, M.; Prajeep, M.; Sonnevend, A.; Coquet, L.; Leprince, J.; Jouenne, T.; Vaudry, H.; King, J. D., Host-defense peptides in skin secretions of the tetraploid frog *Silurana epitropicalis* with potent activity against methicillin-resistant *Staphylococcus aureus* (MRSA). *Peptides* 2012, 37 (1), 113-9.
11. Clinical Laboratory and Standards Institute Methods for Antimicrobial Susceptibility Testing of Anaerobic Bacteria; Approved Standard. M11-A7. 2007; Vol. 7th ed.
12. Casino, P.; Rubio, V.; Marina, A., Structural insight into partner specificity and phosphoryl transfer in two-component signal transduction. *Cell* 2009, 139 (2), 325-36.
13. Marina, A.; Mott, C.; Auyzenberg, A.; Hendrickson, W. A.; Waldburger, C. D., Structural and mutational analysis of the PhoQ histidine kinase catalytic domain. Insight into the reaction mechanism. *The Journal of biological chemistry* 2001, 276 (44), 41182-90.
14. Christopoulos, H. M. a. A., Fitting Models to Biological Data using Linear and Nonlinear Regression. A Practical Guide to Curve Fitting. Oxford University Press: New York, 2004.
15. SwissDock. <http://www.swissdock.ch/>.
16. Mohedano, M. L.; Overweg, K.; de la Fuente, A.; Reuter, M.; Altabe, S.; Mulholland, F.; de Mendoza, D.; Lopez, P.; Wells, J. M., Evidence that the essential response regulator YycF in *Streptococcus pneumoniae* modulates expression of fatty acid biosynthesis genes and alters membrane composition. *Journal of bacteriology* 2005, 187 (7), 2357-67.
17. Velikova, N.; Bem, A. E.; van Baarlen, P.; Wells, J. M.; Marina, A., Walk, the Path towards New Antibacterials with Low Potential for Resistance Development. *ACS Medicinal Chemistry Letters* 2013, 4 (10), 891-894.

18. Celikel, R.; Veldore, V. H.; Mathews, I.; Devine, K. M.; Varughese, K. I., ATP forms a stable complex with the essential histidine kinase Walk (YycG) domain. *Acta crystallographica. Section D, Biological crystallography* 2012, 68 (Pt 7), 839-45.

SUPPLEMENTARY MATERIAL CHAPTER 5

**Figure S1.** Compounds selected for experimental testing

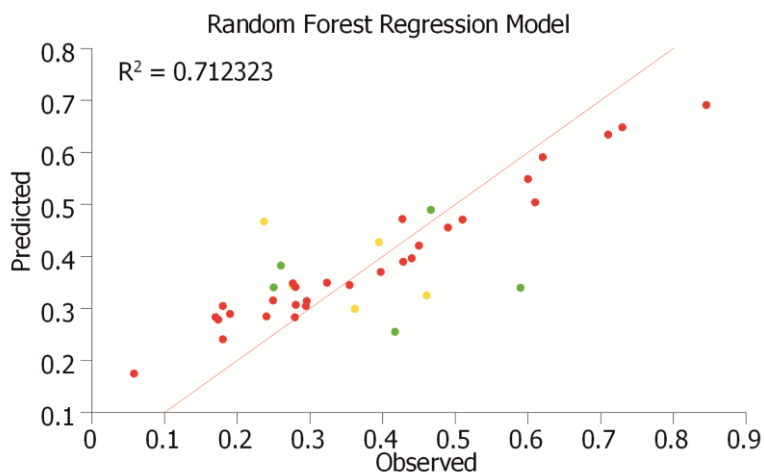


Figure S2. QSAR model for inhibition of *E. coli* PhoR autophosphorylation

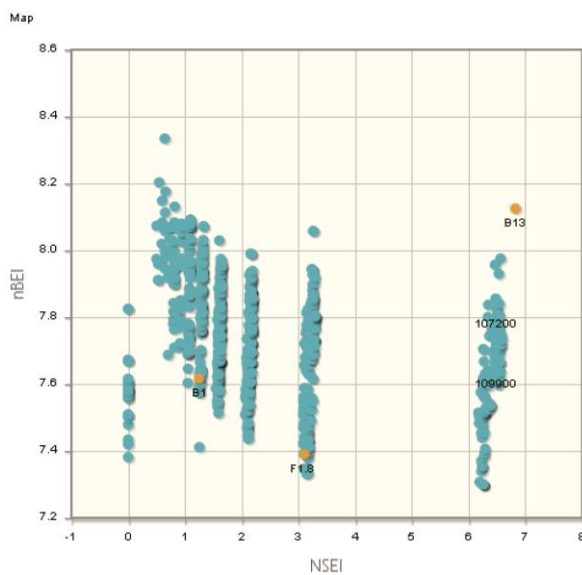


Figure S3. Ligand-efficiency indices facilitate the selection of hits for hit-to-lead optimisation

Table S1. Dataset

Name	% Inhibition PhoR^E	st.error; n=4
B1	42%	9%
B2	73%	7%
B3	29%	3%
B4	36%	6%
B5	17%	3%
B6	46%	4%
B7	62%	3%
B8	35%	2%
B9	28%	5%
B10	28%	4%
B11	71%	5%
B12	25%	7%
B13	85%	2%
B14	40%	10%
B15	43%	1%
B16	28%	5%
B17	59%	2%
B18	28%	13%
B19	43%	8%
B20	47%	9%
B21	32%	9%
B22	30%	6%
B23	24%	6%
B24	39%	7%
B25	6%	13%
F1 (D4.1)	54%	4%
F1.1	45%	3%

Table S1 (continued). Dataset

Name	% Inhibition PhoR^E	st.error; n=4
F1.2	44%	4%
F1.3	26%	3%
F1.4	49%	10%
F1.5	17%	5%
F1.6	28%	4%
F1.7	24%	6%
F1.8	61%	2%
F1.9	18%	2%
F1.10	25%	6%
F2 (G5.9)	74%	2%
F2.4	18%	6%
F2.1	51%	13%
F2.2	60%	6%
F2.3	19%	9%
F2.5	44%	10%
F2.6	25%	13%
F2.7	30%	5%
F2.8	64%	4%
F2.9	80%	10%

2014

CHAPTER 6

PRELIMINARY BIOCHEMICAL STUDIES ON THE INTERACTION OF LACTOFERRICIN B-DERIVED PEPTIDES WITH TWO-COMPONENT SYSTEMS

Nadya Velikova, Jerry Wells, Alberto Marina

BACKGROUND

LactoferricinB (LfcinB) is an antimicrobial peptide with broad-spectrum of antibacterial activity. It has been shown by *in vitro* and *in vivo* experiments that LfcinB inhibits the phosphorylation of the response regulators (RRs), BasR and CreB, and their cognate histidine kinases (HKs), BasS and CreC. Co-crystal structures of (peptide) inhibitors bound to their two-component system (TCS) targets would open up possibilities for the structure based drug design of more potent inhibitors. Here we investigated interaction of LfcinB-derived peptides with the *T. maritima* TCS HK853-RR468, for which X-ray structures of both components have been solved in different conformations.

FINDINGS

We show that LfcinB-derived peptides inhibit the phosphatase activity of *T. maritima* HK853-RR468 and seem to interact with *T. maritima* HK853 and *E. coli* PhoB. However, a possible mechanism of interaction is non-specific protein aggregation.

CONCLUSIONS

LfcinB has been proposed as a promising broad-spectrum inhibitor of bacterial TCS. LfcinB-derived peptides seem to be non-specific TCS inhibitors acting via protein aggregation. The latter would be in agreement with the broad-spectrum of antibacterial activity of LfcinB as protein aggregation would affect multiple targets.

List of abbreviations: TCS – two component systems; HK – histidine kinase; RR – response regulator; LfcinB – lactoferricin B

Key words: Lactoferricin B, antimicrobial peptides, two-component system inhibitors, antibacterials

INTRODUCTION

Antimicrobial peptides have been proposed as a promising alternative to fight resistant bacterial infections and to address the growing problem of multi-drug resistance^{1, 2, 3}. Eukaryotic cationic antimicrobial peptides (AMPs) are produced at sites of infection or inflammation in many different organisms^{4, 5}. Typically they are peptides of 12 to 45 amino acids with a net positive charge and a high proportion of hydrophobic amino acids⁶. There are four structural classes of AMPs, the most common being the β -sheet peptides stabilized by 2–4 disulphide bridges, and the unstructured peptides that fold into amphipathic α -helices upon contact with membranes. Interaction with the membrane may form pores, or act by thinning the membrane or by destabilizing the membrane bilayer. As net result interaction of AMPs and membranes increases permeability of the membrane, leads to loss of pH gradient and cell death. Some cationic peptides have been shown to interact with intracellular targets^{7, 8} but in most cases the exact mechanism of intracellular AMPs action remains unclear.

One of the AMPs proposed to possess intracellular targets is bovine lactoferricin (LfcinB). LfcinB is a typical cationic antibacterial peptide produced by gastric pepsin digestion of the N-terminal region of bovine lactoferrin and has been identified *in vivo*^{9, 10}. The antibacterial core LfcinB includes six residues (positions 20 – 25 in the parental sequence) with the C-terminus amidated (peptide RRWQWR-NH₂)^{11, 12}. A physiologically diverse range of Gram-positive and Gram-negative bacteria have been found to be susceptible to inhibition and inactivation by LfcinB-derived peptides including LfcinB₂₀₋₂₅ and LfcinB₁₇₋₃₁^{13, 14, 9}. Concentrations of LfcinB required to cause complete inhibition of bacterial growth vary within the range of 0.3 to 150 μ g/ml, depending on the strain and the culture medium used⁹. The broad spectrum of antibacterial action of LfcinB suggests a common mechanism of action and/or a widespread intracellular target present in all susceptible strains.

It has been shown that LfcinB-derived peptides (Lfcin₁₇₋₄₁, LfcinB₁₇₋₃₁ and D-Lfcin₁₇₋₃₁) enter the cytoplasm of *E. coli* and *S. aureus*¹⁵. In a recent study the intracellular LfcinB protein targets were identified by hybridisation of biotin-labelled LfcinB to an *Escherichia coli* K12 proteome chip¹⁶. In total 16 proteins were shown to interact with LfcinB, including two response regulators (RRs), BasR and CreB, belonging to the two-component systems (TCS) BasSR and CreCB. TCS are the predominant signalling systems in bacteria. TCS connect input stimuli and output responses with a core phosphotransfer between a membrane bound histidine kinase (HK) and a cognate response regulator (RR)^{17, 18}. Simply described, the signalling pathway is a series of steps including autophosphorylation of the HK, phosphotransfer to the cognate RR, and output modulation, usually via transcription regulation, mediated by the phosphorylated RR^{19, 18}. TCS are highly conserved between bacterial species and TCS signalling inhibition by LfcinB seemed a logical common mechanism explaining the broad-spectrum antibacterial effect of LfcinB. It has been shown by *in vitro* and *in vivo* experiments that LfcinB inhibits the phosphorylation of the RRs (BasR and CreB) by their cognate histidine kinases (HKs), BasS and CreC¹⁶ but does not inhibit the DNA binding capacity of both RRs suggesting that LfcinB-derived

peptides most likely do not interact with the effector domain of RRs, but with the REC domain of RRs. Additionally, antibacterial assays have shown that LfcinB reduced the tolerance of *E. coli* to environmental challenges, such as excessive ferric ions and minimal medium conditions. TCS are known to be involved in the regulation of adaptive response to stress and logically TCS signalling inhibition could be correlated with reduced stress tolerance. Taken together, these results were the first indication that an AMP inhibits the growth of bacteria by influencing the catalytic activities of a TCS directly¹⁶ and seemed to provide a promising starting point for the development of broad-spectrum antimicrobial-peptide drugs targeted at TCS signalling. TCS have been proposed as attractive targets for novel antibacterial as they are well-conserved among bacteria and not present in higher eukaryotes^{20, 21}.

The aim of this study was to investigate the interaction between LfcinB with TCS at atomic level by using X-ray crystallography. The structure of a LfcinB-RR complex would i) elucidate the molecular mechanism of RRs inhibition by LfcinB, ii) identify putative target sites in the RR which can further be exploited in structure-based drug design approaches, and iii) point to RR-peptide interactions and possible peptide modifications which would lead to stronger inhibitory effect. Altogether, these would facilitate the rational design of modified peptides with higher affinity of binding to TCS and may lead to the development of more potent peptide TCS inhibitors. For this purpose we have used the *T. maritima* HK853-RR468 which is a well-studied TCS^{22, 18} and the X-ray structures of both components, HK853 and RR468, alone and in complex are known^{23, 24, 25}. *E. coli* PhoR-PhoB is a prototypical two-component system involved in the regulation of the *pho* regulon and structures of the RR PhoB are known^{26, 27, 26}. As a first step towards a structure of a RR in complex with LfcinB, we verified whether LfcinB-derived peptides inhibit the catalytic activities of *T. maritima* HK853-RR468 and *E. coli* PhoR-PhoB TCS.

RESULTS AND DISCUSSION

INHIBITION OF PHOSPHOTRANSFER AND PHOSPHATASE ACTIVITIES OF PURIFIED BACTERIAL TWO- COMPONENT SYSTEMS.

To check whether LfcinB-derived peptides inhibit the phosphorylation of RR468 and/or PhoB by their cognate HKs, HK853 and PhoR, respectively, phosphotransfer assays were performed in the presence of two LfcinB-derived peptides (LfcinB₁₇₋₂₅ and LfcinB₁₇₋₃₂). The two peptides were chosen as both contain the antibacterial core sequence (positions 20 – 25 in the parental sequence)^{11, 12}. In the phosphotransfer assays the HKs were first auto-phosphorylated using [γ -³²P]ATP²⁴. This leads to accumulation of [γ -³²P]ATP-autophosphorylated HK which in a SDS-PAGE gel appears as a well-defined band (Figure 1). The autophosphorylated HK was then diluted in ATP-free phosphorylation solution containing an equimolar amount (in terms of subunits) of RR and 0.5 mM of analysed peptide. Upon mixture of the HK and the RR phosphotransfer occurs, and in a SDS-PAGE gel the intensity of the band corresponding to the HK becomes lower and a band corresponding to the phosphorylated RR appears. As several HKs have phosphatase activity (i.e. HK853)^{28, 19, 29, 18}, the band corresponding to the phosphorylated RR in the SDS-PAGE gel lower its intensity over time. The time course of the reaction (10 min) showed that in the absence of LfcinB-derived peptides the radioactive band corresponding to autophosphorylated HK853 almost completely disappeared by 1 min and coincided with appearance of a labelled band corresponding to phosphorylated RR468 indicating phosphotransfer from HK853 to RR468 (Figure 1A). However, the intensity of the bands corresponding to the phosphorylated RR468 at 1 min was lower than the intensity of the band corresponding to HK853, confirming dephosphorylation of the RR468 due to HK853 phosphatase activity. In the presence of LfcinB-derived peptides phosphotransfer from HK853 to RR468 did occur but to a lesser extend compared to the negative control evidenced by the slightly higher intensity of the bands corresponding to the autophosphorylated HK853. In the presence of Lfcin B₁₇₋₂₅ or LfcinB₁₇₋₃₂ a proportion of the autophosphorylated HK853 remained visible, indicating either inhibition of phosphotransfer to RR468, or inhibition of the phosphatase activity leading to putative shift in the phosphotransfer/ phosphatase reaction balance. Furthermore, in the presence of LfcinB₁₇₋₂₅ and LfcinB₁₇₋₃₂ the bands corresponding to the phosphorylated RR468 were with higher intensity compared to the negative control or Peptide 3 (a pentapeptide of different sequence) and with similar intensity over time, indicating that the phosphatase activity of HK853 was inhibited. In the case of PhoR-PhoB, the band corresponding to the autophosphorylated PhoR almost completely disappeared by 1 min and a band corresponding to the phosphorylated PhoB appeared. In the presence of LfcinB-derived peptides, the intensity of the bands corresponding to the autophosphorylated PhoR was similar to the assay in the absence of peptide indicating that phosphotransfer was not affected. In the absence of peptide, the intensity of the bands corresponding to the phosphorylated PhoB remained similar over time indicating no or very slow phosphatase activity. Intriguingly, in the presence

of both LfcinB₁₇₋₂₅ and LfcinB₁₇₋₃₂ the amount of phosphorylated PhoB was considerably lower. In the presence of control Peptide3 the intensity of the bands corresponding to autophosphorylated PhoR and phosphorylated PhoB was similar to the assay in the absence of peptides. As it appears that phosphotransfer activity of the PhoR-PhoB TCS is not affected by the LfcinB-derived peptides and the phosphatase activity in the absence of LfcinB-derived peptides is missing or very slow, the lower intensity of the bands corresponding to the phosphorylated PhoB could be explained by activating the PhoB dephosphorylation. Further experiments with *in vitro* phosphorylated PhoB are required to prove or discard this hypothesis.

INHIBITION OF THE PHOSPHOTRANSFER AND PHOSPHATASE ACTIVITY OF HK853-RR468 IS LIKELY MEDIATED VIA INTERACTION WITH HK853

Native polyacrylamide gel electrophoresis (native PAGE) was employed to check whether the observed inhibition of phosphotransfer and phosphatase activity of the HK853-RR468 TCS by LfcinB₁₇₋₂₅ and LfcinB₁₇₋₃₂ is due to interaction with the HK and/ or with the RR. The RR was first phosphorylated *in vitro* by incubation with acetyl phosphate³⁰. The *in vitro* phosphorylated RR468 was combined with LfcinB₁₇₋₂₅ or LfcinB₁₇₋₃₂, or LfcinB₁₇₋₂₅ or LfcinB₁₇₋₃₂ together with the HK853. HK853 alone incubated with or without LfcinB₁₇₋₂₅ or LfcinB₁₇₋₃₂, or with Peptide 3 were run in parallel. In the absence of LfcinB-derived peptides in the native PAGE gel three well defined bands corresponding to RR468 (lowest band), HK853 (intermediate band) and the complex HK853-RR468 (highest band; Figure 2) were evident. Addition of LfcinB₁₇₋₂₅ and LfcinB₁₇₋₃₂ resulted in loss of the band corresponding to HK853. Whereas, in the presence of LfcinB₁₇₋₂₅ and LfcinB₁₇₋₃₂ RR468 was only slightly influenced as a smear was observed. This suggests that the LfcinB-derived peptides interact with HK853 much stronger than RR468 (Figure 2) evidenced by the significant change in the mobility of HK853 in the native gel after incubation with LfcinB-derived peptides. The putative interaction of LfcinB-derived peptides with HK853 does not affect the formation of the complex with RR468 as evidenced by the band corresponding to the HK853-RR468 complex in the presence of the LfcinB-derived peptides. Furthermore, in the presence of LfcinB-derived peptides the complex HK853-RR468 is formed and phosphotransfer and dephosphorylation of the RR can still occur to some extent (Figure 1A). Nevertheless, the amount of complex formed in the presence of the LfcinB peptides was much less than that observed with peptide 3 and control samples (Figure 2). The events observed with HK853 and RR468 were specific to the LfcinB-derived peptides as no change in the mobility of HK853 or smear were evident after incubation with Peptide 3.

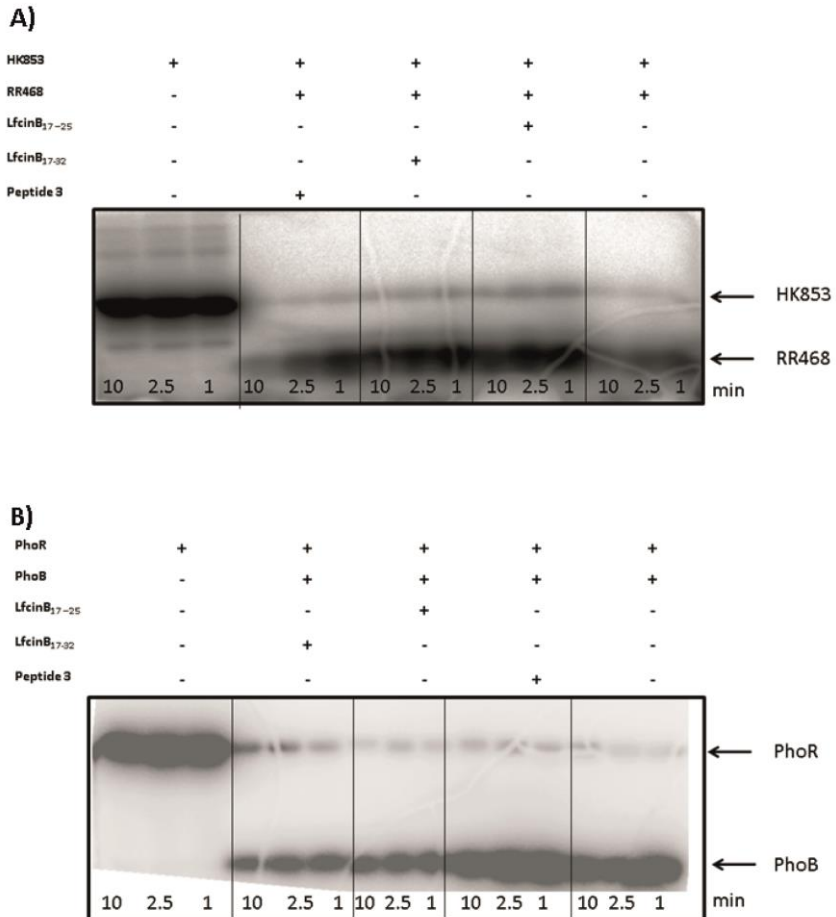


Figure 1. Phosphotransfer assays A) LfcinB₁₇₋₂₅ and LfcinB₁₇₋₃₂ inhibit the phosphorylation of RR468 by HK853 and the phosphatase activity of HK853 as evidenced by the higher intensity of the bands corresponding to autophosphorylated HK853 and the bands corresponding to the phosphorylated RR468, respectively, in the presence of the LfcinB-derived peptides compared to the negative control. B) LfcinB₁₇₋₂₅ and LfcinB₁₇₋₃₂ seem not to inhibit the phosphorylation of PhoB by PhoR as evidenced by the similar intensities of the bands corresponding to the autophosphorylated PhoR. The lower intensities of the bands corresponding to the phosphorylated PhoB in the presence of LfcinB-derived peptides point to the possibility that LfcinB-derived peptides stimulate dephosphorylation of PhoB.

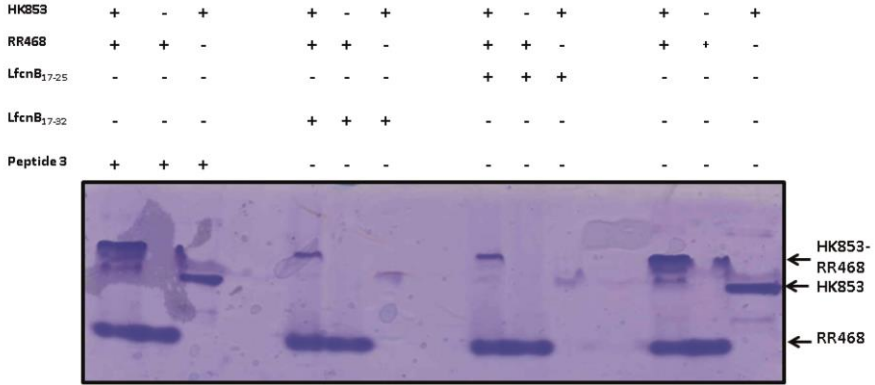


Figure 2. LfcinB₁₇₋₂₅ and LfcinB₁₇₋₃₂ seem to interact with HK853 as evidenced by the disappearance of the band corresponding to HK853 in the presence of the LfcinB-derived peptides. LfcinB₁₇₋₂₅ and LfcinB₁₇₋₃₂ interact with RR468 to a lesser extent compared to HK853 as evidenced by smear of in the presence of the LfcinB-derived peptides. The strong interaction with HK853 and the weaker interaction with RR468 do not prevent the formation of the HK853-RR468 complex and the band corresponding to the complex appears even in the presence of the LfcinB-derived peptides. Nevertheless, the amount of the formed HK853-RR468 complex in the presence of LfcinB-derived peptides less than in the controls.

LFCINB-DERIVED PEPTIDES INTERACT WITH PHO_B IN A CONCENTRATION-DEPENDENT MANNER

Native PAGE indicates that LfcinB-derived peptides interact with PhoB as a smear appeared after incubation of LfcinB-derived peptides with PhoB which had been or had not been *in vitro* phosphorylated (Figure S1 and S2). The interaction with the *in vitro* phosphorylated PhoB seemed to be concentration dependent as the smear was observed only at concentrations higher than 0.125 mM (Figure S2). The putative interaction was specific to the LfcinB-derived peptides as the mobility of *in vitro* phosphorylated PhoB in the native gel was not affected after incubation with Peptide3 (Figure S1).

SUMMARY

In summary, it seems the inhibition of phosphotransfer and phosphatase activities of the *T. maritima* TCS HK853-RR468 caused by LfcinB₁₇₋₂₅ and LfcinB₁₇₋₃₂ can be attributed to interaction with HK853 although some interaction with RR468 might also have contributed to this effect. The LfcinB-derived peptides seem to interact in a concentration dependent manner with *in vitro* phosphorylated *E. coli* response regulator PhoB. Changes in the mobility in native gels of PhoB after incubation with LfcinB-derived peptides indicate possible interaction with this protein. Further experiments are needed to check the hypothesis that incubation with LfcinB-derived peptides might activate the dephosphorylation of *E. coli* PhoB. The observed changes in the mobility of *T. maritima* HK853 and PhoB in native gels could be due to protein aggregation. However, further experiments such as size-exclusion chromatography and/ or protein-aggregation evaluation by cross-linking and SDS-PAGE are required to confirm this hypothesis. Taken together, the results point to the possibility that the antibacterial effect caused by LfcinB-derived peptides might be attributed to interaction with multiple cellular targets after entering into the cell. This is in agreement with the fact that multiple *E. coli* proteins were shown to interact with LfcinB using proteomics¹⁶. Furthermore, non-specific mechanism of action such as protein aggregation could not be excluded at this point. Attempts to solve the structure of *T. maritima* RR468 co-crystallized with LfcinB-derived peptides resulted in high-resolution twinned crystals of RR468 and the LfcinB-derived peptides were not encountered in the asymmetric unit (data not shown). It was not possible to obtain diffracting crystals of PhoB co-crystallized with LfcinB-derived peptides. No attempts have been made to co-crystallize LfcinB-derived peptides with any HK. However, before any future crystallization trials additional biochemical experiments are required to confirm that the mechanism of interaction of LfcinB-derived peptides with TCS is not mediated via non-specific protein aggregation.

MATERIALS AND METHODS

PEPTIDES

Lactoferricin B₁₇₋₂₅ and Lactoferricin B₁₇₋₃₂ were kindly provided by Paloma Manzanares, IATA, CSIC (Valencia, Spain).

PROTEIN EXPRESSION AND PURIFICATION

T. maritima HK853 and RR468, *E. coli* PhoR and PhoB were expressed and purified as previously described^{23, 22, 24, 25, 31, 31}. Shortly proteins were expressed in *E. coli* and purified by anion-exchange (HK853 and RR468) or Ni-affinity chromatography (PhoR and PhoB), and size-exclusion chromatography.

PHOSPHOTRANSFER ASSAY

Phosphotransfer assays were performed as previously described²². HK853 and PhoR were autophosphorylated in kinase buffer (50 mM Tris pH 8.0, 100 mM KCl, 10 mM MgCl₂) with 0.1 μCi μl⁻¹[γ-³²P] ATP (3000 Ci/mmol Perkin Elmer) for 30min (exceeding equilibrium time) at room temperature. Then, each sample was aliquoted into three tubes and phosphotransfer reactions were initiated by the addition of equimolecular amounts of each RR (the final concentration of RRs and HKs in reaction was 2 μM) pre-incubated with 0.5 mM Lactoferricin B₁₇₋₂₅, Lactoferricin B₁₇₋₃₂, Peptide 3 or buffer. Aliquots were removed from each tube at different times (1, 2.5 and 10 min) and the reactions were stopped by adding 1/4 SDS-PAGE loading buffer (62.5 mM Tris pH 6.8, 30% glycerol, 0.01% bromophenol blue) supplemented with 50 mM EDTA. Afterwards, the samples were subjected to SDS-PAGE on a 15% gel to separate the protein from free nucleotide. After drying, the phosphorylated proteins were visualized by phosphorimaging using a Fluoro Image Analyzer FLA-5000 (Fuji).

NATIVE POLYACRYLAMIDE GEL ELECTROPHORESIS (NATIVE PAGE)

Purified PhoB and RR468 were autophosphorylated in kinase buffer (50 mM Tris pH 8.0, 100 mM KCl, 10 mM MgCl₂) containing 12.5 mM acetyl phosphate for 1 h at room temperature. Phosphorylated PhoB and RR468 were mixed with 0.5 mM Lactoferricin B₁₇₋₂₅, Lactoferricin B₁₇₋₃₂, Peptide 3 or buffer. RR468 mixed with 0.5 mM Lactoferricin B₁₇₋₂₅, Lactoferricin B₁₇₋₃₂, Peptide 3 or buffer was incubated with or without equimolar amounts of HK853. After 30 min of incubation at room temperature Native polyacrylamide gel electrophoresis (Native-PAGE) loading buffer was added and samples loaded. Coomassie blue staining was used for protein visualization.

REFERENCES

1. HASSAN, M.; KJOS, M.; NES, I. F.; DIEP, D. B.; LOTFIPOUR, F., NATURAL ANTIMICROBIAL PEPTIDES FROM BACTERIA: CHARACTERISTICS AND POTENTIAL APPLICATIONS TO FIGHT AGAINST ANTIBIOTIC RESISTANCE. *JOURNAL OF APPLIED MICROBIOLOGY* 2012, 113 (4), 723-36.
2. MOK, W. W.; LI, Y., THERAPEUTIC PEPTIDES: NEW ARSENAL AGAINST DRUG RESISTANT PATHOGENS. *CURRENT PHARMACEUTICAL DESIGN* 2014, 20 (5), 771-92.
3. STECKBECK, J. D.; DESLOUCHES, B.; MONTELARO, R. C., ANTIMICROBIAL PEPTIDES: NEW DRUGS FOR BAD BUGS? EXPERT OPINION ON BIOLOGICAL THERAPY 2014, 14 (1), 11-4.
4. PALFFY, R.; GARDLIK, R.; BEHULIAK, M.; KADASI, L.; TURNA, J.; CELEC, P., ON THE PHYSIOLOGY AND PATHOPHYSIOLOGY OF ANTIMICROBIAL PEPTIDES. *MOLECULAR MEDICINE* 2009, 15 (1-2), 51-9.
5. PASUPULETI, M.; SCHMIDTCHEN, A.; MALMSTEN, M., ANTIMICROBIAL PEPTIDES: KEY COMPONENTS OF THE INNATE IMMUNE SYSTEM. *CRITICAL REVIEWS IN BIOTECHNOLOGY* 2012, 32 (2), 143-171.
6. HANCOCK, R. E. W., PEPTIDE ANTIBIOTICS. *LANCET* 1997, 349 (9049), 418-422.
7. FRIEDRICH, C. L.; MOYLES, D.; BEVERIDGE, T. J.; HANCOCK, R. E., ANTIBACTERIAL ACTION OF STRUCTURALLY DIVERSE CATIONIC PEPTIDES ON GRAM-POSITIVE BACTERIA. *ANTIMICROBIAL AGENTS AND CHEMOTHERAPY* 2000, 44 (8), 2086-92.
8. CUDIC, M.; OTVOS, L., JR., INTRACELLULAR TARGETS OF ANTIBACTERIAL PEPTIDES. *CURRENT DRUG TARGETS* 2002, 3 (2), 101-6.
9. BELLAMY, W.; TAKASE, M.; WAKABAYASHI, H.; KAWASE, K.; TOMITA, M., ANTIBACTERIAL SPECTRUM OF LACTOFERRICIN B, A POTENT BACTERICIDAL PEPTIDE DERIVED FROM THE N-TERMINAL REGION OF BOVINE LACTOFERRIN. *THE JOURNAL OF APPLIED BACTERIOLOGY* 1992, 73 (6), 472-9.
10. ARIAS, M.; MCDONALD, L. J.; HANEY, E. F.; NAZMI, K.; BOLSCHER, J. G.; VOGEL, H. J., BOVINE AND HUMAN LACTOFERRICIN PEPTIDES: CHIMERAS AND NEW CYCLIC ANALOGS. *BIOMETALS: AN INTERNATIONAL JOURNAL ON THE ROLE OF METAL IONS IN BIOLOGY, BIOCHEMISTRY, AND MEDICINE* 2014.
11. TOMITA, M.; TAKASE, M.; BELLAMY, W.; SHIMAMURA, S., A REVIEW: THE ACTIVE PEPTIDE OF LACTOFERRIN. *ACTA PAEDIATRICA JAPONICA; OVERSEAS EDITION* 1994, 36 (5), 585-91.
12. (A) SCHIBLI, D. J.; HWANG, P. M.; VOGEL, H. J., STRUCTURE OF THE ANTIMICROBIAL PEPTIDE TRITRPTICIN BOUND TO MICELLES: A DISTINCT MEMBRANE-BOUND PEPTIDE FOLD. *BIOCHEMISTRY* 1999, 38 (51), 16749-55; (B) SCHIBLI, D. J.; HWANG, P. M.; VOGEL, H. J., THE STRUCTURE OF THE ANTIMICROBIAL ACTIVE CENTER OF LACTOFERRICIN B BOUND TO SODIUM DODECYL SULFATE MICELLES. *FEBS LETTERS* 1999, 446 (2-3), 213-7.
13. STROM, M. B.; HAUG, B. E.; REKDAL, O.; SKAR, M. L.; STENSEN, W.; SVENDSEN, J. S., IMPORTANT STRUCTURAL FEATURES OF 15-RESIDUE LACTOFERRICIN DERIVATIVES AND METHODS FOR IMPROVEMENT OF ANTIMICROBIAL ACTIVITY. *BIOCHEMISTRY AND CELL BIOLOGY = BIOCHIMIE ET BIOLOGIE CELLULAIRE* 2002, 80 (1), 65-74.
14. (A) DEL OLMO, A.; MORALES, P.; NUÑEZ, M., BACTERICIDAL EFFECT OF LACTOFERRIN AND ITS AMIDATED AND PEP SIN-DIGESTED DERIVATIVES ON PSEUDOMONAS FLUORESCENS: INFLUENCE OF ENVIRONMENTAL AND PHYSIOLOGICAL FACTORS. *JOURNAL OF FOOD PROTECTION* 2008, 71 (12), 2468-2474; (B) ROSEANU, A.; FLORIAN, P.; CONDEI, M.; CRISTEA, D.; DAMIAN, M., ANTIBACTERIAL ACTIVITY OF

LACTOFERRIN AND LACTOFERRICIN AGAINST ORAL STREPTOCOCCI. ROMANIAN BIOTECHNOLOGICAL LETTERS 2010, 15 (6), 5788-5792.

15. HAUKLAND, H. H.; ULVATNE, H.; SANDVIK, K.; VORLAND, L. H., THE ANTIMICROBIAL PEPTIDES LACTOFERRICIN B AND MAGAININ 2 CROSS OVER THE BACTERIAL CYTOPLASMIC MEMBRANE AND RESIDE IN THE CYTOPLASM. FEBS LETTERS 2001, 508 (3), 389-93.

16. HO, Y. H.; SUNG, T. C.; CHEN, C. S., LACTOFERRICIN B INHIBITS THE PHOSPHORYLATION OF THE TWO-COMPONENT SYSTEM RESPONSE REGULATORS BASR AND CREB. MOLECULAR & CELLULAR PROTEOMICS : MCP 2012, 11 (4), M111 014720.

17. STOCK, A. M.; ROBINSON, V. L.; GOUDREAU, P. N., TWO-COMPONENT SIGNAL TRANSDUCTION. ANNUAL REVIEW OF BIOCHEMISTRY 2000, 69, 183-215.

18. CASINO, P.; RUBIO, V.; MARINA, A., THE MECHANISM OF SIGNAL TRANSDUCTION BY TWO-COMPONENT SYSTEMS. CURRENT OPINION IN STRUCTURAL BIOLOGY 2010, 20 (6), 763-71.

19. KENNEY, L. J., HOW IMPORTANT IS THE PHOSPHATASE ACTIVITY OF SENSOR KINASES? CURRENT OPINION IN MICROBIOLOGY 2010, 13 (2), 168-76.

20. GOTOH, Y.; DOI, A.; FURUTA, E.; DUBRAC, S.; ISHIZAKI, Y.; OKADA, M.; IGARASHI, M.; MISAWA, N.; YOSHIKAWA, H.; OKAJIMA, T.; MSADEK, T.; UTSUMI, R., NOVEL ANTIBACTERIAL COMPOUNDS SPECIFICALLY TARGETING THE ESSENTIAL WALR RESPONSE REGULATOR. THE JOURNAL OF ANTIBIOTICS 2010, 63 (3), 127-34.

21. VELIKOVA, N.; BEM, A. E.; VAN BAARLEN, P.; WELLS, J. M.; MARINA, A., WALK, THE PATH TOWARDS NEW ANTIBACTERIALS WITH LOW POTENTIAL FOR RESISTANCE DEVELOPMENT. ACS MEDICINAL CHEMISTRY LETTERS 2013, 4 (10), 891-894.

22. CASINO, P.; FERNANDEZ-ALVAREZ, A.; ALFONSO, C.; RIVAS, G.; MARINA, A., IDENTIFICATION OF A NOVEL TWO COMPONENT SYSTEM IN THERMOTOGA MARITIMA. COMPLEX STOICHIOMETRY AND CRYSTALLIZATION. BIOCHIMICA ET BIOPHYSICA ACTA 2007, 1774 (5), 603-9.

23. MARINA, A.; WALDBURGER, C. D.; HENDRICKSON, W. A., STRUCTURE OF THE ENTIRE CYTOPLASMIC PORTION OF A SENSOR HISTIDINE-KINASE PROTEIN. THE EMBO JOURNAL 2005, 24 (24), 4247-59.

24. CASINO, P.; RUBIO, V.; MARINA, A., STRUCTURAL INSIGHT INTO PARTNER SPECIFICITY AND PHOSPHORYL TRANSFER IN TWO-COMPONENT SIGNAL TRANSDUCTION. CELL 2009, 139 (2), 325-36.

25. PODGORNAIA, A. I.; CASINO, P.; MARINA, A.; LAUB, M. T., STRUCTURAL BASIS OF A RATIONALLY REWIRED PROTEIN-PROTEIN INTERFACE CRITICAL TO BACTERIAL SIGNALING. STRUCTURE 2013, 21 (9), 1636-47.

26. CREPIN, S.; CHEKABAB, S. M.; LE BIHAN, G.; BERTRAND, N.; DOZOIS, C. M.; HAREL, J., THE PHO REGULON AND THE PATHOGENESIS OF ESCHERICHIA COLI. VETERINARY MICROBIOLOGY 2011, 153 (1-2), 82-8.

27. BACHHAWAT, P.; SWAPNA, G. V.; MONTELIONE, G. T.; STOCK, A. M., MECHANISM OF ACTIVATION FOR TRANSCRIPTION FACTOR PHOB SUGGESTED BY DIFFERENT MODES OF DIMERIZATION IN THE INACTIVE AND ACTIVE STATES. STRUCTURE 2005, 13 (9), 1353-63.

28. GUTU, A. D.; WAYNE, K. J.; SHAM, L. T.; WINKLER, M. E., KINETIC CHARACTERIZATION OF THE WALRKSPN (VICRK) TWO-COMPONENT SYSTEM OF STREPTOCOCCUS PNEUMONIAE: DEPENDENCE OF WALKSPN (VICK) PHOSPHATASE ACTIVITY ON ITS PAS DOMAIN. JOURNAL OF BACTERIOLOGY 2010, 192 (9), 2346-58.

29. ZHU, Y.; QIN, L.; YOSHIDA, T.; INOUE, M., PHOSPHATASE ACTIVITY OF HISTIDINE KINASE ENVZ WITHOUT KINASE CATALYTIC DOMAIN. PROCEEDINGS OF THE NATIONAL ACADEMY OF SCIENCES OF THE UNITED STATES OF AMERICA 2000, 97 (14), 7808-13.

2014

30. RUIZ, D.; SALINAS, P.; LOPEZ-REDONDO, M. L.; CAYUELA, M. L.; MARINA, A.; CONTRERAS, A., PHOSPHORYLATION-INDEPENDENT ACTIVATION OF THE ATYPICAL RESPONSE REGULATOR NBLR. MICROBIOLOGY 2008, 154 (PT 10), 3002-15.

31. BILWES, A. M.; ALEX, L. A.; CRANE, B. R.; SIMON, M. I., STRUCTURE OF CHEA, A SIGNAL-TRANSDUCING HISTIDINE KINASE. CELL 1999, 96 (1), 131-41.

SUPPLEMENTARY MATERIAL CHAPTER 6

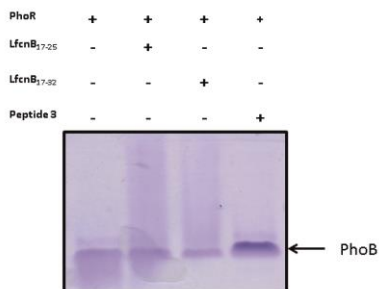


Figure S1. LfcinB₁₇₋₂₅ and LfcinB₁₇₋₃₂ interact with *E. coli* PhoB as evidenced by the smear observed after incubation of PhoB with the LfcinB-derived peptides and not in the negative control or after incubation with Peptide 3.

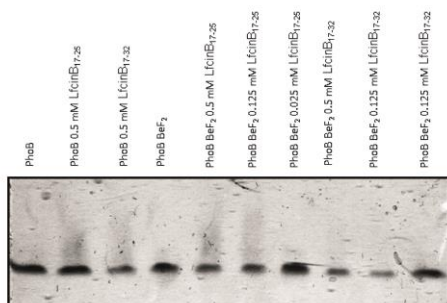


Figure S2. Interaction of LfcinB-derived peptides with *E. coli* PhoB. LfcinB-derived peptides seem to interact with *in vitro* phosphorylated PhoB in a concentration dependent manner as only incubation with LfcinB-derived peptides at concentrations higher than 0.025mM cause change in the mobility of PhoR evidenced by a smear and/ or reduction of the band corresponding to PhoB.

2014

CHAPTER 7

EXPRESSION, PURIFICATION, (CO-)CRYSTALLIZATION AND PRELIMINARY X-RAY DIFFRACTION ANALYSIS OF TWO-COMPONENT SYSTEMS AND TWO-COMPONENT SYSTEM- INHIBITOR CO-CRYSTALS

Nadya Velikova, Alberto Marina

2014

7.1. CO-CRYSTALLIZATION OF HISTIDINE-KINASE AUTOPHOSPHORYLATION INHIBITORS WITH *THERMOTOGA MARITIMA* CHEA

INTRODUCTION

Obtaining the structure of a putative target histidine kinase (HK) and a histidine-kinase autophosphorylation inhibitor (HKAI) would allow the rational structure-based design of more potent and specific inhibitors. The structure of *Thermotoga maritima* CheA CA domain has been previously crystallized in complex with the native ligand ATP/ADP (PDB: 1I58, 1I59) to atomic resolution (1.6 Å), and the conditions to obtain high-resolution well-diffracting crystals are well-known^{1,2}. Thus the aim of this study was to obtain X-ray structures of *T. maritima* CheA in complex with the HKAI discovered in this thesis (Chapter 2, 3, and 5).

The structure of the CA domain of *T. maritima* CheA contains the characteristic ATP-binding Bergerat fold including the ATP-lid (Figure 1). The ATP-lid is a loop variable in sequence and in length crucial for nucleotide binding and catalytic activity^{3, 4}. The ATP-lid is proposed as promising feature for the design of specific HK autophosphorylation inhibitors with reduced adverse effects to host cells^{5, 6}.

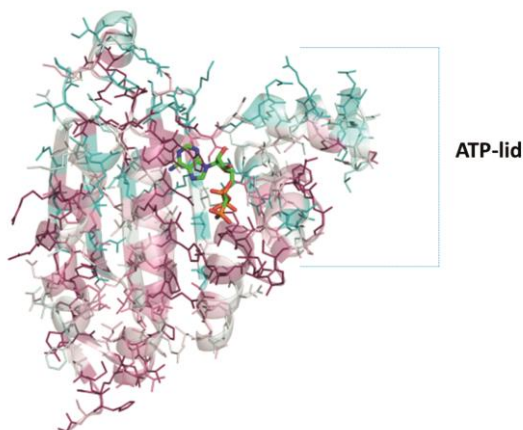


Figure 1. Catalytic and ATP-binding (CA) domain of *T. maritima* CheA (PDB: 1I58, chain A). Residues are coloured based on their conservation score calculated with ConSurf. ATP is shown in sticks. The ATP-lid is a variable loop that can be used to design more specific HK inhibitors.

MATERIALS AND METHODS

PROTEIN EXPRESSION AND PURIFICATION

T. maritima CheA (CA) was expressed and purified as previously described^{1,2}. In brief, protein was expressed in *E. coli* RIL and purified by Ni-affinity and size-exclusion chromatography.

CO-CRYSTALLIZATION AND SOAKING WITH HISTIDINE-KINASE AUTOPHOSPHORYLATION INHIBITORS

Crystals of CheA (25-50 mg/ml) were obtained by the hanging-drop method in solution containing 28-33 % PEG 8000, 0.6M Ammonium acetate, and 0.065 M sodium acetate pH 4.5. Co-crystals with histidine kinase autophosphorylation inhibitors (HKAI) were obtained by incubating CheA with 100 mg/ml of the HKAI for at least 16h at 4°C. In some cases (B13) co-crystals were additionally soaked in crystallization solution containing 100 mg/ml HKAI for at least 3 h.

DATA COLLECTION AND PROCESSING

Single crystals were harvested with a loop and vitrified in liquid nitrogen. Diffraction data of CheA-HKAI crystals (Table 1) were collected at the synchrotrons Diamond Light Source (Didcot, United Kingdom), European Synchrotron Radiation Facility (Grenoble, France), and ALBA (Barcelona, Spain), or at IBV-CSIC (Valencia, Spain) using SuperNova (Agilent). Diffraction images were indexed and integrated using Mosflm⁷, XDS⁸, or CrysAlisPro (Agilent) and the data were scaled using Scala⁹. Data collection and processing statistics of representative crystals are summarized in Table 2. Structures were solved by molecular replacement using as template the previous solved structure of the CheA CA domain (PDB: 1I58, Chain A)) and the software MolRep¹⁰. All models were improved by alternating manual building using Coot^{11, 12} with automatic refinement using Refmac¹² or Phenix Refine^{13, 14, 15}.

RESULTS AND DISCUSSION

Crystals of the CA domain of *T. maritima* CheA co-crystallized with the histidine-kinase autophosphorylation inhibitors (HKAI, Table 1) diffracted at very high resolution between 1.5 to 2.5 Å (Table 2). In the case of inhibitors A5, B13, B14, F1, F1.5, F2, F2.2, F2.4, and H30 (Table 1) the CheA-inhibitor structures, solved by X-ray crystallography, revealed electron density in the ATP-binding site (Figure 2). However, the structures of the HK inhibitors could not be fully resolved, probably due to partial occupancy and/or multiple conformations. In all cases the ATP-lid was not visible.

Table 1. Co-crystals of CheA with inhibitors

Inhibitor	Data set(s) collected at:	Electron density in the ATP-binding site
A1	DLS	No
A5	DLS, Agilent	Yes/No
A6	DLS	No
A11	DLS	No
B7	ALBA	No
B11	ALBA	No
B13	ALBA	Yes
B14	ALBA	Yes
F1	DLS, Agilent, ALBA	Yes/No
F1.5	DLS	Yes
F1.6	DLS	No
F1.7	DLS	No
F1.8	DLS	No
F2	DLS, Agilent, ALBA	Yes
F2.1	DLS	No
F2.2	DLS	Yes
F2.4	DLS	Yes
F2.5	DLS	No
F2.6	DLS	No
F2.7	DLS	No
H30	ALBA	Yes
H31	ALBA	No

Table 2. Data collection and processing statistics for representative CheA-HKAI crystals

	CheA-F2	CheA-B13
Synchrotron	DLS	ALBA
Wavelength (Å)	0.97890	1.07217
Space group	P 2 ₁	P 2 ₁
Cell (Å, °)	a=40.7730 b=60.2130 c=65.6980 α=90.0 β=98.2850 γ=90.0	a=41.01 b=59.24 c=66.79 α=90.0 β=97.68 γ=90.0
Resolution (Å)	28.60 – 2.16 (2.28-2.16)	66.20 – 1.85 (1.95 – 1.85)
R merge	0.029	0.06
I/δ(I)	27.0	11.4
No. of reflections (observed/unique)	62363/16957 (9120/2454)	86960/27188 (12139/3946)
Completeness	99.6 (99.6)	99.3 (99.2)
Multiplicity	3.7 (3.7)	3.2 (3.1)

The data for the outer shell is shown in parenthesis.

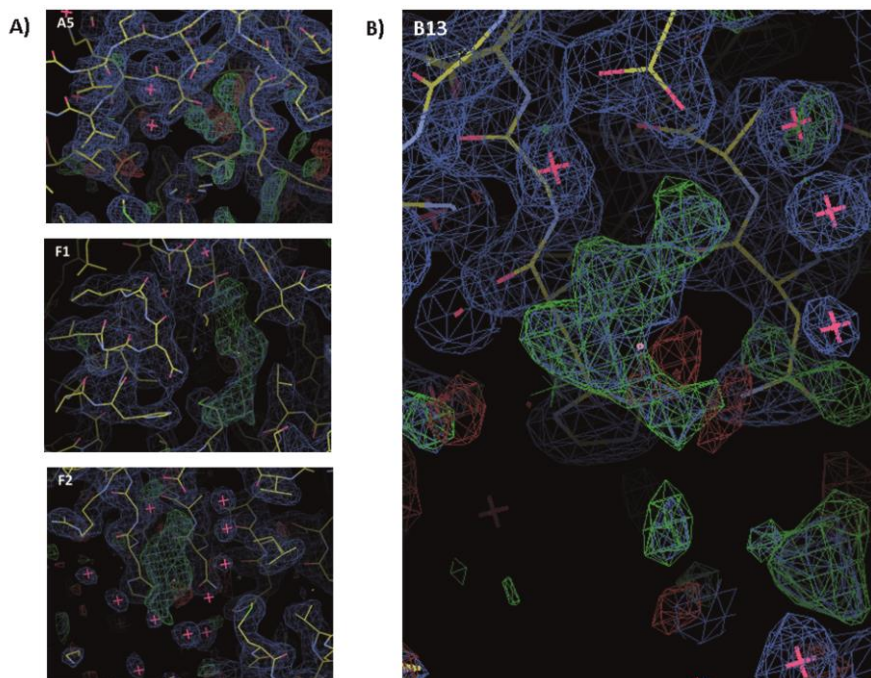


Figure 2. *T. maritima* CheA-HKAI structures solved by X-ray crystallography. A) Co-crystals of *T. maritima* CheA (CA domain) and the initial hits from the structure-based virtual screening (A5, Chapter 2) and the fragment-based screening by differential scanning fluorimetry (F1 and F2) were obtained by co-crystallization with 100 mM HKAI. B) Co-crystal of *T. maritima* CheA and the most promising HKAI described in the thesis B13 (Chapter 2) was obtained by co-crystallization followed by soaking with 100 mM B13. The 2Fo-Fc (blue) and Fo-Fc (green) electron density maps contoured to 1 and 2.5 σ , respectively, showed extra density in the active site that was not possible to explain by the protein model and were ascribed to the HKAI. However, the HKAI could not be fully resolved, probably due to partial occupancy and/or multiple conformations.

7.2. PURIFICATION, CRYSTALLIZATION AND PRELIMINARY X-RAY DIFFRACTION ANALYSIS OF *SYNECCOCYSTIS SPP.* COPM

INTRODUCTION

Copper is an essential trace element for organisms living under aerobic condition¹⁶. It is required in fundamental cellular processes such as oxidative phosphorylation, photosynthesis, and free radical control. However copper is highly toxic when it is present in excess, thus, many organisms have developed homeostatic mechanism to tightly regulate its cellular concentration¹⁷. Cyanobacteria are an attractive model to investigate the systems involved in copper homeostasis since they are unique bacteria with internal copper requirement for two proteins: the blue-copper protein plastocyanin, and the *caa*₃-type cytochrome oxidase¹⁸. These two proteins are localized in the thylakoids, a special internal structure where photosynthesis and respiration take place in cyanobacteria. Cyanobacteria are model microorganisms for the study of photosynthesis, carbon and nitrogen assimilation, evolution of plant plastids, and adaptability to environmental stresses. *Synechocystis* sp. PCC 6803 is one of the most highly studied types of cyanobacteria as it can grow both autotrophically or heterotrophically in the absence of light. Copper resistance in cyanobacteria has been mainly investigated in *Synechocystis* sp. PCC 6803 (hereafter *Synechocystis*), which involves a two-component system, CopRS, a protein of unknown function, CopM, and an HME-RND exports system, CopBAC^{19, 17}. These proteins are encoded by two operons: *copMRS*, and *copBAC*. Both *copM* and *copBAC* are regulated by the CopRS two-component system, and are specifically induced by the presence of Cu²⁺¹⁹. CopM is an unknown protein that contains a predicted periplasmic signal domain and a high number of histidine (8) and methionine (23) residues, which are usually implicated in direct metal binding in proteins. Furthermore, CopM has two domain of unknown function DUF305, which is present in other secretion proteins in bacteria and belongs to the ferritin superfamily²⁰. Herein, we report the purification, crystallization and preliminary X-ray diffraction analysis of *Synechocystis* CopM.

MATERIALS AND METHODS

CLONING, EXPRESSION AND PURIFICATION

A 519-bp band (from *ORF sll0788*) coding for the CopM₂₅₋₁₉₆ periplasmic domain was PCR amplified from genomic DNA with oligonucleotides ACOPMSTF-COPMSTR (Table 1), digested with *KpnI* and *SacI*, and cloned into pET51 digested with the same enzymes. CopM₂₅₋₁₉₆ was expressed in *E. coli* BL21. An overnight pre-culture was used to inoculate Luria broth medium and was grown to an optical density at 600 nm of 0.6. The culture was cooled down on ice for 20 min, protein expression induced by addition of 0.2 mM isopropyl-b-D-thiogalactopyranoside, and incubation continued for 4 h at 25°C. Cells were harvested by centrifugation and frozen at -80°C. Frozen pellets were re-suspended in buffer S (100 mM Tris HCl pH 8, 150 mM NaCl, 1 mM BCSA, 1 mM EDTA, and 2 mM Tris (2-carboxyethyl)-phosphine) and broken by sonication. The suspension was centrifuged 30 min at 30,000 g at 4°C and the supernatant was loaded into a 5-ml streptavidin beads (IBA GmbH) column equilibrated in buffer S. Beads were washed with 50 mL of buffer S and CopM₂₅₋₁₉₆ was eluted with 1x Strep-Tag elution buffer (IBA GmbH). CopM₂₅₋₁₉₆ was further purified by gel filtration in a Hi-Load 75 (GE-Healthcare) column equilibrated with 20 mM Tris HCl pH 8, 150 mM NaCl. The purified protein was concentrated using a 3K Vivaspin concentrator and store at -20 °C until use.

CRYSTALLIZATION

Initial sitting-drop vapour-diffusion crystallization trials to identify promising crystallization conditions for CopM were performed using the commercial crystallization screens JCSG+ (Qiagen, Germany), JBC I and JBC II (Jena Bioscience, Germany). In an attempt to obtain crystals of both the apo and Cu²⁺-bound CopM initial crystallization conditions screenings were performed in the presence of 1 mM EDTA and 1 mM CuSO₄, respectively. Crystallization drops of 0.6 µl (protein:precipitant ratio of 1:1) were set up in 96-well plates containing 75 µl reservoir solution. Initial hits were obtained after 4-6 days in multiple conditions (Table S1). Optimization of the crystallization conditions was attempted by varying the concentration of PEGs and salts under the conditions that initially generated diffracting crystals.

DATA COLLECTION AND PROCESSING

For data collection, the crystals were soaked in cryoprotectant (reservoir solution supplemented with 40% PEG 3350) for 5-10 sec. A single crystal was harvested with a loop and vitrified in liquid nitrogen. Diffraction data were collected the synchrotronsat Diamond Light Source (Didcot, United Kingdom) or European Synchrotron Radiation Facility (Grenoble, France). Diffraction images were indexed and integrated using Mosflm ⁷ or XDS ⁸ and the data were scaled using Scala ⁹. Data collection and processing statistics are summarized in Table 2.

RESULTS AND DISCUSSION

Recombinant CopM was cloned from genomic DNA, overexpressed in *E. coli* and purified to homogeneity using streptavidin-affinity chromatography and size-exclusion chromatography (SEC). The SEC elution profile showed a large peak (data not shown) eluting at apparent molecular mass between 17 and 44 kDa. This suggested that recombinant CopM with a theoretical molecular mass of 22.65 kDa is a monomer or a dimer in solution. Analysis of the purified CopM by SDS-PAGE and Coomassie staining showed a purity of at least 95 % (Figure 1). From a 2 L culture, 4.5 mg pure CopM was obtained. CopM was concentrated to 6.5 mg/ml and used in initial crystallization conditions screenings. Crystals with different shapes grew in various conditions (Table S1). In JBS I C7 (25% PEG 4000, 0.1 M Na MES pH 6.5, 0.2 M MgCl₂) rectangular crystals of CopM diffracting at 4 Å were obtained. In JCSG H9 (25% PEG 3350, 0.1 M Bis-Tris pH 5.5, different salts) in the presence of EDTA CopM crystals diffracting at 2.9 Å and C2 space group were obtained (Figure 2). Based on these initial results optimization of the crystals was attempted by varying PEG, salt and/ or buffer concentrations in the presence or absence of EDTA or Cu²⁺. Crystallization in the presence of EDTA was performed in order to eliminate any possible interacting ions and to obtain unbound CopM crystals (CopM apo). As CopM is related to copper resistance and it is hypothesized that it might interact with CopM we tried to obtain CopM bound to Cu²⁺ (CopM Cu²⁺). CopM was overexpressed in *E. coli* and during the expression and purification it might have bound to ions present in the medium and crystallization of the overexpressed CopM might have resulted in CopM bound to unknown ligands (CopM medium). The optimization of the crystallization conditions resulted in crystals with different shapes diffracting between 2.5 – 2.75 Å with P2₁ (CopM Cu²⁺) and P2₁2₁2₁ space group (CopM apo). Complete datasets from 2.5 to 3 Å resolution were collected from single crystals (Table 2). Data-collection and processing statistics are summarized in Table 2. Preliminary diffraction data analysis using POINTLESS²¹ suggested the presence of 5 (CopM EDTA, space group C2), 1 (CopM medium, space group P2₁) or 2 (CopM Cu²⁺, space group P2₁2₁2₁) molecules per asymmetric unit. Attempts of structure solution of CopM by molecular replacement using the coordinates of a fragment from *Deinococcus radiodurans* DUF305 (PDB: 3BT5) and *Streptomyces coelicolor* DUF305 (PDB: 2QF9) as search models and/ or with MRBUMP²² automatic mode were not successful. *D. radiodurans* DUF305 and *S. coelicolor* DUF 305 share 26.5 and 21.9 % sequence identity with CopM, respectively.

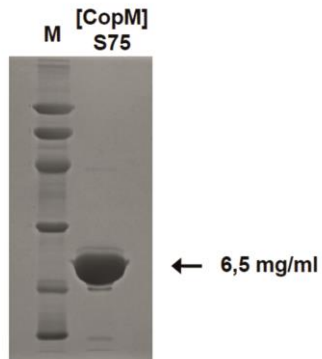


Figure 1. CopM purity assessed by SDS-PAGE

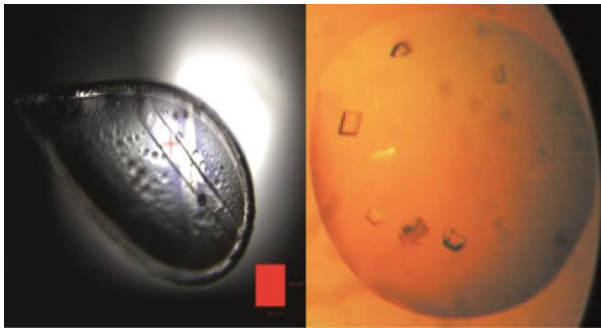


Figure 2. CopM crystals

Table 1. Oligonucleotides used in this work.

Name	Sequence
ACOPMSTF	caggtaccgtatcgcaatcaatctcc
COPMSTR	atgagctctcactgaccataccagt

Table 2. Data collection and processing statistics for CopM crystals

	CopM apo	CopM Cu ²⁺	CopM medium
Synchrotron	DLS	ESRF	ESRF
Wavelength (Å)	0.97889	0.87260	0.87260
Space group	C 2	P 2 ₁ 2 ₁ 2 ₁	P 2 ₁
Cell (Å)	a=199.29 b= 54.09 c=139.38 β=125.970	a=64.43 b=85.35 c=99.12	a=29.84 b=86.49 c=52.18 β=96.21
Resolution (Å)	52.6 - 2.92 (3 - 2.92)	49.56 - 2.90 (3.08 - 2.9)	51.87 - 2.70 (2.83 - 2.70)
R merge	0.062	0.062	0.124
I/σ(I)	11.3	11.1	8.4
No. of reflections (observed/unique)	86654/26359 (5915/1945)	51235/12654 (8263/2002)	53148/7219 (5678/880)
Completeness	99.5 (99.5)	99.9 (100)	99.0 (93.3)
Multiplicity	3.3 (3.0)	4.0 (4.1)	7.4 (6.5)

The data for the outer shell is shown in parentheses

DLS – Diamond Light Source

ESRF – European Synchrotron Radiation Facility

REFERENCES

1. Bilwes, A. M.; Alex, L. A.; Crane, B. R.; Simon, M. I., Structure of CheA, a signal-transducing histidine kinase. *Cell* 1999, 96 (1), 131-41.
2. Bilwes, A. M.; Quezada, C. M.; Croal, L. R.; Crane, B. R.; Simon, M. I., Nucleotide binding by the histidine kinase CheA. *Nature structural biology* 2001, 8 (4), 353-60.
3. Casino, P.; Rubio, V.; Marina, A., The mechanism of signal transduction by two-component systems. *Current opinion in structural biology* 2010, 20 (6), 763-71.
4. Casino, P.; Miguel-Romero, L.; Marina, A., Visualizing autophosphorylation in histidine kinases. *Nat Commun* 2014, 5, 3258.
5. Guarnieri, M. T.; Zhang, L.; Shen, J.; Zhao, R., The Hsp90 inhibitor radicicol interacts with the ATP-binding pocket of bacterial sensor kinase PhoQ. *Journal of molecular biology* 2008, 379 (1), 82-93.
6. Velikova, N.; Bem, A. E.; van Baarlen, P.; Wells, J. M.; Marina, A., Walk, the Path towards New Antibacterials with Low Potential for Resistance Development. *ACS Medicinal Chemistry Letters* 2013, 4 (10), 891-894.
7. Powell, H. R., The Rossmann Fourier autoindexing algorithm in MOSFLM. *Acta Crystallographica Section D: Biological Crystallography* 1999, 55 (10), 1690-1695.
8. Kabsch, W., XDS. *Acta Crystallographica Section D: Biological Crystallography* 2010, 66 (2), 125-132.
9. Evans, P., Scaling and assessment of data quality. *Acta crystallographica. Section D, Biological crystallography* 2006, 62 (Pt 1), 72-82.
10. Vagin, A.; Teplyakov, A., Molecular replacement with MOLREP. *Acta crystallographica. Section D, Biological crystallography* 2010, 66 (Pt 1), 22-5.
11. Emsley, P.; Cowtan, K., Coot: model-building tools for molecular graphics. *Acta crystallographica. Section D, Biological crystallography* 2004, 60 (Pt 12 Pt 1), 2126-32.
12. Emsley, P.; Lohkamp, B.; Scott, W. G.; Cowtan, K., Features and development of Coot. *Acta crystallographica. Section D, Biological crystallography* 2010, 66 (Pt 4), 486-501.
13. Afonine, P. V.; Grosse-Kunstleve, R. W.; Echols, N.; Headd, J. J.; Moriarty, N. W.; Mustyakimov, M.; Terwilliger, T. C.; Urzhumtsev, A.; Zwart, P. H.; Adams, P. D., Towards automated crystallographic structure refinement with phenix.refine. *Acta crystallographica. Section D, Biological crystallography* 2012, 68 (Pt 4), 352-67.
14. Afonine, P. V.; Mustyakimov, M.; Grosse-Kunstleve, R. W.; Moriarty, N. W.; Langan, P.; Adams, P. D., Joint X-ray and neutron refinement with phenix.refine. *Acta crystallographica. Section D, Biological crystallography* 2010, 66 (Pt 11), 1153-63.
15. Headd, J. J.; Echols, N.; Afonine, P. V.; Grosse-Kunstleve, R. W.; Chen, V. B.; Moriarty, N. W.; Richardson, D. C.; Richardson, J. S.; Adams, P. D., Use of knowledge-based restraints in phenix.refine to improve macromolecular refinement at low resolution. *Acta crystallographica. Section D, Biological crystallography* 2012, 68 (Pt 4), 381-90.
16. Bondarczuk, K.; Piotrowska-Seget, Z., Molecular basis of active copper resistance mechanisms in Gram-negative bacteria. *Cell biology and toxicology* 2013, 29 (6), 397-405.
17. Lopez-Maury, L.; Giner-Lamia, J.; Florencio, F. J., Redox control of copper homeostasis in cyanobacteria. *Plant signaling & behavior* 2012, 7 (12), 1712-4.
18. Manna, P.; Vermaas, W., Lumenal proteins involved in respiratory electron transport in the cyanobacterium *Synechocystis* sp. PCC6803. *Plant molecular biology* 1997, 35 (4), 407-16.
19. Giner-Lamia, J.; Lopez-Maury, L.; Reyes, J. C.; Florencio, F. J., The CopRS two-component system is responsible for resistance to copper in the cyanobacterium *Synechocystis* sp. PCC 6803. *Plant physiology* 2012, 159 (4), 1806-18.

20. Uchida, M.; Kang, S.; Reichhardt, C.; Harlen, K.; Douglas, T., The ferritin superfamily: Supramolecular templates for materials synthesis. *Biochimica et biophysica acta* 2010, 1800 (8), 834-45.
21. Evans, P. R., An introduction to data reduction: Space-group determination, scaling and intensity statistics. *Acta Crystallographica Section D: Biological Crystallography* 2011, 67 (4), 282-292.
22. Keegan, R. M.; Winn, M. D., MrBUMP: an automated pipeline for molecular replacement. *Acta crystallographica. Section D, Biological crystallography* 2008, 64 (Pt 1), 119-24.

SUPPLEMENTARY MATERIAL CHAPTER 7.2

Table S1. Crystallization screenings results

Sample	Screening, position, morphology	Condition
CopM glycerol	JBS I, A11	25% PEG 1000, 0.1 M Na HEPES pH 7.5
CopM	JBS I, C7 cubes	25% PEG 4000, 0.1 M Na MES pH 6.5, 0.2 M MgCl ₂
CopM	JBS I, C11 very small	30% PEG 4000, 0.1 M Na HEPES pH 7.5, 0.2 M CaCl ₂
CopM	MIDAS, H3	20% glycerol ethoxylate, 3% polyethylene imine
CopM	MIDAS, G7, needles	30% glycerol ethoxylate, 0.2 M Amm Acetate pH 6.5, 0.1 M MES-NaOH
CopM EDTA	JBS I, G2	10% PEG 8000, 0.1 M Na HEPES pH 7.5, 0.2 mM Na Acetate
CopM, EDTA	JBS I, C8	25% PEG 4000, 0.1 M Tris HCl 8.5, 0.2 M CaCl ₂
CopM EDTA	JCSG+, from H6 to H11	25% PEG 3350, 0.1 M Bis-Tris pH 5.5, different salts
CopM EDTA	JCSG+, G1, needles, thin plates	30% Jeaffamine ED 2001, 0.1 M HEPES pH 7
CopM EDTA	JCSG+, E1	1M Tri-Na citrate, 0.1 M Na cacodylate pH 6.5
CopM EDTA	JCSG+, E2	0.2 N NaCl, 0.1 M Na cacodylate pH 6.5, 2M AmSO ₄
CopM EDTA	JCSG+, G10	0.15 M KBr, 30% PEG MME 2000
CopM EDTA	JCSG+, G11	2M AmSO ₄ , 0.1 M Bis-Tris pH 5.5
CopM	JBS I, F4	15% PEG 6000, 50 mM KCl, 10 mM MgCl
CopM	JBS I, B12	12% PEG 4000, 0.1 M Na HEPES pH 7.5, 0.1 M Na Acetate

CHAPTER 8

WALK, THE PATH TOWARDS NEW ANTIBACTERIALS WITH LOW POTENTIAL FOR RESISTANCE DEVELOPMENT

Nadya Velikova¹, Agnieszka E. Bem², Peter van Baarlen², Jerry M. Wells³, Alberto Marina^{1,3}

¹Instituto de Biomedicina de Valencia, Consejo Superior de Investigaciones Científicas (CSIC), Jaime Roig 11, 46010 Valencia, Spain;

²Host–Microbe Interactomics Chair Group, Animal Sciences, University of Wageningen, 6700 AH Wageningen, The Netherlands;

³CIBER de Enfermedades Raras (CIBERER), ISCIII, 46010 Valencia, Spain

PUBLISHED IN ACS MEDICINAL CHEMISTRY LETTERS, DOI:
10.1021/ML400320S

2014

ABSTRACT

Resistance to antibiotics used in the treatment of bacterial infectious diseases is a global health problem. More than a decade ago, two-component systems such as WalKR were proposed as ideal targets for the development of new antibiotics. Biochemical screens for WalKR inhibitors using compound libraries have identified many hits, some of which were shown to have non-specific effects. The recently published structures of the *S. mutans* and *B. subtilis* WalK provide the opportunity to study inhibitors of WalK autophosphorylation at the atomic level and means to design compounds with improved specificity and affinity using a structure-based approach.

Recently scientists have been watching in awe as bacteria develop resistance to the latest antibiotics. Multidrug resistant tuberculosis (MDR-TB), penicillin-resistant *Streptococcus pneumoniae*, and hospital-acquired infections with vancomycin-resistant enterococci (VRE) or methicillin-resistant *Staphylococcus aureus* (MRSA) are regularly making headline news. The problem is not only one of resistance to front line drugs and the fear that one day, infections will be incurable, but also the increased cost of patient care and the prospect of future inability to perform trivial medical procedures without significant risk.

The scarcity of new antibiotics has been put down to dwindling returns on screening natural sources but also poor incentives for companies to invest in this sector as opposed to treatment for cancer and chronic diseases. However, the challenge of developing anti-infective drugs has been taken up by small enterprises and academia with the support of governments and other funding organizations.

The genomics revolution has accelerated finding new targets for anti-infective drugs, but designing drug-like inhibitors against specific targets remains highly challenging, costly, and not without significant risk of failure.

Against this somewhat gloomy perspective, there are some promising developments unfolding, one of which concerns bacterial two-component systems (TCSs) as drug targets. Bacteria respond and adapt to a large variety of environmental and intracellular signals via TCS signal transduction. The minimum components of a TCS are a sensor histidine kinase (HK) and an effector response regulator (RR)(8)(Figure 1). Typically, the sensor histidine kinase (HK) is membrane-bound, and signal recognition alters the phosphorylation state of a cognate response regulator (RR). HK sensing of specific signals occurs via a variable domain that is commonly exposed to the extracellular milieu, whereas the remaining protein domains are generally conserved, cytoplasmic, and required for signal transduction (8) (Figure1). RRs are usually transcription factors of which the DNA-binding capacity and consequently, gene transcription is determined by their phosphorylation state. TCSs may directly or indirectly control numerous genes, including those involved in the regulation of metabolism, cell physiology, virulence, persistence, and resistance to antibiotics or antimicrobial peptides. Targeting virulence is a promising antibacterial-drug discovery strategy as it exerts less selective pressure on the pathogen and resistance development will be slower.

TCSs were proposed as attractive targets more than 20 years ago because they are absent in mammals and essential or conditionally essential for viability in several important bacterial pathogens. WalKR system (a.k.a., YycGF, VicKR, MicAB) is an obligate essential regulatory system in Firmicutes including MRSA, VRE, and some other notorious pathogens. Other TCSs might not be essential for growth in vitro, but in vivo they can be necessary for survival or persistence (e.g., the DosRS system in *Mycobacterium*). Besides, some bacteria possess as many as 200 TCSs depending on

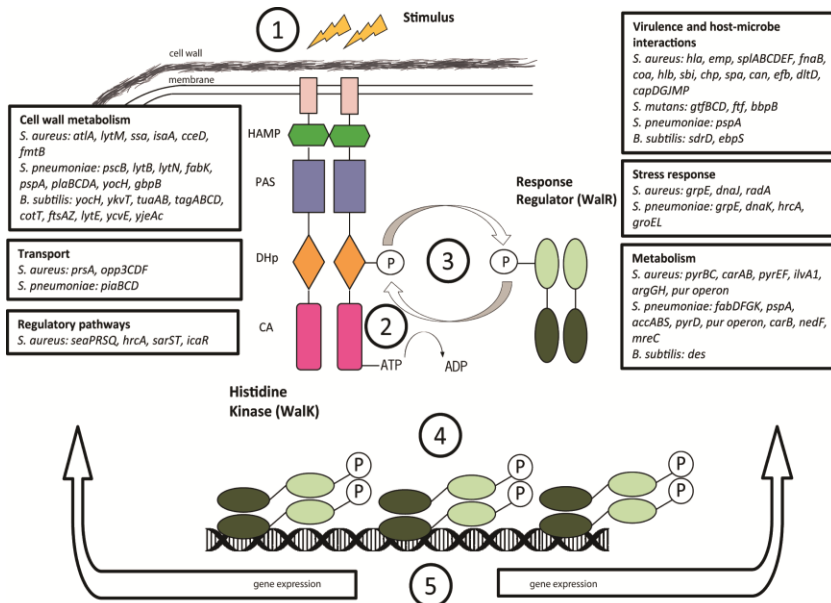


Figure 1. TCS signaling. TCS signaling is triggered by the recognition of the signal (1) by the HK sensor variable domain, which regulates the autophosphorylation of a histidine residue in the conserved portion of HK (2). (8) Signal is then transduced to the cognate RR by the transfer of the phosphoryl group from the histidine to a conserved aspartic residue in the RR (3). Typically, RRs are transcription factors, and their phosphorylation state regulates their DNA-binding capacity (4) and, consequently, gene transcription (5) (1-4)

their lifestyle and requirements for adaptation and metabolism in different environments. Presumably the combined effect of inhibiting all or multiple TCSs and thus the ability of a bacterium to adapt to changing physiological conditions would also greatly weaken their ability to cause infections. Given that the first TCS inhibitors were described more than a decade ago, one might think that finding TCS inhibitors is an intractable problem, and it might be better to focus on other essential pathways in bacteria. Nevertheless, there is no doubt that TCSs are good antibacterial drug targets because they have a high degree of conservation in the active sites of their catalytic domains. This fact implies that inhibitors of one TCS may in fact block multiple TCS regulatory networks, effectively incapacitating the ability of bacteria to adapt to environmental and physiological changes.

Perhaps the lack of drug candidates against WalKR or other TCSs is due to the limitations of the previously adopted approach.

The pioneering work by the Utsumi group identified imidazole and zerumbone derivatives as the first inhibitors of WalK. Afterward, the same group developed biochemical and genetic high-throughput (HTP) screening methods resulting in the discovery of a number of WalKR inhibitors.(5) However, some of these inhibitors were not exclusively selective to WalKR suggesting that HTP screening approach may favor the identification of compounds that inhibit through mechanisms that are not specific for TCSs and may be toxic. A more promising avenue of research seems to be structure-based virtual screenings (SBVS) with tailored libraries or rational structure-based drug design. Targeting WalKR following structure-based approach is expected to help identify specific inhibitors of WalKR and general inhibitors of TCSs. Both these will expedite the urgently needed development of novel antibacterial drugs.

The more druggable component of TCS is the HK due to the presence of the catalytic ATP-binding domain (CA domain). The CA domain contains a well-defined and partially conserved pocket, which accommodates the ATP required for autokinase activation, i.e., initiation of signal transduction (Figure 2A,B). This pocket is hydrophobic in nature but presents two conserved polar residues, aspartic acid (Asp) and asparagine (Asn), which are responsible for ATP selectivity and Mg^{2+} chelation, respectively. In addition, three conserved structural water molecules increase the pocket polarity and are involved in hydrogen bonds between the ATP and the conserved Asp and Asn.

The major bottleneck for structure-based discovery of WalK inhibitors has been the lack of high-resolution structures of WalK. Instead, structural homology models of the CA domain of *S. pneumoniae* and *S. epidermidis* WalK based on the structures of *Thermotoga maritima* HK853 (PDB:2C2A) and *E. coli* EnvZ (PDB:1BXD) were used for SBVS. These screenings yielded WalK autophosphorylation inhibitors belonging to different classes of chemical structures, such as imidazole analogues and derivatives of furan, thiophene, thiazolidinone, benzamide, and pyrimidinone.(6),(7) This suggests that the ATP-binding pocket can accommodate a variety of ligands, a feature that can be exploited to design potent and selective HK inhibitors with a desired ADMET (absorption, distribution, metabolism, elimination, and toxicology) profile. Notably, unfavorable ADMET properties are one of the major reasons for high attrition rates of candidate molecules in drug discovery.

WalK autophosphorylation inhibitors identified by SBVS inhibited the growth of *S. pneumoniae* and *S. epidermidis* and showed bactericidal effects toward both planktonic and biofilm cells. Furthermore, some of them decreased the mortality of mice infected with *S. pneumoniae* in an *in vivo* sepsis model, supporting the idea that SBVS is a viable tool for the identification of WalK inhibitors with therapeutic effect. Nevertheless, the design of potent ATP-competitive inhibitors specific for WalK is challenging, even more so when structural homology models are used. This issue is crucial when attempting to generate a WalK inhibitor with higher specificity and affinity in the hit-to-lead optimization phase. Although the overall fold of the CA domain as well as the catalytic residues is generally conserved, there are large

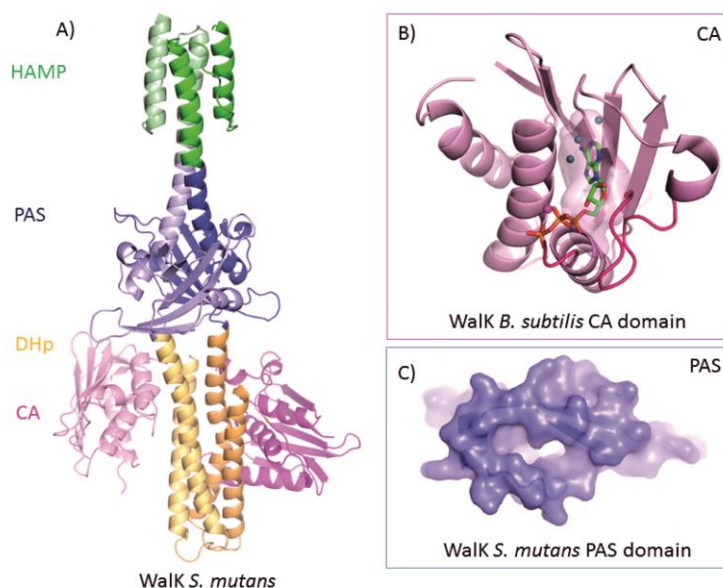


Figure 2. Structure of WalK. (A) *S. mutans* WalK (PDB:4I5S) is a long-rod dimer anchoring a HAMP signal-transducer domain (green) and a PAS sensor domain (blue) directly connected to the catalytic DHp (yellow) and CA (pink) domains. (B) *B. subtilis* WalK CA domain (PDB:3SL2). The ATP-binding site (semitransparent surface, ATP shown as sticks) is generally conserved except for the variable ATP-lid (magenta). More potent and specific WalK inhibitors can be redesigned by optimizing the interactions of previously identified hits with the ATP-binding site, particularly with the conserved structural water molecules (blue spheres) and the ATP-lid. (C) Close up view of *S. mutans* WalK PAS domain shows the putative ligand-binding pockets with a large cavity and a unique tunnel; these structural characteristics can be exploited to identify WalK PAS domain ligands.

variations in size and sequence in the ATP-lid, a HK distinctive flexible loop that covers the ATP-binding pocket and is crucially involved in the autophosphorylation reactions (8)(Figure 2A,B).

Recent elucidation of WalK structures of the entire intracellular portion from *Streptococcus mutans* (PDB:4I5S) (Figure 2A,C) and the CA domain from *Bacillus subtilis* (PDB:3SL2) (Figure 2B) might provide the key to design improved WalK inhibitors. These structures have not only revealed specific characteristics of the WalK CA domain but also insights into the molecular mechanism of WalK autokinase activation. These WalK structures might be used to generate potent and selective WalK inhibitors by the rational redesign of the previously identified hits by optimizing interactions with the ATP-binding site and particularly with the ATP-lid. Moreover, the structure of *S. mutans* WalK has also revealed specific folds of the HAMP transducer, the PAS sensor, and the DHp catalytic domains of WalK (Figure 2), opening up new possibilities to explore these domains for structure-based drug design.

PAS (Per-Arnt-Sim) domains are small sensor modules that bind a chemically diverse range of small molecules and present a conserved three-dimensional architecture but a divergent primary sequence. The *B. subtilis* PAS domain is required for WalK activity and localization to the divisome during cell division. The structure of *S. mutans* WalK shows that the putative ligand binding site forms unique pockets for a variety of ligands to bind (Figure 2C) suggesting that WalK PAS domain might bind ligands differently from other HK PAS domains. Therefore, the WalK PAS domain appears to be a promising target for novel antimicrobials, and its structure might also facilitate the rational design of specific and potent WalK inhibitors. Furthermore, WalK PAS ligands remain unknown, and their identification might generate chemical reagents to facilitate mechanistic studies.

In summary, we argue that discovery of new WalKR, and in general TCS, inhibitors, which will be further developed into antibacterial drugs, is still a realistic scenario. However, the focus should be on structure-based approaches. Certainly, ongoing efforts to solve the structures of HK from other important pathogens will help to design inhibitors with optimized activity. The high homology between TCSs and their wide distribution among bacteria imply that such inhibitors can be developed into broad-spectrum antibiotics. The road ahead is still challenging and arduous, but given the importance of the problem of drug resistance, we are convinced it is a road we should take.

REFERENCES

1. Dubrac,S.; Boneca,I. G.; Poupel,O.; Msadek,T.New insights into the WalK/WalR (YycG/YycF) essential signal-transduction pathway reveal a major role in controlling cell wall metabolism and biofilm formation in *Staphylococcus aureus* *J. Bacteriol.* **2007**,189(22)8257–8269
2. Delauné,A.; Dubrac,S.; Blanchet,C.; Poupel,O.; Mäder,U.; Hiron,A.; Leduc,A.; Fitting,C.; Nicolas,P.; Cavailon,J.-M.; Adib-Conquy,M.; Msadek,T.The WalKR system controls major staphylococcal virulence genes and is involved in triggering host inflammatory response *Infect. Immun.* **2012**,80(10)3438–3453
3. Mohedano,M. L.; Overweg,K.; De La Fuente,A.; Reuter,M.; Altabe,S.; Mulholland,F.; De Mendoza,D.; López,P.; Wells,J. M.Evidence that the essential response regulator YycF in *Streptococcus pneumoniae* modulates expression of fatty acid biosynthesis genes and alters membrane-composition *J. Bacteriol* **2005**,187(7)2357–2367
4. Howden,B. P.; McEvoy,C. R. E.; Allen,D. L.; Bell,J.; Coombs,G.; Bennett-Wood,V.; Porter,J. L.; Robins-Browne,R.; Davies,J. K.; Seemann,T.; Stinear,T. P.Evolution of multidrug resistance during *Staphylococcus aureus* infection involves mutation of the essential two component regulator WalKR *PLoS Pathog* **2011**,7(11)e1002359
5. Okada,A.; Gotoh,Y.; Watanabe,T.; Furuta,E.; Yamamoto,K.; Usumi,R. Targeting two-component signal transduction: a novel drug discovery system *Methods Enzymol.* **2007**,422,386–395
6. Qin,Z.; Zhang,J.; Xu,B.; Chen,L.; Wu,Y.; Yang,X.; Shen,X.; Molin,S.; Danchin,A.; Jiang,H.; Qu,D. Structure-based discovery of inhibitors of the YycG histidine kinase: new chemical leads to combat *Staphylococcus epidermidis* infections *BMC Microbiol.* **2006** 6,96
7. Li,N.; Wang,F.; Niu,S.; Cao,J.; Wu,K.; Li,Y.; Yin,N.; Zhang,X.; Zhu,W.; Yin,Y.Discovery of novel inhibitors of *Streptococcus pneumoniae* based on the virtual screening with the homology-modelled structure of histidine kinase (VikK) *BMC Microbiol* **2009**,9,129
8. Casino,P.; Rubio,V.; Marina, A.The mechanism of signal transduction by two-component systems *Curr. Opin. Struct. Biol.* **2010**,20(6)763–771

2014

CHAPTER 9

GENERAL DISCUSSION

Nadya Velikova

2014

THE NEED OF NEW ANTIBACTERIALS AND THE IDEAL ANTIBACTERIAL TARGETS

The growing problem of bacterial multi-drug resistance (MDR) requires the urgent development of novel antibacterials with different mechanisms of action from known antibiotics^{1, 2}. At the outset of this thesis bacterial two-component systems (TCS) were selected as targets for the discovery of novel lead candidates for the development of antibacterial drugs. At this point it seems prudent to reevaluate TCS suitability as drug targets based on the results presented in the thesis and developments published in the literature. Recent reviews^{3, 4, 5, 6, 7, 8} from opinion leaders in the field suggest that from pharmaceutical point of view novel antibacterial targets should fulfil the following criteria:

Chapter 9

1. Have no human homologues or structurally similar proteins.
2. Be highly conserved among various bacterial species to assure broad-spectrum of antibacterial action.
3. Be strictly essential for bacterial viability such that their inhibition would lead to bacterial death but as targeting essentiality might increase the rise of resistance, targeting virulence targets has been proposed as an alternative.
4. Be "assayable", i.e. should have easy measurable activity, assays amenable to high-throughput screening (HTS), target structural data should be available or easy to disclose and genetic tools should be available to validate the target in a key species.
5. Be patentable.

The suitability of TCS as targets for novel antibacterials is discussed below in relation to the first four criteria listed above.

1. HOMOLOGUES OF TWO-COMPONENT SIGNALLING SYSTEMS ARE ABSENT IN HIGHER EUKARYOTES

In all living organisms cellular processes are regulated via signal transduction. Both prokaryotes and eukaryotes depend on the ability to rapidly sense and respond to changes in intracellular and extracellular signals to adapt and survive. Two-component systems (TCS) are the major mode of signal transduction in bacteria⁹. They are attractive antibacterial (drug) targets because multiple TCS are found in nearly all bacteria and homologues have not been identified in mammals, including humans^{10, 11, 12}. TCS signalling involves autophosphorylation of a membrane-bound histidine kinase (HK), phosphotransfer of the phosphoryl group to a cognate response regulator (RR), and ultimately modulation of the expression of target genes (Figure 1)¹³. The

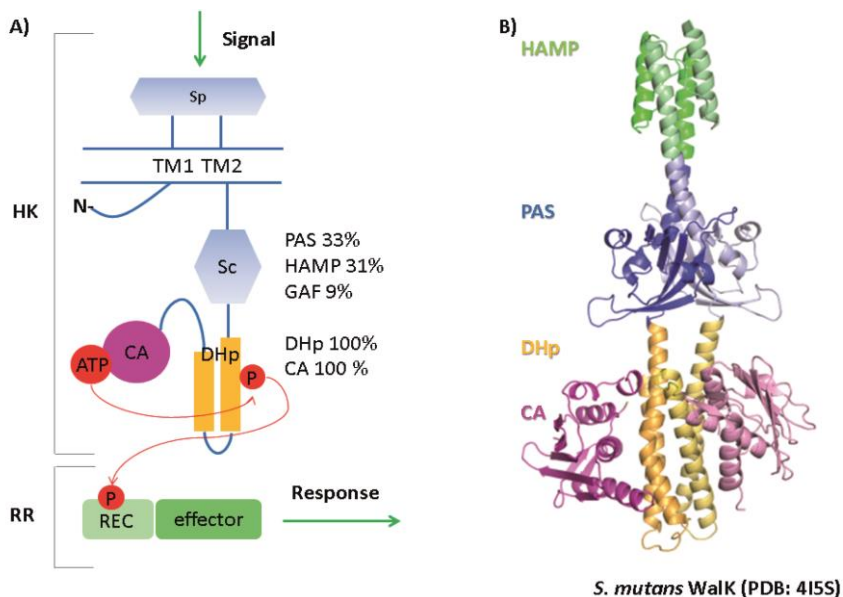


Figure 1. Two-component system domain organization and signalling. A) A two-component system consist of a membrane-bound HK composed of a sensor domain (periplasmic sensor domain, Sp, and/or cytosolic sensor domain, Sc), transmembrane helices (TM1 and TM2) and the DHp and CA domains, and of an RR composed of a REC and an effector domain. ATP is used to first phosphorylate a His in the DHp domain and the phosphoryl group is then transferred to an Asp residue in the RR REC domain. The composition of the Sc can vary and is not always present in all HK, whereas the DHp and the CA domain are present in all HKs (modified from ¹³). B) HK domain organisation exemplified by *S. mutans* Walk (PDB: 4I5S).

phosphorylation levels of the RR are tightly regulated by the phosphatase activity of the HK, the RR or a partner protein ^{13, 14}. HK autophosphorylation is mediated via the catalytic and ATP-binding (CA) domain, which binds ATP and phosphorylates the HK at conserved histidine (His) residues in the dimerization and histidine phosphotransfer (DHp) domain. The CA and DHp domains are conserved and present in all HKs, whereas the remaining sensor domains (periplasmic, PAS; GAF, HAMP) are variable and not present in all HKs (Figure 1) Furthermore, the ATP-binding site of the CA domain is a well-defined and highly conserved binding pocket (Figure 2). The conserved features of the CA domain and its essential role in signal transduction highlight it as an attractive target for structure-based virtual screening and phenotypic screening of biochemical inhibitors¹³. Moreover, the high degree of sequence conservation in the CA catalytic site implies that inhibitors targeted against this site will possess broad-spectrum of antibacterial activity. Altogether, this makes the CA domain the most attractive HK target site for the discovery and development of broad-spectrum antibacterials.

The only caveat with targeting the CA domain is the presence of the ATP-binding Bergerat fold which is shared with GHKL family of proteins, including mammalian proteins as Hsp90 or MutL[4] (Figure 3). The Bergerat fold includes four conserved motifs common to the GHKL family of proteins. Three of the four motifs correspond to the conserved N, G1 and G2 boxes in the HK CA domain¹³. These similarities might lead to off target inhibitory effects of putative HK autophosphorylation inhibitors (HKAI)s and therefore toxicity to mammalian cells. Indeed, the novel HKAI)s described in this thesis (Chapter 2 and 3) were cytotoxic to Caco-2 cells. The observed IC₅₀ values for cell viability were mostly lower than the observed minimal inhibitory concentrations (MICs) against the bacterial strains tested suggesting off-target activities. Nevertheless, these were small molecule hits and there is considerable potential to improve their specificity and target selectivity through structure-based drug design and medicinal chemistry approach.

The similarity between the CA domain of bacterial TCS and eukaryotic proteins containing the Bergerat fold is exemplified by the demonstration that the eukaryotic Hsp90 inhibitor radicicol is an inhibitor of PhoQ autophosphorylation and was co-crystallized with the CA domain of PhoQ¹⁵. However, other GHKL family member protein inhibitors, such as novobiocin and geldanamycin, could not be co-crystallized successfully with PhoQ and had no inhibitory effect on PhoQ autophosphorylation¹⁵. The differences between radicicol and the other Hsp90 inhibitors with respect to PhoQ inhibition were attributed to differences in the putative interaction with the ATP-lid and the ATP-lid conformation in the CA domain. The ATP-lid (Figure 1) is a variable loop that connects the G1 and G2 boxes or the corresponding motifs in other GHKL family members. The ATP-lid is crucially involved in autophosphorylation^{13, 16}. Although HKs are structurally similar to eukaryotic proteins belonging to the GHKL family, the differences in the ATP-lid can be a valuable feature for designing inhibitors that are specific to HKs with limited effect on eukaryotic GHKL proteins and therefore with low toxicity to host cells¹⁵.

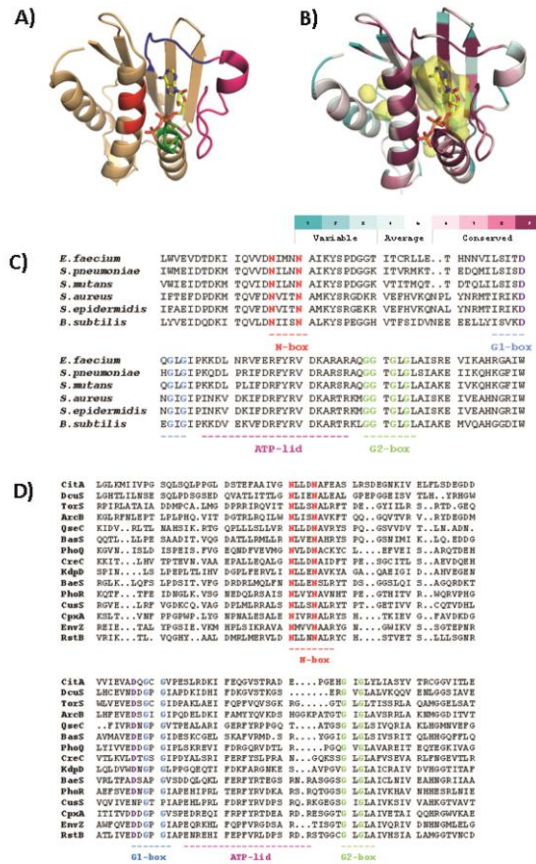


Figure 2. The ATP-binding site of HK CA domain is a well-defined and highly conserved pocket and allows the discovery and design of HK autophosphorylation inhibitors with broad-spectrum antibacterial activity following structure-based approaches A) Structure of *B. subtilis* Walk CA domain (PDB: 3SL2). The conserved N-, G1- and G2-boxes are shown in red, blue and green, respectively. The variable ATP-lid is shown in pink. B) *B. subtilis* Walk CA domain (PDB:3SL2) coloured by conservation. The conservation scores were calculated using ConSurf ¹⁰⁶. The ATP-binding pocket was calculated using PyMol ¹⁰⁷ and is shown as a semi-transparent yellow surface. ATP is shown as ball-and-stick in A and B. C) Alignment of Walk CA domains from different organisms D) Alignment of the CA domains of different *E. coli* HKs

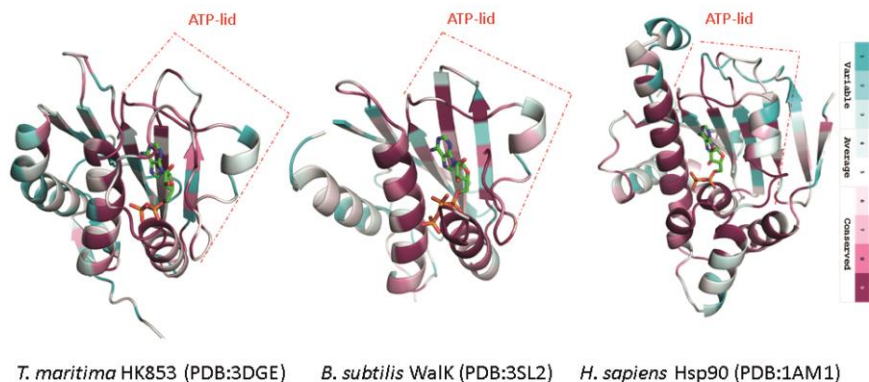


Figure 3. The ATP-lid is a flexible loop variable in length and in sequence playing a critical role in ligand-binding and catalytic activity of members of the GHKL-superfamily of proteins. Features of the ATP-lid can be exploited to design histidine-kinase autophosphorylation inhibitors with higher specificity to bacterial histidine kinases and reduced off-target effects to mammalian members of the GHKL-superfamily, i.e. with lower toxicity. Conservation scores were calculated using ConSurf¹. Ligands are shown in sticks.

2. TCS ARE HIGHLY CONSERVED IN THE BACTERIAL KINGDOM AND TCS INHIBITORS ARE EXPECTED TO SHOW BROAD-SPECTRUM OF ANTIBACTERIAL ACTIVITY AND LOWER POTENTIAL FOR RESISTANCE DEVELOPMENT

TCS and especially the HK CA domains are highly conserved among various bacterial species (Figure 1). The high conservation on the one hand assures broad-spectrum of antibacterial activity and on the other hand simultaneous inhibition of multiple targets. Simultaneous inhibition of multiple targets (drug polypharmacology) has been proposed as a strategy to slow down resistance development to drugs including to novel antibacterials^{17, 18, 19, 19, 20}. As bacteria possess multiple sometimes as many as 160 TCSs, inhibitors of the highly conserved CA domain are likely to shut down multiple signaling pathways compromising the ability of the bacteria to rapidly adapt to environmental changes including those encountered in the host during infection. For some bacteria TCS inhibition may not be bactericidal but it is likely to compromise efficient growth, especially under the physiological stresses encountered by pathogens in the host.

The notion that inhibitors of TCS could inhibit multiple TCS targets is supported by the activity studies performed on the novel histidine kinase autophosphorylation inhibitors (HKAI) described in this thesis (Chapter 2 and 3). Promising HKAI were discovered by structure-based virtual screening (SBVS) and fragment-based screening (FBS) for putative ligands of three or two different HKs, respectively. Inhibition of autophosphorylation was then shown in biochemical assays with HKs not used for screening, indicating the potential to identify inhibitors with a broad-spectrum of HK autophosphorylation inhibitory activity using such approaches. The broad spectrum of activity against HKs was also reflected in the capacity of these inhibitors to prevent growth of several species of Gram-positive bacteria (Chapter 2 and 3). Furthermore, the most promising inhibitors were effective against multi-drug resistant (MDR) clinical isolates, including MRSA strains resistant to a wide range of β -lactam and non- β -lactam antibiotics²¹. These results suggest that the HKAI possess different mechanism of action than the known antibiotics and/or the mechanisms of resistance present in the MDR strains are not active against the HKAI. The activity of the novel HKAI against Gram-negative bacteria was initially found to be low (minimal inhibitory concentrations (MICs) ≥ 63 $\mu\text{g/ml}$ for the active compounds, and > 500 $\mu\text{g/ml}$ for the majority of the tested inhibitors) but when combined with ϵ -poly-L-lysine capped nanoparticles (Chapter 4) the activity increased more than 10-fold. The antibacterial activity of the nanoparticles was only observed when combined with the HKAI, suggesting that the cell envelope of Gram-negative bacteria is most likely limiting intracellular uptake of the HKAI. Despite the evidence stated above, it remains possible that the antibacterial activity is due to inhibition of targets other than TCS HKs. Until this is proven we cannot unequivocally conclude that inhibition of multiple HKs is the reason for their antibacterial activity of the identified HKAI.

3. SOME TCS ARE ESSENTIAL FOR BACTERIAL GROWTH AND/OR INVOLVED IN THE REGULATION OF VIRULENCE

Ideally novel antibacterials should target essential proteins or processes to assure bactericidal effect but most TCS are not essential for viability of bacteria in their normal habitat. This has been demonstrated by the systematic knock out of TCS in different bacteria^{22, 23, 24}. However, this approach does not rule out the possibility that simultaneous inhibition of multiple TCS would cause bacterial death. In only a few organisms, more than one TCS has been genetically deleted or inactivated and this is restricted to typically just two or three TCS²⁴. One TCS that is known to be essential for bacterial viability is WalKR, which is highly conserved among Gram-positives with a low G+C content in their genomic DNA (Figure 1)²⁵.

In this thesis (Chapter 3) inhibitors of *S. pneumoniae* WalK autophosphorylation with moderate antibacterial effect for Gram-positive strains, including *S. pneumoniae* and MRSA²¹, and Gram-negative strains, including multidrug resistant *Acinetobacter baumannii*²⁶ were discovered by FBS for putative ligands of *S. pneumoniae* WalK and then ligand-based similarity searches (LBS) with the two best hits. The SBVS hits, A5 and A6 (Chapter 2), also inhibited *S. pneumoniae* WalK autophosphorylation *in vitro* and showed antibacterial effect for Gram-positive bacteria. Nevertheless it is difficult

to demonstrate that the antibacterial effect is due to inhibition of WalKR even more so when multiple-target inhibition is expected. Possible approaches to demonstrate target specificity and to elucidate the mechanism of action of the novel antibacterial HKAI include overexpression of the putative target and checking of inhibitor-induced changes in the growth rate or the morphology of the mutant strain²⁷; transcriptomics signatures²⁸, transcriptional profiling of conditional mutants²⁹. Furthermore, some of the identified fragment-like HKAI (Chapter 3) showed antibacterial effect against the Gram-negative *A. baumannii*, *S. maltophilia* and/ or *E. coli*. WalKR is not present in Gram-negative bacteria. The high IC₅₀ values of the fragment-like HKAI for WalK autophosphorylation inhibitors ($\geq 2\text{mM}$) and their antibacterial effect for Gram-negative strains where WalKR is not present indicate that the identified HKAI inhibit more HK targets and/ or possess mechanism of action different than HK autophosphorylation inhibition.

It has been suggested that inhibiting essential targets would lead to fast(er) development of resistance than inhibition of virulence mechanisms because there would only be selection for resistance in pathogens causing an infection in the host²⁵,³⁰. High throughput screening for ligands of *E. coli* QseC periplasmic domain identified Led209 as a promising hit for the development of antibacterials that act via inhibiting virulence. QseCB is a TCS involved in the response to host adrenergic signals and in quorum sensing mediated via AI-2^{31, 32, 33, 34}. Led209 was shown to inhibit the binding of signals to QseC, preventing its autophosphorylation and consequently inhibiting QseC-mediated activation of virulence gene expression³⁰. Altogether, this led to inhibition of virulence *in vitro* and *in vivo* of several susceptible pathogens such as UPEC and *Salmonella* spp.³⁰. The results obtained with Led209 highlight the potential of targeting virulence for the development of novel antibacterials. Other TCS such as PhoQP and PhoRB involved in responses to environmental stimuli have also been linked to regulation of virulence^{35, 36} and therefore might also be promising targets for the discovery of antibacterials reducing virulence. Interestingly the HKAI identified in this thesis (Chapter 2 and 3) inhibited autophosphorylation activity of *E. coli* PhoR and *S. aureus* PhoR. In the future it would be interesting to study their specific effects on the regulation of genes controlled by the PhoRB TCS under phosphate limiting conditions in order to demonstrate that these inhibitors act on the targets that are inhibited *in vitro*. Furthermore, evaluation of the effect of these HKAI in *phoR* knockout strains will give crucial information about the specificity of the compounds.

An example of a promising antimicrobial target that is crucial for virulence and persistent infections is the Mycobacterium DosRST composed of the RR DosR and the HKs DosS and DosT. DosRST plays an essential role in triggering and maintaining dormancy and in enabling resuscitation in tuberculosis^{37, 38, 39, 40}. The metabolic adaptations occurring in non-duplicating, drug resistant dormant *M. tuberculosis* are triggered by hypoxia and respiratory poisons (i.e. NO, CO), and are regulated by the DosR RR. DosR is activated by phosphorylation catalyzed by two HKs, DosS and DosT. Due the conservation of the CA domains of HKs a future possibility is to test the activity of the discovered HKAI (Chapter 2 and 3) against DosS and DosT and their antimicrobial effect against *M. tuberculosis*. In a genomics-based *in silico* target identification pipeline for *M. tuberculosis* incorporating a network analysis of the protein-protein interactome, a flux balance analysis of the reactome, a structural

assessment of targetability as well as experimentally derived phenotype essentiality data, DosS was selected as a high-confidence target for dormant mycobacteria⁴¹.

4. A VARIETY OF DRUG-DISCOVERY APPROACHES CAN BE APPLIED TO TCS INHIBITORS DISCOVERY

The first published TCS inhibitors were discovered by high-throughput screenings of natural products or chemical libraries for biochemical inhibition of the target⁴². With the elucidation of TCS structures, structure-based virtual screenings were employed to identify TCS inhibitors hits^{43, 43, 43, 44, 45} and some of the hits have been further improved by rational design^{46, 47, 45}. Drug design strategies for identifying TCS inhibitors with broad spectrum of inhibition as well as specific TCS inhibitors is facilitated by the available structural and genomic information for TCS as well as the large body of research on their role in bacterial physiology and virulence. Virtual structure-based or in vitro fragment-based screenings with multiple targets (Chapter 2 and 3, respectively) and selecting for common hits facilitates the discovery of broad-spectrum inhibitors, whereas selecting hits specific to particular target will facilitate the discovery of narrow-spectrum inhibitors. In this case high-resolution structures of TCS targets in complex with their inhibitors are still needed to facilitate the rational design of improved inhibitors against specific TCS targets that are either essential or controlling key virulence factors. With the advance of high-throughput crystallography^{48, 49, 50} it seems feasible to crystallize the kinome of a bacterial pathogen or promising HK targets from different pathogens and use the structural information to design more potent and/or specific inhibitors following structure-based design approach. Complementary approaches should include the structural determination of co-crystals of putative target HK CA domains that has been previously crystallized (e.g. WalK from *B. subtilis*, PDB:3SL2) with fragment libraries or known kinase inhibitors and co-crystals with mammalian members of the GHKL protein family (e.g. Hsp90) to facilitate structure-based design of inhibitors with improved affinity and specificity.

APPROACHES FOR TCS INHIBITORS DISCOVERY

STRUCTURE-BASED VIRTUAL SCREENINGS USING MULTIPLE HK STRUCTURES INCREASES THE CHANCES OF IDENTIFYING HK INHIBITORS WITH BROAD SPECTRUM OF INHIBITION

Molecular docking and receptor-based virtual screening have been an indispensable component within structure-based drug discovery, including TCS inhibitors discovery, for hits identification and hit-to-lead optimization^{43, 51, 44, 35, 45, 52, 53, 54, 55}. Although, ligand flexibility can be handled by variety of algorithms in current docking implementations^{56, 57}, receptor flexibility remains a major outstanding challenge in the practice of molecular docking-based virtual screening^{58, 59}. The

challenge is mainly because of the high dimensionality of the conformational space and the complexity of scoring energy function. It is generally accepted protein flexibility to be often coupled to ligand binding in numerous experimental and theoretical studies^{60, 61}. Two kinds of ligand-binding mechanisms have been well discussed⁶². The first is conformational selection, which assumes that the ligand binds to a pre-existing receptor conformation in an equilibrated ensemble; and the second is induced fit, which presumes that the binding of the ligand induces conformational changes in the receptor. In both cases, structural conformations of the receptors need to be taken into account in molecular docking studies and, ideally, (multiple) ligand-bound structures should be used instead of apo-structures.

Various modeling methods have been developed to account for receptor flexibility in molecular docking and structure-based virtual screening.^{58, 63} Soft docking, which docks ligands to a rigid receptor with a soft scoring function tolerating some steric clashes, has been reported to be worse for identifying known ligands than the hard scoring function when multiple receptor conformations were used.⁶⁴ Several docking programs limit protein flexibility to side chains by exploration of rotamer libraries and make the problem of protein flexibility less computationally demanding⁶⁵. However, this approach cannot deal with backbone movement or other major structural rearrangements. Another implementation is docking of ligands to multiple receptor conformations⁶⁶, which may either be obtained experimentally by X-ray crystallography and NMR spectroscopy or computationally by molecular dynamics, normal-mode analysis, and other techniques.

In Chapter 2 we applied an approach combining structure-based virtual screenings for putative ligands of three different HK X-ray structures followed by ligand-based similarity searches with the most promising hits as query molecules. The problem of receptor flexibility in the docking approach was addressed by using three different receptor structures. The use of multiple structures in the docking experiments increases the chance of finding broad-spectrum ligands because it implicitly considers the receptors plasticity, sequence and conformation variability in the docking approach. This approach mimics an ensemble based docking which has been shown to improve the overall performance of virtual screening experiments⁶⁷.

Screening by molecular docking for putative ligands of three different HKs successfully identified two hits, A5 and A6, which inhibited the autophosphorylation activity of multiple HKs and showed weak antibacterial effects. A5 and A6 inhibited the autophosphorylation of three HKs not employed in the virtual screenings (i.e. *E. coli* and *S. aureus* PhoR, and *S. pneumoniae* WalK). Therefore, A5 and A6 were used as query molecules in ligand-based similarity searches (LBSS). The LBSS successfully identified B13 as a promising lead candidate. B13 (R,S)-4-[1-Ethyl-2-(4-fluorophenyl)butyl]phenol inhibited the autophosphorylation of *E. coli* PhoR and *S. aureus* PhoR with IC₅₀ values of 16 and 212 μM, respectively (Chapter 2). The fact that B13 inhibited the autophosphorylation of multiple HKs including targets not used in the structure-based virtual screening supports the concept that use of multiple structures in the virtual screening by molecular docking, facilitates the identification of broad-spectrum inhibitors. Furthermore, even the next generation hits identified by other methods, in this case ligand-based similarity search (LBSS), possessed broad-spectrum inhibitory capacity. The putative broad spectrum HK autophosphorylation

inhibitory capacity of B13 was reflected in its broad-spectrum antibacterial effect (Chapter 2). B13 showed antibacterial effect for a range of Gram-positive bacteria, including MRSA clinical isolates. The MICs for the different Gram-positive strains ranged between 1 and 16 $\mu\text{g/ml}$.

Antibacterials should not cause adverse effects to host cells. Furthermore, one of the main causes of high attrition rates in drug discovery is so called adverse "off-target" effects. Therefore, as early as possible in the developmental program the toxicity of the hits has to be evaluated. B13 inhibited cell viability of Caco-2 cells and macrophages with IC_{50} values of 29 $\mu\text{g/ml}$ and $> 20 \mu\text{g/ml}$, respectively (Chapter 2 and 4). The selectivity index ($\text{IC}_{50}/\text{MICs}$) > 1 indicates that B13 is a promising candidate for hit-to-lead optimisation in the preclinical development of antibacterials for Gram-positive bacteria. B13 showed no antibacterial effect for Gram-negative bacteria. We hypothesized that this was most probably due to inability of B13 to cross the outer membrane of Gram-negative bacteria and explored the possibility to use nanoparticles for enhanced delivery to Gram-negative bacteria (Chapter 4). Indeed, as part of a nano-formulation for delivery of antibacterials to Gram-negative bacteria⁶⁸ B13 showed antibacterial effect for the uropathogenic *E. coli* CFT 073 with MIC of 25 $\mu\text{g/ml}$ (Chapter 4). The latter is in agreement with B13 autophosphorylation inhibitory capacity for HKs from Gram-negative bacteria (Chapter 2). This is encouraging because it might be possible to enhance the permeability of next generation hits based on B13 using medicinal chemistry approaches⁶⁹.

The other two promising hits coming from the LBSS following SBVS (Chapter 2), B7 and B14, showed lower HK autophosphorylation inhibitory capacity, weaker antibacterial effect and stronger cytotoxicity to Caco-2 cells than B13. Nevertheless, B7 and B14 are worth considering as starting points for the design of improved HK inhibitors because they are predicted to interact with the ATP-lid. The ATP-lid is a highly flexible and variable in sequence component of the ATP-binding site of HKs and is critically involved in autophosphorylation^{13, 16}. The variability of the ATP-lid has been proposed as a valuable feature for the design of inhibitors that are specific to bacterial HKs with limited off-target effects on eukaryotic proteins sharing the ATP-binding Bergerat fold (the so called GHKL proteins, including Hsp90 and MutL)¹⁵ or for the design of strain-specific HK inhibitors²⁰.

FRAGMENT-BASED SCREENING BY DIFFERENTIAL SCANNING FLUORIMETRY IS A POTENT TOOL FOR THE DISCOVERY OF HK AUTOPHOSPHORYLATION INHIBITORS WITH DESIRED SPECTRUM OF INHIBITION

So far, TCS inhibitors have been discovered mainly by high-throughput screenings (HTS)^{70, 30, 71} or by structure-based virtual screenings^{43, 51, 44, 35, 45}. Fragment-based screening (FBS) is a more recent approach and the methodology behind it is complementary to HTS^{72, 73}. Fragments are small molecules with low affinity (usually $K_d > 0.1 \text{ mM}$) following the rule of three ($\text{MW} < 300$, $\text{ClogP} < 3$, number of hydrogen bond donors and hydrogen bond acceptors < 3 , number of

rotatable bonds < 3)^{74, 75}. Fragments serve as starting point for the elaboration of more potent inhibitors by rational design⁷⁶. The main advantage of FBS over HTS is that fragment libraries are much smaller than conventional compound libraries^{77, 78, 79}. It has been estimated that there are only $\sim 10^7$ molecules of up to 11 heavy atoms which are also fragment-like ($MW \leq 300$ Da), compared to $\sim 10^{63}$ molecules of molecular weight less than 500 Da, i.e. drug-like. This means that a library of 10^3 fragments covers 0.01 % of the fragment-like chemical space compared to 10^{-58} % of the chemical drug-like space.

The low molecular weight of fragments (typically ≤ 300 Da) and their corresponding reduced functionality implies that they will generally bind a target protein with weak affinity ($K_d > 0.1$ mM), if at all. Despite their weak affinities, fragments possess high intrinsic binding energy to overcome a large entropic barrier upon binding⁸⁰ and often exhibit high ligand efficiency (ΔG of binding per non-hydrogen atoms)⁸¹. Therefore, fragments are suitable starting points for elaboration into larger, more potent inhibitors.

Considering the advantages of FBS over HTS mentioned above, we performed fragment-based screenings (FBS) by differential scanning fluorimetry (DSF) for ligands of multiple HKs (Chapter 3). By choosing the hits identified with different targets we were able to identify HKAI s that inhibited the autophosphorylation of HKs that were not used in the screens, showing that the use of multiple targets selects for inhibitors with broad-spectrum inhibitory capacity. The hits identified by FBS by DSF were used as query molecules in ligand-based similarity searches (LBSS) and the LBSS hits showed broad-spectrum antibacterial effect against multi-drug resistant Gram-positive and Gram-negative strains (Chapter 3). Probably due to their small size, the fragment-like HKAI s showed lower affinity to HKs (indicated by their IC_{50} s for *E. coli* PhoR autophosphorylation) and higher cytotoxicity to Caco-2 cells compared to the hits identified by SBVS and LBSS in Chapter 2. The antibacterial activity of the FBS hits was comparable to the less potent hits identified by SBVS and LBSS, B7 and B14 (Chapter 2). The comparable antibacterial effect despite of the lower affinity to HKs and the higher cytotoxicity might be related to off-target effects as these hits are fragment-like and most likely bind also to multiple prokaryotic and eukaryotic targets. The structural similarity with previously published TCS inhibitors (F1 and F1.6,^{43, 46, 47}) and the limited options for further improvement of the carbazoles from drug discovery perspective (F2.1, F2.3 and F2.8) makes these hits unattractive for further investigation. Nevertheless, F1.8 (4-N-(4-bromophenyl)pyrimidine-2,4-diamine) seems to present a promising starting point for structure-based drug design of HK inhibitors with broad-spectrum antibacterial effect. F1.8 possess weak HK autophosphorylation inhibitory capacity, however, it shows broad-spectrum antibacterial activity including against multi-drug Gram-negative strains. The latter suggests that F1.8 scaffold is attractive for the development of antibacterials with improved permeability for Gram-negative bacteria.

COMPUTER-AIDED APPROACHES CAN FACILITATE HIT IDENTIFICATION AND OPTIMISATION PROVIDED SCREENINGS ARE PERFORMED BY STANDARDISED METHODS

Nowadays early-stage antibacterial drug discovery is largely done by academic organisations or SMEs. It is unlikely that such organisations would have the resources for extensive screening⁸². However, if screening and *in vitro* evaluation of screening hits are performed under standardized conditions in different laboratories and the information is made (publicly) available different computational methods can be exploited to speed up the discovery and optimisation of hits. These include predictive quantitative structure-activity relationship (QSAR)^{83, 84} models and ligand-efficiency indices (LEIs) approaches^{85, 86} (Chapter 5).

MOLECULAR MODELING CAN GUIDE RATIONAL OPTIMISATION OF HITS IN THE ABSENCE OF EXPERIMENTAL TARGET-INHIBITOR STRUCTURES

The hits identified by SBVS, FBS, LBSS, QSAR and LEIs approaches (Chapter 2, 3 and 6) were co-crystallized with the CA domain of *T. maritima* CheA HK as a model system (data not shown)⁸⁷. In some cases, such as A5, B13, B14, F1, F2, F2.3, H30 the CheA-inhibitor structures, solved by X-ray crystallography, revealed electron density in the binding site, although the structures of the HK inhibitors could not be fully resolved, probably due to partial occupancy and/or multiple conformations. Unfortunately, these structures could not be used to guide rational design of more potent inhibitors following structure-based drug design approach. Therefore, the putative binding mode of the HK inhibitors was predicted by molecular docking to the structure of the CA domain of *T. maritima* HK853⁸⁸ or *B. subtilis* WalK⁸⁹. The predicted binding modes of the HKAIIs (Chapter 2 and 3) resembled the binding mode of the natural substrate ATP/ADP. The most potent inhibitors, e.g. B13, were predicted to form contacts with conserved residues in the N-, G1- and G2-boxes in the ATP-binding site. Some inhibitors, such as B7, were predicted to interact with the variable ATP-lid and showed significant differences in the autophosphorylation inhibitory capacity for different HKs. Other inhibitors predicted to interact with the ATP-lid, e.g. F1.8 (Chapter 3), showed broad spectrum HK inhibitory activity and antibacterial action. Although the ATP-lid is more variable compared to the remaining parts of the ATP-binding site of the CA domains (Figure 2), it contains conserved residues, such as Arg, Ile or Leu, and Tyr (Figure 2B). These residues are conserved among HKs from different species or different HKs from the same bacteria (Figure 2C and 2D). The binding modes predicted by molecular modeling can serve as starting point for the structure-based design of more potent and specific or broad-spectrum inhibitors with lower off-target effects by exploring the features of the ATP-lid.

ANTIMICROBIAL PEPTIDES AND TWO-COMPONENT SYSTEMS INHIBITION

Eukaryotic cationic antimicrobial peptides (AMPs) are produced at sites of infection or inflammation in many different organisms^{90, 91, 92}. Usually, AMPs increase the permeability of the bacterial membrane, leading to loss of pH gradient and cell death. Some AMPs have been shown to interact with intracellular targets^{93, 94} but in most cases the exact mechanism of action of intracellular AMPs remains unclear.

INHIBITION OF *T. MARITIMA* HK853-RR468 BY LACTOFERRICIN B-DERIVED PEPTIDES IS NOT SUITABLE FOR STRUCTURAL STUDIES ON TCS INHIBITION BY AMPs

Chapter 9

LactoferricinB (LfcinB) is an AMP with broad-spectrum antibacterial activity^{95, 96}. It has been shown by *in vitro* and *in vivo* experiments and bioinformatics methods that LfcinB inhibits the phosphorylation of the RRs (BasR and CreB) by their cognate histidine kinases (HKs), BasS and CreC⁹⁷. We showed that LfcinB-derived peptides inhibit the phosphotransfer and phosphatase activity of *T. maritima* HK853-RR468 (Chapter 6). However, the LfcinB-derived peptides seemed to induce aggregation of *T. maritima* HK853 and *E. coli* PhoB. Therefore, *T. maritima* HK853-RR468 and *E. coli* PhoRB might not be suitable for structural studies of TCS inhibition by LfcinB-derived peptides. Furthermore, the described results taken together with the broad-spectrum of antibacterial activity of LfcinB point to the possibility that the antibacterial effect caused by LfcinB and LfcinB-derived peptides might be attributed to non-specific protein aggregation and might act on multiple cellular targets after entering into the cell. On this basis further work on LfcinB-derived peptide inhibitors was abandoned.

SYNERGY EFFECT BETWEEN ANTIMICROBIAL PEPTIDES AND TCS INHIBITORS

Antimicrobial peptides have been proposed as a way to overcome the lower permeability of Gram-negatives cell envelope^{98, 99}. Therefore, we tested the synergistic effect of three frog AMPs with antibacterial effect against Gram-negative bacteria and B13, as the most potent HK inhibitor described in this thesis. The AMPs tested were [E4k]alyteserin-1c, [E6K]hymenochirin-1B and [K20K27]esculentin-2Cha^{100, 101}. Unfortunately, no synergistic antibacterial effect against *E. coli* CFT 073 was observed (data not shown). ϵ -Poly-L-lysine (ePLL) is a homo-polypeptide with demonstrated antibacterial effect¹⁰². Similar to the frog AMPs, ePLL showed no synergistic effect with HK inhibitors on antibacterial activity against *E. coli* CFT073 (Chapter 4). The MICs against *E. coli* CFT073 of the tested frog AMPs and ePLL

were ≥ 63 $\mu\text{g/ml}$. Combinations of more potent AMPs and/or more potent HKAIs might be required to achieve synergistic effect and ultimately to observe antibacterial effect against Gram-negative pathogens.

HK INHIBITOR SPECTRUM CAN BE BROADENED AND THE CYTOTOXICITY REDUCED VIA THE USE OF NANOTECHNOLOGY

Although the best hits described in Chapter 2 and 3 have weak or no activity (MICs in the range of 125-500 $\mu\text{g/ml}$) against Gram-negative pathogens, they do inhibit autophosphorylation of HKs from Gram-negative bacteria suggesting permeability of the Gram-negative cell envelope is limiting their anti-bacterial effects. This assumption was shown to be correct using histidine kinase autophosphorylation inhibitors (HKAs) loaded mesoporous silica-based nanoparticles capped with ϵ -poly-L-lysine as a strategy for effective drug delivery (Chapter 4)⁶⁸. Whereas the nanoparticles themselves had no antibacterial activity, the MICs of HKAs combined with nanoparticles was decreased more than 10-fold (Chapter 4). The free HKAs showed relatively low toxicity to human cells and even lower toxicity when combined with nanoparticles. Taken together these data indicate high potential for developing a new structural class of antibacterial lead compounds with activity against multiple targets in several MDR Gram-positive and Gram-negative pathogens.

COMPARISON OF THE NOVEL HK INHIBITORS WITH OTHER PUBLISHED TCS INHIBITORS

Structure-based virtual screenings for *S. epidermidis* WalK ligands yielded inhibitors which have been subsequently further optimized by rational design^{43, 46, 47}. The last generation of *S. epidermidis* WalK inhibitors had MICs for *S. epidermidis* and *S. aureus* lower than 3.1 μM , corresponding to lower than 1.66 $\mu\text{g/ml}$ ⁴⁷. B13, the most potent hit described in this thesis (Chapter 2), possess MICs for *S. epidermidis* laboratory strains and clinical isolates in the range of 1 to 8 $\mu\text{g/ml}$. B13 MICs for reference strains of *S. aureus* and clinical isolates of MRSA are in the range of from 8 to 16 $\mu\text{g/ml}$ (Chapter 2). Therefore, in terms of antibacterial activity B13 is comparable to the last generation of published *S. epidermidis* WalK inhibitors. *S. epidermidis* WalK inhibitors inhibited *S. epidermidis* WalK autophosphorylation with IC_{50} values in the range of 24.2 to 71.2 μM ⁴⁷. B13 has not been tested for its autophosphorylation inhibitory capacity for any WalK, however, it inhibits *E. coli* PhoR and *S. aureus* PhoR with IC_{50} of 16 and 212 μM , respectively (Chapter 2). Considering the differences in the experiments used to determine the IC_{50} s of the *S. epidermidis* WalK inhibitors and B13 and the fact that different HKs Km differ in the range 2 and 200 μM ¹⁰³, it is difficult to conclude how B13 compares to the last generation of published *S. epidermidis* WalK inhibitors. The cytotoxicity of the *S.*

epidermidis WalK inhibitors was evaluated with Vero Cells using the MTT assay and the IC₅₀ were higher than 100 µg/ml⁴⁷ corresponding to > 60 selectivity index (IC₅₀viability/MIC). B13 cytotoxicity was evaluated with Caco-2 cells using the neutral-red uptake assay (Chapter 2) and with macrophages in cell culture (Raw cells) using the XTT assay (Chapter 4) and the IC₅₀ were 29 µg/ml and ≤ 20 µg/ml, respectively, corresponding to selectivity index ≥ 1.25 for the different *S. epidermidis* and *S. aureus* strains tested (Chapter 2). Even though the cell viability was evaluated using different cell lines and methods, it is clear that B13 selectivity is worse than the selectivity of the last generation published *S. epidermidis* WalK inhibitors and needs to be improved. However, B13 (MW 272.4) is a relatively smaller compound compared to the last generation *S. epidermidis* WalK inhibitors (MW between 498.02 and 534.02) implying that it possesses higher ligand efficiency and more possibilities for further improvements using an iterative structure-based drug design approach.

FUTURE CHALLENGES AND PERSPECTIVES OF THE DISCOVERY OF TCS INHIBITORS

Both SBVS and FBS seem to be promising tools for the discovery of TCS inhibitors. The application of multidisciplinary screening approach (including SBVS, FBD, and LBSS) allowed us to identify HK inhibitors with activity against multiple HKs and a broad-spectrum antibacterial effect. Furthermore, the identified inhibitors are predicted to interact with different parts of the ATP-binding sites. The latter together with the relatively small size of the identified HK inhibitors (MW < 300) provides the possibility to design improved inhibitors by combining chemical moieties from the different hits to generate inhibitors with stronger affinity and higher specificity to bacterial HKs.

Although a very promising starting point for development of novel antibacterials, the identified HKAls have a number of shortcomings that need to be addressed in the hit-to-lead optimisation process:

- The affinity to model HKs such as *T. maritima* CheA is most likely not high enough and/ or multiple conformations of the inhibitors are possible and therefore, the CheA-inhibitors structures cannot be resolved and used for structure-based drug design. This liability can be addressed by discovering more potent HK autophosphorylation inhibitors and/ or by solving the structures of the discovered inhibitors with other putative target HKs, such as the recently published *B. subtilis* and *S. mutans* WalK (PDB: 3SL2 and 4I5S) or *E. coli/T. maritima* EnvZ (PDB: 4KP4)^{89, 104}.

- The identified HKs inhibitors are not sufficiently permeable to Gram-negative bacteria. This can be overcome by using nanoparticles (Chapter 4). The latter however, raises additional issues related to the following steps of the drug discovery process related to the safety of such complex therapeutic agents. Therefore, it is desirable to apply medicinal chemistry approaches to design inhibitors with improved permeability for Gram-negatives⁶⁹. Addition of functional groups to the identified

HKAIs, given their small size, could increase the permeability in Gram-negatives. Nevertheless, increasing the specificity of the identified inhibitors to Gram-positive targets such as the obligatory essential WalKR can be a promising strategy to develop narrow-spectrum antibacterials against Gram-positive bacterial infections.

- The identified HKAI s showed some cytotoxicity to Caco-2 cells evaluated by neutral-red uptake assays (Chapter 2 and 3) and B13 showed cytotoxic effect to macrophages (Raw cells) evaluated by the XTT assay (Chapter 4). The most promising and most potent HK inhibitor B13 possesses a selectivity index for Gram positives (IC_{50} viability/ MICs) ≥ 1.25 . Increasing the potency and the selectivity of the HK inhibitors will most likely lead to decrease in their cytotoxicity. To facilitate the discovery of more selective HK inhibitors, the next generation of HK inhibitors should be tested also for their inhibitory activity on the structurally closely related mammalian members of the GHKL superfamily^{15, 105}.

In summary, following structure-based and ligand-based virtual screenings and fragment-based *in vitro* screenings, we have successfully identified HK autophosphorylation inhibitors (HKAI s) that can serve as a starting point for the design of HKAI s with improved target affinity and selectivity, which would lead to stronger antibacterial effect and lower toxicity.

SUMMARY

2014

The growing problem of bacterial multi-drug resistance requires the urgent establishment of pipelines for discovery of novel antibacterials. Two-component systems (TCS) have been proposed for years as promising novel antibacterial targets. Inhibitors of TCS, especially autophosphorylation inhibitors targeted at the CA domains of multiple histidine kinases (HKs) are expected to show broad-spectrum of antibacterial activity and low toxicity to host cells.

Using structure-based virtual screenings (SBVS) for putative ligands of three different HKs followed by ligand-based similarity search with the most promising SBVS hits (**Chapter 2**) we identified HK autophosphorylation inhibitors of multiple HKs from both Gram-positive and Gram-negative bacteria. The inhibitors showed broad-spectrum antibacterial activity for Gram-positive bacteria, including clinical isolates of MRSA strains resistant to a wide range of β -lactam and non- β -lactam antibiotics. The most promising hit, B13, showed relatively low cytotoxicity and hemolytic activity and therefore presents a promising starting point for hit-to-lead optimisation using a structure-based drug design approach. The predicted binding modes of the other less potent hits, B7 and B14, point to possibilities to design more potent and selective inhibitors by combining chemical moieties belonging to the different hits.

In **Chapter 3** fragment-based in vitro screenings (FBS) by differential scanning fluorimetry (DSF) were performed for ligands of two different HKs followed by ligand-based similarity searches with the two identified hits. Weak HK autophosphorylation inhibitors with broad spectrum of antibacterial activity were identified. Compounds F1.8 and F2.3 showed antibacterial effect for both Gram-positive and Gram-negative strains, including clinical isolates of MRSA and multi-drug resistant *Acinetobacter baumannii* and *Stenotrophomonas maltophilia*. The identified hits present a promising starting point for the design of HK autophosphorylation inhibitors with improved permeability.

In *Chapter 5* a computer-aided approach was used in an attempt to identify more promising hits for HK autophosphorylation inhibitors using

Nanoparticles delivery was employed to show that the most potent HK inhibitors, e.g. B13, possess antibacterial effect against Gram-negative bacteria (**Chapter 4**). Mesoporous silica-based nanoparticles loaded with HK autophosphorylation inhibitors showed 10-fold lower MICs compared to the free HK autophosphorylation inhibitors for UPEC *E. coli* CFT 073 and *Serratia marcescens*. Despite the lower MICs of HK autophosphorylation inhibitors loaded in nanoparticles for bacteria they were less cytotoxic than the free inhibitors at equivalent concentrations

Lactoferricin (LfcinB) has been shown to inhibit TCS from *E. coli*. We demonstrated that LfcinB-derived peptides interact with *T. maritima* HK853-RR468 and *E. coli* PhoRB however, the mechanism of interaction was most likely non-specific and due to protein aggregation. (**Chapter 6**). Therefore efforts to co-crystallize these peptides with TCS for the rational structure-based drug design of improved inhibitors was not pursued further.

Co-crystallization of the HK autophosphorylation inhibitors with *T. maritima* CheA is described in **Chapter 7.1**. Furthermore, the purification, crystallization and

preliminary X-ray analysis of the periplasmic domain of CopM, a protein suggested to be involved in copper resistance, is presented in **Chapter 7.2**.

Chapter 8 is a discussion on the possibility to develop novel antibacterials with low potential for resistance development by targeting TCS signalling in general and the essential WalKR in particular.

Chapter 9 is a discussion of the main results of this thesis in the context of current literature on antibacterial drug discovery and published research on discovery of TCS inhibitors.

SAMENVATTING

2014

Het toenemende probleem van bacteriële multidrug resistentie vereist het vlotte opzetten van onderzoeks-structuren om nieuwe antibiotica te ontdekken. Enkele jaren geleden werd voorgesteld dat twee-component systemen (TCSen) veelbelovende nieuwe antibacteriële doelwitten zouden kunnen vormen. Het is de verwachting dat remmers van TCSen, vooral autofosforylatie remmers gericht op de zogenoemde "CA" domeinen van histidine kinases (HKs), een breed spectrum van antibacteriële activiteit en lage toxiciteit voor gastheercellen zullen vertonen.

Met behulp van structuur-gebaseerde virtuele screenings (SBVS) voor vermeende liganden van drie verschillende HKs, gevolgd door zoeken naar liganden die het sterkst lijken op de meest veelbelovende SBVS treffers (**Hoofdstuk 2**) identificeerden we HK autofosforylatie remmers van HKs van zowel Gram-positieve als Gram-negatieve bacteriën. De remmers toonden breed-spectrum antibacteriële activiteit ten aanzien van Gram-positieve bacteriën, inclusief klinische isolaten van MRSA-stammen met resistentie tegen diverse β -lactam en niet- β -lactam antibiotica. De meest veelbelovende treffer, B13, liet een relatief lage cytotoxiciteit en hemolytische activiteit zien en lijkt daarom een veelbelovend uitgangspunt voor de zogenoemde "hit-to-lead" optimalisatie waarbij een structuur-gebaseerde drug ontwerp aanpak wordt gevolgd. De voorspelde bindingscapaciteit van twee minder krachtige treffers, B7 en B14, biedt mogelijkheden om krachtiger en selectievere remmers te ontwerpen, door het combineren van chemische groepen die behoren tot de verschillende treffers.

In **hoofdstuk 3** is beschreven hoe fragment-gebaseerde in vitro screenings (FBS) door differentiële scanning fluorimetrie (DSF) werden uitgevoerd om liganden van twee verschillende HKs te zoeken, gevolgd door het zoeken naar chemische verbindingen die een ligand-gebaseerde gelijkenis vertonen, met als uitgangspunt de twee in hoofdstuk 2 geïdentificeerde treffers. Zwakke HK autofosforylatie remmers met een breed spectrum van antibacteriële activiteit werden gevonden. De verbindingen F1.8 en F2.3 toonden antibacteriële werking tegen zowel Gram-positieve als Gram-negatieve stammen, met inbegrip van klinische isolaten van MRSA en multiresistente *Acinetobacter baumannii* en *Stenotrophomonas maltophilia*. De geïdentificeerde treffers bieden een veelbelovend uitgangspunt voor het ontwerp van HK autofosforylatie remmers met verbeterde doorlaatbaarheid voor bacterie membranen.

In **hoofdstuk 5** werd een computer-gebaseerde benadering gebruikt in een poging om meer veelbelovende treffers van HK autofosforylatie remmers te vinden.

Nanodeeltjes werden gebruikt om te laten zien dat de meest potente HK-remmers, bijvoorbeeld B13, een antibacteriële werking hebben tegen Gram-negatieve bacteriën (**Hoofdstuk 4**). Mesoporeuze silica-gebaseerde nanodeeltje gevuld met HK autofosforylatie remmers toonden 10-voudig lagere MICs in vergelijking met de MIC van de pure HK autofosforylatie remmers; deze remmers hadden aantoonbare activiteit tegen UPEC *E. coli* CFT 073 en *Serratia marcescens*. Ondanks het feit dat de in nanodeeltjes verpakte HK autofosforylatie remmers een lagere MIC hadden wanneer toegepast om bacteriën te bestrijden, waren deze verpakte remmers minder cytotoxisch dan de pure remmers bij dezelfde concentraties.

Het is aangetoond dat Lactoferricine (LfcinB) TCSen uit *E. coli* kan remmen. We toonden aan dat van LfcinB afgeleide peptides activiteit bezitten tegen *T. maritima* HK853-RR468 en *E. coli* PhoRB, en dat het mechanisme van interactie

hoogstwaarschijnlijk niet specifiek was maar werd bepaald door eiwit aggregatie (**Hoofdstuk 6**). Pogingen om deze peptiden samen te kristalliseren met TCSen om betere remmers te vinden via een rationele structuur-gebaseerde drug ontwerp benadering werden daarom niet doorgezet.

Het tegelijk kristalliseren van HK autofosforylatie remmers met het *T. maritima* CheA TCS wordt beschreven in **hoofdstuk 7.1**. In **hoofdstuk 7.2** worden eveneens de zuivering, kristallisatie en voorlopige röntgenanalyse van het periplasmatische domein van CopM, een eiwit dat gedacht wordt betrokken te zijn bij koper resistentie, beschreven.

Hoofdstuk 8 presenteert een discussie over de mogelijkheid om nieuwe antibacteriële middelen met een lage kans op ontwikkeling van resistentie te ontwikkelen, door middelen te ontwikkelen die het doorgeven van cellulaire signalen via TCSen in het algemeen, en in het bijzonder de essentiële WalKR, blokkeren.

In **hoofdstuk 9** worden de belangrijkste resultaten van dit proefschrift en hun inbedding in de huidige literatuur over antibacteriële drug ontdekking in het algemeen, en de specifiekere literatuur over de ontdekking van TCS-remmers, bediscussieerd.

Translated from English to Dutch by Peter van Baarlen

ACKNOWLEDGEMENTS

2014

Those who know me well/ long enough are aware of my difficulties in expressing positive thoughts especially gratitude, but I will do my best to thank the people who have helped me reach the final stage of my formal education (at least in Biology), and who have been an inspiration and example to follow.

Obtaining a PhD degree takes around four years, “a moment”, and the “journey” to starting a graduate programme takes at least six times longer. First, I would like to thank the people involved in the “journey” in retrospective order:

- My family for letting me grow independent, taking my own decisions and for their support in times when it was needed.

- The dentist who took the initiative, responsibility and the risk in probably my first fight with multi-drug resistant bacteria when I was 2-3-years-old.

- My primary school teacher Neli Koshnicharova for holding my hand to my first competition in Mathematics in my future high school.

- All the amazing people who still work in this high school for their extraordinary professionalism. Despite minor distractions such as electricity and water regimens, no fuel for public transport and heating in the winter, wars in neighbouring countries etc. they managed to keep us excited and curious about life and science, and motivated to make a difference. Special gratitudes to Elena Stancheva, Mima Ilieva, Penka Nikolova, Miroslava Georgieva, Elena Yordanova-Kostadinova, and Antoaneta Velikova.

- To my classmates whose success in their personal and professional life makes me proud and keeps me optimistic. Especially to Peter, Ayshe and Marina.

- My teacher and friend Nikolina Stoyanova. Unfortunately, I still sound bored during presentations.

- Lyubo, whenever I feel down I know I can count on you for a ridiculous remark full of wisdom.

- Iliana Ivanova for being an example of a dedicated, positive, optimistic and down-to-earth researcher and teacher.

- My classmates and friends in the Faculty of Biology for the parties, wisdom and talks and walks, hiking in Vitosha, the tripe soup, the “conference calls”, trainings in the gym etc. crazy memories. Especially to Nadezhda, Velmira, Sylvia, Apo, and Niki.

- Eugene Semenov (RIP) for the great opportunity to work on an international project already as a BSc student and for sharing his wisdom. I try to always remember that “All people are nice, but sometimes it is difficult to work with them.”

- My colleagues at the Molecular Neurobiology, and especially Shazie, for the friendly and relaxed atmosphere. Working in the lab and chilling can be the same action.

- My classmates and friends at WUR, Christina, Agata, Christos, Man, and George for making the bad weather in the Netherlands seem “not so bad”.

- All the Bulgarians in Wageningen, especially Nikolay P., Daniela and Slav, Radostina and her mother, and Denica B.

- All the people I have met at IC, especially Michiel, Mensur, Jessin, Hida, Remko, and the wild dancer Alexander.

- The people at the Toxicology Department and at RIKILT, especially Si, Alexandros, Ana, and Jaime. Laura, Jac, Ivonne, Ad, Toine, and Tinca you gave me an opportunity but apparently I was not ready for it and now I am extremely grateful for helping me take the right decision.

- Prof. Iliana Ionkova for confirming what I already knew.

- Nikolay R. for the countless hours of skype and phone calls, the helpful distraction, moral support, the nice presents and the life lessons.

And now the people involved in the "moment" called PhD studies:

- Alberto for the coolest job interview I have ever had/ will have. For being a great example of a dedicated, passionate, focused structural biologist (... however, sometimes too focused), and relatively patient and fair group leader, flexible about rules and deadlines. I have learned (some) Structural Biology in your group and hopefully one day I will publish a protein structure, or even better protein-inhibitor structure. And furthermore, everytime I feel upset and dissatisfied I try to remember that "There are plenty of people in the world who dream to have my problems." and sometimes it helps.

- Paqui for being an inspiring example of a structured, organized, efficient, calm, open-minded, confident and friendly female scientist from a country where women had no rights up until 40 years ago.

- My colleagues at UCM-IBV, for forcing me to learn Spanish and for training my patience, which in long-term is probably more useful than any lab technique I could have learnt from them.

- El president de la CdF and the others responsible for the party atmosphere at IBV. I regret I haven't enjoyed more.

- InhibOx for hosting my first secondment and for being involved in the project. As a frustrated, unlucky crystallographer, without your contribution I would have had a much shorter thesis.

- Especially to Simone who did all the scripting and computational experiments. She also taught me how to do some experiments myself, and to me she is an example of a professional, organized, reliable, and very helpful person. Although this project was not exactly what she was meant to work on, she was sincerely interested in the progress, provided me with moral support and advice in times of disappointment and frustration, and I hope we'll stay in touch and remain friends.

- Prof. Conlon, Milena, Manju, Akela, Agnes Sonnevend and Tibor Pal, and everyone else at UAEU, Al Ain, for the productive, exotic and exciting secondment!

- Ana and Marco for the MICs and MBCs with *S. pneumoniae*.

- Nuria, Ramon and anyone else from UPV for synthesizing the nanoparticles. Your collaboration made the coolest and the fastest chapter of my thesis! Thank you!

- My Bulgarian friends in Valencia, Associacio L'orneta blanca, Daniel, Pavel, for helping me feel at home and stimulating me to keep in shape.

- Everyone in the STARS ITN for the nice times during our "paid holidays".

- Everyone at the Host-microbe Interactomics group at WUR for the friendly and happy atmosphere. Nico, Ellen, Edo and his students for their contribution to my coolest chapter, I promise to publish it asap. Loes and Mayo for their help on administrative, printing, publishing etc issues, and for their positivism. Aga for writing together a viewpoint and a review before having solid results. Rogier for his help, I can't remember a particular example right now, but I've bothered him few times. Peter for his thorough proof-reading of the viewpoint, the review and translation of the summary.

- Jerry for letting me and helping me finish my PhD studies on time at HMI, for his "contagious" multidisciplinary scientific curiosity and enthusiasm to make it possible to continue working on TCS inhibitors discovery and development, and for creating an atmosphere where you see everything as easy and feasible. Unfortunately, in the 6-7 months at HMI I couldn't accomplish all ideas you've given me during our meetings but hopefully in future I can do more.

3 hours to thank people I have met for 30 years ... I thank also everyone else who is not mentioned due to dehydration, my short memory or "blindness" to their impact, and last but not least laziness to read the text again ...

2014

PERSONALIA

CURRICULUM VITAE LIST OF PUBLICATIONS

2014



Nadya Velikova (Надя Великова) was born on 17th of January 1984 in Burgas, Bulgaria. She finished her secondary school education in the High School for Mathematics and Natural Sciences "Akad. Nikola Obreshkov", Burgas, Bulgaria, in 2002. In the same year she was among the winners of the National Olimpiad in Biology, the winner of the National Contest for High School Students Projects in Ecology and Environmental protection and participant in the finals of the National Competition in Chemistry. The first granted her admission to the Bachelor of Science programme in Molecular Biology at the Faculty of Biology, Sofia University "St. Kliment Ohridski", Sofia, Bulgaria. In parallel to her BSc studies she worked in Eugene Semeonov's group at the Department of Molecular Neurobiology, Institute of Molecular Biology, Bulgarian Academy of Sciences, on ivermectin resistance. After finishing her BSc studies in 2007, Nadya continued her education in the Master of Science programme in Medical Biotechnology at Wageningen University, The Netherlands. She did a MS thesis at the Department of Toxicology under the supervision of Dr. ir. Jac Aarts, and an internship at the Toxicology and Bioassays Business Unit at RIKILT-Institute of Food Safety, under the supervision of Dr. ir. Toine Bovee. Both the the thesis and the internship were related to design, development and implementation of reporter-gene assays for nuclear-hormone receptors ligands. In 2010 In 2010, Nadya continued her education and research experience in Dr. Alberto Marina's group in the Institute of Biomedicine of Valencia, Spanish National Research Council, Valencia, Spain, working on the structure-based discovery of two-component system inhibitors as part of the EU FP7-funded Marie Curie ITN STARS – Scientific Training in Antimicrobial Research Strategies. The project included secondments at InhibOx, Oxford, United Kingdom, and at the Department of Biochemistry, United Arab Emirates University, Al Ain, United Arab Emirates. In 2014 Nadya continued her PhD studies as an external PhD candidate at the Host-Microbe Interactomics Group at Wageningen University under the supervision of Prof. dr. Jerry Wells.

PUBLICATIONS

PUBLICATIONS RELATED TO THE CURRENT THESIS

Velikova, N.; Bem, A. E.; van Baarlen, P.; Wells, J. M.; Marina, A., WalK, the Path towards New Antibacterials with Low Potential for Resistance Development. ACS Medicinal Chemistry Letters 2013, 4 (10), 891-894.(viewpoint)

Velikova, N., Fulle, S., Manso, A.S., Mechkarska, M., Finn, P., Conlon, M.J., Oggioni, M.R., Wells, J.M., Marina, A., Identification of putative fragment-like histidine-kinase inhibitors active against multi-drug resistant bacterial strains, submitted to the European Journal of Medicinal Chemistry

Bem, A., Velikova, N., Pellicer, T., van Baarlen, P., Marina, A., Wells, J.M., Bacterial Histidine Kinases as Novel Antibacterial Drug Targets, submitted to ACS Chemical Biology (review)

Velikova, N., Fulle, S., Manso, A.S., Mechkarska, M., Conlon, M.J., Wells, J.M., Oggioni, M.R., Finn, P., Marina, A., Discovery of bacterial histidine kinase inhibitors with antibacterial activity against clinical isolates of MRSA and *Staphylococcus epidermidis*, in preparation

Velikova, N., Mas, N., Stolte, E., Zaccaria, E., Cao, R., Taverne, N., Murgina, J.R., Martinez-Manez, R., Marina, A., Wells, J.M., Broadening the Antibacterial Spectrum of Histidine-kinase Autophosphorylation Inhibitors via the use of ϵ -poly-L-lysine Capped Mesoporous Silica-based Nanoparticles, in preparation

Velikova, N., Marina, A., Purification, Crystallization and Preliminary X-ray Diffraction Analysis of *Syneccocystis spp.* CopM, in preparation

OTHER PUBLICATIONS

Loonen, L.M.P., Taverne, N., Velikova, N., Stolte, E.H., Marina, A., Dekker, J., Wells, J.M., Purification and characterization of recombinant mouse RegIII proteins, thesis chapter, Wageningen University, ISBN 987-94-6173-672-7, 2013

Sotoca, A.M., Bovee, T.F.H., Brand, W., Velikova, N., Boeren, S., Vervoort, J., Rietjens, I.M.C.M., Superinduction of estrogen receptor mediated gene expression in luciferase based reporter gene assays is mediated by a post-transcriptional mechanism, The Journal of Steroid Biochemistry and Molecular Biology, Volume 122, Issue 4, October 2010, Pages 204-211, ISSN 0960-0760, 10.1016/j.jsbmb.2010.06.010.

Yusein, S., Velikova, N., Kупenova, R., Hardie, R., Wolstenholme, A., Semenov, E., Altered ivermectin pharmacology and defective visual system in *Drosophila* mutants for histamine receptor HCLB, Invertebrate Neurosciences 2008 Dec; 8(4):211-22. doi: 10.1007/s10158-008-0078-2

The research described in this thesis was financially supported by the European Union Framework Programme 7-funded Marie Curie Initial Training Network **STARS** (Contract No. PITN-GA-2009-238490)

Cover design: Nadya Velikova

Layout: Nadya Velikova

Printed by: GVO drukkers & vormgevers B.V. Ponsen & Looijen